

**STUDIES ON THE PHOTOVOLTAIC AND METAL ION  
BINDING PROPERTIES OF A FEW HETEROCYCLIC  
DONOR- $\pi$ -ACCEPTOR SYSTEMS**

*Thesis submitted to the  
Cochin University of Science and Technology  
In partial fulfilment of the requirements for the degree of*

*Doctor of Philosophy  
in  
Chemistry*

*In the Faculty of Science  
By*

**Kala, K.**

*(Reg. No: 4024)*

*Under the supervision of*

**Dr. N. Manoj**



**DEPARTMENT OF APPLIED CHEMISTRY  
COCHIN UNIVERSITY OF SCIENCE AND TECHNOLOGY  
KOCHI- 682 022, KERALA, INDIA**

*July 2016*



*Dedication*

*To my respected teachers and beloved family*







DEPARTMENT OF APPLIED CHEMISTRY  
COCHIN UNIVERSITY OF SCIENCE AND TECHNOLOGY  
KOCHI – 682 022, KERALA, INDIA

---

**Dr. N. Manoj**  
Associate Professor  
E-mail: manoj.n@cusat.ac.in  
Ph: 0484-2575804

### CERTIFICATE

This is to certify that the thesis entitled “**STUDIES ON THE PHOTOVOLTAIC AND METAL ION BINDING PROPERTIES OF A FEW HETEROCYCLIC DONOR- $\pi$ -ACCEPTOR SYSTEMS**” is a genuine record of research work carried out by **Ms. Kala, K.**, under my supervision, in partial fulfilment of the requirements for the degree of Doctor of Philosophy of Cochin University of Science and Technology, and further that no part thereof has been presented before for the award of any other degree. All the relevant corrections and modifications suggested by the audience and recommended by the doctoral committee of the candidate during the pre-synopsis seminar have been incorporated in the thesis.

*Kochi-22*  
*July, 2016*

*Dr. N. Manoj*  
*(Thesis Supervisor)*



## DECLARATION

I hereby declare that the work presented in the thesis entitled **“STUDIES ON THE PHOTOVOLTAIC AND METAL ION BINDING PROPERTIES OF A FEW HETEROCYCLIC DONOR- $\pi$ -ACCEPTOR SYSTEMS”** is the result of genuine research carried out by me under the supervision of **Dr. N. Manoj**, Associate Professor of Organic Chemistry, Department of Applied Chemistry, Cochin University of Science and Technology, Kochi-22, and the same has not been submitted elsewhere for the award of any other degree.

*Kochi-22*  
*July, 2016*

*Kala, K,*



## ***Acknowledgements***

*A piece of work to become perfect, one needs the blessings and help of many. For the completion of this research work, I am indebted to many for their generous contributions, be it in the form of a piece of advice or suggestions for improvement. I would like to take this opportunity to acknowledge and extend my sincere thanks for those who help me to make this Ph. D. thesis possible.*

*First and foremost, I express my sincere gratitude and obligation to my thesis supervisor **Dr. N. Manoj**, Associate Professor, Department of Applied Chemistry, Cochin University of Science and Technology, for giving me an opportunity to be in his research group, for his patience, inspiration, valuable suggestions and boundless support throughout my research work. His guidance helped me in all the time of research and writing of this thesis. I could not have imagined having a better advisor and mentor for my Ph. D study.*

*I express my sincere thanks to Dr. S. Prathapan, Associate Professor, Department of Applied Chemistry, CUSAT for his valuable suggestions and fruitful discussions throughout the research, being my doctoral committee member.*

*I wish to thank Prof. M. R. Prathapachandra Kurup, Head, Department of Applied Chemistry, CUSAT for the immense support and encouragement extended to me.*

*I gratefully acknowledge the former Head of the Department, Dr. K. Sreekumar for providing me with all the necessary facilities of the department for carrying out my research work. I would like to extend my sincere thanks to all the former and present members of the Faculty of the Department of Applied Chemistry. I thank the administrative staff of the Department and University office, CUSAT.*

*I express my heartfelt gratitude to Dr. K. R. Gopidas, NIIST, Trivandrum for providing me the facilities to study the solar cell fabrication. I*

*sincerely thank Mr. Mohammed Yousaf for his patience and support to teach the fabrication of solar cell.*

*My thanks are also due to,*

- *Prof. C. T. Aravindakumar and Ms. Manju Mathew, School of Environmental Studies, M. G. University, Kottayam, for the analytical support.*
- *Dr. A. R. Biju, Assistant Professor, Sir Syed College, Thaliparamba, Kannur, for theoretical calculations.*
- *Dr. K. R. Haridas and Dr. Siji Mathew, School of Chemical Sciences, Kannur University, for the analytical support.*
- *Dr. Manju Thankomoni, Assistant Professor Sree Sankara College Kalady, for valuable suggestions during thesis correction.*
- *Mr. Saji T. K. SAIF, CUSAT, for NMR analyses whenever I needed.*
- *Mrs. Thahira, A. for the LC-MS analysis*
- *Dr. Priya Vijayaraghavan, NTHU, Taiwan for the analytical support.*
- *Dr. Akhil K. Nair, Assistant Professor, SVNSS College, Wadakkanchery and Dr. Jaimy K. B., Assistant professor, VTMNSS college, Thiruvananthapuram for their immense support and care throughout my research.*
- *Mr. Fredi Francis, Ms. Vidya Kattoor and Mr. Sujith for their support and cooperation.*
- *Ms. Vineetha, Mr. Kiran James, Ms. Aswathy and Ms. Parvathy for their support and patience.*
- *Mr. Varun, Ms. Athira, Ms. Anjali Mahadevan, Ms. Neelima, Ms. Sangeetha, Ms. Rinu and Ms. Gismi for the partial experimental assistance.*
- *My seniors, Dr. Jomon P. Jacob, Ms. Seena S, Ms. Pravitha N. P., Dr. Sandhya R, Dr. Eason M. Mathew, Dr. Sajitha T. S., Dr. Rakesh N., Dr. Reshma G., Ms. Suma C.S, Mr. Senju D. for their boundless help and support throughout the work.*

- *Dr. Bineesh P. B. for giving wise advices and suggestions.*
- *Late Mr. Vishnu P., Alpha Chemicals and Diagnostics for supplying chemicals in time.*
- *My colleagues., Ms. Manjula K., Ms. Minu J., Ms. Cisy A., Ms. Remya L. Ms. Saumya, T. S., Ms. Nithya C., Ms. Ligi M. L., Mr. Shandev P. P., Mr. Tomson D., Ms. Nishad K. M., Mr. Jith C. J., Ms. Amrutha U., Ms. Rani M., Ms. Jyothy C. Mary, Ms. Lekshmipriya R., Ms. Aswathy C. S., Ms. Nayana R., Shabeeb K. H. and Ms. Ananjana K., Ms. Jesna A. for making a homely atmosphere in the lab.*
- *Friends of other groups in the Department of Applied Chemistry for their endless care and support.*
- *All my respected teachers and well-wishers.*
- *SAIF, CUSAT for the analytical and spectral data.*
- *University Grants Commission (UGC) for the research fellowship.*

*My amma and acha deserves special mention for their consistent support and encouragements. They have shown that persistent hard work and respecting the dignity of fellow beings is the road to success. They sincerely raised me with their caring and constant prayers. It is a pleasure to pay tribute for the care and prayers given by my dearest sister Sreekutty, when I was very much tensed. I express my extreme gratitude and thanks to my in laws, they supported me a lot that I can't explain.*

*The unconditional love and encouragement provided by my beloved husband Anokh served as a secure anchor during the hard and easy times; thank you. Without his whole hearted support it would not have been possible me to complete this work.*

*Above all, I thank **God Almighty** for his blessings.*

***Kala, K.***





## PREFACE

Organic molecules with  $\pi$ -conjugated scaffolds end-capped with electron donor and acceptor groups are widely investigated due to their immense application potentials and hence belong to a promising area of organic chemistry. Donor-acceptor materials have found wide variety of applications such as dyes in dye-sensitised solar cells (DSSCs), organic photovoltaics, organic light emitting diodes, nonlinear optical devices, chemosensors, diagnostic probes and as therapeutic agents. Despite their use in such a wide range of applications, many fundamental properties of donor acceptor materials are still poorly understood. Even simple structural modifications can bring unexpected electronic and photophysical properties and wider understanding of the interaction between donor and acceptor is thus required. Furthermore, many such systems show diversity in properties in solution state or in their condensed state such as crystalline or amorphous forms. For example, some of these molecules show aggregation induced quenching or enhancement in emission in the solid state. Thus, structural motifs that facilitate intermolecular interaction via hydrophobic association, hydrogen bonding or electrostatic effects can lead to excellent control over their supramolecular functions. Some of the important structural types which used as donors are triarylamines, carbazoles, phenothiazine, fluorenes, thiophenes, and oligothiophenes. Strongly electron withdrawing groups or electron deficient heterocyclic systems such as oxadiazoles, diarylborons, quinolines, quinoxalines, thienopyrazines, and benzothiadiazoles, cyanoacetic acid, rhodanine-3-acetic acid, barbituric acid, and thiobarbituric acid etc., have been used as the acceptors in the

design of donor-acceptor systems. In this context, the thesis entitled **“STUDIES ON THE PHOTOVOLTAIC AND METAL ION BINDING PROPERTIES OF A FEW HETEROCYCLIC DONOR- $\pi$ -ACCEPTOR SYSTEMS”** portrays our attempt to expand the scope of D- $\pi$ -A systems and their applications in photovoltaics and heavy metal ion sensing.

The thesis is divided into five chapters, in which chapter one is an extensive review on  $\pi$ -conjugated donor-acceptor systems and their applications. Chapter 2 discusses the design, synthesis and characterisation of the donor- $\pi$ -acceptor systems. The acceptors used were rhodanine-3-acetic acid, barbituric acid and thiobarbituric acid and the prepared dyes were compared with a widely used acceptor cyanoacrylic acid. The compounds were synthesised by a multi-step synthesis where carbazole or phenothiazine (donors) were alkylated using n-octyl bromide followed by formylation by Vilsmeier-Haack reaction. The carbaldehydes thus obtained were made to react with the acceptors by Knoevenagel condensation reaction. All the compounds were characterised by FT-IR,  $^1\text{H}$  NMR,  $^{13}\text{C}$  NMR, GC-MS and HRMS techniques. The electronic properties of the synthesised compounds were studied by UV-Vis absorption spectroscopy, diffuse reflectance spectroscopy, steady-state and time-resolved fluorescence spectroscopy.

All the systems exhibited intramolecular charge transfer properties characterised by their absorption bands in the visible region of the electromagnetic spectrum. The thiobarbituric acid conjugate PTBA showed the maximum red shifted absorption band at 553 nm and cyanoacetic acid conjugate CCAA showed absorption maximum around

400 nm commensurate with their respective electron affinities. A detailed theoretical study of the absorption and emission behaviour of CTBA was to account for the marked difference in its ground state and excited state properties.

The third chapter deals with the photovoltaic application of these synthesized dyes. The acceptor moieties such as cyanoacetic acid, rhodanine-3-acetic acid, barbituric acid, thiobarbituric acid are acidic compounds which expected to bind to TiO<sub>2</sub> either via deprotonation or through chelation. The n-octyl group at the N (9) and N (10) positions of carbazole and phenothiazine increase the hydrophobicity of the dye and expected to act as a barrier to prevent moisture as well as the electrolyte from reaching the semiconductor and thereby reducing the leakage of dark current. The HOMO and LUMO levels of the dyes were experimentally determined by cyclic voltammetry and verified by DFT calculations using GUASSIAN-09 programme. A prominent solar energy-to-electricity conversion efficiency ( $\eta$ ) is achieved in a DSSC based on n-octylphenothiazine as donor and rhodanine-3-acetic acid as acceptor.

Literature reports suggest that cyclic amides such as thiamine and uracil are potential ligands to metals. Tiziana Marino reported that Hg<sup>2+</sup> gets inserted between the base pairs via deprotonation in DNA and has been ascribed as the major reason for the genotoxic action of mercury. The thiamine and uracil have structure similarity to barbituric acid and thiobarbituric acid. Among the compounds synthesised, CBA showed high solid-state luminescence and CTBA showed dual emission characteristic. The high luminescence of CBA in the solid state is due to

the aggregation induced emission and we expected a mercury insertion via deprotonation in CBA aggregates as seen in the DNA base pairs. In CTBA, the existence of emission from the local excited state and charge transfer state offer an excellent ratiometric response in the presence of heavy metal ions. In chapters 4 and 5, we narrated the results of metal ion binding studies of CBA and CTBA respectively.

The fourth chapter deals with the investigation of interaction of the various mono- and bivalent metal ions with the carbazole-barbituric acid conjugate (CBA). CBA showed unusual selectivity for the  $\text{Hg}^{2+}$  ions among the various metal ions investigated. Our investigations revealed that the metal ion complexation involves the deprotonation of NH protons of barbituric acid moiety as characterized by  $^1\text{H}$  NMR spectral analysis. Upon  $\text{Hg}^{2+}$  binding, CBA molecules in 1:1 methanol water mixture gave a 150 fold an enhancement in emission. Similarly, a four enhancement in emission was also observed when CBA used in anionic SDS micellar solution. The binding stoichiometry, detection limit and association constants were determined by photophysical analysis. Addition of cysteamine hydrochloride resulted in decomplexation of CBA- $\text{Hg}^{2+}$  complex through changes in the photophysical properties evidenced the reversibility of the complexation process. The proper arrangement of the donor acceptor units in the CBA molecule made it an ideal candidate as a chemosensor for the selective and sensitive detection of  $\text{Hg}^{2+}$  ions reversibly in aqueous medium.

Finally, the fifth chapter report the results of our investigations on the metal binding properties of CTBA. We investigated the interaction of metal ions with CTBA in homogeneous media such as acetonitrile and

9:1 THF/H<sub>2</sub>O and in micro heterogeneous media such as SDS surfactant solution in water. We obtained a ratiometric behaviour in the UV-Vis titration as well as in fluorescence titration in acetonitrile and 9:1 THF/H<sub>2</sub>O respectively. Addition of mercuric ions to CTBA resulted in visual colour changes made it as colorimetric probe in aqueous medium. The colourimetry and fluorescence response was selective to Hg<sup>2+</sup> and Cd<sup>2+</sup> ions and Hg<sup>2+</sup> showed highest sensitivity. The CTBA-Hg complex can be reverted to free CTBA by the addition of cysteamine hydrochloride. The mechanism of binding was established through UV-Vis, fluorescence and <sup>1</sup>H NMR spectroscopy.

Since each chapter of the thesis has organized as an independent unit, the structural formulae, schemes, tables and figures are numbered chapter-wise. All new compounds are fully characterised on the basis of spectral and analytical data. Relevant references are included at the end of individual chapters.



## *List of Abbreviations*

A	: acceptor
AIE	: aggregation induced emission
AIEE	: aggregation induced emission enhancement
AIQ	: aggregation induced quenching
BA	: barbituric acid
BH	: Benesi–Hildebrand
BHJ	: bulk heterojunction
C	: centigrade
CE	: carbazole type emission
CHEF	: chelation enhanced fluorescence
CMC	: critical micelle concentration
CT	: charge transfer
Cys. HCl	: cysteamine hydrochloride
D	: donor
dd	: doublet of doublet
DCM	: dichloromethane
DFT	: density functional theory
DMA	: dimethyl aniline
DMF	: dimethylformamide
DMSO	: dimethyl sulphoxide
EPA	: environmental protection agency
DSSC	: dye sensitized solar cell
ESIPT	: excited-state intramolecular proton transfer
EtOH	: ethanol
FF	: fill factor
$\Phi_f$	: fluorescence quantum yield
FRET	: fluorescence resonance energy transfer
FTO	: fluorine doped tin oxide
FT IR	: fourier transform infrared
g	: gram
h	: hour
GC-MS	: gas chromatography-mass spectrometry
HOMO	: highest occupied molecular orbital
ICP-AES	: inductively coupled plasma atomic emission
ICP-MS	: inductively coupled plasma mass spectrometry
ICT	: intramolecular charge transfer

IPCE	: incident photon to current efficiency
$J_{sc}$	: short circuit photocurrent
LE	: local excited state
LUMO	: lowest unoccupied molecular orbital
m	: multiplet
MALDI	: matrix-assisted laser desorption/ionization
TOF	: time of flight
Me	: methyl
MeCN	: acetonitrile
MeOH	: methanol
mg	: milligram
min	: minute
mL	: millilitre
mp	: melting point
nm	: nanometre
ns	: nanosecond
NMR	: nuclear magnetic resonance
OFET	: organic field effect transistors
OLED	: organic light emitting diode
OPV	: organic photo voltaic
PCE	: power/photo conversion efficiency
PCM	: polarizable continuum model
PCT	: Photo-induced charge transfer
PET	: Photo-induced electron transfer
ppm	: parts per million
ppb	: parts per billion
KOH	: potassium hydroxide
NaOH	: sodium hydroxide
s	: singlet
SDS	: sodium dodecyl sulphate
SQV	: square wave voltammograms
t	: triplet
TBA	: thiobarbituric acid
TD-DFT	: time dependent density functional theory
THF	: tetrahydrofuran
TBET	: through-bond energy transfer (TBET)
TICT	: twisted intramolecular charge transfer



TLC : thin layer chromatography  
TMS : tetramethylsilane  
UV : ultraviolet  
 $V_{oc}$  : open circuit photovoltage  
WHO : world health organisation



# CONTENTS

Page No.

## CHAPTER 1

### **An Overview of Donor- $\pi$ -Acceptor systems: Applications in Photovoltaics and Heavy Metal Ion Sensing** **1-62**

1.1	<i>Introduction</i>	1
1.2	<i>Electronic Structure of D-<math>\pi</math>-A systems</i>	2
1.2.1	<i>Donor-Acceptor molecules in Photovoltaics</i>	5
1.2.1.1	<i>Incident Photon to Current Efficiency (IPCE)</i>	8
1.2.1.2	<i>Open Circuit Photo voltage (<math>V_{oc}</math>)</i>	8
1.2.1.3	<i>Short Circuit Photocurrent (<math>J_{sc}</math>)</i>	8
1.2.1.4	<i>Fill Factor (FF)</i>	9
1.2.1.5	<i>Sensitizers</i>	10
1.2.1.6	<i>Phenothiazine based dyes for dye sensitized solar cells (DSSC)</i>	12
1.2.1.7	<i>Triphenylamine based dyes for dye sensitized solar cells (DSSC)</i>	14
1.2.1.8	<i>Carbazole based dyes for dye sensitized solar cells (DSSC)</i>	16
1.2.2	<i>Donor-Acceptor molecules as Sensor Systems for Heavy Metals</i>	20
1.2.2.1	<i>Fluorescent sensors</i>	20
1.2.2.1.1	<i>Classification of fluorescent sensors</i>	22
1.2.2.1.1.1	<i>Photo-induced electron transfer (PET) and turn-on probes</i>	22
1.2.2.1.1.2	<i>Photo-induced charge transfer (PCT) and ratiometric probes</i>	23
1.2.2.1.1.3	<i>Excimer formation and ratiometric probes</i>	24

1.2.2.1.1.4	<i>Fluorescence resonance energy transfer (FRET) and ratiometric probes</i>	25
1.2.2.2	<i>Heavy metals in the environment</i>	26
1.2.2.2.1	<i>Arsenic sensors</i>	27
1.2.2.2.2	<i>Lead sensors</i>	29
1.2.2.2.3	<i>Cadmium sensors</i>	30
1.2.2.2.4	<i>Mercury sensors</i>	32
1.2.2.2.4.1	<i>Colorimetric sensors for Hg<sup>2+</sup> ion</i>	32
1.2.2.2.4.1.1	<i>Polyether-based sensors</i>	33
1.2.2.2.4.1.2	<i>Squaraine-based sensors</i>	35
1.2.2.2.4.1.3	<i>Rhodamine-based sensors</i>	38
1.2.2.2.4.1.4	<i>Other organic molecular sensors</i>	39
1.2.2.2.4.2	<i>Fluorescent sensors and ratiometric detection</i>	41
1.2.2.2.4.3	<i>Other fluorescent Hg<sup>2+</sup> sensors</i>	43
1.3	<i>Objectives</i>	46
1.4	<i>References</i>	47

## **CHAPTER 2**

### **Synthesis and Photophysical Properties of Donor- $\pi$ -Acceptor Systems 63-119**

2.1	<i>Abstract</i>	63
2.2	<i>Introduction</i>	63
2.3	<i>Results and Discussion</i>	71
2.3.1	<i>Synthesis</i>	71
2.3.2	<i>Photophysical Studies</i>	74
2.3.2.1	<i>Absorption Properties of Carbazole dyes</i>	74
2.3.2.2	<i>Emission Properties of Carbazole dyes</i>	77
2.3.2.3	<i>Intramolecular Charge Transfer in Carbazole dyes</i>	81
2.3.2.4	<i>Absorption Properties of Phenothiazine dyes</i>	97
2.3.2.5	<i>Emission Properties of Phenothiazine dyes</i>	99

2.3.3	<i>A survey of mercury binding studies of carbazole and phenothiazine dyes</i>	103
2.4	<i>Conclusions</i>	107
2.5	<i>Experimental Section</i>	108
2.6	<i>Reference</i>	117
	<b>CHAPTER 3</b>	
	<b>Dye-Sensitized Solar Cell Performance Using Simple Phenothiazine and Carbazole - Based Dyes</b>	121-150
3.1	<i>Abstract</i>	121
3.2	<i>Introduction</i>	121
3.3	<i>Results and Discussion</i>	123
3.3.1	<i>UV–Visible Absorption Properties</i>	124
3.3.2	<i>Evaluation of the Binding Properties of the Dyes with TiO<sub>2</sub></i>	125
3.3.2.1	<i>Absorption spectral properties</i>	125
3.3.2.2	<i>Electron Transfer and Electrochemical Properties</i>	130
3.3.4	<i>Theoretical Calculations</i>	137
3.3.5	<i>Photovoltaic Performance</i>	138
3.4	<i>Conclusions</i>	141
3.5	<i>Experimental section</i>	143
3.5	<i>References</i>	146
	<b>CHAPTER 4</b>	
	<b>A Carbazole Based “Turn on” Fluorescent Sensor for Selective Detection of Hg<sup>2+</sup> in an Aqueous Medium</b>	151-200
4.1	<i>Abstract</i>	151
4.2	<i>Introduction</i>	151
4.3	<i>Results and Discussion</i>	154
4.3.1	<i>Photophysical Properties</i>	154

4.3.2	<i>Metal ion binding studies of CBA in 1:1 MeOH/H<sub>2</sub>O</i>	156
4.3.2.1	<i>Stoichiometry and Reversibility of Complexation</i>	159
4.3.2.2	<i>Nature of Complexation</i>	162
4.3.2.3	<i>Determination of Lowest Detection Limit</i>	171
4.3.2.4	<i>Selectivity of Metal ion Recognition</i>	172
4.3.3	<i>Study of the Effect of Microheterogeneous medium on the Metal Binding Properties of CBA</i>	175
4.3.3.1	<i>Photophysical Properties of CBA in Micellar Medium</i>	178
4.3.3.2	<i>Metal ion binding studies of CBA in 100 mM SDS</i>	180
4.3.3.3	<i>Stoichiometry and Reversibility of Complexation in Micellar Medium</i>	181
4.3.3.4	<i>Nature of Complexation in Micellar Medium</i>	185
4.3.3.5	<i>Determination of Lowest Detection Limit in Micellar Medium</i>	187
4.3.3.6	<i>Selectivity of Metal ion Recognition by CBA in SDS micelles</i>	189
4.4	<i>Conclusions</i>	191
4.5	<i>Experimental Section</i>	193
4.6	<i>References</i>	196

## **CHAPTER 5**

	<b>Highly selective ratiometric and colorimetric detection of mercury (II) ions in aqueous medium with a carbazole thiobarbituric acid based fluorescent probe</b>	201-240
5.1	<i>Abstract</i>	201
5.2	<i>Introduction</i>	202
5.3	<i>Results and Discussion</i>	205
5.3.1	<i>Intramolecular Charge Transfer and Dual Emission</i>	205

	<i>in CTBA</i>	
5.3.2	<i>Metal ion Binding Studies of CTBA in MeCN</i>	208
5.3.3	<i>Effect of water on the emission spectrum of CTBA in THF</i>	212
5.3.4	<i>Metal ion Binding Studies of CTBA in 9:1 THF/H<sub>2</sub>O</i>	213
5.3.4.1	<i>Stoichiometry of Complexation</i>	216
5.3.4.2	<i>Reversibility of Complexation</i>	218
5.3.4.3	<i>Mechanism of Complexation</i>	220
5.3.4.4	<i>Determination of Lowest Detection Limit</i>	222
5.3.4.5	<i>Selectivity of Recognition of Hg<sup>2+</sup> Ions</i>	223
5.3.5	<i>Detection of Hg<sup>2+</sup> Ions in Aqueous Medium Containing Micelles</i>	225
5.5	<i>Conclusions</i>	232
5.6	<i>Experimental Section</i>	234
5.7	<i>References</i>	236
	<i>Summary and Conclusions</i>	241
	<i>List of Publications</i>	245

## Chapter 1

# **An Overview of Donor- $\pi$ -Acceptor systems: Applications in Photovoltaics and Heavy Metal Ion Sensing**

---

### **1.1 Introduction**

Organic molecules of push-pull type  $\pi$ -conjugated structure with electron rich donor groups linked to acceptor groups having high electron affinity have attracted academic and technological research for decades. Even now this is an active area of research and novel molecules having interesting properties are reported regularly in the current literature. Such molecules are characterised by their low energy gap between the HOMO and LUMO levels. This is manifested in their long wavelength absorption maxima extending up to near-infrared region of the electromagnetic spectrum. These electronic transitions often possess very high molar absorptivity values often show high luminescence characteristics. These electronic transitions are due to intramolecular charge transfer (ICT) from donor (D) to the electron deficient acceptor (A) through the conjugated  $\pi$  bridge. In the last four or five decades, organic  $\pi$ -systems have become a broadly investigated, growing area of organic chemistry, and have led to the development of extensive applications across various branches of current research. Some of the domains of the technological application of these systems are optoelectronics,<sup>1-3</sup> photovoltaics<sup>4,5</sup> field-effect transistors (OFET) for sensors,<sup>6</sup> light-emitting diodes (OLED)<sup>7</sup> and in nonlinear optics. The properties of these systems are largely depending on the donor and acceptor strengths, characterised by their individual redox properties.



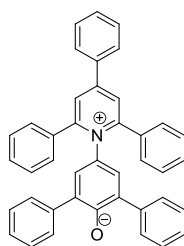
Therefore, modifications in the structure of donor, as well as acceptor moiety, offer the possibility of tuning of their electronic properties.

## **1.2 Electronic Structure of D- $\pi$ -A Systems**

In “push-pull” D- $\pi$ -A molecules, due to the electronic coupling between the donor (D) and the acceptor (A) group orbitals, a new set of low energy molecular orbitals (MO) are formed which usually result in a reduced energy gap between the HOMO and LUMO levels. This makes such molecules for absorbing light in the visible region of the electromagnetic spectrum and therefore push-pull molecules are generally coloured. These types of push-pull molecules or groups generally have intramolecular charge-transfer (ICT) character.<sup>8-11</sup> Nitroaniline is a typical example of a D- $\pi$ -A molecule to demonstrate the ICT character. When compared to nitrobenzene and aniline which absorb light below 300 nm, *p*-nitroaniline has an absorption maximum at 350 nm. The interaction between the nitro group and the amino group through the benzene  $\pi$ -system is demonstrated in the resonance forms that are possible for *p*-nitroaniline<sup>12</sup> (Scheme 1.1). The extent of ICT character depends on the strength of electronic coupling between donor and acceptor orbitals, which often lead to polarization of the molecule and creation of a permanent molecular dipole.



Being inherently polarised with permanent dipoles, these molecules respond profoundly to the environmental changes. This makes them an excellent choice for the development of solvatochromic probes. Depending on the structure, they show either negative solvatochromism i.e., a hypsochromic shift to the absorption maximum with increased polarity of the medium or an inverse effect termed as positive solvatochromism.<sup>36</sup> An example is the pyridinium betaine dye (Figure 1.1) based on which the well-known ET-30 solvent polarity scale is developed.<sup>37</sup> In nonlinear optics, the second- and third-order optical nonlinearities are mainly affected by the extent of the ICT of push-pull system and result in prepolarization of the  $\pi$ -system.<sup>32-34</sup> In push-pull system, the ICT embodies the HOMO–LUMO gap, so that the optical properties and NLO response can be tailored by (i) attaching different electron donors and acceptors and assuring efficient D–an interaction, (ii) extension and spatial arrangement of the  $\pi$ -linker, and (iii) planarization of the entire molecule.<sup>38-42</sup> Thus, in order to get better performance, we can tune the donor,  $\pi$ -linker and acceptor moiety.



**Figure 1.1** Structure of pyridinium betaine dye

The present thesis work focuses on two major applications of donor-acceptor systems, the photovoltaic and the heavy metal ion sensing

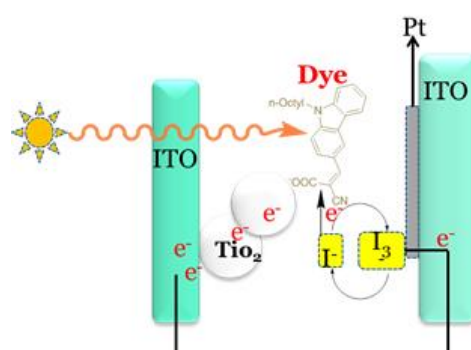
property. The preceding section is a review of the application of organic molecules in photovoltaics and heavy metal ion sensing systems.

### 1.2.1 Donor-Acceptor Molecules in Photovoltaics

The chemistry of organic D- $\pi$ -A systems and their applications in photovoltaics (OPV) is a highly active area of research nowadays due to the versatile properties of organic materials. The diverse synthesis routines in organic chemistry offer the possibility of introducing mixed functionalities that are often required in the materials development, for example with appropriate structural modifications, their electronic properties, solubility, hydrophobicity or hydrophilicity, crystallinity or amorphous nature, coulombic properties etc. can be tuned. The major motivation for developing OPV is the drastic reduction of the cost and environmental impact during the production of solar cells compared to the established silicon technology. The area of organic photovoltaics includes polymer-based solar cells and DSSC. Although soluble conjugated polymers remain a major class of donor materials for single layered and multi-layered bulk heterojunction OPV cells.<sup>43-46</sup> In recent years many research groups reported the use of small molecules as sensitizers for OPV owing to their well-defined chemical structures in terms of repeatable and scalable synthesis methods and ease of purification.<sup>47-51</sup> After an innovative work published in 2005 by Roncali, J. *et al.*, the design of soluble molecular donors has generated considerable research efforts<sup>52-55</sup> and solution-processed bulk heterojunction (BHJ) cells with power conversion efficiency (PCE) of 8.0–10% have been reported in 2013 and 2014.<sup>53-55</sup> However, these results have been obtained with solar cells of small active areas.

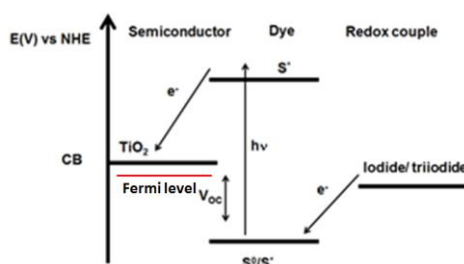
Moreover, the active materials used have more complex chemical structures and can be prepared only through multi-step syntheses with low overall yield, high cost, heavy environmental impact and poor scalability. One of the crucial factors for the large-scale development of OPV technology lies in the substantial reduction of the cost with preparative routines having lesser environmental impact.<sup>56-58</sup> In this context, rather than more focus on PCE, the development of OPV should consider high-yield, environmentally benign and scalable synthesis routines for the preparation of active materials.

Dye-sensitized solar cells (DSSC), which are regarded as the new generation solar cells,<sup>59-62</sup> were invented in 1991 by Grätzel and O'Regan. The DSSC, popularly known as Grätzel cell, is a complex system wherein three different components, namely, a nanocrystalline semiconductor, a chromophore and an electrolyte are brought together to generate electric power from light without suffering from any permanent chemical transformation (Figure 1.2)



**Figure 1.2** Schematic picture of a dye-sensitized solar cell

The nanocrystalline semiconductor is usually  $\text{TiO}_2$ , although alternative wide band gap oxides such as  $\text{ZnO}$  and  $\text{SnO}$  can also be used.<sup>63</sup> A monolayer of the chromophore, i.e. the sensitizer, is attached to the surface of the semiconductor. Photoexcitation of the chromophore results in the injection of an electron into the conduction band of the semiconductor (Figure 1.3). The chromophore is regenerated by the electrolyte, usually an organic solvent containing a redox couple, such as iodide/triiodide. The electron donation to the chromophore by iodide is compensated by the reduction of triiodide at the counter electrode and the circuit is completed by electron migration through the external load. The overall voltage generated by the cell corresponds to the difference between the Fermi level of the semiconductor and the redox potential of the electrolyte. The position of the  $\text{TiO}_2$  conduction band depends on the surface charge, which is affected by the electrolyte composition. Adsorption of negatively charged ions or Lewis bases shifts the conduction band edge to more negative potentials, and can be used to increase the efficiency of the solar cells, as it improves the open-circuit voltage.



**Figure 1.3** Schematic representation of the electron flow in the DSSC

The performance of a solar cell can be quantified with parameters such as incident photon to current efficiency (IPCE), short circuit photocurrent ( $J_{sc}$ ), open circuit photovoltage ( $V_{oc}$ ) and the overall efficiency of the photovoltaic cell ( $\eta_{cell}$ ). The efficiency of the DSSC is related to a large number of parameters. The present thesis will focus only on the synthesis of sensitizers and their photovoltaic properties; even so, it is important to have some general concepts in mind.

### **1.2.1.1 Incident Photon to Current Efficiency (IPCE)**

IPCE is also known as the “external quantum efficiency” and describes how efficiently the light of a specific wavelength is converted to current i.e. (electrons out) / (photons in). The IPCE can be calculated according to equation

$$\text{IPCE (\%)} = 1240 \frac{J_{SC}}{\lambda \Phi_{in}} 100$$

$J_{sc}$  is the short circuit current density,  $\lambda$  is the wavelength of the incident light and  $\Phi_{in}$  is the intensity of the incident light.

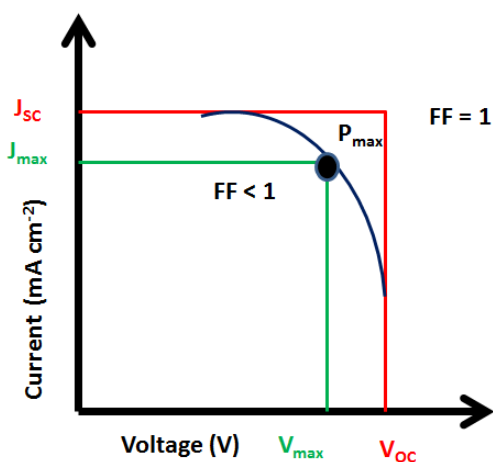
### **1.2.1.2 Open Circuit Photo Voltage ( $V_{oc}$ )**

$V_{oc}$  is the difference in potential between the two terminals in the cell under light illumination when the circuit is open. It depends on Fermi level of the semiconductor and the level of dark current.

### **1.2.1.3 Short Circuit Photocurrent ( $J_{sc}$ )**

$J_{sc}$  is the photocurrent per unit area ( $\text{mA}/\text{cm}^2$ ) when an illuminated cell is short circuited. It is dependent on several factors such

as light intensity, light absorption, injection efficiency and regeneration of the oxidized dye.



**Figure 1.4** Illustration of current-voltage characteristics of a solar cell. Blue line: measured current-voltage curve. Area under Red line:  $V_{oc} \times J_{sc}$ ; Area under Green line:  $V_{max} \times J_{max}$

#### 1.2.1.4 Fill Factor (FF)

The fill factor measures the quality of the device and is defined as the ratio of the maximum power output per unit area to the product of  $V_{oc}$  and  $J_{sc}$

$$FF = \frac{J_{max} \cdot V_{max}}{J_{sc} \cdot V_{oc}}$$

The overall solar energy to electricity conversion efficiency of a solar cell is defined as the ratio of the maximum output of the cell divided by the power of the incident light. It can be determined by the photocurrent density measured at short circuit ( $J_{sc}$ ), the open circuit



photovoltage ( $V_{oc}$ ), the fill factor of the cell (FF), and the intensity of the incident light ( $\Phi_{in}$ ).

$$\eta = \frac{J_{sc} \cdot V_{oc} \cdot FF}{\phi_{in}}$$

### 1.2.1.5 Sensitizers

The dyes, used in organic dye-based solar cells should satisfy some basic features for efficient conversion of solar energy to electrical energy, as follows:

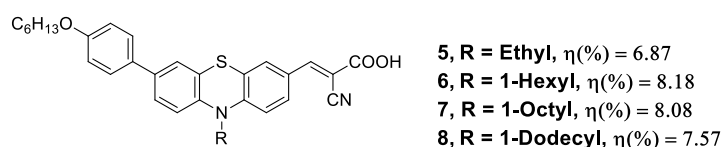
- The dye must absorb light in the visible region (400-700 nm). That means, the dye should possess an energy bandgap of about 1.35 eV, which is essential for single-layer solar cells.
- The dye must be strongly adsorbed on the surface of the semiconductor.
- The excited state energy of the dye (LUMO) must be slightly above the energy of the conduction band of semiconductor and energy difference must be sufficient to permit the transfer of electrons. Also, ground state energy level of the dye (HOMO) must be slightly below the reduction-oxidation potential of the electrolyte used. This is necessary to obtain the efficient conversion of solar energy to the electric energy and to maintain minimum energy losses.
- The electron transfer from the excited state of the dye to the conduction band of semiconductor must be very fast in order to avoid fluorescence and phosphorescence which may otherwise result in charge recombination.

- The dye adsorbed on semiconductor surface must remain stable for a sufficiently long time in the working conditions. i.e., there should be no interaction between the interface of the semiconductor and electrolyte.
- The dye should be highly soluble in organic solvents and must contain an anchoring group to bind the surface of the semiconductor.
- In a solar cell, light must be absorbed only by the dye molecule. If the other layers such as the semiconductor or the electrolyte absorb light, it may lead to side reactions and may adversely affect the stability and efficiency of the cell.

A wide range of dyes is used in organic dye-based solar cells (DSSC) such as porphyrins, phthalocyanines, poly pyridyls, coumarins, indoline, triphenylamines, conjugated polymers, perylenes,<sup>63-74</sup> phenothiazines, carbazoles, etc. The highest efficiency still reported is for cells based on polypyridyl ruthenium derivatives<sup>75,76</sup> (Grätzel cells). Although polypyridyl ruthenium dyes have the highest yield obtained until now, these are not desired category of dyes for the cell systems due to the tedious synthesis procedure, the requirement of high-cost starting materials, low molar absorption coefficients and a very narrow absorption range in the visible region. Organic dyes have higher molar absorption coefficient than ruthenium-based dyes and are amenable to chemical modifications, whereby, a variety of dyes can be synthesised which can absorb light in desired range of the spectrum.

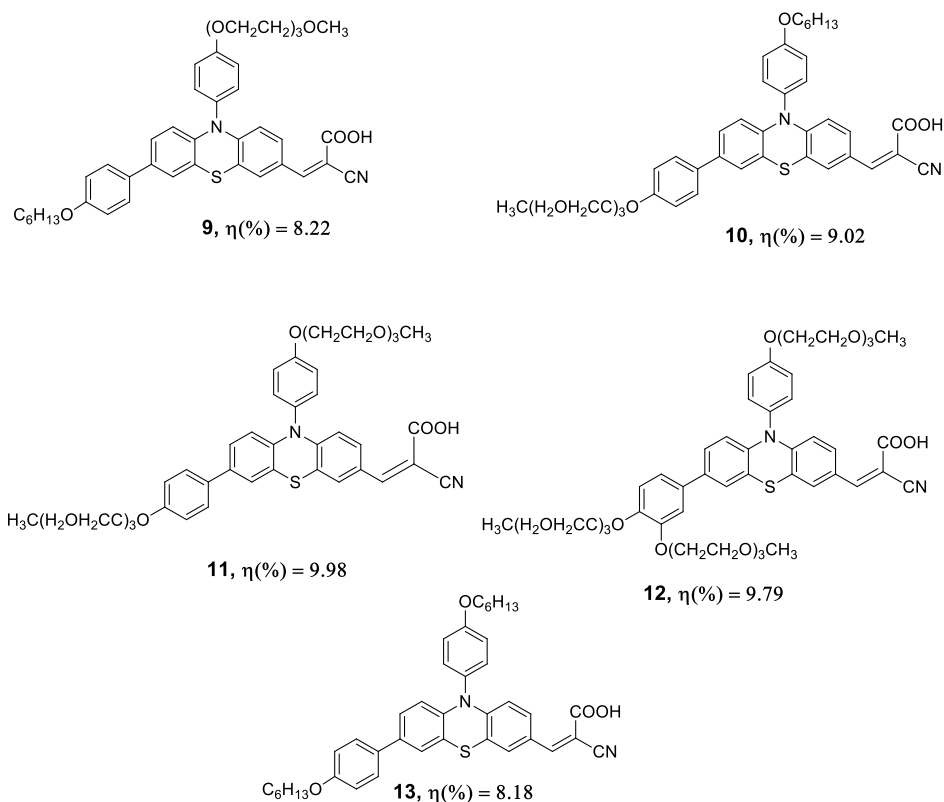


Hua *et al.* have reported a set of substituted phenothiazine based dyes having cyanoacetic acid as acceptor/anchoring moiety. For dye **6**, they obtained a maximum photoconversion efficiency of 8.18%.<sup>78</sup>



**Figure 1.7** Structure of substituted phenothiazine dyes **5**, **6**, **7** and **8**

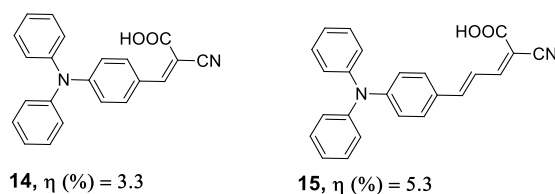
When 4-alkoxyphenyl groups are fixed on N-10 and C-7 positions of phenothiazine ring, the corresponding PCE values can become very high. Lin *et al.* in 2015 reported that sensitizer **11** has a solar-to-electric power conversion efficiency of 9.98%, which represents the maximum of all up to now investigated phenothiazine-based DSSCs. Its short-circuit current is extremely high and its open-circuit voltage reaches the theoretical maximum. They reported a series of phenothiazine dyes, their N-10 and C-7 positions of phenothiazine ring was substituted by simple O-bridged donor groups.<sup>79</sup>



**Figure 1.8** Structure of substituted phenothiazine dyes **9**, **10**, **11**, **12** and **13**

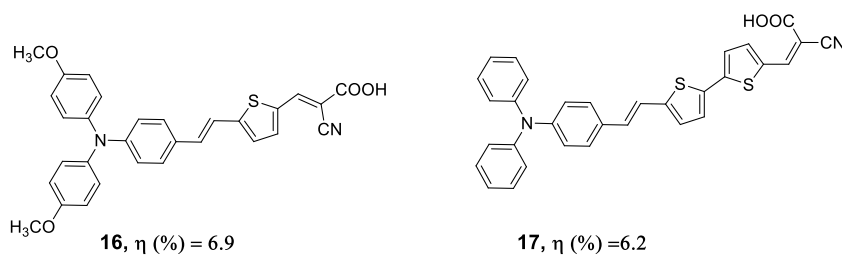
### 1.2.1.7 Triphenylamine Based Dyes

Triphenylamine is an excellent electron donor and widely used in organic photovoltaic functional materials. Yanagida and co-workers<sup>80</sup> first introduced the triphenylamine unit as an electron donor in organic dyes and obtained overall DSSC efficiencies of 3.3 and 5.3% for dye **14** and **15**, respectively in comparison with N719 (7.7%).



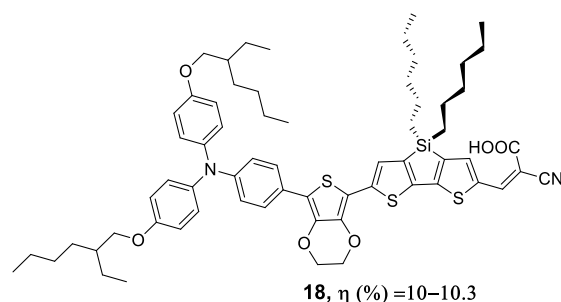
**Figure 1.9** Structure of substituted triphenylamine dyes **14** and **15**

Dye **16** and **17** containing thienylenevinylene and bithiophene group, which was reported by Hagberg *et al.*,<sup>81</sup> and Justin Thomas *et al.*,<sup>82</sup> respectively, showed photoelectric conversion efficiency 6.9% and 6.2% respectively. The presence of additional electron-donating methoxy groups in **16** is responsible for a better efficiency (6.9%) compared to **17** (6.2%).



**Figure 1.10** Structure of substituted triphenylamine dyes **16** and **17**

Zeng *et al.*, in 2010 reported a triphenyl amine based Dye **18** showing highest efficiency (10.0–10.3%) ( $J_{sc} = 17.94 \text{ mA cm}^{-2}$ ,  $V_{oc} = 0.770 \text{ V}$ ,  $FF = 0.730$ ) at the AM 1.5 irradiation ( $100 \text{ mW cm}^{-2}$ ). In the range of 500–540 nm the IPCE reached to 90%.<sup>83</sup>

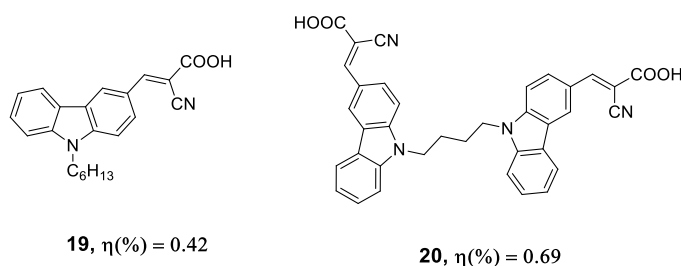


**Figure 1.11** Structure of substituted triphenylamine based dye **18**

### 1.2.1.8 Carbazole Based Dyes

Carbazole-based organic materials have been widely employed as active ingredients in DSSC due to their unique charge transporting properties and pronounced thermal stability.

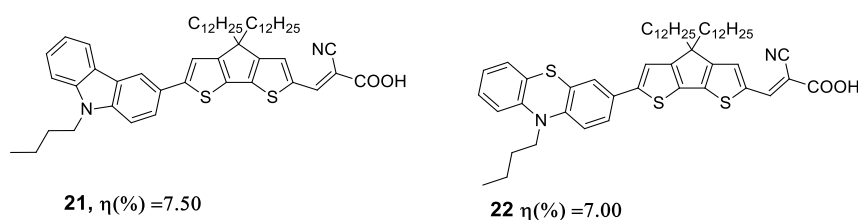
Simple carbazole-based dyes (**19**, **20**) containing carbazole as a donor and cyano acrylic acid as acceptor have been reported by Kim *et al.*<sup>84</sup> They have systematically investigated the effect of a number of chromophores on the performance of the DSSCs. The short circuit current density ( $J_{sc}$ ) of the dyes increased from **19** (1.29 mA cm<sup>-2</sup>) to **20** (2.31 mA cm<sup>-2</sup>) due to the increase of molar extinction coefficient



**Figure 1.12** Structure of carbazole based dyes **19**, and **20**

Grätzel and co-workers reported<sup>85</sup> two dyes containing carbazole or phenothiazine donors (**21**, **22**). The dye **21**, having 4,4-didodecyl- 4H-cyclopenta[1,2-b:5,4-b']dithiophene as a linker displayed longer

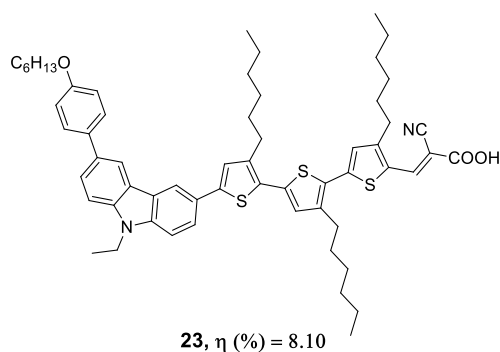
wavelength absorption band at 532 nm with a very high molar extinction coefficient ( $57500 \text{ M}^{-1} \text{ cm}^{-1}$ ). The carbazole dye **21** exhibited higher efficiency (7.50%) when compared to a similar dye **22** (7.00%) containing phenothiazine as a donor ( $\epsilon = 46500 \text{ M}^{-1} \text{ cm}^{-1}$ ). Better efficiency of the dye **21** is due to the higher molar absorption coefficient which led to the larger photocurrent.



**Figure 1.13** Structure of substituted carbazole and phenothiazine based dyes **21** and **22**

Koumura, *et al.* reported<sup>86</sup> that alkyl chains present on the thiophene unit and the nature of alkoxy phenyl fragment attached to the carbazole nucleus (scheme 1.12) significantly altered the  $V_{oc}$  (0.71V) as well as  $J_{sc}$  ( $16 \text{ mA cm}^{-2}$ ) of the device.<sup>54</sup> Due to the optimized structural components, the dye **23** exhibited very high efficiency (8.10%) in DSSC. This is the highest obtained efficiency in the case of carbazole based dyes.





**Figure 1.14** Structure of substituted carbazole based dye **23**

Cyanoacrylic acid unit is considered as a good acceptor as well as an efficient anchoring group for prospective binding of dye molecules on  $\text{TiO}_2$  thin films. Other major anchoring groups are pyridine,<sup>87-97</sup> phosphonic acid,<sup>98-102</sup> tetracyanate,<sup>103</sup> perylene dicarboxylic acid anhydride,<sup>104-108</sup> 2-hydroxylbenzotrile,<sup>109</sup> 8-hydroxylquinoline,<sup>110</sup> pyridine-N-oxide,<sup>111</sup> hydroxypyridium,<sup>112</sup> catechol,<sup>113-117</sup> hydroxamate,<sup>118-120</sup> sulfonic acid,<sup>121-125</sup> acetylacetonate,<sup>126-128</sup> boronic acid,<sup>129</sup> nitro,<sup>130</sup> tetrazole,<sup>131</sup> rhodanine<sup>132-140</sup> and salicylic acid<sup>141-144</sup> substituents. Several studies were conducted on the effect of anchoring groups<sup>145</sup> on the overall efficiency of the DSSCs.

Barbituric acid and Thiobarbituric acid are cyclic amides, which can also be very good electron acceptors and found to interact with donor group's orbitals producing ICT states. However, their usages as anchoring groups in DSSC are limited. A few reports exist, where the N-alkylated barbituric acid and thiobarbituric acid are used as acceptors in dyes for DSSC. In our study, we have used 9-octylcarbazole and 10-octylphenothiazine as the donor moieties. Though these simple systems possess good optical and electrochemical properties, no report exist on

their application in DSSC. The present thesis reports the study on the application of these molecules in DSSC and is compared with 9-octylcarbazole and 10-octylphenothiazine based dyes having cyanoacrylic or rhodanine-3-acetic acid anchoring/acceptor groups.

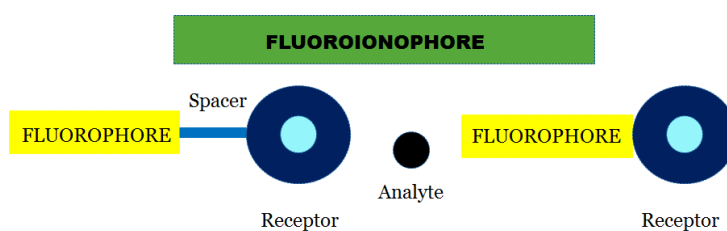
### **1.2.2 Donor-Acceptor Molecules as Sensor Systems for Heavy Metals**

A molecule containing conjugated electron donor (D) and an electron acceptor (A) usually undergoes an intramolecular charge transfer (ICT) upon electronic excitation. One of the major applications of the D- $\pi$ -A system is as a chemo responsive unit in the development of sensor systems. Recently, many studies reported in the literature focuses on recognition of heavy metals using D- $\pi$ -A systems. In most of such chemosensors, the acceptor part is the recognition site and upon binding, the ICT state get perturbed and the subsequent electronic effects are reflected as changes in the absorption as well as fluorescence spectra of D- $\pi$ -A systems.

#### **1.2.2.1 Fluorescent sensors**

Fluorescent sensors consist of a fluorophore linked to a docking site for interaction with an analyte and if the docking site is an ionophore, such systems are termed as fluoro ionophores (Figure 1.15). In the case of fluoro ionophore, the ionophore is the recognition moiety whereas the fluorophore is the signaling moiety. The recognition and signaling moieties are the key components in the design of sensors. In a typical design, the signalling moiety can be integrated to the receptor via direct coupling or through a spacer. In both cases, the signalling moiety and the receptor are covalently attached via single or conjugated bonds. In the directly coupled systems, the MO's show extensive delocalization over the signalling and receptor moieties, whereas in an uncoupled system i.e., through a non-conjugating spacer this delocalization is absent.<sup>146</sup> When the analyte binds the probe, there is a change in the photophysical

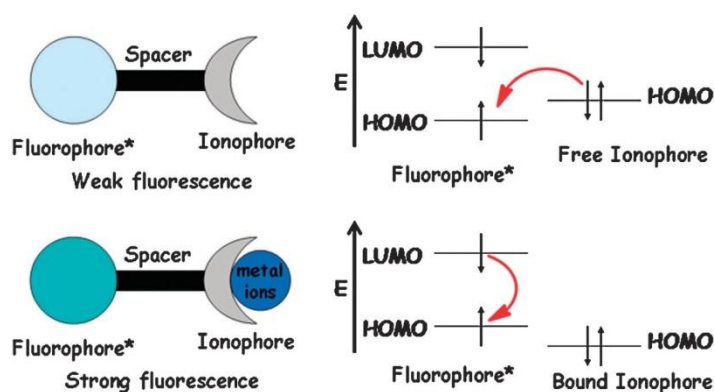
characteristics of the fluorophore and the information is converted into an optical signal through changes in the fluorescence emission. The nature of the change in fluorescence depends on the mechanism of interaction between the analyte and the probe. The changes may manifest as increase or decrease of fluorescence quantum yield or fluorescence lifetime or in certain mechanism a complete quenching or a “turn-on” of a new emission. The mechanisms such as Photo-induced Electron Transfer (PET),<sup>147,148</sup> Photo-induced Charge Transfer (PCT),<sup>149</sup> Fluorescence Resonance Energy Transfer (FRET)<sup>150</sup> and excimer/excimer formation have been normally found operating in some of the reported fluoro ionophores.<sup>151,152</sup> In addition to these mechanisms, a number of dynamic events with a bearing on fluorescence properties such as metal ion coordination inhibited excited-state intramolecular proton transfer (ESIPT) and aggregation-induced emission (AIE), have also been exploited in designing novel and selective probes.<sup>153</sup>



**Figure 1.15** Schematic representation of fluoro ionophore

**1.2.2.1.1 Classification of Fluorescent Sensors****1.2.2.1.1.1 Photoinduced Electron Transfer (PET) and Turn-on Probes**

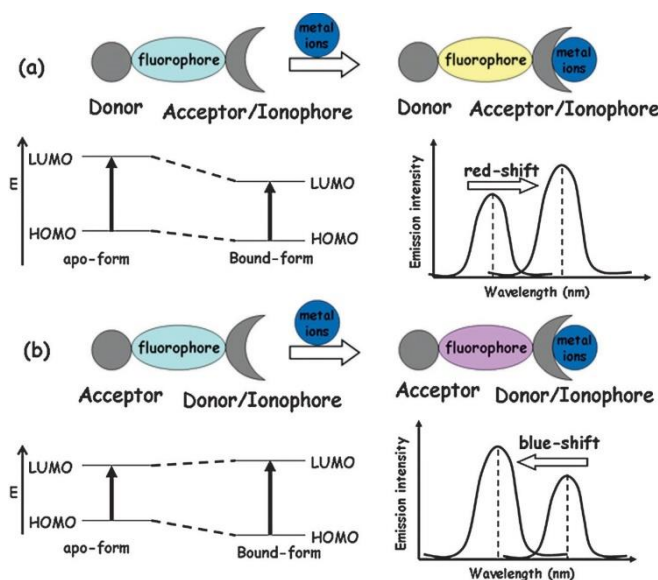
One of the most commonly employed mechanisms for the design of fluorescence probes is PET.<sup>148</sup> Standard PET probes for metal ions contain three parts: fluorophore, spacer, and ionophore (Figure 1.16). In this design Ionophores are usually electron donors such as a group containing amino nitrogen, while electron accepting fluorophores are made the signalling unit. Here, the electron occupied in the highest occupied molecular orbital (HOMO) of the fluorophore gets promoted to the lowest unoccupied molecular orbital (LUMO) upon light absorption. If the energy level of the ionophore HOMO is just higher than that of the fluorophore, a second electron transfer from the ionophore HOMO to the HOMO of the excited fluorophore and thus blocks the emission by radiative deactivation of the excited electron to the HOMO of the fluorophore. This PET quenching of fluorescence gets prevented once the ionophore coordinates with an appropriate metal ion. This metal coordination can affect the energy gap between the two HOMO orbitals in a manner that makes the PET quenching endergonic and thus the fluorescence of the probe gets recovered. This metal binding triggered enhanced fluorescence is also termed as metal chelation-enhanced fluorescence (MCHEF).



**Figure 1.16** PET fluorescent probes for metal cations and their “turn-on” sensing mechanism.<sup>154</sup>

#### 1.2.2.1.1.2 Photo-Induced Charge Transfer (PCT) and Ratiometric Probes

Fluorophores of D- $\pi$ -A type of intramolecular charge transfer (ICT) states normally exhibit large Stokes shift, visible light absorption and in the presence of metal ions and depending on the chelating ability of the donor or acceptor moiety show a metal coordination-induced emission changes. Choosing a chelating donor or acceptor is an effective strategy to develop ratiometric metal ion probes. The Figure 1.17 shows that metal coordination to the donor of an ICT fluorophore will decrease the HOMO energy level leading to a consequent red shifted excitation or emission maxima. If the metal coordination is at acceptor site, the reverse is observed. This type of sensing behaviours is desirable for ratiometric probes, whose self-calibration effect of its excitation/emission bands can remove the interference due to photobleaching, local probe concentration, and other experimental errors. Therefore, the PCT mechanism is an efficient strategy for the construction of ratiometric metal ion probes.

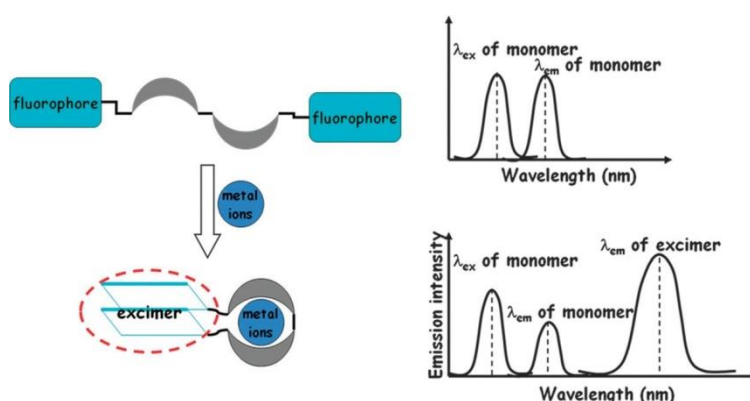


**Figure 1.17** PCT fluorescent probes for metal cations and their ratiometric sensing mechanisms.<sup>154</sup>

### 1.2.2.1.1.3 Excimer Formation and Ratiometric Probes

An excimer is a dimer in an electronic excited state where the excitation energy is shared between the monomer units. They are usually formed by a  $\pi$ - $\pi$  stacking interaction between an excited and ground state fluorophore.<sup>155</sup> A typical design of an excimer-based probe consists of two identical fluorophore moieties spaced by a flexible ionophoric spacer. Upon metal ion coordination, the flexible spacer brings the two fluorophore moieties closer and often within van der Waals contact. This will result in the formation of an excimer and a consequent change in emission spectral profile with the appearance of a new red-shifted broad emission band. In most of the cases, both emission bands from the monomer and the excimer can be observed simultaneously. Hence, the metal coordination by the spacer ionophore controls the ratio between

monomer emission and excimer emission making the system a ratiometric probe for metal cations (Figure 1.18). The length and number of chelating sites can be changes to achieve the desired selectivity of metal binding in these cases.



**Figure 1.18** Excimer formation-based fluorescent sensing<sup>154</sup>

#### 1.2.2.1.1.4 Fluorescence Resonance Energy Transfer (FRET) and Ratiometric Probes

Fluorescence resonance energy transfer, also known as Förster resonance energy transfer (FRET), is a non-radiative process in which the resonance energy transfers from an excited state of a donor fluorophore (D-F) to the ground state of an acceptor fluorophore (A-F) via a non-radiative “dipole–dipole coupling”.<sup>156</sup> The emission spectrum of D-F should have a certain overlap with the absorption spectrum of A-F and if the overlap is high, there will be more effective FRET. Moreover, FRET processes are distance dependant so that the distance between D-F and A-F should be in between 10 to 100 Å for an effective FRET (Figure



1.19).<sup>156</sup> The FRET mechanism is commonly used for the design of ratiometric fluorescent probes with large pseudo Stokes shifts.

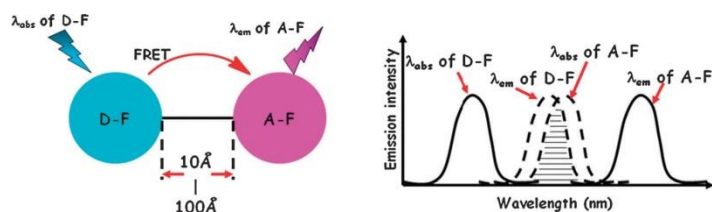


Figure 1.19 Schematic diagram of the FRET process<sup>154</sup>

### 1.2.2.2 Heavy Metals in the Environment

Heavy metals<sup>157</sup> are defined as metals of a density higher than 5 g/cm<sup>3</sup> and occur as pure metals, ions, and complexes. They are of natural origin and forms part of the earth's crust. WHO lists about 10 heavy metals and their excessive presence in the environment as a major public concern. They are cadmium, mercury, lead, chromium, manganese, cobalt, nickel, copper, zinc, silver, thallium and metalloids such as arsenic, selenium, and antimony. Among this cadmium, mercury, lead, and antimony are the common concern due to their alarmingly increasing concentration and damages that cause to the ecosystem. They enter the environment by human activities such as petroleum exploration, refining and their use, mining etc. For example, crude oil contains 3.4 ppm mercury and the firing of coal causes the worldwide emission of  $2.4 \times 10^4$  t of lead per year.<sup>158</sup> Among these heavy metals, mercury, cadmium and arsenic are deadly toxic and in accordance with the toxicity data and scientific studies, WHO (World Health Organization) recommended limits for the amount of heavy metals allowed in drinking water (Table 1.1)

**Table 1.1** Standards and guidelines for heavy metals in drinking water<sup>159</sup>

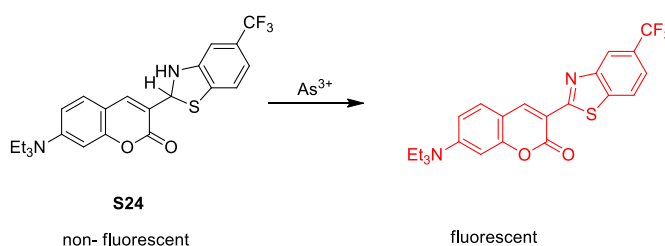
Metal	WHO allowed level (mg L <sup>-1</sup> )
As	0.01
Cd	0.003
Hg	0.001
Pb	0.01

#### 1.2.2.2.1 Arsenic Sensors

The abundance of arsenic (As) compounds in the environment causes major health problems in biological systems. Arsenic contaminates drinking water sources and in water, it exists as arsenic acid (H<sub>3</sub>AsO<sub>4</sub>) and arsenous acid (H<sub>3</sub>AsO<sub>3</sub>). It is introduced into the habitat through mining of sulphide ores,<sup>160</sup> industrial operations,<sup>161</sup> and agricultural activities such as the use of an antimicrobial additive roxarsone.<sup>162</sup> Arsenic oxidation states range from <sup>-3</sup> to <sup>+5</sup> and the trivalent As<sup>3+</sup> state being the most toxic.<sup>163</sup> In mammals, arsenic (III) compounds like H<sub>3</sub>AsO<sub>3</sub> show a strong affinity for thiol biomolecules like cysteine and glutathione<sup>164</sup> which lead to the distraction of vital enzymes such as pyruvate dehydrogenase<sup>165</sup> and the arsenic (V) compound HAsO<sub>4</sub><sup>2-</sup> interrupts the Krebs cycle by acting as a phosphate mimic.<sup>166</sup> Humans get affected by exposure to arsenic through drinking water and contaminated food<sup>167</sup> and can lead to an increased risk of liver, bladder, and lung cancer.<sup>168</sup> The prolonged arsenic exposure causes a skin condition known as arsenicosis.

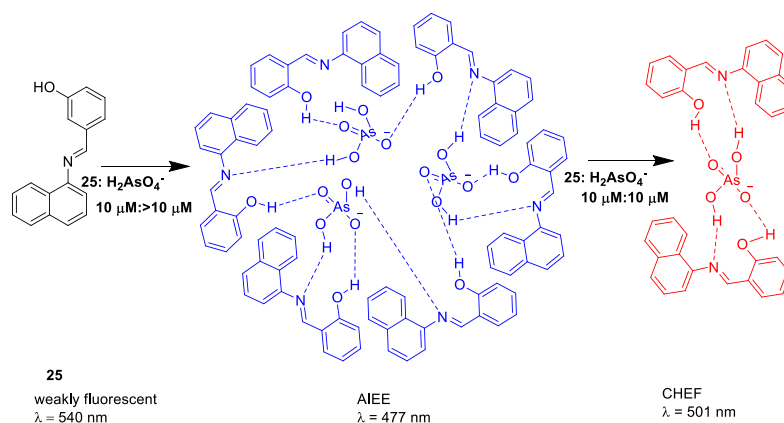
Vivian C. Ezeh *et al.* developed<sup>169</sup> very sensitive and selective fluorescent chemical probe **24**, for the detection of As<sup>3+</sup>, which is the first

example of a chemosensor for  $\text{As}^{3+}$  detection in organic solvents at 298 K. The sensor exhibits a 25-fold fluorescence enhancement in the presence of  $\text{As}^{3+}$  at  $\lambda_{\text{em}} = 496 \text{ nm}$  in THF, and displays a sub-ppb detection limit.



**Scheme 1.2** Turn-on fluorescent probe **24** for  $\text{As}^{3+}$  detection

Debasis Das and co-workers reported<sup>170</sup> a novel turn on fluorescence probe naphthalene–salicylaldehyde conjugate **25**, for the selective detection of arsenate and can detect as low as  $5 \times 10^{-9} \text{ M}$   $\text{H}_2\text{AsO}_4^-$  in HEPES buffered EtOH : water (1 : 9, v/v, pH 7.4). Hydrogen bonding assisted CHEF and AIEE was responsible for the sensing.

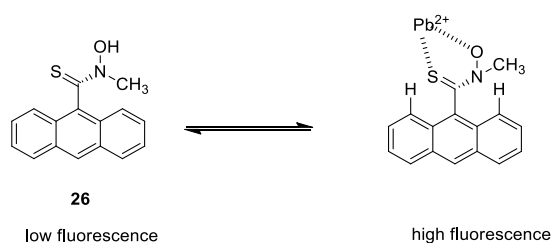


**Scheme 1.3** Probable mechanism for binding of  $\text{H}_2\text{AsO}_4^-$  with **25**.

### 1.2.2.2.2 Lead Sensors

Lead is another toxic metal in the earth's crust and one of the important metal used in batteries, fuel additive and in pigments.<sup>171</sup> Lead pollution is a long-lasting danger to human health because over 300 million tons of lead mined to date are circulating mostly in soil and ground water.<sup>172</sup> Even very little amount of lead exposure can induce reproductive, neurological, cardiovascular, and developmental disorders such as slowed responses, decreased IQs, and hypertension<sup>173</sup> in children.

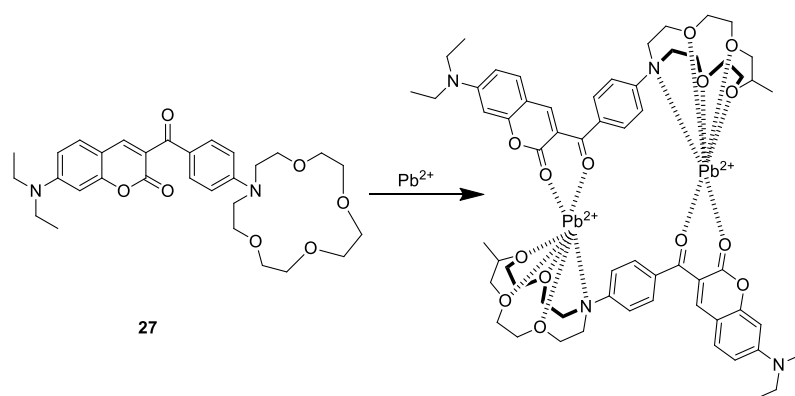
Czarnik and co-workers reported a fluorescent chemosensor **26**<sup>174</sup> for  $\text{Pb}^{2+}$ , which exhibited strongly quenched fluorescence due to the photo-induced electron transfer (PET). Complexation of the sensor with  $\text{Pb}^{2+}$  induced a 13-fold fluorescence enhancement at pH 9, which can be attributed to the steric protection of the thiocarbonyl group by two peri hydrogens (Scheme 1.4). Even though there were few competitive metal ions such as  $\text{Ag}^+$ ,  $\text{Co}^{2+}$ , and  $\text{Hg}^{2+}$ , this is one of the earlier examples of fluorescent chemosensors for  $\text{Pb}^{2+}$



**Scheme 1.4** Probable mechanism for binding of  $\text{Pb}^{2+}$  with **25**.

Chen and Huang reported a new chemosensor **27**<sup>175</sup> (Scheme 1.5) which can selectively detect  $\text{Pb}^{2+}$  and a 2:2 binding stoichiometry was

observed while  $\text{Pb}^{2+}$  binding. The sensor displayed 40-fold fluorescence enhancement for  $\text{Pb}^{2+}$  due to the photo-induced charge transfer (PCT) and metal binding-induced conformational restriction.



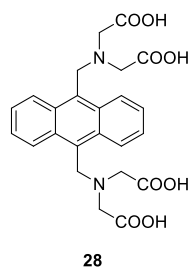
**Scheme 1.5** Proposed 2:2 binding mode of the **27** with  $\text{Pb}^{2+}$

### 1.2.2.2.3 Cadmium Sensors

Cadmium is also an extremely toxic and carcinogenic metal<sup>176</sup> and the main source of exposure is smoking and through food, but the most dangerous route is the inhalation of cadmium-containing dust. Cadmium can be found in electroplated steel, electric batteries, and pigments in plastics etc<sup>177</sup> and high level of exposure is associated with increased risks of cardiovascular diseases, cancer, and also harmful to liver and kidneys.<sup>178</sup>

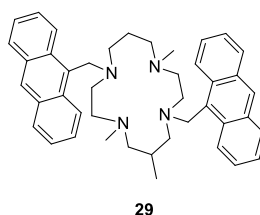
Yoon *et al.* synthesized anthracene derivative<sup>179</sup> **28** bearing the iminomethyl diacetic acid moieties at 9, 10- positions for selective detection of cadmium (Figure 1.20). Fluorescence studies of **28** indicated a selective and large CHEF effect by a PET mechanism with  $\text{Cd}^{2+}$  at pH

10, in 0.1 M CAPS buffer, even though there was a relatively small CHEF effect with  $Zn^{2+}$ .



**Figure 1.20** Structure of chemosensor **28**

Youn and Chang reported<sup>180</sup> a di-substituted bis(anthrylmethyl) derivative of 1,8-dimethylcyclam, **29** (Figure 1.21), for the detection of  $Hg^{2+}$  and  $Cd^{2+}$  in aqueous MeCN solution. The water content of the aqueous MeCN solution can dominate the signaling type of the recognition of  $Hg^{2+}$  and  $Cd^{2+}$ . An OFF–ON type signaling was observed for  $Hg^{2+}$  and  $Cd^{2+}$  ions in low water content solutions (MeCN : H<sub>2</sub>O = 90 : 10, v/v ), whereas in 50% aqueous MeCN solution the signalling mode was reversed (ON–OFF) towards  $Hg^{2+}$  ions.



**Figure 1.21** Structure of sensor **29**

#### 1.2.2.2.4 Mercury Sensors

In earlier days, mercury was used as an important component for various medicines such as diuretics, antibacterial agents, antiseptics, and laxatives. It was also a technologically important metal and was extensively used in thermometers, barometers, manometers, button cells and electronic devices. However, the adverse role of mercury in the biological system on prolonged exposure was realized over the years and now mercury is being considered as one of the most powerful neurotoxins for humans and mammals. The most dangerous form of mercury is organic mercury compared to two other forms of mercury, namely, elemental mercury and inorganic salts. Reports suggest that microbes in water bodies convert inorganic mercury to methylmercury which bioaccumulates in living aquatic organisms and enter into the food chain. Methylmercury is lipophilic and very well absorbed through biological membranes, such as skin, respiratory, and gastrointestinal tissues, which eventually damages the central nervous and endocrine systems.

##### 1.2.2.2.4.1 Colorimetric Sensors for $\text{Hg}^{2+}$ Ion

The colorimetric chemosensors of  $\text{Hg}^{2+}$  can be constructed through the proper combination of receptors and chromophores.<sup>181-183</sup> Here, we are discussing the recent developments and mechanisms of colorimetric sensors for  $\text{Hg}^{2+}$  according to their receptors. There are varieties of colorimetric sensors such as organic molecules, metal complexes, polymers and nanoparticle-based colorimetric sensors. Colorimetric response remains a popular technique due to the factors

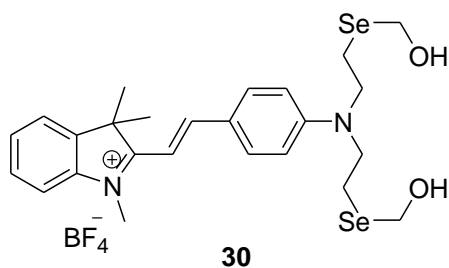
such as low cost, naked eye detection, easy handling and inexpensive consumables. At this point, we are discussing the organic molecule based colorimetric sensors such as polyether, squaraine, rhodamine etc based systems.

#### 1.2.2.2.4.1.1 Polyether Based Sensors

The sensors, which derived from organic dyes, have attracted more attention because of their facile and scalable synthesis in addition to their tunable chemical and physical properties via the molecular design. Many types of organic materials with different structures and tunable optical properties have been effectively used as colorimetric chemosensors.<sup>184–187</sup> Among the known organic sensors, polyether compounds having one or more amino nitrogen or sulphide groups can act as multidentate ligands and which effectively and selectively coordinate to different heavy metal ions especially  $\text{Hg}^{2+}$ .

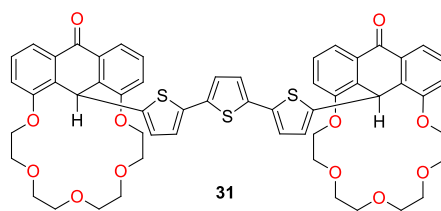
A water soluble  $\text{Hg}^{2+}$  chemosensor (**30**) based on hemicyanine as colorimetric reporting unit and dialkylamine having Se and hydroxyl groups as the chelating unit was developed by Y. Lu and co-workers.<sup>188</sup> The chemosensor shows good selectivity to  $\text{Hg}^{2+}$  over other heavy metal ions. While  $\text{Hg}^{2+}$  binds to **30**, the red colour of the chemosensor turned to colourless. The detection limit was estimated to be  $5.0 \times 10^{-8}$  M and which matches the regulatory requirements. The binding mechanism of  $\text{Hg}^{2+}$  was attributed to the intramolecular charge transfer (ICT), through which the metal ionophore incorporated into the electron donor moiety of the chromophore.



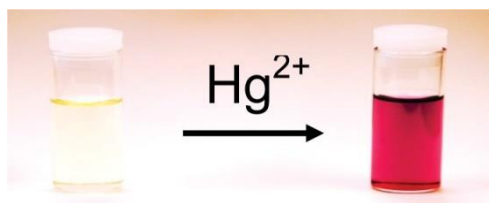


**Figure 1.22** Structure of the chemosensor **30**

A. G. Sykes and co-workers reported<sup>189</sup> a terthiophene based colorimetric sensor, which was composed of linear  $\pi$ -conjugated aromatic compounds and annular macrocycles. Upon Hg<sup>2+</sup> addition, the sensor showed an intense colour change from light yellow to red. This colour change is due to the interaction between Hg<sup>2+</sup> ions and the sulphur atoms of the terthiophene unit, which can lead to the formation of a charge transfer band as a result of the partial oxidation of the terthiophene unit. This simple mercury ion sensing mechanism considerably differs from other numerous photoinduced electron transfer (PET) sensors, which combine a selective receptor to the fluorophore.



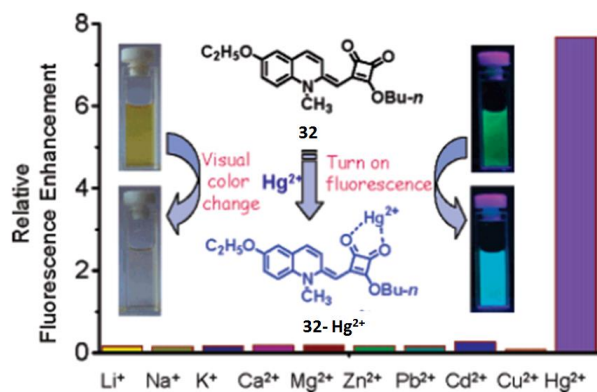
**Figure 1.23** Structure of the chemosensor **31**



**Figure 1.24** Visual changes with addition Hg (II) to **31**<sup>189</sup>

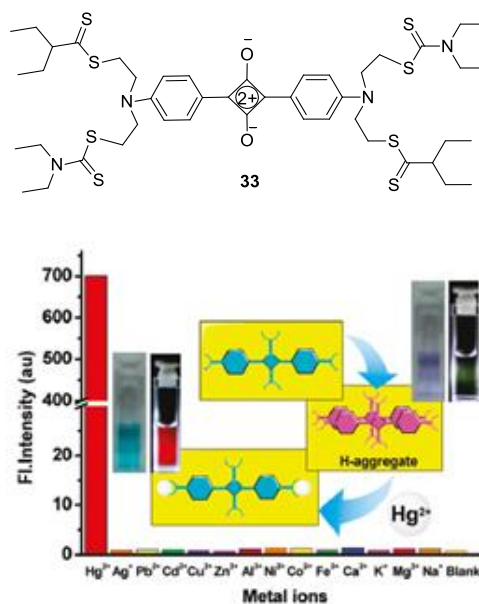
#### 1.2.2.2.4.1.2 Squaraine Based Sensors

Squaraine is one of the most common classes of colorimetric molecular sensors. The rigid D- $\pi$ -A- $\pi$ -D conjugation provides the molecule with a strong absorption from red to the near-IR region. Many squaraine derivatives have been designed and applied for detecting heavy metal ions. For example, D. Ramaiah and co-workers<sup>190</sup> reported a semi-squaraine dye (**32**) (Figure 1.25) as a novel probe for the qualitative detection of Hg<sup>2+</sup> in the micellar medium. Upon the addition of Hg<sup>2+</sup> to the solution of **32** colour changes from deep yellow to colourless. The high selectivity for Hg<sup>2+</sup> is attributed to the soft acid nature and the size of the mercury ion. The interfacing oxygen atoms of the carbonyl groups in the **32** can exclusively coordinate with Hg<sup>2+</sup> and result in an obvious colour change.



**Figure 1.25** Selectivity of binding in **32**<sup>190</sup>

C. Chen *et al.* designed a squaraine-based colorimetric sensor<sup>191</sup> (**33**) using (phenylazanediyli)-bis-(ethane-2,1-diyl)-bis-diethyl-carbamodithioate as the binding group by taking the advantage of the specific aggregation effect of squaraine molecules. Upon  $\text{Hg}^{2+}$  binding, the colour of the sensor solution is dramatically changed from purple to blue. The detection limit was calculated as  $7.1 \times 10^{-9}$  M and the colour change was attributed to the formation of the 1:2 binding stoichiometry of squaraine to  $\text{Hg}^{2+}$ . The colour change was observed only for  $\text{Hg}^{2+}$  ions which can be attributed to the “H”-aggregate de-aggregation process as shown in Figure **1.26**.



**Figure 1.26** Metal ion sensitivity of **33** sensor<sup>191</sup>

In 2013, S. Das and co-workers<sup>192</sup> reported an unsymmetrical squaraine as a colorimetric probe (**34**) for the detection of Hg<sup>2+</sup> ion in methanol medium. Hg<sup>2+</sup> binding resulted in a colour change of the sensor solution from blue to violet with the lowest detection concentration of Hg<sup>2+</sup> ion is  $18.0 \times 10^{-6}$  M. The sensor and Hg<sup>2+</sup> ions showed a 1:1 binding stoichiometry and the Hg<sup>2+</sup> binds through the phenylsquarate carbon-carbon bond, as shown in Figure 1.27

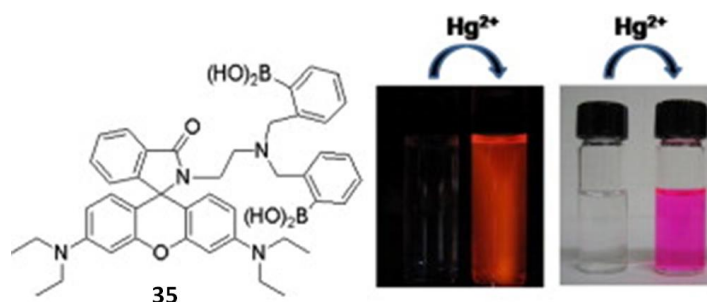


**Figure 1.27** Binding mechanism of **34**.<sup>192</sup>

### 1.2.2.2.4.1.3 Rhodamine Based Sensors

Rhodamine and its derivatives have special photophysical properties and they are used as chemodosimetric sensors for various heavy metal ions.<sup>193,194</sup> Rhodamine derivatives are non-fluorescent and colourless, but the ring-opening of the spirolactam moiety produces a strong fluorescent centre, which gives a clear signal for a colorimetric detection.

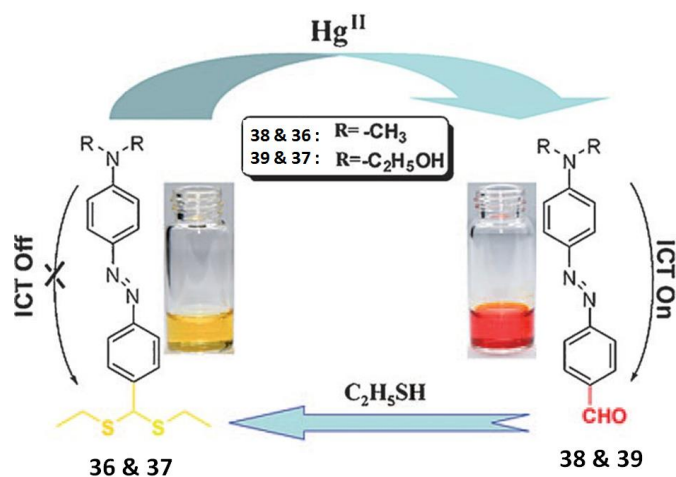
J. Yoon and co-workers<sup>195</sup> reported a reversible chemosensor (**35**) for  $\text{Hg}^{2+}$  detection derived from rhodamine B bearing mono and bis-boronic acid groups as the binding sites. The addition of  $\text{Hg}^{2+}$  resulted in a colour change from colourless to dark pink with a detection limit of 30  $\mu\text{M}$  and the colour change is due to the opening of the non-fluorescent spirolactam ring to form a strongly fluorescent amide. This study successfully reveals that the boronic acid group can serve as a unique and novel ligand for metal ion identification.



**Figure 1.28** Fluorescent changes and colorimetric changes of **35** (30  $\mu\text{M}$ ) with  $\text{Hg}^{2+}$  (50 equiv) in MeCN.<sup>195</sup>

#### 1.2.2.2.4.1.4 Other Organic Molecular Sensors

Z. Li and co-workers<sup>196</sup> reported two colorimetric chemosensors (**36** and **37**) for  $\text{Hg}^{2+}$  detection (Figure 1.29), in which the azobenzene moiety act as the electron donor and the aldehyde group act as the electron acceptor. Upon  $\text{Hg}^{2+}$  addition the sensors changed their colour from light yellow to deep red, which could be easily observed with the naked eye. The binding mechanism is the highly selective  $\text{Hg}^{2+}$ -promoted deprotection of dithioacetal. The  $\text{Hg}^{2+}$  ions converted the protected aldehyde group back to the original aldehyde, and thus the D- $\pi$ -D structures in **38** and **39** were converted into D- $\pi$ -A structures, which accordingly increased the degree of ICT and resulted in a red shift of the absorption bands of the compound.



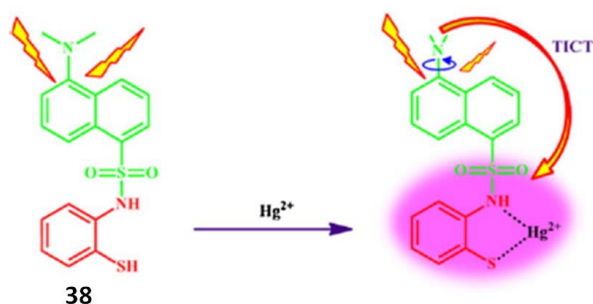
**Figure 1.29**  $\text{Hg}^{2+}$  sensing process of **36** and **37**<sup>196</sup>

K. Pitchumani and co-workers<sup>197</sup> reported a colorimetric chemosensor for  $\text{Hg}^{2+}$  containing 5-(dimethylamino)-N-(2-

mercaptophenyl)naphthalene-1-sulfonamide (**38**) via a twisted intramolecular charge transfer (TICT) mechanism. The sensor shows a colour change from colourless to gray upon  $\text{Hg}^{2+}$  binding (Figure 1.30). While adding  $\text{Hg}^{2+}$ , TICT from the electron-rich group such as N,N'-dimethylamino group to the electron withdrawing group such as thiophenol ring with sulphonamide group takes place because of the interaction between the probe molecule and  $\text{Hg}^{2+}$  with a binding stoichiometry of 1:1. The detection limit is as low as  $5.0 \times 10^{-10}$  M.



**Figure 1.30** Visual color change of probe **38** ( $5.0 \times 10^{-5}$  M) with different cations: Sensor,  $\text{Hg}^{2+}$ ,  $\text{K}^+$ ,  $\text{Na}^+$ ,  $\text{Ag}^+$ ,  $\text{Mn}^{2+}$ ,  $\text{Ca}^{2+}$ ,  $\text{Ba}^{2+}$ ,  $\text{Fe}^{2+}$ ,  $\text{Zn}^{2+}$ ,  $\text{Pb}^{2+}$ ,  $\text{Cu}^{2+}$ ,  $\text{Sn}^{2+}$ ,  $\text{Cd}^{2+}$ ,  $\text{Ni}^{2+}$  and  $\text{Co}^{2+}$  ( $5.0 \times 10^{-5}$  M)<sup>197</sup>

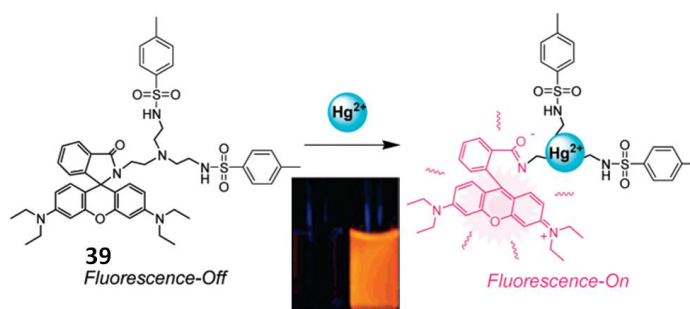


**Figure 1.31** Illustration of sensing mechanism of mercury (II) ion by **38**<sup>197</sup>

### 1.2.2.2.4.2 Fluorescent Sensors and Ratiometric Detection

Fluorescence based detection usually depends on the intensity change at a single wavelength and more sensitive compared to absorption spectroscopy, but the signal output could be easily overshadowed by the experimental errors and the background noise of the sample media. To overcome the above-mentioned drawback, ratiometric fluorescent sensing has been used to permit the measurement of relative fluorescence intensities at two different wavelengths and can serve as an internal reference for self-correction, therefore the reliability of the measurements is substantially enhanced.

J. S. Kim and co-workers synthesized a novel tren-based tripodal “turn on” fluorescent chemosensor **39** bearing a rhodamine and two tosyl groups.<sup>198</sup> The sensor served as a sensitive and selective detection of  $\text{Hg}^{2+}$  in MeCN and 9:1 MeCN/  $\text{H}_2\text{O}$  with a pH scan of 3-6 and a 1:1 binding stoichiometry was observed between the sensor and  $\text{Hg}^{2+}$  ions.

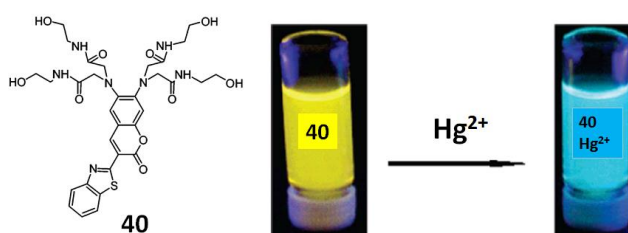


**Figure 1.32** Binding mechanism in chemosensor **39**<sup>198</sup>

X. Qian and co-workers reported<sup>199</sup> a selective, ratiometric, ICT fluorescent  $\text{Hg}^{2+}$  ion sensor **40** by incorporating an *o*-phenylenediamine derived tetraamide receptor into a coumarin platform. The working of the

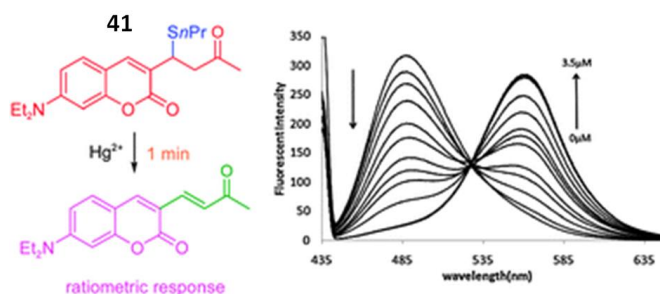


sensor is based on the ICT mechanism and could be used to selectively detect  $\text{Hg}^{2+}$  ions in a neutral buffered water solution with  $\sim 100\text{-nm}$  blue shift in emission spectra. The **40**- $\text{Hg}^{2+}$  binding constant was comparatively low and was effective for  $\text{Hg}^{2+}$  ion concentrations only in the micromolar range.



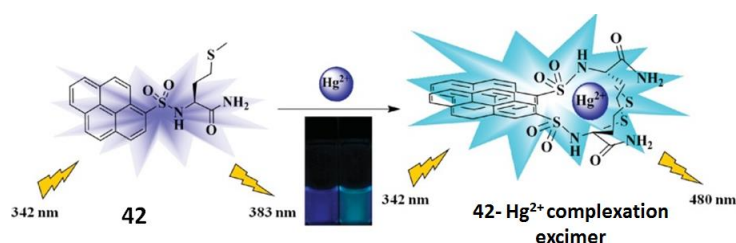
**Figure 1.33** Structure and fluorescence response of **40** in the presence  $\text{Hg}^{2+}$ <sup>199</sup>

W. Wang and co-workers developed<sup>200</sup> a novel ratiometric ICT fluorescent probe **41** for the detection of  $\text{Hg}^{2+}$ . The probe displayed excellent sensitivity and selectivity towards  $\text{Hg}^{2+}$  in aqueous buffer solutions. Especially, significant ratiometric fluorescent response with a large emission redshift was observed, which allowed suitable detection and quantification of the toxic metal ion in a complex system.



**Figure 1.34** Ratiometric detection of  $\text{Hg}^{2+}$  by **41**.<sup>200</sup>

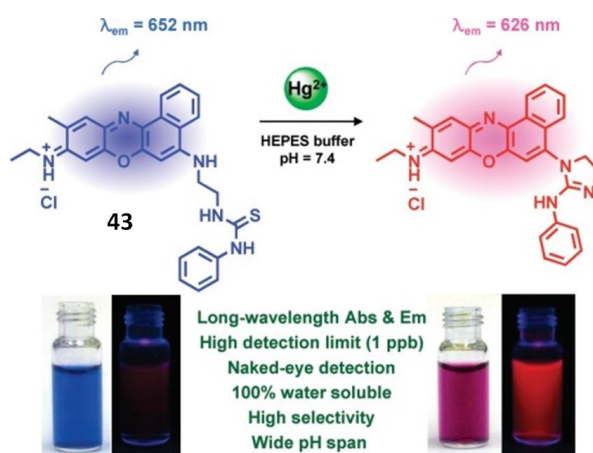
K. Lee and co-workers reported a novel pyrene derivative sensor (**42**) based on amino acid and binding interactions with  $\text{Hg}^{2+}$  was investigated in water.<sup>201</sup> After  $\text{Hg}^{2+}$  binding, the sensor exhibited a considerable excimer emission at 480 nm along with a decrease of monomer emission at 383 nm. Sensor allowed a selective and sensitive ratiometric detection of  $\text{Hg}^{2+}$  with a binding stoichiometry of 2:1



**Figure 1.35** Binding mechanism in **42**<sup>201</sup>

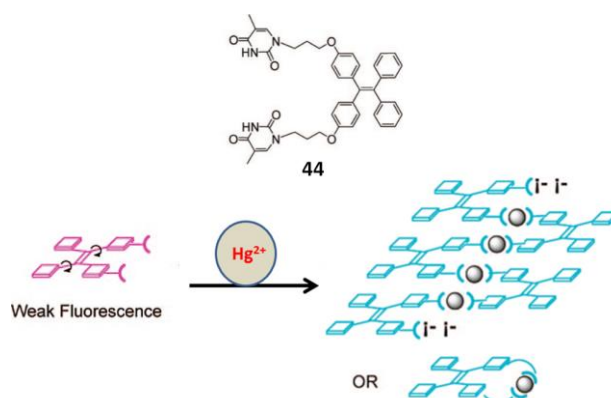
#### 1.2.2.2.4.3 Other Fluorescent $\text{Hg}^{2+}$ Sensors

J. S. Kim and co-workers reported a Nile blue based chemodosimeter (**43**), and its application for detection of the  $\text{Hg}^{2+}$  ion in 100% aqueous solution was demonstrated.<sup>202</sup> Upon the addition of  $\text{Hg}^{2+}$  ion, sensor exhibited a considerable blue shift in its absorption and emission spectra, driven by a desulfurization reaction. Detection of an emission of 652 nm was extremely sensitive (less than 1.0 ppb), even in biological media such as blood plasma and albumin.



**Figure 1.36** Mechanism of  $\text{Hg}^{2+}$  binding in chemodosimeter **43**<sup>202</sup>

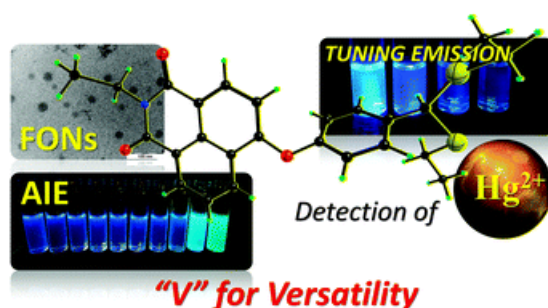
An interesting tetraphenylethylene (TPE) compound bearing thymine moieties (**44**) for the selective detection of  $\text{Hg}^{2+}$  was reported by D. Zhang and co-workers reported.<sup>203</sup> The sensor was found to be fluorescence “turn-on” chemosensors for  $\text{Hg}^{2+}$  by making use of the AIE feature of TPE motif and the specific binding of thymine with  $\text{Hg}^{2+}$



**Figure 1.37** AIE binding mechanism of TPE based sensor **44** with  $\text{Hg}^{2+}$

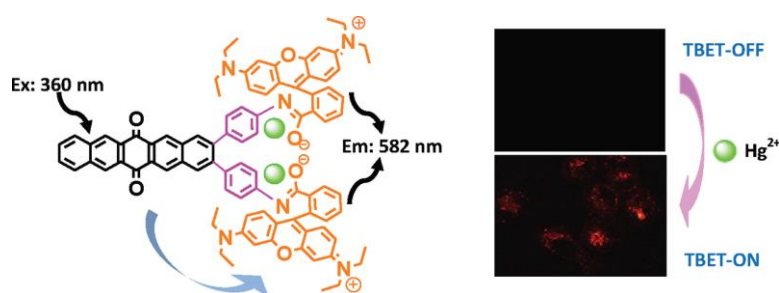
203

A “V” shaped 1,8-naphthalimides based sensor (**45**) for the selective detection of  $\text{Hg}^{2+}$  via a chemodosimetric approach was reported by S. Mukherjee and P. Thilagar.<sup>204</sup> The sensor was an AIE active molecule with the formation of fluorescent nanoaggregates with  $\text{Hg}^{2+}$  binding.



**Figure 1.38** Mechanism of  $\text{Hg}^{2+}$  binding in chemodosimeter **45**<sup>204</sup>

M. Kumar and co-workers synthesized<sup>205</sup> new pentaquinone derivative **46** having rhodamine moieties, which can undergo ‘through-bond energy transfer’ (TBET) in the presence of  $\text{Hg}^{2+}$  ions among the various cations such as  $\text{Cu}^{2+}$ ,  $\text{Pb}^{2+}$ ,  $\text{Fe}^{2+}$ ,  $\text{Fe}^{3+}$ ,  $\text{Zn}^{2+}$ ,  $\text{Ni}^{2+}$ ,  $\text{Cd}^{2+}$ ,  $\text{Co}^{2+}$ ,  $\text{Ag}^+$ ,  $\text{Ba}^{2+}$ ,  $\text{Mg}^{2+}$ ,  $\text{K}^+$ ,  $\text{Na}^+$ , and  $\text{Li}^+$  tested in 9.5:0.5(v/v) THF/  $\text{H}_2\text{O}$ .



**Figure 1.39** TBET on binding mechanism of pentaquinone sensor **46** with  $\text{Hg}^{2+}$  ions<sup>205</sup>

The present thesis reports the design, synthesis, and studies of a series of heterocyclic D- $\pi$ -A systems. The design of the D- $\pi$ -A in the present study was made with a view to developing potential dyes for thin film photovoltaic devices like dye-sensitized solar cells (DSSC) as well as chemosensors for toxic metal ion detection. With this in mind, we designed a series of carbazole and phenothiazine based D- $\pi$ -A systems with a few heterocyclic electron acceptor groups. The electron acceptor groups are chosen such that they act as anchoring groups for binding to TiO<sub>2</sub>, the photoanode in the DSSC. A few of the acceptor groups selected are potential recognition sites for metal ion sensing.

### **1.3 Objectives**

**The main objectives are:**

- Synthesis, characterization and photophysical studies of the n-octylcarbazole and n-octylphenothiazine based D- $\pi$ -A systems
- Study of photovoltaic properties of the n-octylcarbazole or n-octylphenothiazine – cyclic amide conjugates.
- Study of metal ion binding properties of selected n-octylcarbazole – cyclic amide conjugates

The detailed discussion of the above mentioned objectives will be narrated in the second chapter.

## 1.4 References

1. Forrest, S. R.; Thompson, M. E. *Chem. Rev.*, **2007**, *107*, 923.
2. Miller, R. D.; Chandross, E. A. *Chem. Rev.*, **2010**, *110*, 1.
3. Mayor, M. *Chimia*, **2010**, *64*, 348.
4. Bredas, J. L.; Durrant, J. R. *Acc. Chem. Res.*, **2009**, *42*, 1689.
5. Lin, Y.; Li, Y.; Zhan, X. *Chem. Soc. Rev.*, **2012**, *41*, 4245.
6. Allard, S.; Forster, M. B.; Souharce, H.; Scherf, U. *Angew. Chem., Int. Ed.*, **2008**, *47*, 4070.
7. Ohmori, Y. *Laser Photonics Rev.*, **2009**, *4*, 300.
8. Kivala, M.; Diederich, F. *Acc. Chem. Res.*, **2009**, *42*, 235.
9. Kato, S.; Diederich, F. *Chem. Commun.*, **2010**, *46*, 1994
10. Meier, H. *Angew. Chem., Int. Ed.*, **2005**, *44*, 2482.
11. Kivala, M.; Diederich, F. *Pure Appl. Chem.*, **2008**, *80*, 411.
12. Bure, F. *RSC Adv.*, **2014**, *4*, 58826.
13. *Handbook of thiophene-based materials, applications in organic electronics and photonics*, ed. I. F. Perepichka and D. F. Perepichka, Wiley, Chicester, **2009**, vol. 1 and 2.
14. Andreu, R.; Carrasquer, L.; Franco, S.; Garín, J.; Orduna, J.; de Baroja, N. M.; Alicante, R.; Villacampa, B.; Allain, M. *J. Org. Chem.* **2009**, *74*, 6647.
15. Andreu, R.; Galán, E.; Garín, J.; Herrero, V.; Lacarra, E.; Orduna, J.; Alicante, R.; Villacampa, B. *J. Org. Chem.* **2010**, *75*, 1684.
16. Achelle, S.; Baudequin, C.; Plé, N. *Dyes Pigm.* **2013**, *98*, 575.
17. Achelle, S.; Plé, N.; Turck, A. *RSC Adv.* **2011**, *1*, 364.

18. Hrobárik, P.; Hrobáriková, V.; Sigmundová, I.; Zahradník, P.; Fakis, M.; Polyzos, I.; Persephonis, P. *J. Org. Chem.* **2011**, *76*, 8726.
19. Hrobáriková, V.; Hrobárik, P.; Gajdoš, P.; Fitis, I.; Fakis, M.; Persephonis, P.; Zahradník, P. *J. Org. Chem.* **2010**, *75*, 3053.
20. Kulhánek, J.; Bureš, F. *J. Org. Chem.*, **2012**, *8*, 25.
21. Huo, L.; He, C.; Han, M.; Zhou, E.; Li, Y.F. *J. Polym. Sci. Part A: Polym. Chem.* **2007**, *45*, 3861.
22. Tian, H.; Yang, X.; Chen, R.; Pan, Y.; Li, L.; Hagfeldt, A.; Sun, L. *Chem. Commun.* **2007**, 3741.
23. Kivala, M.; Diederich, F. *Acc. Chem. Res.* **2009**, *42*, 235.
24. Kato, S.; Diederich, F. *Chem. Commun.* **2010**, *46*, 1994.
25. Bureš, F.; Pytela, O.; Kivala, V.; Diederich, F. *J. Phys. Org. Chem.* **2011**, *24*, 274.
26. Lee, J. Y.; Kim, K. S.; Mhin, B. J. *J. Chem. Phys.* **2001**, *115*, 9484.
27. Perepichka, D. F.; Bryce, M. R. *Angew. Chem., Int. Ed.* **2005**, *44*, 5370.
28. Van Mullekom, H. A. M.; Vekemans, J. A. J. M.; Havinga, E. E.; Meijer, E. W. *Mater. Sci. Eng., R* **2001**, *32*, 1.
29. Lasitha, P.; Prasad, E. *RSC Adv.* **2015**, *5*, 41420.
30. Agarwal, C.; Prasad, E. *RSC Adv.* **2014**, *4*, 8015.
31. Rajamalli, P.; Prasad, E. *Soft Matter* **2012**, *8*, 8896.
32. Sullivan, P. A.; Dalton, L. R. *Acc. Chem. Res.* **2010**, *43*, 10.
33. Chen, F.; Zhang, J.; Wan, X. *Chem. - Eur. J.* **2012**, *18*, 4558.
34. Coe, B. J. *Chem. - Eur. J.* **1999**, *5*, 2464.

35. Raymo, F. M.; Tomasulo, M. *Chem. - Eur. J.* **2006**, *12*, 3186.
36. Lekha, P. K.; Prasad, E. *Chem. -Eur. J.* **2011**, *17*, 8609.
37. Reichardt, C. *Chem. Rev.* **1994**, *94*, 2319.
38. Kulhánek, J.; Bureš, F.; Wojciechowski, A.; Makowska- Janusik, M.; Gondek, E.; Kityk, I. V. *J. Phys. Chem. A* **2010**, *114*, 9440.
39. Würthner, F.; Effenberger, F.; Wortmann, R.; Krämer, P. *Chem. Phys.* **1993**, *173*, 305.
40. Stiegman, A. E.; Graham, E.; Perry, K. J.; Khundkar, L. R.; Cheng, L.-T.; Perry, J. W. *J. Am. Chem. Soc.* **1991**, *113*, 7658.
41. Dehu, C.; Meyers, F.; Brédas, J. L. *J. Am. Chem. Soc.* **1993**, *115*, 6198.
42. Marder, S. R.; Cheng, L.-T.; Tiemann, B. G. *J. Chem. Soc.* **1992**, 672.
43. Brabec, C.; Scherf, U.; Dyakonov, V. *Organic Photovoltaics. John Wiley & Sons*, **2014**.
44. Guñes, S.; Neugebauer, H.; Sariciftci, N. S. *Chem. Rev.* **2007**, *107*, 1324.
45. Chen, Y.-J.; Yang, S.-H.; Hsu, C.-S. *Chem. Rev.* **2009**, *109*, 5868.
46. Liang, Y.; Yu, L. *Acc. Chem. Res.* **2010**, *43*, 1227.
47. Roncali, J. *Acc. Chem. Res.* **2009**, *42*, 1719.
48. Würthner, F.; Meerholz, K. *Chem-Eur. J.* **2010**, *16*, 9366.
49. Walker, B.; Kim, C.; Nguyen, T. Q. *Chem. Mater.* **2011**, *23*, 470.
50. Lin, Y.; Li, Y.; Zhan, X. *Chem. Soc. Rev.* **2012**, *41*, 4245.
51. Roncali, J.; Leriche, P.; Blanchard, P. *Adv. Mater.* **2014**, *26*, 3821.
52. Roncali, J. *Thin Solid Films* **2006**, *511*, 567.



53. Chen, Y.; Wan, X.; Long, G. *Acc. Chem. Res.* **2013**, *46*, 2645.
54. Coughlin, J. E.; Henson, Z. B.; Welch, G. C.; Bazan, G. *Acc. Chem. Res.* **2014**, *47*, 257.
55. Kan, B. *J. Am. Chem. Soc.* **2014**, *136*, 15529.
56. Burke, D. J.; Lipomi, D. J. *Energy Environ. Sci.* **2013**, *6*, 2053.
57. Osedach, T. P.; Andrew, T. L.; Bulovic, V. *Energy Environ. Sci.* **2013**, *6*, 711.
58. Marzano, G. *Eur. J. Org. Chem.* **2014**, *30*, 6583.
59. O'Regan, B.; Grätzel, M. *Nature*, **1991**, *353*, 737.
60. Grätzel, M. *Chem. Lett.* **2005**, *34*, 8.
61. Bard, A. J. *J. Phys. Chem.* **1982**, *86*, 172.
62. Hagfeldt, A.; Grätzel, M. *Chem. Rev.* **1995**, *95*, 49.
63. Jose, R.; Thavasi, V.; Ramakrishna, S. *J. Am. Ceram. Soc.* **2009**, *92*, 289.
64. Kay, A.; Graetzel, M. *J. Phys. Chem.*, **1993**, *97*, 6272.
65. Cherian, S.; Wamser, C. C. *J. Phys. Chem.: B*, **2000**, *104*, 3624.
66. Komori, T.; Amao, Y. *J. Porphyrins Phthalocyanines*, **2003**, *7*, 131.
67. Islam, A.; Sugihara, H.; Arakawa, H. *J. Photchem. Photobiol. A* **2003**, *158*, 131.
68. Hara, K.; Sayama, K.; Arakawa, H.; Ohga, Y.; Shinpo, A.; Suga, S. *Chem. Commun.* **2001**, 569.
69. Hara, K.; Kurashige, M.; Dan-oh, Y.; Kasada, C.; Shinpo, A.; Suga, S.; Sayama, K.; Arakawa, H. *New J. Chem.* **2003**, *27*, 783.

70. Hara, K.; Wang, Z.S.; Sato, T.; Furube, A.; Katoh, R.; Sugihara, H.; Dan-oh, Y.; Kasada, C.; Shinpo, A.; Suga, S. *J. Phys. Chem. B.* **2005**, *109*, 15476.
71. Ferrere, S.; Gregg, B. A. *New J. Chem.* **2002**, 1155.
72. Jiang, K. J.; Masaki, N.; Xia, J. B.; Noda, S.; Yanagida, S. *Chem. Commun.* **2006**, *21*, 2460.
73. Hwang, S.; Lee, J.H.; Park, C.; Lee, H.; Kim, C.; Lee, M.H.; Lee, W.; Park, J.; Kim, K.; Park, N. G. *Chem. Commun.* **2007**, *14*, 4887.
74. Horiuchi, T.; Miura, H.; Sumioka, K.; Uchida, S. *J. Am. Chem. Soc.* **2004**, *126*, 12218.
75. Nazeeruddin, Md. K.; Kay, A.; Rodicio, I.; Humphry-Baker, R.; Muller, E.; Liska, P.; Vlachopoulos, N.; Grätzel, M. *J. Am. Chem. Soc.* **1993**, *115*, 6382.
76. Nazeeruddin, Md. K.; Zakeeruddin, S. M.; Humphry-Baker, R.; Jirousek, M.; Liska, P.; Vlachopoulos, N.; Shklover, V.; Fischer, C. H.; Grätzel, M. *Inorg. Chem.* **1999**, *38*, 6298.
77. Tian, H.; Yang, X.; Chen, R.; Pan, Y.; Li, L.; Hagfeldt, A.; Sun, L. *Chem. Commun.* **2007**, 3741.
78. Hua, Y.; Chang, S.; Huang, D.; Zhou, X.; Zhu, X.; Zhao, J.; Chen, T.; Wong, W. Y.; Wong, W. K. *Chem. Mater.* **2013**, *25*, 2146.
79. Lin, R. Y. Y.; Wu, F. L.; Li, C. T.; Chen, P. Y.; Ho, K. C.; Lin, J. T. *ChemSusChem*, **2015**, *8*, 2503.
80. Kitamura, T.; Ikeda, M.; Shigaki, K.; Inoue, T.; Anderson, N.A.; Ai, X.; Lian, T.Q.; Yanagida, S. *Chem. Mater.* **2004**, *16*, 1806.
81. Hagberg, D.P.; Yum, J.-H.; Lee, H.; De Angelis, F.; Marinado, T.; Karlsson, K. M.; Humphry-Baker, R.; Sun, L.; Hagfeldt, A.;

- Gratzel, M.; Nazeeruddin, M. K. *J. Am. Chem. Soc.* **2008**, *130*, 6259.
82. Justin Thomas, K.R.; Hsu, Y.-C.; Lin, J. T.; Lee, K.-M.; Ho, K.-C.; Lai, C.-H.; Cheng, Y.-M.; Chou, P.-T. *Chem. Mater.* **2008**, *20*, 1830.
83. Zeng, W.; Cao, Y.; Bai, Y.; Wang, Y.; Shi, Y.; Zhang, M.; Wang, F.; Pan, Y.; Wang, P. *Chem. Mater.* **2010**, *22*, 1915.
84. Kim, M. S.; Yang, H. S.; Jung, D. Y.; Han, Y. S.; Kim, J. H. *Colloid Surface A* **2013**, *420*, 22.
85. Marszalek, M.; Nagane, S.; Ichake, A.; Humphry-Baker, R.; Paul, V.; Zakeeruddin, S. M.; Grätzel, M. *RSC Adv.* **2013**, *3*, 7921.
86. Koumura, N.; Wang, Z.-S.; Miyashita, M.; Uemura, Y.; Sekiguchi, H.; Cui, Y.; Mori, A.; Mori, S.; Hara, K. *J. Mater. Chem.* **2009**, *19*, 4829.
87. Ooyama, Y.; Inoue, S.; Nagano, T.; Kushimoto, K.; Ohshita, J.; Imae, I.; Komaguchi, K.; Harima, Y. *Angew. Chem., Int. Ed.* **2011**, *123*, 7567.
88. Ooyama, Y.; Nagano, T.; Inoue, S.; Imae, I.; Komaguchi, K.; Ohshita, J.; Harima, Y. *Chem. Eur. J.*, **2011**, *17*, 14837.
89. Zhang, M.-D.; Xie, H.-X.; Ju, X.-H.; Qin, L.; Yang, Q.-X.; Zheng, H.-G.; Zhou, X.-F. *Phys. Chem. Chem. Phys.* **2013**, *15*, 634.
90. Ooyama, Y.; Yamaguchi, N.; Imae, I.; Komaguchi, K.; Ohshita, J.; Harima, Y. *Chem. Commun.* **2013**, *49*, 2548.
91. Mao, J.; Wang, D.; Liu, S.-H.; Hang, Y.; Xu, Y.; Zhang, Q.; Wu, W.; Chou, P.-T.; Hua, J. *Asian J. Org. Chem.* **2014**, *3*, 153.

92. Wang, L.; Yang, X.; Li, S.; Cheng, M.; Sun, L. *RSC Adv.* **2013**, *3*, 13677.
93. Massin, J.; Ducasse, L.; Toupance, T.; Olivier, C. *J. Phys. Chem. C* **2014**, *118*, 10677.
94. Daphnomili, D.; Landrou, G.; Prakash Singh, S.; Thomas, A.; Yesudas, K.; Bhanuprakash, K.; Sharma, G. D.; Coutsolelos, A. G. *RSC Adv.* **2012**, *2*, 12899.
95. Daphnomili, D.; Sharma, G. D.; Biswas, S.; Justin Thomas, K. R.; Coutsolelos, A. G. *J. Photochem. Photobiol. A Chem.*, **2013**, *253*, 88.
96. Lu, J.; Xu, X.; Li, Z.; Cao, K.; Cui, J.; Zhang, Y.; Shen, Y.; Li, Y.; Zhu, J.; Dai, S.; Chen, W.; Cheng, Y.; Wang, M. *Chem. Asian J.* **2013**, *8*, 956.
97. Zhang, L.; Cole, J. M.; Dai, C. *ACS Appl. Mater. Interfaces* **2014**, *6*, 7535.
98. Péchy, P.; Rotzinger, F. P.; Nazeeruddin, M. K.; Kohle, O.; Zakeeruddin, S. M.; Humphry-Baker, R.; Grätzel, M. *Chem. Commun.* **1995**, 65.
99. Odobel, F.; Blart, E.; Lagrée, M.; Villieras, M.; Boujtita, H.; El Murr, N.; Caramori, S.; Alberto Bignozzi, C. *J. Mater. Chem.* **2003**, *13*, 502.
100. Park, H.; Bae, E.; Lee, J.-J.; Park, J.; Choi, W. *J. Phys. Chem. B* **2006**, *110*, 8740.
101. López-Duarte, I.; Wang, M.; Humphry-Baker, R.; Ince, M.; Martínez-Díaz, M. V.; Nazeeruddin, M. K.; Torres, T.; Grätzel, M. *Angew. Chem., Int. Ed.* **2012**, *51*, 1895.

102. Mulhern, K. R.; Orchard, A.; Watson, D. F.; Detty, M. R. *Langmuir* **2012**, *28*, 7071.
103. Michinobu, T.; Satoh, N.; Cai, J.; Li, Y.; Han, L. *J. Mater. Chem. C* **2014**, *2*, 3367.
104. Ferrere, S.; Gregg, B. A. *New J. Chem.* **2002**, *26*, 1155.
105. Zafer, C.; Kus, M.; Turkmen, G.; Dincalp, H.; Demic, S.; Kuban, B.; Teoman, Y.; Icli, S. *Sol. Energy Mater. Sol. Cells* **2007**, *91*, 427.
106. Edvinsson, T.; Li, C.; Pschirer, N.; Schöneboom, J.; Eickemeyer, F.; Sens, R.; Boschloo, G.; Herrmann, A.; Müllen, K.; Hagfeldt, A. *J. Phys. Chem. C* **2007**, *111*, 15137.
107. Li, C.; Yum, J.-H.; Moon, S.-J.; Herrmann, A.; Eickemeyer, F.; Pschirer, N. G.; Erk, P.; Schöneboom, J.; Müllen, K.; Grätzel, M.; Nazeeruddin, M. *ChemSusChem* **2008**, *1*, 615.
108. Planells, M.; Céspedes-Guirao, F. J.; Forneli, A.; Sastre-Santos, Á.; Fernández-Lázaro, F.; Palomares, E. *J. Mater. Chem.* **2008**, *18*, 5802.
109. Li, S.-F.; Yang, X.-C.; Cheng, M.; Zhao, J.-H.; Wang, Y.; Sun, L.-C. *Tetrahedron Lett.* **2012**, *53*, 3425.
110. He, H.; Gurung, A.; Si, L. *Chem. Commun.* **2012**, *48*, 5910.
111. Wang, L.; Yang, X.; Li, S.; Cheng, M.; Sun, L. *RSC Adv.* **2013**, *3*, 13677.
112. Zhao, J.; Yang, X.; Cheng, M.; Li, S.; Sun, L. *ACS Appl. Mater. Interfaces* **2013**, *5*, 5227.
113. Cherepy, N. J.; Smestad, G. P.; Grätzel, M.; Zhang, J. Z. *J. Phys. Chem. B* **1997**, *101*, 9342.

114. Tae, E. L.; Lee, S. H.; Lee, J. K.; Yoo, S. S.; Kang, E. J.; Yoon, K. B. *J. Phys. Chem. B* **2005**, *109*, 22513.
115. An, B.-K.; Hu, W.; Burn, P. L.; Meredith, P. J. *J. Phys. Chem. C* **2010**, *114*, 17964.
116. Ooyama, Y.; Yamada, T.; Fujita, T.; Harima, Y.; Ohshita, J. *J. Mater. Chem. A* **2014**, *2*, 8500.
117. Abuabara, S. G.; Cady, C. W.; Baxter, J. B.; Schmuttenmaer, C. A.; Crabtree, R. H.; Brudvig, G. W.; Batista, V. S. *J. Phys. Chem. C* **2007**, *111*, 11982.
118. McNamara, W. R.; Snoeberger, R. C., III; Li, G.; Richter, C.; Allen, L. J.; Milot, R. L.; Schmuttenmaer, C. A.; Crabtree, R. H.; Brudvig, G. W.; Batista, V. S. *Energy Environ. Sci.* **2009**, *2*, 1173.
119. McNamara, W. R.; Milot, R. L.; Song, H.; Snoeberger, R. C., III; Batista, V. S.; Schmuttenmaer, C. A.; Brudvig, G. W.; Crabtree, R. H. *Energy Environ. Sci.* **2010**, *3*, 917.
120. Brewster, T. P.; Konezny, S. J.; Sheehan, S. W.; Martini, L. A.; Schmuttenmaer, C. A.; Batista, V. S.; Crabtree, R. H. *Inorg. Chem.* **2013**, *52*, 6752.
121. Ma, T.; Inoue, K.; Noma, H.; Yao, K.; Abe, E. *J. Photochem. Photobiol. A Chem.* **2002**, *152*, 207.
122. Yan, Z.; Guang, S.; Su, X.; Xu, H. *J. Phys. Chem. C* **2012**, *116*, 8894.
123. Wang, Z.-S.; Li, F.-Y.; Huang, C.-H. *Chem. Commun.* **2000**, *20*, 2063.

124. Wang, Z.-S.; Li, F.-Y.; Huang, C.-H. *J. Phys. Chem. B* **2001**, *105*, 9210.
125. Yao, Q.-H.; Shan, L.; Li, F.-Y.; Yin, D.-D.; Huang, C.-H. *New J. Chem.* **2003**, *27*, 1277.
126. Heimer, T. A.; D’Arcangelis, S. T.; Farzad, F.; Stipkala, J. M.; Meyer, G. J. *Inorg. Chem.* **1996**, *35*, 5319.
127. Warnan, J.; Guerin, V.-M.; Anne, F. B.; Pellegrin, Y.; Blart, E.; Jacquemin, D.; Pauporté, T.; Odobel, F. *J. Phys. Chem. C* **2013**, *117*, 8652.
128. McNamara, W. R.; Snoeberger, R. C.; Li, G.; Schleicher, J. M.; Cady, C. W.; Poyatos, M.; Schmuttenmaer, C. A.; Crabtree, R. H.; Brudvig, G. W.; Batista, V. S. *J. Am. Chem. Soc.* **2008**, *130*, 14329.
129. Altobello, S.; Bignozzi, C.; Caramori, S.; Larramona, G.; Quici, S.; Marzanni, G.; Lakhmiri, R. *J. Photochem. Photobiol. A Chem.* **2004**, *166*, 91.
130. Cong, J.; Yang, X.; Liu, J.; Zhao, J.; Hao, Y.; Wang, Y.; Sun, L. *Chem. Commun.* **2012**, *48*, 6663.
131. Massin, J.; Ducasse, L.; Toupance, T.; Olivier, C. *J. Phys. Chem. C* **2014**, *118*, 10677.
132. Marinado, T.; Hagberg, D. P.; Hedlund, M.; Edvinsson, T.; Johansson, E. M. J.; Boschloo, G.; Rensmo, H.; Brinck, T.; Sun, L.; Hagfeldt, A. *Phys. Chem. Chem. Phys.* **2009**, *11*, 133.
133. Mao, J.; He, N.; Ning, Z.; Zhang, Q.; Guo, F.; Chen, L.; Wu, W.; Hua, J.; Tian, H. *Angew. Chem., Int. Ed.* **2012**, *51*, 9873.

134. Ganesan, P.; Chandiran, A.; Gao, P.; Rajalingam, R.; Grätzel, M.; Nazeeruddin, M. K. *J. Phys. Chem. C* **2014**, *118*, 16896.
135. Li, S.-L.; Jiang, K.-J.; Shao, K.-F.; Yang, L.-M. *Chem. Commun.* **2006**, *2*, 2792.
136. Tian, H.; Yang, X.; Chen, R.; Pan, Y.; Li, L.; Hagfeldt, A.; Sun, L. *Chem. Commun.* **2007**, 3741.
137. Horiuchi, T.; Miura, H.; Uchida, S. *Chem. Commun.* **2003**, 3036.
138. Horiuchi, T.; Miura, H.; Sumioka, K.; Uchida, S. *J. Am. Chem. Soc.* **2004**, *126*, 12218.
139. Ito, S.; Miura, H.; Uchida, S.; Takata, M.; Sumioka, K.; Liska, P.; Comte, P.; Péchy, P.; Grätzel, M. *Chem. Commun.* **2008**, 5194.
140. Horiuchi, T.; Miura, H.; Uchida, S. *J. Photochem. Photobiol. A Chem.* **2004**, *164*, 29.
141. Gou, F.; Jiang, X.; Li, B.; Jing, H.; Zhu, Z. *ACS Appl. Mater. Interfaces* **2013**, *5*, 12631.
142. Gou, F.; Jiang, X.; Fang, R.; Jing, H.; Zhu, Z. *ACS Appl. Mater. Interfaces* **2014**, *6*, 6697.
143. Tang, J.; Qu, S.; Hu, J.; Wu, W.; Hua, J. *Sol. Energy* **2012**, *86*, 2306.
144. Ooyama, Y.; Hagiwara, Y.; Oda, Y.; Mizumo, T.; Harima, Y.; Ohshita, J. *New J. Chem.* **2013**, *37*, 2336.
145. Zhang, L.; Cole, J. M. *ACS Appl. Mater. Interfaces* **2015**, *7*, 3427.
146. Quang, D. T.; Kim, J. S. *Chem. Rev.* **2010**, *110*, 6280.



147. Valeur, B.; Leray, I. *Coord. Chem. Rev.* **2000**, 205, 3.
148. De Silva, A. P.; Moody, T. S.; Wright, G. D. *Analyst* **2009**, 134, 2385.
149. Jiang, P. J.; Guo, Z. J. *Coord. Chem. Rev.* **2004**, 248, 205.
150. Carlson, H. J.; Campbell, R. E. *Curr. Opin. Biotechnol.* **2009**, 20, 19.
151. Kim, J. S.; Quang, D. T. *Chem. Rev.* **2007**, 107, 3780.
152. Lodeiro, C.; Pina, F. *Coord. Chem. Rev.* **2009**, 253, 1353.
153. Wu, J.; Liu, W.; Ge, J.; Zhang, H.; Wang, P. *Chem. Soc. Rev.* **2011**, 40, 3483.
154. Liu, Z.; He, W.; Guo, Z. *Chem. Soc. Rev.* **2013**, 42, 1568.
155. Moragues, M. E.; Martínez-Mañé, R.; Sanceno, F. *Chem. Soc. Rev.* **2011**, 40, 2593.
156. Sapsford, K. E.; Berti, L.; Medintz, I. L. *Angew. Chem., Int. Ed.* **2006**, 45, 4562.
157. *Römpps Chemie Lexikon*, Thieme, Stuttgart, **1995**.
158. Merian, E. *Metals and their Compounds in the Environment*, VCH, Weinheim **1991**.
159. World Health Organization, *Guidelines for drinking water quality*, 2nd ed., Geneva, **1998**.
160. Ferguson, J. F.; Gavis, J. *A Review of the Arsenic Cycle in Natural Waters*; Pergamon Press: London, **1972**.
161. Saha, J. C.; Dikshit, A. K.; Bandyopadhyay, M.; Saha, K. C. *Crit. Rev. Environ. Sci. Technol.* **1999**, 29, 281.
162. Christen, K. *Environ. Sci. Technol. A Pages* **2001**, 35, 184A.
163. Cullen, W. R.; Reimer, K. J. *Chem. Rev.* **1989**, 89, 713.

164. Rey, N. A.; Howarth, O. W.; Pereira-Maia, E. C. *J. Inorg. Biochem.* **2004**, *98*, 1151.
165. Lin, S.; Cullen, W. R.; Thomas, D. *J. Chem. Res. Toxicol.* **1999**, *12*, 924.
166. Spuches, A. M.; Kruszyna, H. G.; Rich, A. M.; Wilcox, D. E. *Inorg. Chem.* **2005**, *44*, 2964.
167. Meacher, D. M.; Menzel, D. B.; Dillencourt, M. D.; Bic, L. F.; Schoof, R. A.; Yost, L. J.; Eickhoff, J. C.; Farr, C. H. *Hum. Ecol. Risk Assess.* **2002**, *8*, 1697.
168. Yu, H.-S.; Liao, W.-T.; Chai, C.-Y. *J. Biomed. Sci.* **2006**, *13*, 657.
169. Ezeh, V. C.; Harrop, T. C. *Inorg. Chem.* **2012**, *51*, 1213.
170. Sahana, A.; Banerjee, A.; Lohar, S.; Panja, S.; Mukhopadhyay, S. K.; Matalobos, J. S.; Das, D. *Chem. Commun.* **2013**, *49*, 7231.
171. Flegal, A. R.; Smith, D. R. *Environ. Res.* **1992**, *58*, 125.
172. Claudio, E. S.; Godwin, H. A.; Magyar, J. S. *Prog. Inorg. Chem.* **2003**, *51*, 1.
173. *Department of Health and Human Services and Prevention, Center for Disease Control (2003) Surveillance for Elevated Blood Lead Levels Among Childrens: United States, 1997–2001, Morbidity and Mortality Weekly Rep.* *52*, 1.
174. Chae, M.-Y.; Yoon, J.; Czarnik, A. W. *J. Mol. Recognit.* **1996**, *9*, 297.
175. Chen, C.-T.; Huang, W.-P. *J. Am. Chem. Soc.* **2002**, *124*, 6246.

176. Lauwerys, R. R.; Bernard, A. M.; Reels, H. A.; Buchet, J.-P. *Clin. Chem.* **1994**, *40*, 1391.
177. Nordberg, G. F.; Herber, R. F. M.; Alessio, L. *Cadmium in the Human Environment*, Oxford University Press, Oxford, UK, **1992**.
178. McFarland, C. N.; Bendell-Young, L. I.; Guglielmo, C.; Williams, T. D. *J. Environ. Monit.* **2002**, *4*, 791.
179. Choi, M.; Kim, M.; Lee, K. D.; Han, K.-N.; Yoon, I.-A.; Chung, H.-J.; Yoon, J. *Org. Lett.* **2001**, *3*, 3455.
180. Youn, N. J.; Chang, S.-K. *Tetrahedron Lett.* **2004**, *46*, 125.
181. Yan, Z. Q.; Guang, S. Y.; Xu, H. Y.; Liu, X. Y. *Analyst* **2011**, *136*, 1916.
182. Liu, R. L.; Lu, H. Y.; Li, M.; Hu, S. Z.; Chen, C. F. *RSC Adv.* **2012**, *2*, 4415.
183. Lee, J. S.; Han, M. S.; Mirkin, C. A. *Angew. Chem., Int. Ed.*, **2007**, *46*, 4093.
184. Yan, Z. Q.; Guang, S. Y.; Xu, H. Y.; Liu, X. Y. *Dyes Pigm.* **2013**, *99*, 720.
185. Sun, J.; Zhu, G. H.; Sun, X. Q.; Li, T.; Gao, W. N.; Zhang, D. M.; Hou, A. L. *Chin. Phys. Lett.* **2009**, *26*.
186. Sajjan, D.; Joe, I. H.; Jayakumar, V. S.; Zaleski, J. *J. Chem. Sci.* **2008**, *120*, 405.
187. Yan, Z. Q.; Guang, S. Y.; Su, X. Y.; Xu, H. Y. *J. Phys. Chem. C* **2012**, *116*, 8894.
188. Li, Y.; He, S.; Lu, Y.; Zeng, X. *Org. Biomol. Chem.* **2011**, *9*, 2606.

189. Kadarkaraisamy, M.; Thammavongkeo, S.; Basa, P. N.; Caple, G.; Sykes, A. G. *Org. Lett.* **2011**, *13*, 2364.
190. Avirah, R. R.; Jyothish, K.; Ramaiah, D. *Org. Lett.* **2007**, *9*, 121.
191. Chen, C.; Wang, R.; Guo, L.; Fu, N.; Dong, H.; Yuan, Y. *Org. Lett.* **2011**, *13*, 1162.
192. Shafeekh, K. M.; Rahim, M. K. A.; Basheer, M. C.; Suresh, C. H.; Das, S. *Dyes Pigm.* **2013**, *96*, 714.
193. Nunez, C.; Diniz, M.; Dos Santos, A. A.; Capelo, J. L.; Lodeiro, C. *Dyes Pigm.* **2014**, *101*, 156.
194. Chen, Y. T.; Mu, S. Y. *Sens. Actuators, B* **2014**, *192*, 275.
195. Kim, S. K.; Swamy, K. M. K.; Chung, S. Y.; Kim, H. N.; Kim, M. J.; Jeong, Y.; Yoon, J. *Tetrahedron Lett.* **2010**, *51*, 3286.
196. Cheng, X. H.; Li, Q. Q.; Li, C. G.; Qin, J. G.; Li, Z. *Chem.–Eur. J.* **2011**, *17*, 7276.
197. Tharmaraj, V.; Pitchumani, K. *Anal. Chim. Acta* **2012**, *751*, 171.
198. Lee, M. H.; Wu, J-S.; Lee, J. W.; Jung, J. H.; Kim, J. S. *Org. Lett.* **2007**, *9* 2501.
199. Wang, J.; Qian, X.; Cui, J. *J. Org. Chem.* **2006**, *71*, 4308.
200. Xuan, W.; Chen, C.; Cao, Y.; He, W.; Jiang, W.; Liu, K.; Wang, W. *Chem. Commun.* **2012**, *48*, 7292.
201. Yang, W. H.; Thirupathi, P.; Lee, K. H. *Org. Lett.* **2011**, *13*, 5028.
202. Lee, M. H.; Lee, S. W.; Kim, S. H.; Kang, C.; Kim, J. S. *Org. Lett.* **2009**, *11*, 2101.

203. Liu, L.; Zhang, G.; Xiang, J.; Zhang, D.; Zhu, D. *Org. Lett.* **2008**, *10*, 4581.
204. Mukherjee, S.; Thilagar, P. *Chem. Commun.* **2013**, *49*, 7292.
205. Bhalla, V.; Kumar, M.; Sharma, P. R.; Kaur, T. *Inorg. Chem.* **2012**, *51*, 2150.

## Chapter 2

# Synthesis and Photophysical Properties of Donor- $\pi$ -Acceptor Systems

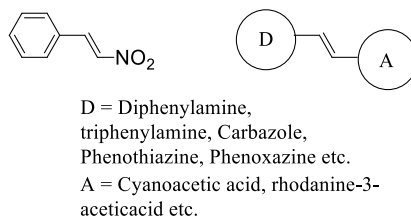
---

### 2.1 Abstract

Organic dyes comprising carbazole, or phenothiazine moieties as the electron donors, and cyanoacetic acid, rhodanine-3-acetic acid, barbituric acid and thiobarbituric acid moieties as the electron acceptors were synthesized and characterized. The influence of different heterocyclic acceptor groups on their absorption and emission properties were studied by photophysical and theoretical methods.

### 2.2 Introduction

The present thesis reports the design, synthesis and studies of a series of heterocyclic D- $\pi$ -A systems. The design of D- $\pi$ -A in the present study was made with a view to develop potential dyes for thin film photovoltaic devices like dye sensitized solar cells (DSSC) as well as chemosensors for toxic metal ion detection. The typical structure of a directly coupled D- $\pi$ -A is an arylidene derivative having a structure similar to  $\beta$ -nitrostyrene (Figure 2.1).



**Figure 2.1** The typical structure of D- $\pi$ -A system

In  $\beta$ -nitrostyrene, the phenyl ring is in conjugation with nitro group, which is an acceptor. Dyes with a similar design are commonly used for solar cell applications (Figure 2.1). The following are some of the important considerations to be adopted while designing dyes for DSSC applications.

- The electronic properties such as HOMO and LUMO energies should be conducive for an exergonic electron injection to the conduction band of the semiconductor and an exergonic regeneration of the dye by the redox electrolyte. For a DSSC based on  $\text{TiO}_2$  as semiconductor and Iodine triiodide as electrolyte, the LUMO and HOMO level of the dye should lie above -0.5 V and below 0.5 V respectively.
- The absorption spectrum of the dye should cover the visible region of the solar spectrum i.e., 400-700 nm.
- The dye should have sufficient solubility to allow good dye loading on the semiconductor surface.
- The affinity towards semiconductor surfaces is an important factor for a better binding and subsequent

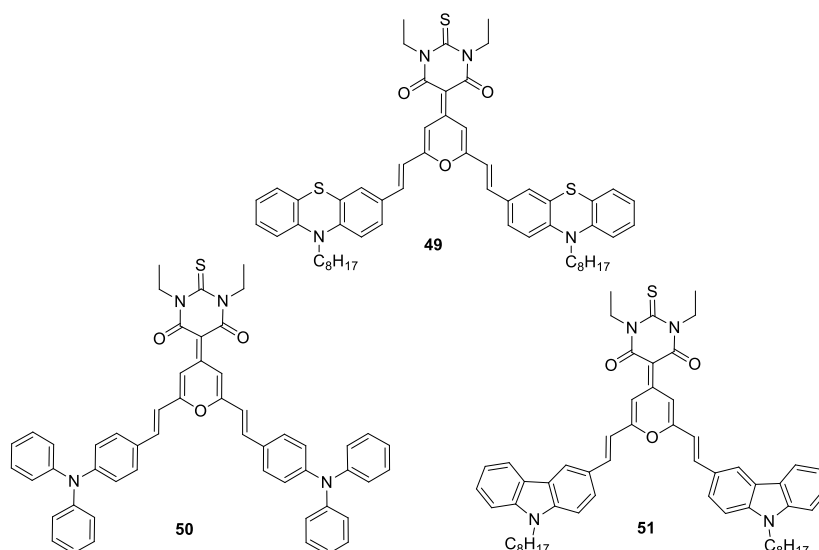
electronic interaction with the LUMO orbitals and the conduction band of the semiconductor.

- The dye should have sufficient hydrophobicity to insulate the electrolyte from reaching the semiconductor surface.
- The dye with long hydrocarbon chains is a necessary structure design to prevent aggregation of the dye on the semiconductor surface.

Figure 2.1 lists the type of donor and acceptor moieties used in the design of D- $\pi$ -A type of dyes. Triphenylamine, carbazole, phenoxazine and phenothiazine are typical donor moieties. However, cyanoacrylic acid is the most commonly used acceptor group, it has its own advantages and disadvantages such as greater affinity towards TiO<sub>2</sub> and the absorption spectrum haven't sufficient overlap with the visible region of the solar spectrum respectively. Some of the alternative acceptor groups reported in the literature are rhodamine-3-acetic acid and its bis rhodanine derivative.<sup>1</sup> These acceptors possess good affinity towards semiconductor surfaces due to their carboxylic acid groups and the dyes synthesised with these acceptor moieties have suitable LUMO levels for efficient electron injection.

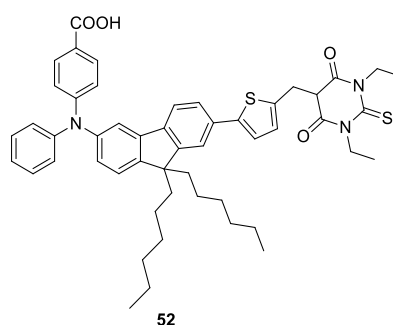
Z. Li *et al.* reported<sup>2</sup> a series of dyes **49**, **50**, and **51** with N-ethyl substituted thiobarbituric acid as the acceptor unit. DSSC device based on **51** showed the highest photoconversion efficiency ( $\eta = 2\%$ ) and the lowest was for **49** ( $\eta = 0.28\%$ ) (Figure 2.2).





**Figure 2.2** Dyes containing N-ethyl substituted thiobarbituric acid as the acceptor unit

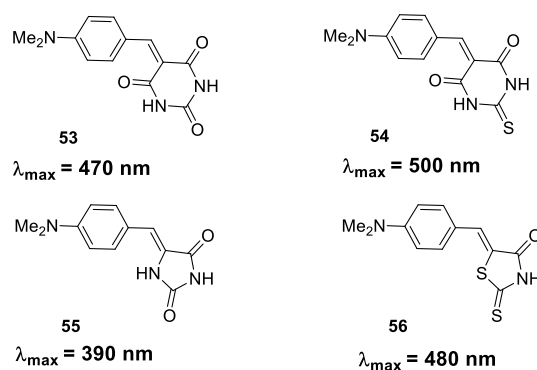
In a report<sup>3</sup> by Yen *et al.*, the N-alkylated derivatives of thiobarbituric acid (Figure 2.3) have been used as the acceptor in a *p*-type DSSC device where the donor moiety was anchored to NiO via -COOH groups. The efficiency reported was very low ( $\eta = 0.053\%$ )



**Figure 2.3** Sensitizer with N-alkylated derivative of thiobarbituric acid as acceptor

The acceptor groups of the above mentioned dyes are alkylated cyclic amides. The noticeable thing is that, compared to cyanoacetic acid based dyes, the category listed above doesn't have suitable anchoring groups at the acceptor site.

In the present thesis, we propose the use of barbituric acid and thiobarbituric acid as acceptor groups, which can bring the excitation energy considerably down and thereby ensuring better overlap with the visible solar spectrum. This has been demonstrated by Ikeda and co-workers<sup>4</sup> in their study of push-pull aniline-cyclic amide conjugates **53**–**56** (Figure 2.4). In these molecules, the DMA (dimethyl aniline) donor was linked to acceptors such as N-unsubstituted barbituric acid (**53**), thiobarbituric acid (**54**), hydantoin (**55**) and rhodanine (**56**). The optical absorption ( $\lambda_{\text{max}}$ ) was shifted by 30 nm from barbituric acid to thiobarbituric acid acceptors. On the other hand, the replacement of six membered BA derivative **53** by the five membered hydantoin derivative **55** resulted in considerable hypsochromic shift. Compared to **55**, two sulphur atoms in rhodanine derivative **56** shifted the CT-band by 90 nm and thus, the ring size and heteroatoms attached on the acceptor play an important role in the overall performance of the given heterocyclic acceptor.

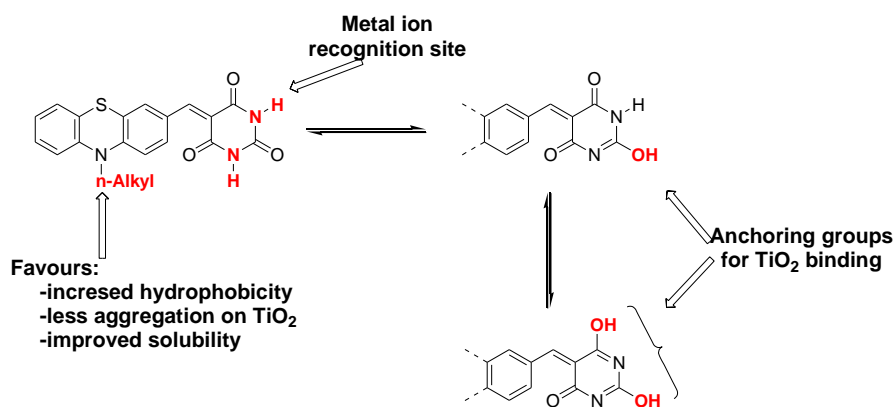


**Figure 2.4** The absorption maxima changes in push-pull dimethyl substituted aniline-cyclic amide conjugates

A keto-imido tautomerization can be expected for barbituric acid and thiobarbituric acid acceptors and thus have a tendency to deprotonate and bind with the TiO<sub>2</sub> surface (Scheme 2.1). The use of barbituric acid or thiobarbituric acid with free NH groups as the acceptor/anchoring group in photovoltaic applications was not reported so far to the best of our knowledge. With this in mind, we have designed a series of carbazole and phenothiazine based D- $\pi$ -A systems with a few heterocyclic electron acceptor groups such as rhodanine-3-acetic acid, barbituric acid and thiobarbituric acid.

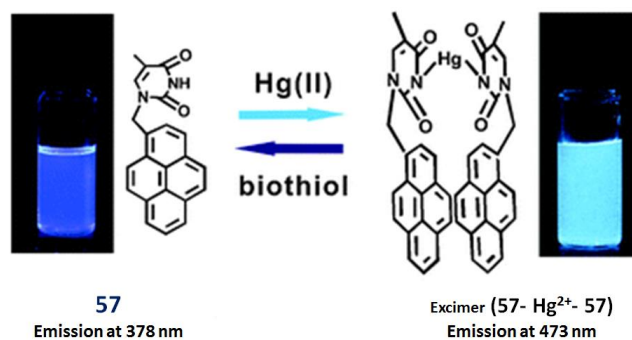
The chosen donor moieties are carbazole and phenothiazine, their conjugates with cyanoacrylic acid show suitable HOMO levels for using with a Gratzel type solar cell. These are well studied cases and the results can be used to validate our studies. N-alkylation in these types of donors can generate better results as these groups make the semiconductor surface hydrophobic, which can prevent electrolyte from reaching the surface and reducing the leakage of dark current. They also prevent close

packing of the dye, a factor that reduces the power conversion efficiency in organic dye based DSSC devices.



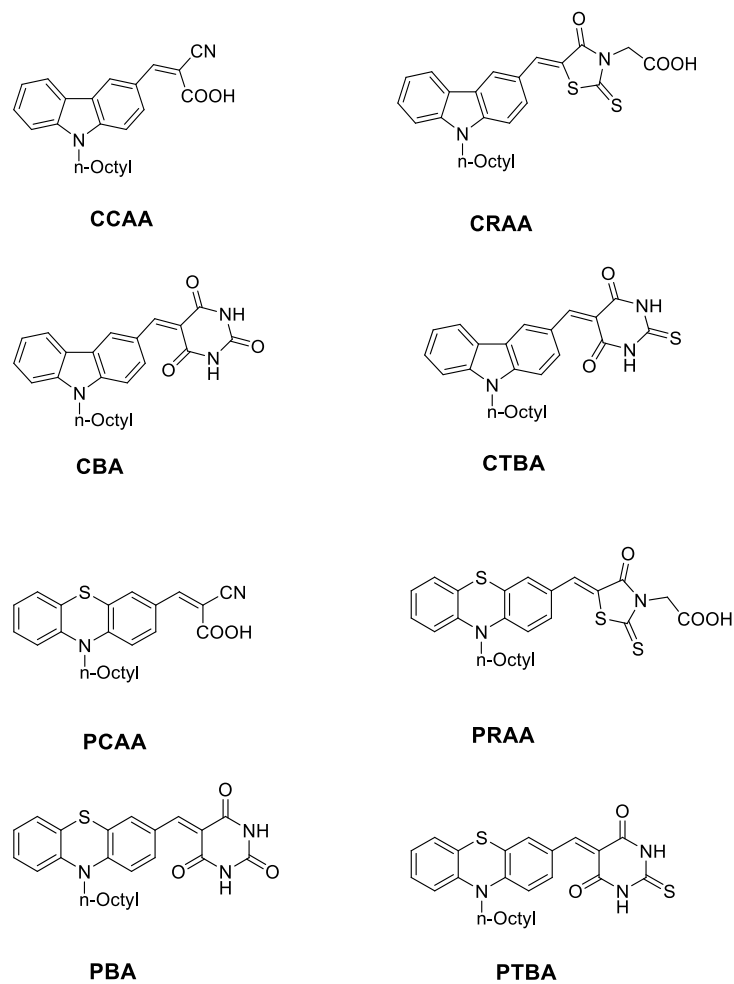
**Scheme 2.1** Proposed TiO<sub>2</sub> binding sites of barbituric acid moiety.

Barbituric acid and thiobarbituric acid are pyrimidine triones and are known to form metal complexes with Co, Ni, Cu, Pd and Pt. The nucleic acid base thymidine as well as DNA itself are known to interact with metal ions such as Ag<sup>+</sup> and Hg<sup>2+</sup>. These cations deprotonate the amide NH and subsequently form divalent species of T-M-T type divalent metal organic structures. B. Ma *et al.* have successfully used this in the development of a ratiometric fluorescent sensor for biothiols and Hg<sup>2+</sup> (Figure 2.5). The mechanism of binding involves the monomer–excimer transformation of pyrene moieties.<sup>5</sup> A 2:1 binding stoichiometry is formed between the pyrene based sensor and Hg<sup>2+</sup> ions. In this method, the difference in the binding affinity between thymine–Hg<sup>2+</sup> and biothiol–Hg<sup>2+</sup> was employed to understand the detection. This excimer–monomer emission change affords the **57**–Hg<sup>2+</sup>–**57**, a reversible and sensitive fluorescent ratiometric sensor for biothiols.



**Figure 2.5** Mechanism of binding in **57** with Hg<sup>2+</sup>

These reports motivated us to proceed with the current design of D- $\pi$ -A systems which can be potential dyes for DSSC applications and as chemosensor systems for metal ion detection. These D- $\pi$ -A molecules have inherent intramolecular charge transfer (ICT) character which is expected to respond to the electron distribution changes by metal ion binding. Thus, these acceptor groups are chosen, such that they act as anchoring groups for binding to TiO<sub>2</sub>, the photoanode in the DSSC. Few of these acceptor groups are also potential recognition sites for metal ion sensing. The general design principle is illustrated with a phenothiazine – barbituric acid conjugate in Scheme 2.1 and Figure 2.6 which show the D- $\pi$ -A systems synthesised and studied in the present thesis.

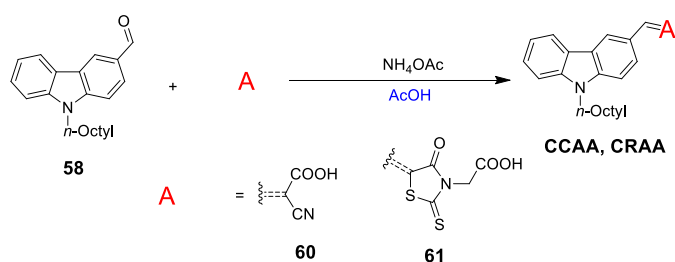


**Figure 2.6** Chart showing the D- $\pi$ -A systems synthesised and studied.

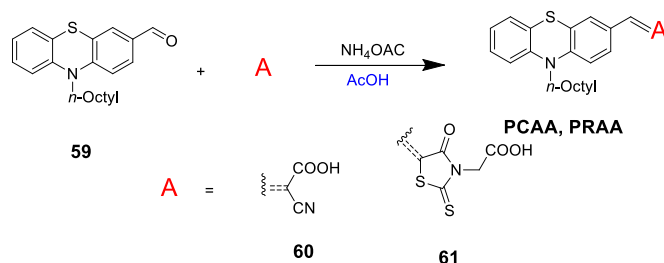
## 2.3 Results and Discussion

### 2.3.1 Synthesis

Knoevenagel condensation reaction was used for the synthesis of above mentioned dyes. Here, 9-octyl-9*H*-carbazole-3-carbaldehyde (**58**) or 10-octyl-10*H*-phenothiazine-3-carbaldehyde (**59**) was prepared by Vilsmyer formylation of respective *n*-octyl carbazole or *n*-octylphenothiazine in acetic acid. These were refluxed with cyano acetic acid or rhodanine-3- acetic acid in the presence of ammonium acetate which resulted in the dyes **CCAA**, **CRAA**, **PCAA** and **PRAA** respectively in good yields (scheme 2.2 & 2.3)

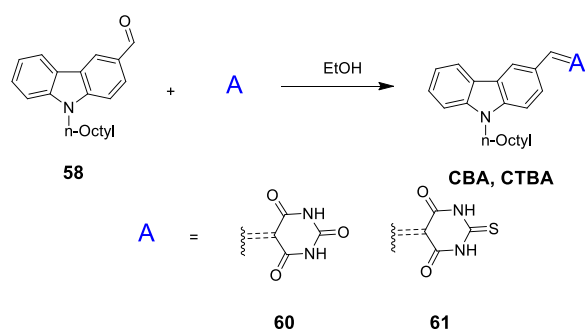


**Scheme 2.2** Synthesis of CCAA and CRAA

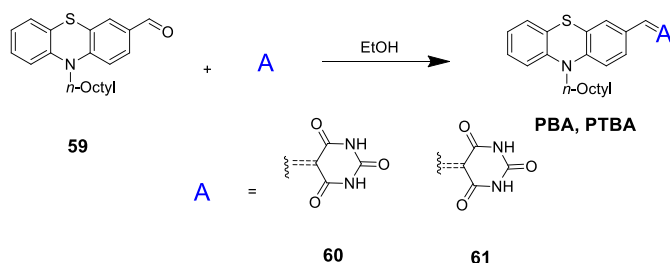


**Scheme 2.3** Synthesis of PCAA and PRAA

The other four dyes CBA, PBA, CTBA and PTBA were synthesised by refluxing 9-octyl-9*H*-carbazole-3-carbaldehyde (**58**) or 10-octyl-10*H*-phenothiazine-3-carbaldehyde (**59**) with barbituric acid or thiobarbituric acid in ethanol (Scheme 2.4 & 2.5).



**Scheme 2.4** Synthesis of CBA and CTBA



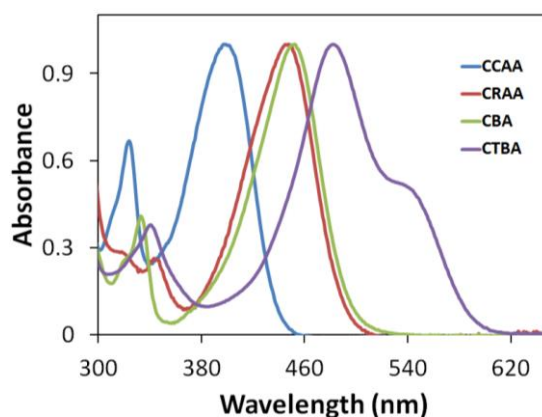
**Scheme 2.5** Synthesis of PBA and PTBA

All the prepared dyes were characterised by spectroscopic techniques such as FT-IR,  $^1\text{H}$  NMR,  $^{13}\text{C}$  NMR and ESI-MS/HRMS.

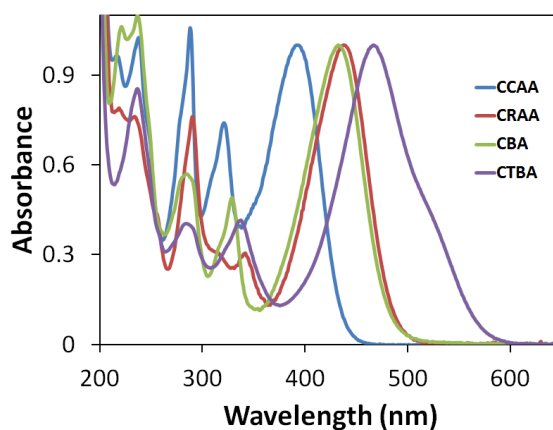


## 2.3.2. Photophysical Studies

### 2.3.2.1 Absorption Properties of Carbazole Dyes



**Figure 2.7** Absorption spectra of carbazole compounds in  $\text{CHCl}_3$



**Figure 2.8** Absorption spectra of carbazole compounds in MeCN

The absorption spectral properties of the four carbazole dyes have been investigated in different solvents. The absorption spectra of these dyes possess the characteristic features of a  $\pi$ -conjugated donor-acceptor

system with a prominent intramolecular charge transfer herein referred to as ICT absorption band. The absorption maximum due to this ICT state shifts to the visible region of the electromagnetic spectrum with increase in the electron affinity of the acceptor group. CCAA and CRAA show an ICT absorption band at  $\lambda_{\text{max}}$  399 and 448 nm respectively, while CBA and CTBA exhibited an absorption maximum at 452 and 482 nm in chloroform as shown in Figure 2.7. A red shift of 83 nm in the absorption maximum is observed as we change the acceptor from cyanoacetic acid to thiobarbituric acid. Based on the absorption maximum of the ICT band observed, the order of electron affinity of the acceptor groups is cyanoacetic acid < rhodanine-3-acetic acid < barbituric acid < thiobarbituric acid. The absorption spectra of these conjugates were found to be dependent on the polarity of the solvent medium. The absorption maximum of the ICT band in different solvents is summarized in Table 2.1 and the absorption spectra of these dyes in acetonitrile is presented in Figure 2.7. As observed for typical D- $\pi$ -A systems, the absorption spectrum is red shifted in a less polar solvent such as chloroform. In a highly polar solvent such as acetonitrile, the absorption maximum is blue shifted by 7 nm for CCAA, 10 nm for CRAA, 20 nm for CBA and 15 nm for CTBA. For CCAA and CRAA, the absorption maximum did not show much variation among Toluene, THF, acetone, methanol and acetonitrile. In toluene, the absorption maximum observed for CCAA and CRAA are blue shifted compared to that observed in chloroform and this is unusual for a less polar solvent like toluene. Similarly, the spectrum is further blue shifted in ethyl acetate which is slightly polar compared to chloroform and toluene and less polar than acetonitrile. For CBA and

CTBA, the response to polarity in chloroform and acetonitrile is as expected for a molecule having ICT character. However, no specific trend is seen among other solvents. This may be due to the fact that these molecules possess hydrogen bond donating and accepting sites in addition to the inherent dipolar nature due to the ICT character. Hydrogen bonding with the solvent along with dipole–dipole interaction may lead to complex solvatochromic responses in this type of systems. Molar extinction coefficients of carbazole dyes are calculated and listed in the Table 2.1. All these dyes show high molar extinction coefficients for typical ICT states in D- $\pi$ -A systems. The dyes CCAA, CBA and CTBA show maximum molar absorptivity in toluene and CRAA has molar absorptivity maximum in ethyl acetate (Table 2.1).

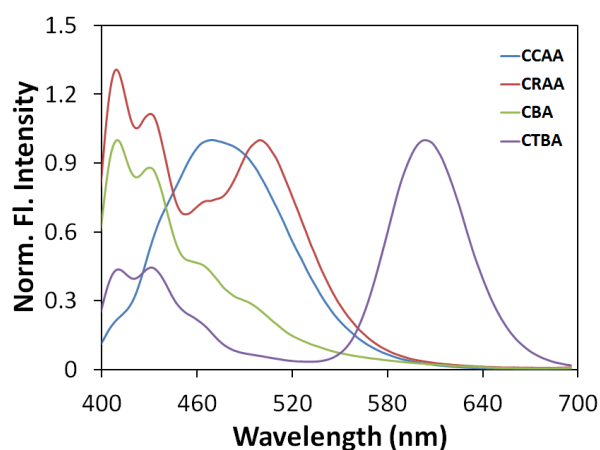
**Table 2.1** Absorption spectral properties of n-octylcarbazole based D- $\pi$ -A systems.

Solvent	CCAA		CRAA		CBA		CTBA	
	$\lambda_{\max}$ (nm)	$\epsilon_{\max}$ $\text{cm}^{-1}\text{M}^{-1}$ $\times 10^4$	$\lambda_{\max}$ (nm)	$\epsilon_{\max}$ $\text{cm}^{-1}\text{M}^{-1}$ $\times 10^4$	$\lambda_{\max}$ (nm)	$\epsilon_{\max}$ $\text{cm}^{-1}\text{M}^{-1}$ $\times 10^4$	$\lambda_{\max}$ (nm)	$\epsilon_{\max}$ $\text{cm}^{-1}\text{M}^{-1}$ $\times 10^4$
Toluene	394	3.53	440	3.29	437	3.66	467	5.67
CHCl <sub>3</sub>	399	2.97	448	2.77	452	3.23	482	4.54
THF	391	3.19	438	3.34	428	2.85	460	4.93
EtOAc	388	3.23	428	3.47	428	3.30	460	4.41
MeOH	390	2.71	438	3.33	438	3.16	469	4.61
Acetone	392	3.28	441	3.02	430	2.94	461	4.65
MeCN	392	2.95	438	2.98	432	3.10	467	5.00

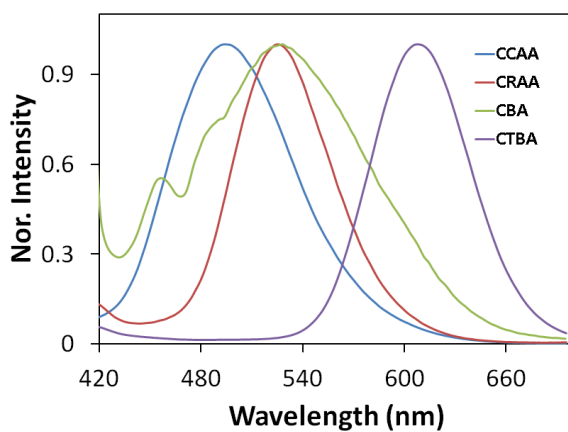
### 2.3.2.2 Emission Properties of Carbazole Dyes

The emission properties of the four carbazole dyes have been investigated under different solvents. Figure 2.9 & 2.10 show the emission spectra of all the compounds recorded in chloroform and acetonitrile by exciting at 370 nm. In chloroform, the emission spectrum of these dyes shows carbazole type emission band in the range of 400-440 nm having vibrational fine structure. CCAA, CRAA and CTBA show dual emission bands and in these molecules apart from the carbazole type emission, a broad and unstructured emission band is also observed which is assigned to the ICT state. These molecules thus possess two emissive states; one, a carbazole based excited state (CE) and an intramolecular charge transfer state (ICT). In the case of CCAA in chloroform, two states are not resolved very well and the fine structure expected for the CE state appear as small shoulders at 410 and 427 nm. The maximum at 497 nm observed in chloroform is primarily due to the ICT state. For CRAA and CTBA, the dual emission is well resolved and for CTBA, they are 170 nm apart from the observed ICT emission maximum at 600 nm. Since these compounds have overlapping absorption band in this region, the observed spectrum do not represent the actual intensity and emission spectral profile. The carbazole type CE emission intensity is lower in acetonitrile and the spectra is characterised by strong ICT emission band for all compounds. The large red shift in the ICT emission band in CTBA could be due to a highly stabilized CT excited state possible in such molecules possessing strong electron acceptor groups. The effect of solvent polarity on the relative intensity of the CE and ICT emission bands were compared and presented in Figure

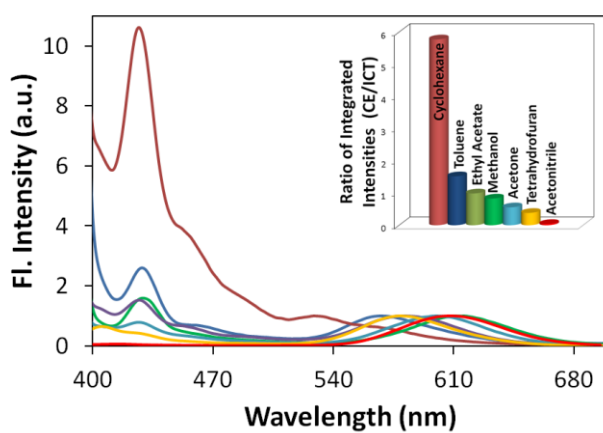
**2.11.** The inset in the bar diagram shows the ratio of integrated intensities for the CE and ICT band and it is evident that, there is strong polarity dependence to the ICT emission. However, in methanol, though polar do have significant CE emission compared to that observed in acetonitrile. This may be due to the polar-protic character and hydrogen bonding interaction of the solvent with the carbonyl/thiocarbonyl groups which may facilitate a faster non-radiative deactivation and lower quantum yield of ICT emission.



**Figure 2.9** Emission spectra of carbazole compounds in  $\text{CHCl}_3$ ,  $\lambda_{\text{ex}} = 370$  nm



**Figure 2.10** Emission spectra of carbazole compounds in MeCN,  $\lambda_{\text{ex}} = 370$  nm



**Figure 2.11** Fluorescence emission spectra of CTBA in different solvents (Normalized at the ICT emission maximum). Inset: Ratio of integrated emission intensity due to carbazole type emission (**CE**) and charge transfer excited state (**ICT**).

The fluorescence lifetime at 600 nm for CCAA, CBA, and CTBA were recorded in acetonitrile and the data were fitted well to a multi-exponential equation. The lifetime values with >5% contribution are reported in the Table 2.2. CCAA and CBA emissions have a lifetime of 0.019 ns whereas that of CTBA is long lived with a lifetime 0.58 ns. The fluorescence quantum yields ( $\phi_f$ ) were also determined by relative actinometry using perylene bisimide as the reference. All compounds show weak emissions and CBA has the lowest quantum yield of fluorescence.

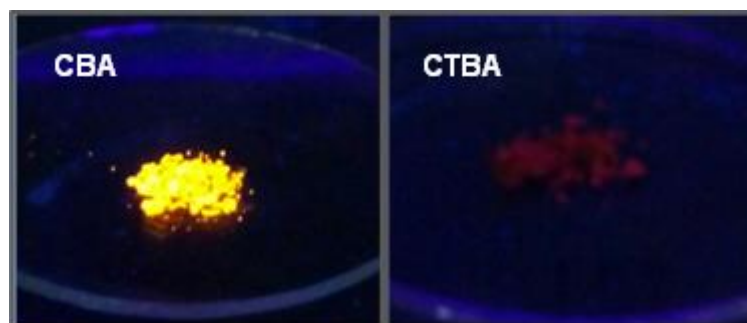
**Table 2.2** Emission spectral properties of *n*-octylcarbazole based D- $\pi$ -A

Solvent	CCAA $\lambda_{\text{max}}$ (nm)	CRAA $\lambda_{\text{max}}$ (nm)	CBA $\lambda_{\text{max}}$ (nm)	CTBA $\lambda_{\text{max}}$ (nm)
Cyclohexane	425, 452	485	490, 564	427, 527
Toluene	438	512	510	427, 564
CHCl <sub>3</sub>	470	429, 500	429, 490	429, 600
THF	455	495	491	424, 574
EtOAc	453	527	491	425, 576
MeOH	460	565	495	426, 608
Acetone	478	545	513	424, 595
MeCN	494	550	524	427, 604
$\tau$ (ns)*	0.019	--	0.019	0.58
$\phi_f$ *	0.013	0.015	0.0015	0.01

\*Solvent: Acetonitrile

Since CBA and CTBA possess multiple hydrogen bonding donor and acceptor sites, they can form organised assemblies in the solid state. Such organized assemblies of carbazole derivatives were shown to have high luminescence properties in the solid state.<sup>6</sup> CBA showed strong

solid state emission than CTBA when observed under UV illumination (Figure 2.12). This behaviour may be due to an aggregation induced emission arising from the close packing of molecules in the solid state. Such aggregation induced emission has been reported earlier for carbazole derivatives and the property has been used earlier in photonic applications.<sup>7</sup>



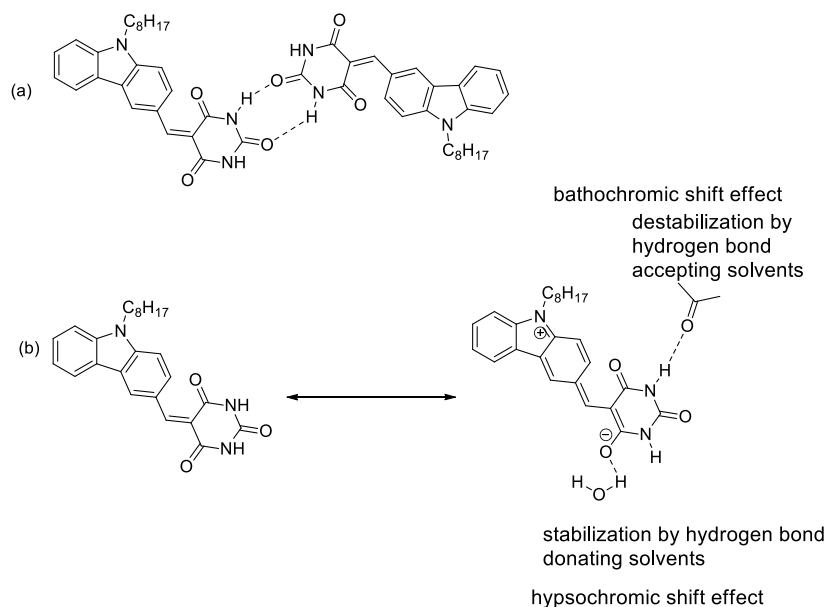
**Figure 2.12** Photographs showing solid state emission of CBA and CTBA

### 2.3.2.3 Intramolecular Charge Transfer in Carbazole Dyes

Mohamad-Ali, T. *et al.* in their report on the push-pull systems in photosensitized radical and cationic polymerization reactions using CBA and CTBA made some interesting observation related to their absorption and emission behaviour in various solvents.<sup>8</sup> The authors suggested a zwitterionic form, which gets stabilized by hydrogen bond donating solvents causing a blue shift in the absorption spectrum and hydrogen bond accepting solvents like acetone or THF destabilizes the ground state and causing a red shift in the absorption spectrum (Scheme 2.6). This explanation lacks clarity and is contradictory to what is observed in



hydrogen bond donating solvents such as methanol and polar solvents like acetonitrile where a red shift in the absorption spectrum is observed. Similarly in hydrogen bond accepting solvents such as acetone and ethyl acetate, a blue shifted absorption spectrum is observed. In the case of CTBA, we have observed a weak shoulder like absorption around 500 nm in all solvents and are more prominent in chloroform. (See Figures 2.7 and 2.8)



**Scheme 2.6** (a) Formation of hydrogen bonded "dimers" in solution and (b) schematic representation of the different effects involved in the solvatochromic behaviour of CBA reported by Mohamad-Ali, T. *et al.*<sup>8</sup>

Major discrepancies were also observed in the emission properties reported by this group. They did not observe the dual emission property of these compounds and this may be due to choosing an excitation wavelength along the onset of the absorption band. We have

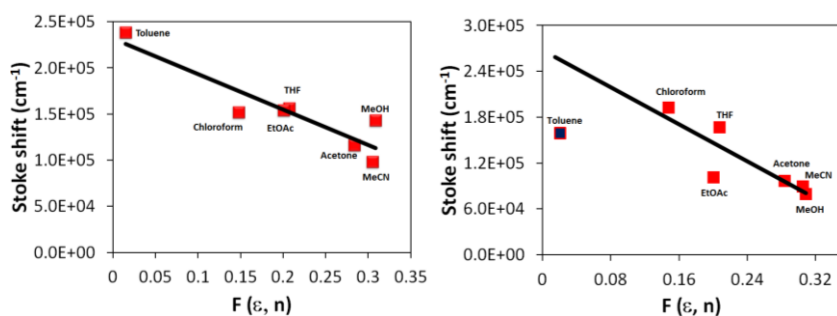
chosen an excitation wavelength of 370 nm, which may lead to population of both LE and CT states. According to this report, in acetonitrile, CTBA showed emission maximum at 557 nm whereas we have observed the emission maximum at 604 nm. This emission maximum was found to be less affected by the solvent polarity and the stokes shift values ( $\nu_{st}$ ) obtained in different solvents were plotted against  $\Delta f$ , a function that was dependent on the dielectric constant ( $\epsilon$ ) and refractive index ( $n$ ) of the medium as described by the Lippert equation.<sup>9,10</sup>

$$\nu_{st} = \frac{2(\mu_e - \mu_g)^2 \Delta f}{hca^3} + \text{Constant}$$

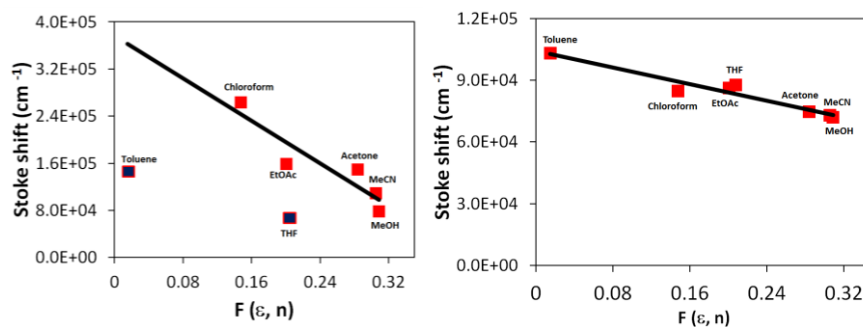
where  $\mu_e$  and  $\mu_g$  are the excited and ground state dipole moments,  $\Delta f = \left[ \frac{(\epsilon-1)}{(2\epsilon+1)} \right] - \left[ \frac{(n^2-1)}{(2n^2+1)} \right]$ ,  $h$  is the Planck's constant,  $c$  is the speed of light and  $a$  is the radius of the solvent shell where the fluorophore resides. The slope ( $m$ ) of a plot of  $\nu_{st}$  vs.  $\Delta f$  gives the value of  $2\Delta\mu^2/hca^3$ . For the carbazole derivative  $a$  is assumed as  $4 \text{ \AA}$ <sup>0</sup>

Since these compounds in particular, CRAA, CBA and CTBA, possessing hydrogen bond donating and accepting functionalities showed mixed solvatochromic behaviour they did not give very good correlation with the Lippert model. Figures 2.13–2.14 show the Lippert–Mataga plots obtained for CCAA, CRAA, CBA and CTBA and Table 2.3 summarises the experimental data and the estimated dipole moment difference ( $\Delta\mu$ ) between the excited state and the ground states. All the compounds except CTBA showed ground and excited state dipole

moment differences typical for molecules with ICT. In the case of CTBA  $\Delta\mu$  calculated was small indicating a highly polarised ground state leading to very little charge shift in the excited state.



**Figure 2.13** Lippert- Mataga plots obtained for CCAA and CRAA



**Figure 2.14** Lippert- Mataga plots obtained for CBA and CTBA

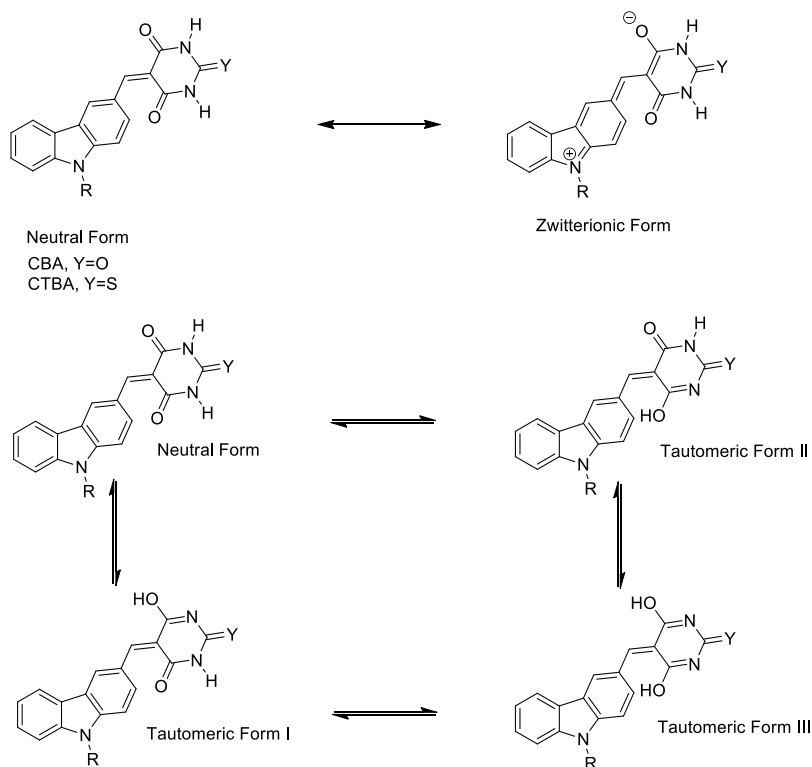
**Table 2.3** Stokes shift values in different solvents, solvatochromic slopes ( $m$ ), and  $\Delta\mu$  values for CCAA, CRAA, CBA and CTBA

Compound/Solvent		CCAA	CRAA	CBA	CTBA
Stokes shift, (cm <sup>-1</sup> )	Toluene	238095			103092
	CHCl <sub>3</sub>	151515	192307	63157	84745
	THF	156250	166666		87719
	EtOAc	153846	101010	158730	86206
	Acetone	116279	96153	149253	74626
	MeOH	142857	78740	78125	71942
	MeCN	98039	89285	108695	72992
Slope, $m$ (cm <sup>-1</sup> )		384348	647534	902372	101567
$\Delta\mu$ (D)		28.5	43.5	53.1	17.8

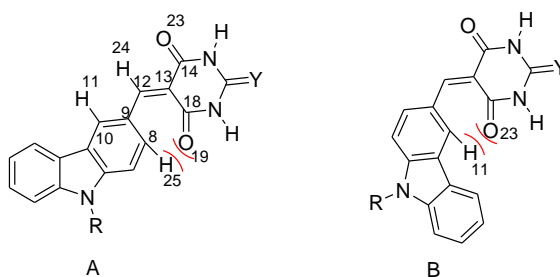
This unusual behaviour of CTBA along with the marked difference in the absorption and emission characteristics prompted us to undertake a detailed theoretical study of this molecule.

CTBA can exist in various forms such as the neutral form, a zwitterionic form, and in three different tautomeric forms (Scheme 2.7). Relative proportions of these forms depend on the nature of the solvents used. For example, zwitterionic form is more probable in polar solvents and tautomeric forms to get stabilized or destabilized by hydrogen bonding interactions. In order to get more insight into these aspects, we have carried out DFT and TD-DFT calculations at 6-311G (2d, p) level<sup>11,12</sup> on a model N-methylated carbazole derivative considering the higher time required for the computational work on n-octyl substituted

derivative (CTBA). The calculations were carried out for acetonitrile medium by using polarizable continuum model (PCM). The results of the calculations are presented in the Table 2.4 and 2.5. Both CBA and CTBA molecules show a planar geometry in the ground state for the neutral form, zwitterionic form and the tautomeric form III. Scheme 2.8 shows two possible planar conformers for the neutral form. Here two important steric interactions raise the energy of the planar conformer. In conformer A, there is steric interaction between the H25 and carbonyl oxygen O19. Similarly in conformer B, the steric interaction is between H11 and O23. The atom numbering used was taken from the z-matrix used for the DFT calculations. The results of the DFT calculations show that, conformer A is the lowest energy one where the steric interaction is minimized by adopting a wide angle (angle C9-C12-C13~138°-139°) for the bridging  $sp^2$  hybridized methylene carbon.



**Scheme 2.7** Different structural forms possible for CBA and CTBA



**Scheme 2.8** The two planar conformers for the neutral form

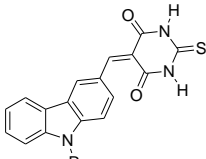
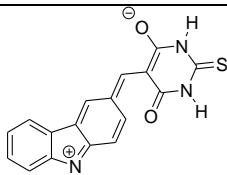
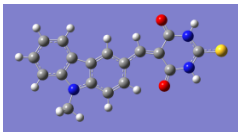
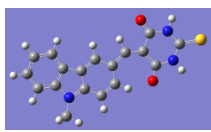
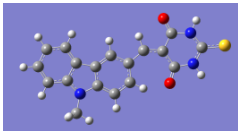
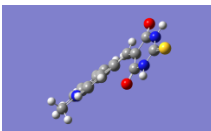
This wide angle is adopted by both CBA and CTBA in their neutral form, zwitterionic form and in the tautomeric form I and thus maintains a planar geometry. The tautomeric forms II and III adopt a

twisted geometry and thus relieve the excessive steric strain arising from the change of hybridization from  $sp^2$  hybrid O19 carbonyl oxygen to  $sp^3$  hybrid enolic oxygen. The dipole moments calculated for the tautomeric form I and II were  $\sim 5$  Debye units higher than that obtained for the neutral form. Moreover, the energy difference between the neutral and the tautomeric forms was  $\sim 16$  kcal/mol making their inter-conversion by intramolecular proton transfer facile. This intramolecular proton transfer may occur even in the excited state via Excited State Intramolecular Proton Transfer (ESIPT) pathway reported for such systems where tautomeric forms are possible. Due to the higher dipole moment for the tautomeric form, they may get stabilized by polar aprotic or polar protic solvents.

The results of the calculations for both CBA and CTBA in their neutral and zwitterionic forms gave identical results and show no difference between the respective neutral and zwitterionic forms. Both forms gave identical energies, dipole moments and molecular orbitals. TD-DFT calculations also gave identical excitation energies and UV-Vis absorption transitions. CBA gave excellent correlation with the experimental absorption spectrum in acetonitrile. Since there is no difference in the electronic properties of neutral and zwitterionic forms, it is safer to assume a dipolar charge transfer model for the ground state molecule considering the solvatochromic responses of CBA. However calculated data obtained for CTBA showed marked deviation from the experimental values. In the case of CTBA, HOMO and LUMO are delocalized over carbazole and thiobarbituric acid moieties. HOMO has its largest coefficients contributed by carbazole and LUMO has major

contribution from thiobarbituric acid. HOMO-1 is less delocalized over thiobarbituric acid and mainly located on carbazole. LUMO+1 is also a carbazole centered orbital. The lowest energy electronic state calculation shows electronic transitions based on HOMO-1 to LUMO transition as well as between HOMO and LUMO. Based on the orbitals involved, this transition is having a  $\pi$ - $\pi^*$  character and involves a charge shift from carbazole to thiobarbituric acid typical for such molecules with ICT character.

**Table 2.4.** Comparison of the electronic properties of various forms of CTBA obtained by DFT and TD-DFT calculations.

Property	 Neutral Form	 Zwitterionic Form
Heat of Formation	-38.29 keV	-38.29 keV
Dipole moment, (Debye)	12.5896 Debye	12.5907 Debye
UV-Vis Absorption	457.86 (0.8675, $\pi$ - $\pi^*$ ) 422.41 (0.2640, $\pi$ - $\pi^*$ )	457.85 (0.8674, $\pi$ - $\pi^*$ ) 422.41 (0.2640, $\pi$ - $\pi^*$ )
Emission	553.08 (0.5990, $\pi$ - $\pi^*$ )	565.57 nm (0.4357, $\pi$ - $\pi^*$ )
Optimized Geometry (Ground State)		
Optimized Geometry (Excited State)		



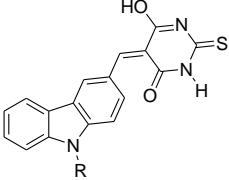
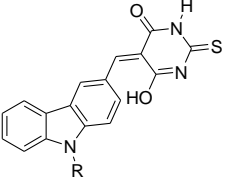
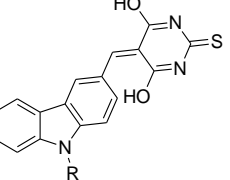

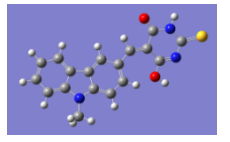
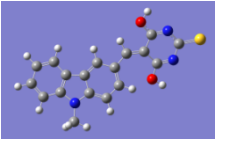

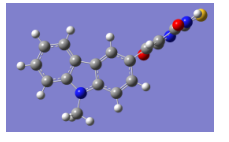
Property	 Tautomeric Form I	 Tautomeric Form II	 Tautomeric Form III
Heat of Formation	-38.29 keV	-38.29 keV	-38.28 keV
Dipole moment, (Debye)	17.40 Debye	18.26 Debye	21.94 Debye
UV-Vis Absorption (Oscillator Strength, nature of transition)	512.99 nm (0.0000, $\pi$ - $\pi^*$ ) 472.19 nm (1.1633, $\pi$ - $\pi^*$ ) 431.14 nm (0.2356, $\pi$ - $\pi^*$ ) 617.59 nm (0.0000, $\pi^*$ -n)	525.5 nm (0.0001, n- $\pi^*$ ) 495.46 nm (1.1029, $\pi$ - $\pi^*$ ) 456.55 nm (0.2022, $\pi$ - $\pi^*$ ) 867.95 nm (0.0000, $\pi^*$ - $\pi$ )	646.87 nm (0.0001, n- $\pi^*$ ) 510.97 nm (1.3213, $\pi$ - $\pi^*$ ) 470.19 nm (0.1808, $\pi$ - $\pi^*$ )
Emission (Oscillator Strength, nature of transition)	561.32 nm (1.5758, $\pi^*$ - $\pi$ ) 492.16 nm (0.1182, $\pi^*$ - $\pi$ ) 432.71 nm (0.0104, $\pi^*$ - $\pi$ )	602.3 nm (0.0000, $\pi^*$ - $\pi$ ) 576.15 nm (0.0000, $\pi^*$ -n) 425.44 nm (0.7849, $\pi^*$ - $\pi$ )	
Optimized Geometry (Ground State)			
Optimized Geometry (Excited State)			

Table 2.5 MOs of N- methyl substituted CTBA

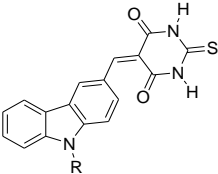
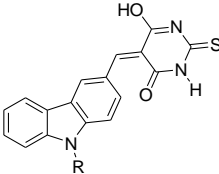
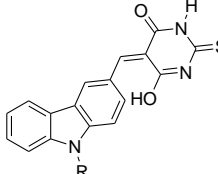
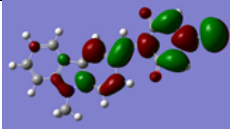
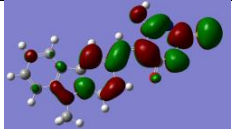
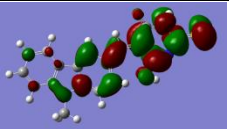
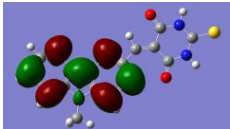
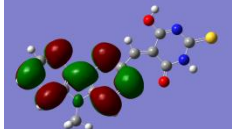
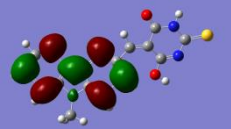
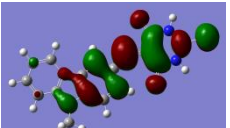
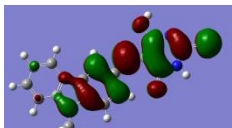
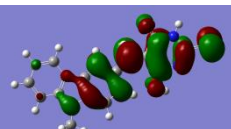
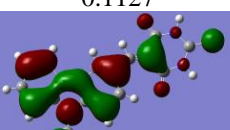
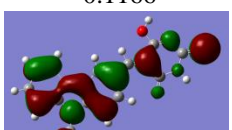
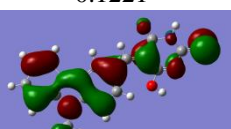
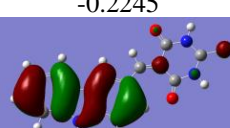
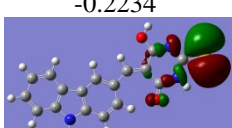
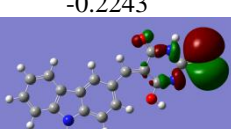
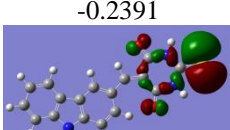
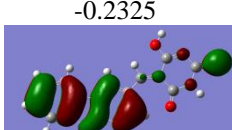
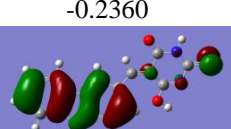
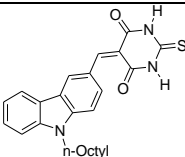
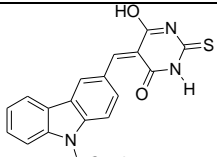
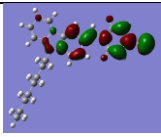
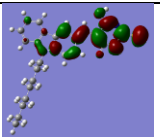
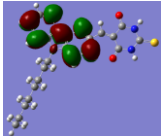
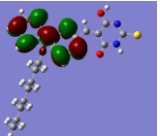
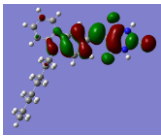
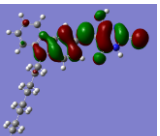
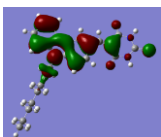
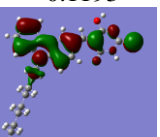
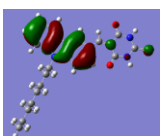
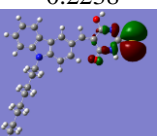
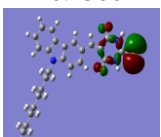
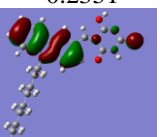
HOMO/ LUMO (Orbital Number)	 Neutral Form	 Tautomeric Form 1	 Tautomeric Form 2
LUMO+2 (90)	 -0.0472	 -0.0415	 -0.0467
LUMO+1 (89)	 -0.0547	 -0.0531	 -0.0574
LUMO (88)	 0.1127	 -0.1166	 -0.1221
HOMO (87)	 -0.2245	 -0.2234	 -0.2243
HOMO-1 (86)	 -0.2391	 -0.2325	 -0.2360
HOMO-2 (85)	 -0.2461	 -0.2402	 -0.2400

Table 2.6 MOs of CTBA

HOMO/LUMO(Orbital Number)	 Neutral	 Tautomeric form 1
LUMO+1	 -0.0472	 -0.0455
LUMO+1 (89)	 -0.0547	 -0.0558
LUMO (88)	 -0.1127	 -0.1193
HOMO (87)	 -0.2236	 -0.2238
HOMO-1 (86)	 -0.2386	 -0.2351
HOMO-2 (85)	 -0.2461	 -0.2394

Tautomeric forms also share similar orbitals as found in the neutral form or zwitterionic form. However, there is a reordering of

energy levels and in these forms; the HOMO-1 is now the non-bonding lone pair orbital on the thiocarbonyl sulfur atom. In general, tautomerization leads to destabilization of the HOMO and stabilization of the LUMO in all tautomeric forms. This destabilization is partly due to the increasing twist angle between the Donor and acceptor moieties causing lesser overlap between  $\pi$  type orbitals. Table 2.4 and 2.5 shows a comparison of frontier orbitals of neutral form and the three tautomeric forms (I - III).

TD-DFT calculations provided insights on how these forms contribute to the excited state properties of CTBA. Though computationally expensive, calculations at the 6-311G (2d, p) level gave better correlations with the experimental data. The results show significant lowering in the excitation energy of the  $\pi$ - $\pi^*$  transitions in these forms along with significant involvement of a new a weakly allowed n- $\pi^*$  transition at 525 nm. This n- $\pi^*$  transition involve nonbonding sulfur lone pair orbital and LUMO in the twisted tautomeric form II. This becomes significant due to the increasing twist angle between the donor and the acceptor moieties in the tautomeric forms making the forbidden n- $\pi^*$  transition allowed. In terms of energy this transition further shifts to 646nm in form III. In form II and III, twisting is due to the steric strain due to buttressing of sp<sup>3</sup> hybrid enolic O-atom with the C-H on the carbazole ring. In comparison to the planar forms in form II and III this this twisting is preferred between the carbazole and the thiobarbituric acid moiety rather than a widening of the C-C-C bond angle of the methylene bridge. Other transitions are also affected due to this twist and occur the reordering of energy levels. The charge transfer

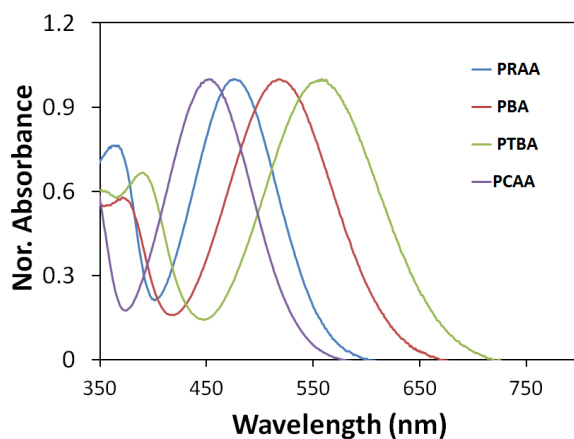
transition of the  $\pi$ - $\pi^*$  type also shows progressive red shift in tautomeric form I-III. Based on these results and the observed experimental data, it can be assumed that the CTBA molecule adopts a tautomeric form preferably the form I or II in solution with slight twist making the  $n$ - $\pi^*$  transitions weakly allowed. This explains the appearance of a shoulder around 510 nm and the absorption maximum at 567 nm in the experimental spectrum obtained for CTBA in acetonitrile. This also explains similar results obtained in other solvents. Additional evidence exists in the  $^1\text{H}$  NMR spectrum recorded in DMSO- $d_6$ . The spectrum shows evidence for the existence of tautomeric forms, as an additional peak at  $\delta$  12.23 ppm along with the peaks corresponding to the NH protons of thiobarbituric acid moiety (Figure 2.29)

The TD-DFT calculations with geometry optimization in the excited state gave a clearer picture on the allowed radiative transitions (emission) from the excited state. The optimized geometry obtained for the neutral form was a planar one and the lowest energy radiative transition calculated was at 553 nm. The optimized geometry for the zwitterionic form shows a twist between the carbazole and the thiobarbituric acid moiety and the calculated radiative transition is at 565 nm, which is red shifted compared to that calculated for the neutral form. The tautomeric form I also shows a planar excited state and a strongly allowed emission at 561 nm. This form also showed a weak radiative transition around 617 nm and this transition is mainly between the LUMO and the orthogonal nonbonding orbital. In tautomeric form II, the excited state geometry is a  $90^\circ$  twisted excited state, where the carbazole and barbituric acid moieties were orthogonal to each other. In this case,

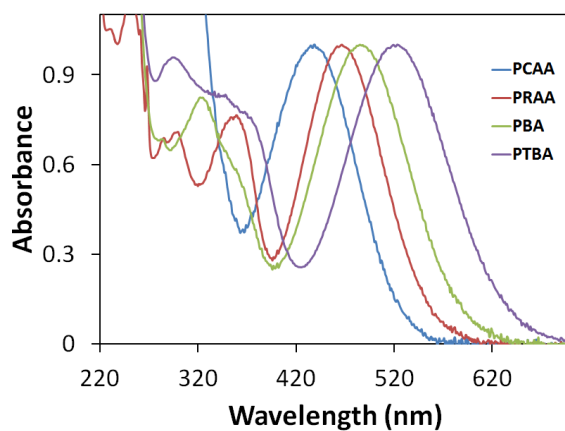
four significant radiative transitions were noted. Three weakly allowed transitions at 867.95 nm (0.0000), 602.3 nm (0.0000) and 576.15 nm (0.0002) and a strongly allowed transition at 425.44 nm (0.7849). All transitions except the one at 576 nm are between  $\pi$  type orbitals. The one calculated at 576 nm is between the LUMO and the nonbonding orbital on sulfur atom of the thiocarbonyl group. The average emission maximum observed for this transition in the intermediate geometries obtained was about 600 nm. This data correlate with the experimentally observed emission maximum in MeCN which was at 604 nm and similar maximum was observed in MeOH (608 nm) and  $\text{CHCl}_3$  (600 nm). Moreover, the theoretical radiative transition at 425.44 nm correlates with the experimentally observed higher energy band at 427 nm. These results further support the experimentally observed dual emission characteristics of CTBA in various solvents. The emission band around 427 nm was also found to be not affected by the solvent polarity ruling out any potential charge transfer nature. The orbitals involved in this transition are the more delocalized LUMO and the carbazole based  $\pi$  type HOMO-3 orbital. The fine structure observed in this emission band further supports this argument. The second red shifted emission band responds to the solvent polarity and this is supported by the charge transfer character of this transition. This band is an envelope of transitions involving the  $\pi$  type delocalized LUMO to the delocalized  $\pi$  type HOMO and an orthogonal nonbonding (n-type) orbital which are known to be stabilized by polar solvents causing prominent solvatochromic effects in emission. Thus, the theoretical data find agreement between the experimental absorption maximum (467 nm) with

a shoulder at 510 nm and the dual emission characteristics with bands at 425 nm and the second red shifted emission maximum around 600 nm. The study points to the fact that, there exists a tautomeric pre-twisted ground state and a twisted excited state with a greater role of the non-bonding lone pair orbital on thiocarbonyl group contributes in the photophysical properties of CTBA. The longer fluorescence lifetime (0.58 ns) and one order higher fluorescence quantum yield (0.01) observed for the 604 nm emission in acetonitrile further supports the twisted and a more stabilized excited state. Similar results due to twisting of geometry were observed in the case of cyanine and polymethine dyes.<sup>13-16</sup> **In summary, the absorption and emission behavior of CTBA depend on the relative orientation of the donor and the acceptor groups and possess two experimentally observable emissive states, which are carbazole based excited state (CE) and twisted intramolecular charge transfer state (TICT) involving radiative transition between the LUMO and nonbonding orbital.**

### 2.3.2.4 Absorption Properties of Phenothiazine Dyes



**Figure 2.15** Absorption spectra of Phenothiazine compounds in  $\text{CHCl}_3$



**Figure 2.16** Absorption spectra of phenothiazine compounds in MeCN.

Absorption spectra of phenothiazine dyes PCAA, PRAA, PBA and PTBA show similar ICT character as seen in the carbazole type dyes CCAA, CRAA, CBA and CTBA. The absorption spectrum was shifted to longer wavelength with increasing electron affinity of the acceptor



moiety. For example, the cyanoacetic acid conjugate, PCAA showed an absorption maximum of 450 nm in chloroform and the thiobarbituric acid conjugate PTBA at 553 nm. In a polar solvent like acetonitrile, all spectra showed a blue shift. The blue shift was about 10 nm for PCAA and PRAA whereas the spectra was shifted to blue region by 36 nm and 30 nm respectively for PBA and PTBA. Similar to carbazole dyes, PCAA, PRAA, PBA and PTBA showed an unusual solvent dependent blue shift in hydrogen bond accepting solvents such as ethyl acetate compared to acetonitrile.

The broad absorption spectrum of PBA and PTBA overlaps well with the visible region of the solar spectrum. This is advantageous as these dyes can be used as sensitizers in solar energy harvesting applications. The extinction coefficients of the phenothiazine dyes were determined and the values were slightly lower than that observed for carbazole dyes. The absorption maximum and the molar extinction coefficients of all compounds are listed in Table 2.6. The next chapter discusses the results of our studies on the photovoltaic properties of both carbazole and phenothiazine based donor – acceptor systems.

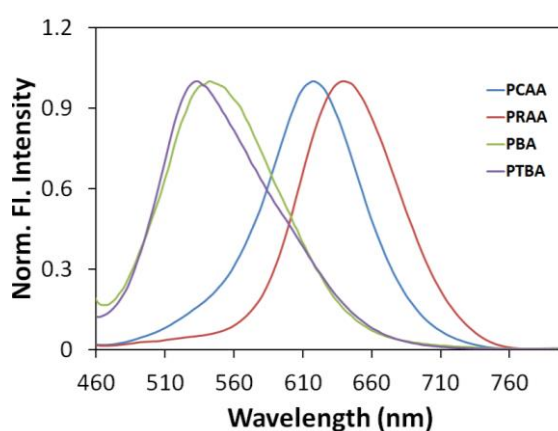
**Table 2.6** Absorption spectral properties of n-octylphenothiazine based D- $\pi$ -A systems

	PCAA		PRAA		PBA		PTBA	
	$\lambda_{\text{abs}}$ (nm)	$\epsilon_{\text{max}}$ ( $\text{cm}^{-1}\text{M}^{-1}$ ) $\times 10^4$	$\lambda_{\text{abs}}$ (nm)	$\epsilon_{\text{max}}$ ( $\text{cm}^{-1}\text{M}^{-1}$ ) $\times 10^4$	$\lambda_{\text{abs}}$ (nm)	$\epsilon_{\text{max}}$ ( $\text{cm}^{-1}\text{M}^{-1}$ ) $\times 10^4$	$\lambda_{\text{abs}}$ (nm)	$\epsilon_{\text{max}}$ ( $\text{cm}^{-1}\text{M}^{-1}$ ) $\times 10^4$
Toluene	438	1.94	465	2.0	490	1.31	525	1.33
CHCl <sub>3</sub>	450	1.98	477	1.72	521	1.27	553	1.23
THF	440	1.97	467	1.91	479	1.20	510	1.24
EtOAc	440	2.15	462	2.01	478	1.28	510	1.27
MeOH	432	1.76	467	1.94	490	1.25	525	1.25
Acetone	441	2.20	467	2.06	481	1.27	518	1.27
MeCN	439	1.93	467	2.17	485	1.15	523	1.29

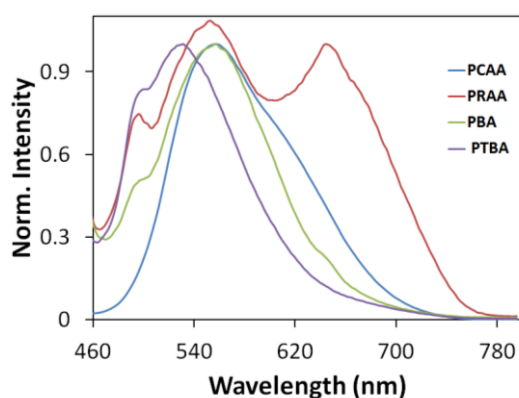
### 2.3.2.5 Emission Properties of Phenothiazine Dyes

All the compounds show weak emission spectra with negligible solid state luminescence except PCAA. The emission properties of the phenothiazine dyes were recorded in different solvents. PCAA and PRAA showed emission band around 600 nm with significant polarity dependence showing the charge transfer nature of the state involved. Figure 2.17 and 2.18 show the emission spectra of phenothiazine dyes in chloroform and acetonitrile respectively. PRAA, PBA and PTBA showed two emission bands as observed in the case of CTBA (Figure 2.9, 2.10 2.11 and § 2.3.2.2). For PRAA this property was mainly observed in acetone and acetonitrile. For PBA the dual emission property was observed in nonpolar and hydrogen bond accepting solvents. PTBA showed dual emission properties only in cyclohexane. The observed data is insufficient to draw conclusions on the nature of the excited states of these molecules. Based on the results obtained in the case of CTBA, a

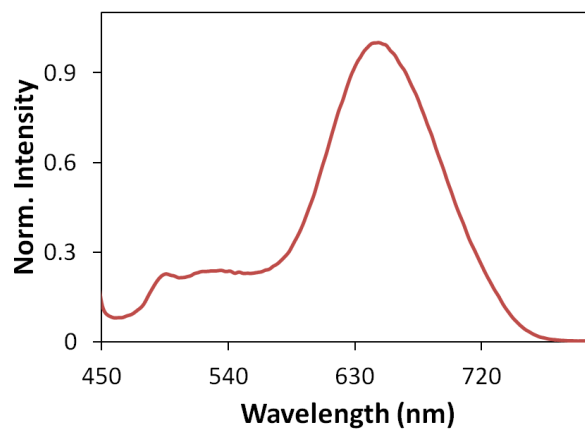
fair assumption is that, these molecules do possess two emissive states: one based on the phenothiazine and the other predominantly of charge transfer nature involving a delocalised LUMO and the nonbonding orbitals on the carbonyl or thiocarbonyl groups in the rhodanine, barbituric acid or thiobarbituric acid groups.



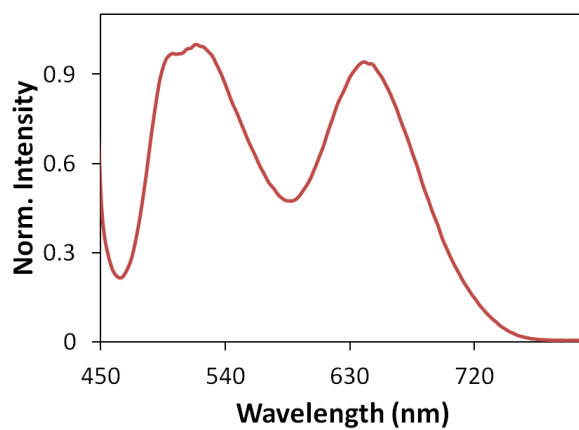
**Figure 2.17** Emission spectrum of phenothiazine compounds in  $\text{CHCl}_3$ ,  $\lambda_{\text{ex}} = 440 \text{ nm}$



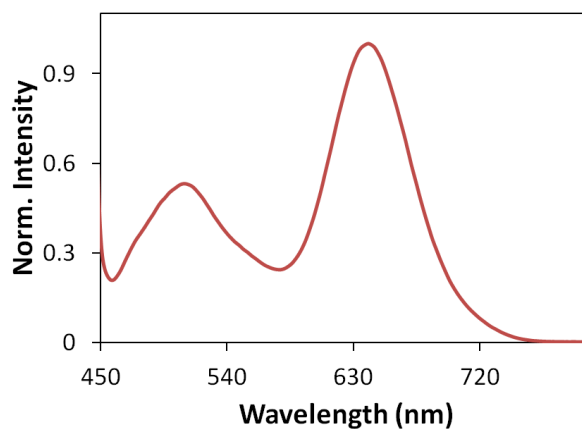
**Figure 2.18** Emission spectrum of phenothiazine compounds in  $\text{MeCN}$ ,  $\lambda_{\text{ex}} = 440 \text{ nm}$



**Figure 2.19** Emission spectrum of PRAA in acetone,  $\lambda_{\text{ex}} = 440$  nm



**Figure 2.20** Emission spectrum of PBA in toluene,  $\lambda_{\text{ex}} = 440$  nm



**Figure 2.21** Emission spectrum of PTBA in cyclohexane,  $\lambda_{\text{ex}} = 440$  nm

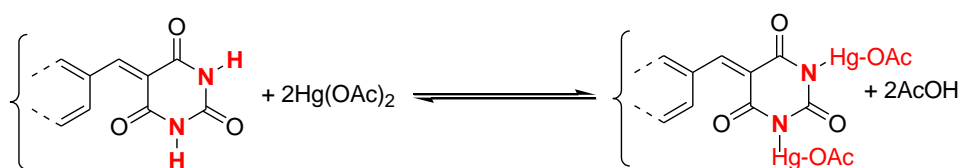
**Table 2.7** Emission spectral properties of n-octylcarbazole based D- $\pi$ -A systems.

	PCAA	PRAA	PBA	PTBA	
	$\lambda_{\text{max}}$ (nm)	$\lambda_{\text{max}}$ (nm)	$\lambda_{\text{max}}$ (nm)	$\lambda_{\text{max}}$ (nm)	
Cyclohexane	558	557	475, 607	510, 641	
Toluene	600	602	511, 634	527	
THF	602	629	533, 627	495	
CHCl <sub>3</sub>	618	639	554	533	
EtOAc	604	627	527, 640	517	
MEOH	593	617	570	492	
Acetone	617	517, 646	524	529	
MECN	557	517, 645	544	531	
$\tau$ (ns)*	0.458 (47.68)	4.71 (52.32)	1.74 (18.41)	5.06 (72.05)	0.0238 (9.54)
$\phi_f^*$	0.261	0.002	0.003	0.004	

\* Solvent: acetonitrile. Values in parenthesis are contributions in % to the overall decay.

### 2.3.3. A Survey of Mercury Binding Studies of Carbazole and Phenothiazine Dyes

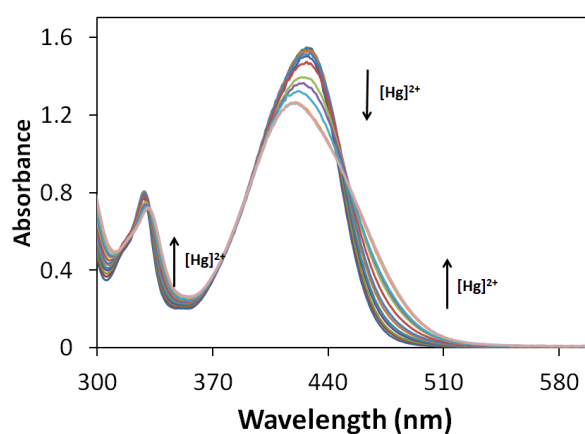
In order to verify the metal binding capability as stated in the objectives, we have made a quick survey of the mercury binding properties of the barbituric acid (CBA & PBA) and thiobarbituric acid (CTBA & PTBA) conjugate compounds by UV-Vis spectroscopy. The spectra obtained in the presence of Hg (II) acetate in THF were compared with the spectra obtained in the absence of Hg (II) acetate. Figures 2.22, 2.23, 2.24 & 2.25 show the effect of Hg (II) acetate on the absorption spectrum of CBA, CTBA, PBA and PTBA respectively. Except CBA, all compounds responded with a slight redshift in the absorption maximum with a broadened spectral profile along with visual colour changes. CBA however showed a slight blue shift in the absorption maximum in the presence of Hg (II) acetate. The interaction of the dye with the Hg (II) acetate is expected to be according to the acid-base equilibrium illustrated in Scheme 2.9 as barbituric acid and thiobarbituric acid are acidic enough to cause protonation of Hg (II) acetate.



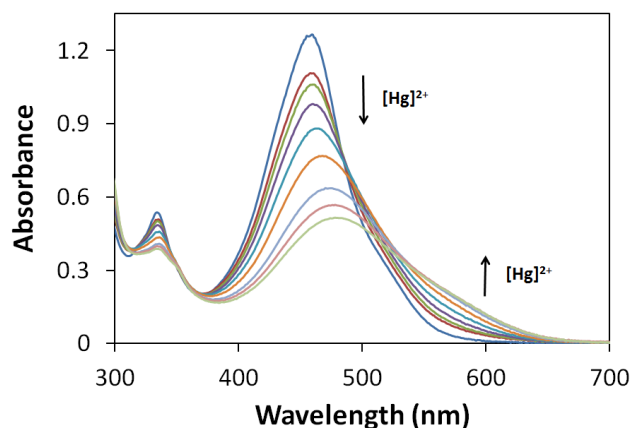
**Scheme 2.9** Proposed binding interaction of mercuric acetate with barbituric acid moiety

Due to the presence of multiple binding sites, the proposed binding interaction may involve different stoichiometry. The exact

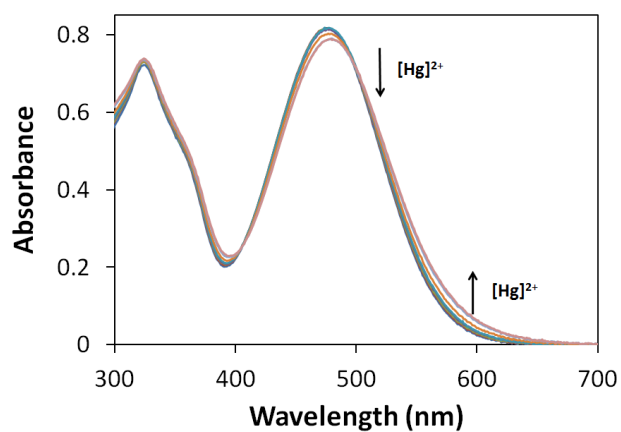
mechanism of binding and stoichiometry can be established through a systematic study of UV-Vis, Fluorescence and  $^1\text{H}$  NMR spectra in the presence of varying concentration of the Hg (II) acetate or other metal salts. We choose CBA and CTBA as the probes as their photophysical properties are well established by theory and supporting experimental data. The results of these studies are presented in Chapter 4 and 5.



**Figure 2.22** Evolution of absorption spectra of CBA in the presence of an aqueous solution of Hg (OAc) $_2$  in THF ([CBA] = 35.6  $\mu\text{M}$ , [Hg (OAc) $_2$ ] = 0–25  $\mu\text{M}$ )

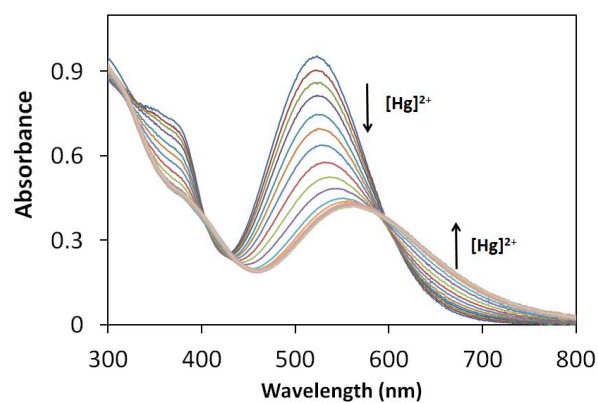


**Figure 2.23** Evolution of absorption spectra of CTBA in the presence of an aqueous solution of  $\text{Hg}(\text{OAc})_2$  in THF ( $[\text{CTBA}] = 23 \mu\text{M}$ ,  $[\text{Hg}(\text{OAc})_2] = 0\text{--}72 \mu\text{M}$ )



**Figure 2.24** Evolution of absorption spectra of PBA in the presence of an aqueous solution of  $\text{Hg}(\text{OAc})_2$  in THF ( $[\text{PBA}] = 73 \mu\text{M}$ ,  $[\text{Hg}(\text{OAc})_2] = 0\text{--}55 \mu\text{M}$ )





**Figure 2.25** Evolution of absorption spectra of PTBA in the presence of an aqueous solution of  $\text{Hg}(\text{OAc})_2$  in THF ( $[\text{PTBA}] = 52 \mu\text{M}$ ,  $[\text{Hg}(\text{OAc})_2] = 0\text{--}73 \mu\text{M}$ )

## 2.4 Conclusions

Eight D- $\pi$ -A compounds having either N-octyl carbazole or N-octyl phenothiazine as the donor and cyanoacetic acid, rhodanine-3-acetic acid, barbituric acid or thiobarbituric acid as the acceptor units were synthesised and characterised. The intramolecular charge transfer nature of their excited states were characterised by UV-Vis absorption spectroscopy and fluorescence spectroscopy. Marked difference in the absorption and emission properties of CTBA was studied in detail by DFT calculations at the 6-311+ G (2d,p) level. Tautomerization and subsequent reordering of HOMO levels was attributed to the difference in the absorption spectral properties in comparison to CBA. The dual emission behaviour was attributed to a twisted excited state geometry for the tautomeric form. All barbituric acid and thiobarbituric acid conjugates showed affinity to heavy metal ion such as Hg<sup>2+</sup>. The suitable electronic properties and the metal ion binding behaviour make them suitable for photovoltaic applications or as chemosensors for heavy metal ion detection.

## 2.5. Experimental Section

### 2.5.1 General Techniques

All reactions were carried out using oven dried glasswares. The solvents used were distilled and dried prior to use. All reagents and starting materials were purchased from either Sigma-Aldrich or Spectrochem Pvt. Ltd and were used as received. Progress of the reaction and chromatographic separations were monitored by dried and activated fluorescent silica gel TLC plates (Aluminium sheets coated with silica gel, E. Merck). Visualisation of TLC plates was made by exposure to iodine vapours or UV lamp. Separation and purification of compounds were done by column chromatography using silica gel (Spectrochem Pvt. Ltd, 60-120 mesh). The products were further purified by recrystallization from suitable solvent systems. Fractions collected in the column chromatography or in preparation steps were concentrated using IKA- RV-10B rotary evaporator. Melting points are uncorrected and were determined on a Neolab melting point apparatus. The  $^1\text{H}$  and  $^{13}\text{C}$  NMR spectra were recorded using 400 MHz Bruker Avance III FT-NMR spectrometer with tetramethylsilane (TMS) as internal standard. Chemical shifts ( $\delta$ ) are reported in parts per million (ppm) downfield of TMS. High resolution mass spectra of new compounds were obtained using a WATERS SYNAPT G2S spectrometer. Absorption spectra were recorded using Evolution 201 UV-visible spectrophotometer. Fluorescence spectra were recorded using a Perkin Elmer fluorescence spectrophotometer (model LS 45).

9-octyl-9*H*-carbazole (93%, mp: 45 °C Lit: 46-47), 9-Octyl-9*H*-carbazole-3-carbaldehyde (**9**, 84%, mp 55 °C: Lit: 54-56 °C), 10-Octyl-10*H*-phenothiazine (90%, mp 48 °C: Lit: 48 °C) and 10-Octyl-10*H*-phenothiazine-3-carbaldehyde (85%, mp 50 °C: Lit: 50-52 °C) were prepared according to reported procedures.<sup>17-19</sup>

### 2.5.2 Synthesis of 2-cyano-3-(9-octyl-9*H*-carbazol-3-yl)acrylic acid (CCAA)

A mixture of precursor **58** (0.5g, 1.6 mmol) and cyanoacetic acid **11** (0.69g, 8.14 mmol) in acetic acid (5 mL) was refluxed in the presence of ammonium acetate (0.62 g) overnight under N<sub>2</sub> atmosphere. The product was filtered and washed with hot hexane and ether. Yield: 0.43g (70 %). mp 146°C; FT- IR (cm<sup>-1</sup>) 1628, 2217, 2856, 3437. <sup>1</sup>H NMR (400 MHz, DMSO-d<sub>6</sub>) δ (ppm): 0.80 (t, 3H), 1.16–1.25 (m, 10H), 1.77–1.80 (m, 2H), 4.45 (t, 2H), 7.32 (t, 1H), 7.53 (t, 1H), 7.70 (d, 2H), 7.80 (d, 1H), 8.16 (d, 1H), 8.27 (d, 1H), 8.46 (s, 1H), 8.85 (s, H); <sup>13</sup>C NMR (DMSO d<sub>6</sub>) δ (ppm): 13.83, 21.95, 26.29, 28.39, 28.49, 28.59, 31.06, 42.59, 98.30, , 110.29, 117.27, 120.34, 120.60, 121.94, 122.27, 122.48, 125.50, 126.91, 127.72, 140.73, 142.73, 155.26, 164.12, 179.19; HRMS (ESI MS) m/z: theoretical: 375.2073, found: 375.2058 ([M + H]<sup>+</sup> detected

### 2.5.3 Synthesis of 2-(5-((9-octyl-9*H*-carbazol-3-yl)methylene)-4-oxo-2-thioxothiazolidin-3-yl)acetic acid (CRAA)

A mixture of precursor **58** (0.5g, 1.6 mmol) and rhodamine-3-acetic acid **12** (0.307g, 8.14 mmol) in acetic acid (5 mL) was refluxed in

the presence of ammonium acetate (0.62 g) overnight under N<sub>2</sub> atmosphere. The precipitate was collected and washed with ether to yield 0.48g (62 %). mp 218 °C; FT- IR (cm<sup>-1</sup>) 1235, 1448, 1708, 2990, 3434. <sup>1</sup>H NMR (400 MHz, DMSO-d<sub>6</sub>) δ (ppm): 0.85 (t, 3H), 1.23–1.37 (m, 10H), 1.83–1.89 (m, 2H), 4.13 (s, 1H), 4.29 (t, 2H), 4.94 (s, 2H), 7.29 (m, 1H), 7.44 (t, 2H), 7.52 (t, 1H), 7.59 (d, 1H), 8.00 (s, 1H), 8.10 (d, 1H), 8.23 (s, 1H); <sup>13</sup>C NMR (DMSO d<sub>6</sub>) δ (ppm): 13.83, 21.95, 26.29, 28.39, 28.49, 28.59, 31.06, 42.59, 98.30, , 110.29, 117.27, 120.34, 120.60, 121.94, 122.27, 122.48, 125.50, 126.91, 127.72, 140.73, 142.73, 155.26, 164.12, 179.19; HRMS (ESI MS) m/z: theoretical: 481.1620, found: 481.1615 ([M + H]<sup>+</sup> detected).

#### 2.5.4 Synthesis of 5-((9-octyl-9H-carbazol-3-yl)methylene)pyrimidine-2,4,6(1H,3H,5H)-trione (CBA)

CBA was synthesized according to a reported procedure<sup>8</sup> by Knoevenagel condensation between 9-octyl-9H-carbazole-3-carbaldehyde and barbituric acid in ethanol. Yield: 85%. mp 268°C, FT-IR (cm<sup>-1</sup>) 1664, 2924, 3432. <sup>1</sup>H NMR (DMSO d<sub>6</sub>) δ (ppm): 0.80 (t, 3H), 1.17–1.28 (m, 10H), 1.75–1.81 (m, 2H), 4.45 (t, 2H), 7.31 (t, 1H), 7.52 (t, 1H), 7.65 (dd, 2H), 8.18 (d, 1H), 8.53 (s, 1H), 8.60 (dd, 1H), 9.30 (s, 1H), 11.15 (s, 1H), 11.27 (s, 1H); <sup>13</sup>C NMR (DMSO d<sub>6</sub>) δ (ppm): 13.84, 21.94, 26.34, 28.45, 28.51, 28.62, 31.08, 42.61, 109.24, 110.22, 114.06, 120.42, 120.47, 122.18, 122.38, 123.43, 126.69, 129.46, 133.27, 140.75, 143.12, 150.23, 156.86, 162.37, 164.18; HRMS (ESI MS) m/z: theoretical: 418.2125, found: 418.2115 ([M + H]<sup>+</sup> detected).

### 2.5.5 Synthesis of 5-((9-octyl-9H-carbazol-3-yl)methylene)-2-thioxodihydropyrimidine-4,6(1H,5H)-dione (CTBA)

CTBA was also synthesized according to a reported procedure<sup>8</sup> by Knoevenagel condensation between 9-octyl-9H-carbazole-3-carbaldehyde and thiobarbituric acid in ethanol. Yield: 80%. mp 276 °C, FT- IR (cm<sup>-1</sup>) 1533, 1642, 2922, 3436. <sup>1</sup>H NMR (DMSO d<sub>6</sub>) δ (ppm): 0.80 (t, 3H), 1.12–1.35 (m, 10H), 1.75–1.81 (m, 2H), 4.45 (t, 2H), 7.31 (t, 1H), 7.56 (t, 1H), 7.70 (m, 2H), 8.20 (d, 1H), 8.56 (s, 1H), 8.70 (m, 1H), 9.36 (s, 1H), 12.27 (s, 1H), 12.36 (s, 1H); <sup>13</sup>C NMR (DMSO d<sub>6</sub>) δ (ppm): 13.84, 21.94, 26.33, 28.44, 28.51, 28.62, 31.08, 42.61, 109.41, 110.34, 114.02, 120.42, 120.47, 120.64, 122.18, 122.35, 122.93, 123.62, 126.82, 130.05, 133.74, 140.78, 142.41, 143.56, 157.95, 160.14, 162.49, 178.10; HRMS (ESI MS) m/z: theoretical: 437.2137, found: 437.1669 ([M + 4H]<sup>+</sup> detected).

### 2.5.6 Synthesis of 2-cyano-3-(10-octyl-10H-phenothiazin-3-yl)acrylic acid (PCAA)

PCAA was synthesized according to a reported procedure<sup>20</sup> by Knoevenagel condensation between 9-octyl-9H-carbazole-3-carbaldehyde (**59**) and cyanoacetic acid in the presence of ammonium acetate in acetic acid. Yield: 75%. mp-140 °C (Lit: 138-140 °C). FT- IR (cm<sup>-1</sup>) 1671, 2233, 2854, 3432. <sup>1</sup>H NMR (DMSO d<sub>6</sub>) δ (ppm): 0.80 (t, 3H), 1.30–1.38 (m, 8H), 1.70–1.77 (m, 4H), 3.80 (t, 2H), 4.48 (s, 1H), 6.8 (m, 2H), 6.91 (dd, 1H), 7.00 (t, 1H), 7.10 (t, 1H), 7.6 (s, 1H), 7.82 (d, 1H), 8.00 (s, 1H); <sup>13</sup>C NMR (DMSO d<sub>6</sub>) δ (ppm): 14.06, 22.59, 26.73, 26.80, 29.12, 29.16, 31.70, 48.12, 114.96, 115.92, 123.31, 123.86,

124.77, 125.34, 127.59, 127.63, 130.45, 131.86, 142.84, 150.27, 154.58, 192.70,; HRMS (ESI MS) m/z: theoretical: 407.1793, found: 407.1785 ([M + H]<sup>+</sup> detected)

### 2.5.7 Synthesis of 2-(5-((10-octyl-10H-phenothiazin-3-yl)methylene)-4-oxo-2-thioxothiazolidin-3-yl)acetic acid (PRAA)

PRAA was also synthesized according to a reported procedure<sup>21</sup> by Knoevenagel condensation between 9-octyl-9H-carbazole-3-carbaldehyde (**59**) and rhodanine-3-acetic acid in presence of ammonium acetate in acetic acid, Yield: 80%. mp 244 °C FT- IR (cm<sup>-1</sup>) 1248, 1458, 1703, 2982, 3422. <sup>1</sup>H NMR (DMSO d<sub>6</sub>) δ (ppm): 0.79 (t, 3H), 1.18–1.2 (m, 8H), 1.70–1.77 (m, 4H), 3.28(s,1H), 3.79 (t, 2H), 4.84 (s, 1H), 6.80 (m, 2H), 6.90 (m, 1H,), 7.08 (t, 1H), 7.12 (t, 1H), 7.20 (s, 1H), 7.22 (d, 1H), 7.56 (s, 1H); <sup>13</sup>C NMR (DMSO d<sub>6</sub>) δ (ppm): 14.06, 22.59, 26.76, 26.83, 29.13, 29.16, 31.70, 44.27, 47.92, 115.35, 115.79, 119.28, 123.47, 125.51, 127.21, 127.58, 129.28, 130.94, 133.40, 143.43, 147.83, 167.07, 169.91, 192.70 ; HRMS (ESI MS) m/z: theoretical: 513.1340, found: 513.1380 ([M + H]<sup>+</sup> detected)

### 2.5.8 Synthesis of 5-((10-octyl-10H-phenothiazin-3-yl)methylene)pyrimidine-2,4,6(1H,3H,5H)-trione (PBA)

9-Octyl-10H-phenothiazine-3-carbaldehyde (**59**, 2.21 g, 6.50 mmol) and barbituric acid (0.83 g, 6.50 mmol) were refluxed in absolute ethanol (100 mL) for 8 h. After cooling, the precipitate was filtered off, washed several times with hot hexane and ether. The product was dried under vacuum to yield 2.19 g (75 %). mp-289 °C, FT- IR (cm<sup>-1</sup>) 1678,

2852, 3069,  $^1\text{H}$  NMR ( $\text{CDCl}_3$ )  $\delta$  (ppm): 0.80 (t, 3H), 1.18–1.38 (m, 10H), 1.72–1.79(m, 2H), 3.83 (t, 2H), 4.48 (s, 1H), 6.79 (m, 2H), 6.90 (m, 1H), 7.00 (t, 1H), 7.10 (t, 1H), 7.6 (s, 1H), 7.74 (d, 1H), 8.14 (s, 1H), 8.15 (s, 1H), 8.27 (s, 1H);  $^{13}\text{C}$  NMR ( $\text{DMSO}-d_6$ )  $\delta$  (ppm): 14.06, 22.59, 26.73, 26.80, 29.12, 29.16, 31.70, 48.12, 114.96, 115.92, 123.31, 123.86, 124.77, 125.34, 127.59, 127.63, 130.45, 131.86, 142.84, 150.27, 154.58, 192.70; HRMS (ESI MS)  $m/z$ : theoretical: 450.1859, found: 450.1835 ( $[\text{M} + \text{H}]^+$  detected).

### 2.5.9 Synthesis of (5-((10-octyl-10*H*-phenothiazin-3-yl)methylene)-6-thioxodihydropyrimidine-2,4(1*H*,3*H*)-dione (PTBA)

9-Octyl-10*H*-phenothiazine-3-carbaldehyde (**59**, 2.21 g, 6.50 mmol) and thiobarbituric acid (0.94 g, 6.50 mmol) were refluxed in absolute ethanol (200 mL) for 8 h. After cooling, the precipitate was filtered off, washed several times with hot hexane and ether. The compound was dried under vacuum to yield 2 g (70 %). mp-293 °C. FT-IR ( $\text{cm}^{-1}$ ) 15412853, 2920, 3067, 3437.  $^1\text{H}$  NMR ( $\text{DMSO}-d_6$ )  $\delta$  (ppm): 0.80 (t, 3H), 1.20–1.37 (m, 8H), 1.64–1.69 (m, 4H), 3.90 (t, 2H), 6.96 (m, 1H), 7.08 (m, 2H), 7.16 (m, 1H), 7.22 (t, 1H), 7.6 (d, 1H), 7.75(d, 1H), 8.13 (s, 1H), 8.37 (s, 1H);  $^{13}\text{C}$  NMR ( $\text{DMSO}-d_6$ )  $\delta$  (ppm): 13.89, 21.96, 25.86, 26.06, 28.39, 31.03, 31.98, 48.22, 114.85, 116.79, 121.64, 123.82, 125.34, 126.97, 127.59, 127.94, 133.27, 137.39, 138.12, 154.60, 178.58; HRMS (ESI MS)  $m/z$ : theoretical: 466.1623, found: 466.1610 ( $[\text{M} + \text{H}]^+$  detected).



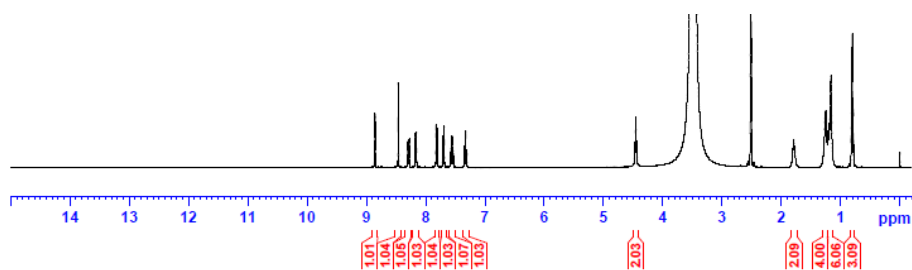


Figure 2.26  $^1\text{H}$  NMR spectrum of CCAA

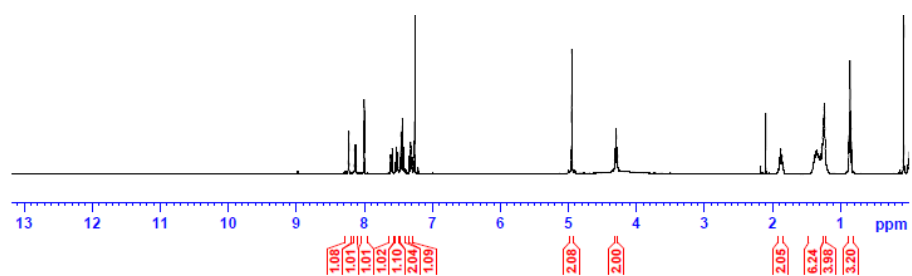


Figure 2.27  $^1\text{H}$  NMR spectrum of CRAA

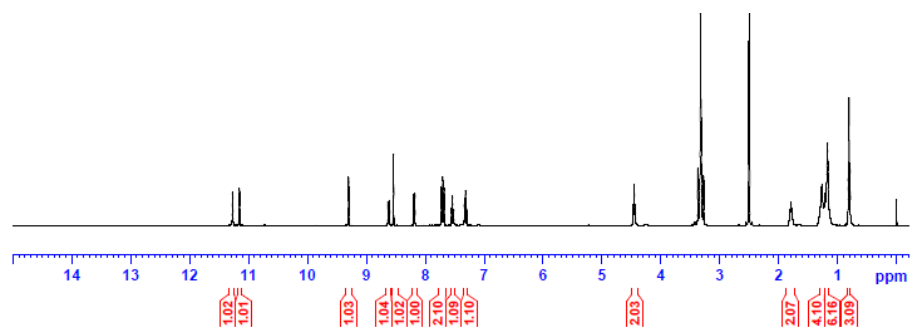


Figure 2.28  $^1\text{H}$  NMR spectrum of CBA

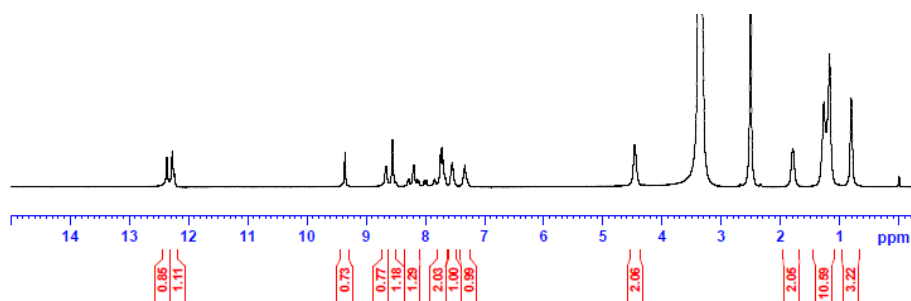


Figure 2.29  $^1\text{H}$  NMR spectrum of CTBA

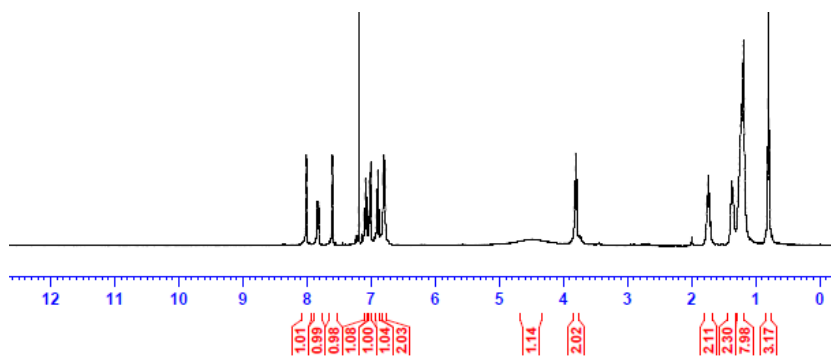


Figure 2.30  $^1\text{H}$  NMR spectrum of PCAA

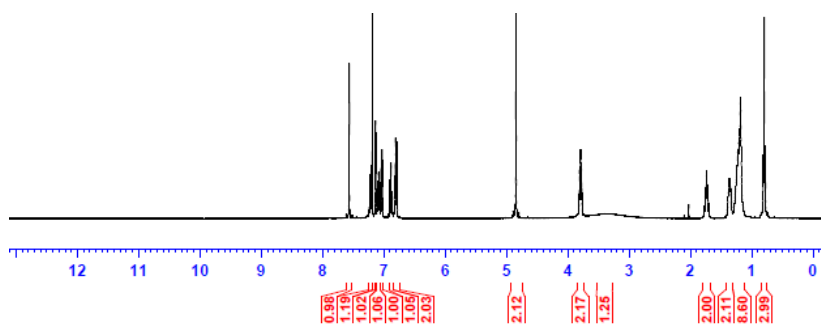


Figure 2.31  $^1\text{H}$  NMR spectrum of PRAA

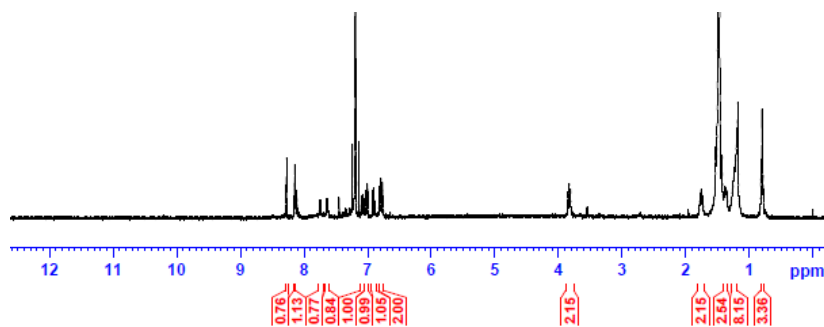


Figure 2.32  $^1\text{H}$  NMR spectrum of PBA in  $\text{DMSO-}d_6$   $\text{CDCl}_3$

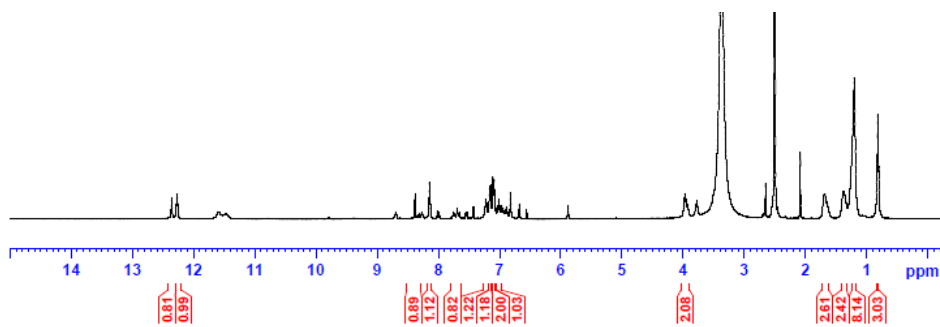


Figure 2.33  $^1\text{H}$  NMR spectrum of PTBA

## 2.6 References

1. Tian, H.; Yang, X.; Chen, R.; Zhang, R.; Hagfeldt, A.; Sun, L. *J. Phys. Chem. C* **2008**, *112*, 11023.
2. Li, Z.; Dong, Q.; Yao, S.; Qian, J.; Wang, Y.; Jiang, F.; Yang, H.; Zhao, Q.; Hou, Q.; Jinhui Tong, W. M.; Xiong, S.; Tian, W. *J Mater. Sci.* **2015**, *50*, 937.
3. Yen, Y. S.; Chen, W. T.; Hsu, C. Y.; Chou, H. H.; Lin, J. T.; Yeh, M. C. P. *Org. Lett.* **2011**, *13*, 4930.
4. Ikeda, H.; Kawabe, Y.; Sakai, T.; Kawasaki, K. *Chem. Lett.* **1989**, 1803.
5. Ma, B.; Zeng, F.; Lia, X.; Wu, S. *Chem. Commun.* **2012**, *48*, 6007.
6. Zhang, X.; Chi, Z.; Zhang, J.; Li, H.; Xu, B.; Li, X.; Liu, S.; Zhang, Y.; Xu, J. *J. Phys. Chem. B* **2011**, *115*, 7606.
7. Singh, G.; Bhalla, V.; Kumar, M. *Phys. Chem. Chem. Phys.* **2015**, *17*, 22079.
8. Tehfe, M. A.; Dumur, F.; Graff, B.; Savary, F. M.; Gigmes, D.; Fouassier, J. P.; Lalevee, J. *Polym. Chem.*, **2013**, *4*, 3866.
9. Lippert, E. Z. *Naturforsch.* **1955**, *10A*, 541.
10. Manoj, N.; Gopidas, K. R. *Chem. Phys. Lett.* **1997**, *267*, 567.
11. Becke, A. D. *J. Chem. Phys.* **1993**, *98*, 5648.
12. Gaussian 09, Revision D.01, M. J. Frisch, G. W. Trucks, H. B. Schlegel, G. E. Scuseria, M. A. Robb, J. R. Cheeseman, G. Scalmani, V. Barone, B. Mennucci, G. A. Petersson, H. Nakatsuji, M. Caricato, X. Li, H. P. Hratchian, A. F. Izmaylov, J. Bloino, G. Zheng, J. L. Sonnenberg, M. Hada, M. Ehara, K.

- Toyota, R. Fukuda, J. Hasegawa, M. Ishida, T. Nakajima, Y. Honda, O. Kitao, H. Nakai, T. Vreven, J. A. Montgomery, Jr., J. E. Peralta, F. Ogliaro, M. Bearpark, J. J. Heyd, E. Brothers, K. N. Kudin, V. N. Staroverov, T. Keith, R. Kobayashi, J. Normand, K. Raghavachari, A. Rendell, J. C. Burant, S. S. Iyengar, J. Tomasi, M. Cossi, N. Rega, J. M. Millam, M. Klene, J. E. Knox, J. B. Cross, V. Bakken, C. Adamo, J. Jaramillo, R. Gomperts, R. E. Stratmann, O. Yazyev, A. J. Austin, R. Cammi, C. Pomelli, J. W. Ochterski, R. L. Martin, K. Morokuma, V. G. Zakrzewski, G. A. Voth, P. Salvador, J. J. Dannenberg, S. Dapprich, A. D. Daniels, O. Farkas, J. B. Foresman, J. V. Ortiz, J. Cioslowski, and D. J. Fox, *Gaussian, Inc.*, Wallingford CT, **2013**.
13. Sanchez-Galvez, A.; Hunt, P.; Robb, M. A.; Olivucci, M. Vreven, T.; Schlegel, H. B. *J. Am. Chem. Soc.* **2000**, *122*, 2911.
14. Nairat, M.; Konar, A.; Lozovoy, V. V.; Beck, W. F.; Blanchard, G. J.; Dantus, M. *J. Phys. Chem. A* **2016**, *120*, 1876.
15. Liu, R. S. H.; Hammond, G. S. *PNAS*, **2000**, *97*, 11153.
16. Rettig, W.; Weigel, W. Highlighting Excited Molecules *Humboldt-Spektrum* **2003**, ISSN 0946-641X.
17. Qiu, X.-P.; Lu, R.; Zhou, H.-P.; Zhang, X.-F.; Xu, T.-H.; Liu, X.-L. *Tetra. Lett.* **2007**, *48*, 7582.
18. Xue, P.; Yao, B.; Liu, X.; Sun, J.; Gong, P.; Zhang, Z.; Qian, C Zhang, Y.; Lu, R. *J. Mater. Chem. C* **2015**, *3*, 1018.
19. Zhang, J.-B.; Xu, B.; Chen, J.-L.; Wang, L.-J.; Tian, W. *J Phys. Chem. C* **2013**, *117*, 23117.

20. Dai, X.-X.; Feng, H.-L.; Huang, Z.-S.; Wang, M.-J.; Wang, L.; Kuang, D.-B.; Meier, H.; Cao, D. *Dyes Pigm.* **2015**, *114* 47.
21. Anumala, U. R.; Gu, J.; Monte, F. L.; Kramer, T.; Haußen, R. H-V.; Hölzer, J.; Schön, C.; V. G.-Meyer.; Mall, G.; Hilger, I.; Czech, C.; Herms, J.; Schmidt, B. *Bioorg. Med. Chem.* **2013**, *21*, 5139.

## Chapter 3

### **Application of Simple Phenothiazine and Carbazole based dyes in Dye-Sensitized Solar Cell.**

---

#### **3.1 Abstract**

A series of simple phenothiazine and carbazole based dyes have been applied as sensitizers in Dye-Sensitized Solar Cell (DSSC), where the sensitizers differ by their acceptor moiety, such as cyano acetic acid, rhodanine-3-acetic acid, barbituric acid, thiobarbituric acid. The dyes exhibit a distinct donor- $\pi$ -acceptor behaviour comprising of carbazole and phenothiazine derivatives as electron donors and cyano acetic acid, rhodamine-3-acetic acid, barbituric acid and thiobarbituric acid as electron acceptors. A significant solar energy-to-electricity conversion efficiency ( $\eta$ ) of 2.63 % was achieved for a DSSC based on n-octyl phenothiazine as a donor and rhodamine-3-acetic acid as acceptor.

#### **3.2 Introduction**

Research in the direction towards the development of sources of clean, sustainable and cost effective energy has tremendously increased nowadays because of the depletion of fossil fuel resources and the rising expenses to meet such energy needs. In this context, development of more efficient and cost effective photovoltaic cells has attracted the attention of researchers worldwide. Photovoltaic cells or simply solar cells, include inorganic, organic, perovskite, etc., are electrical devices which convert light energy directly into electricity by the photovoltaic effect and some other physical and chemical processes.

There are so many organic donor- $\pi$ -acceptor (D- $\pi$ -A) compounds have been studied experimentally and theoretically as sensitizers for solar cells. In the D-A systems, the hole injection and transport is done by donor moiety while the electron injection and transport by acceptor group. Carbazole is one of the best donor moieties, which has been widely employed as active ingredients in electronic devices such as organic light-emitting diodes (OLEDs)<sup>1-3</sup> and DSSCs<sup>4-6</sup> due to the unique charge transporting properties and distinct thermal stability. Carbazole is an attractive building block due to its efficient nuclear sites for functional group incorporation.<sup>7,8</sup> Carbazole derivatives with different chromophores attached at C-2, C-3, C-6, C-7, and N-9 positions have applications in organic light-emitting diodes and photovoltaic devices. Mainly, carbazole has been used either as a peripheral donor or a  $\pi$ -linker in DSSCs. Carbazole can act as a good donor due to the presence of electron rich amine functionality and also can increase the donor capacity by suitable substitution of electron realising groups.<sup>9-13</sup> If the highly electron rich C-3 and C-7 positions substitute with any acceptor or anchoring group will result in a better overlap between HOMO and LUMO orbitals.<sup>14</sup>

Phenothiazine is a heterocyclic molecule with electron-rich nitrogen and sulphur atoms in the central ring and better donor than triphenylamine, tetrahydroquinoline, carbazole, and iminobenzyles. Phenothiazine ring is nonplanar with a butterfly conformation in the ground state, which can prevent the formation of intermolecular excimers by molecular aggregation. The N-substituted simple phenothiazines are colourless and cannot absorb visible light, however, the introduction of

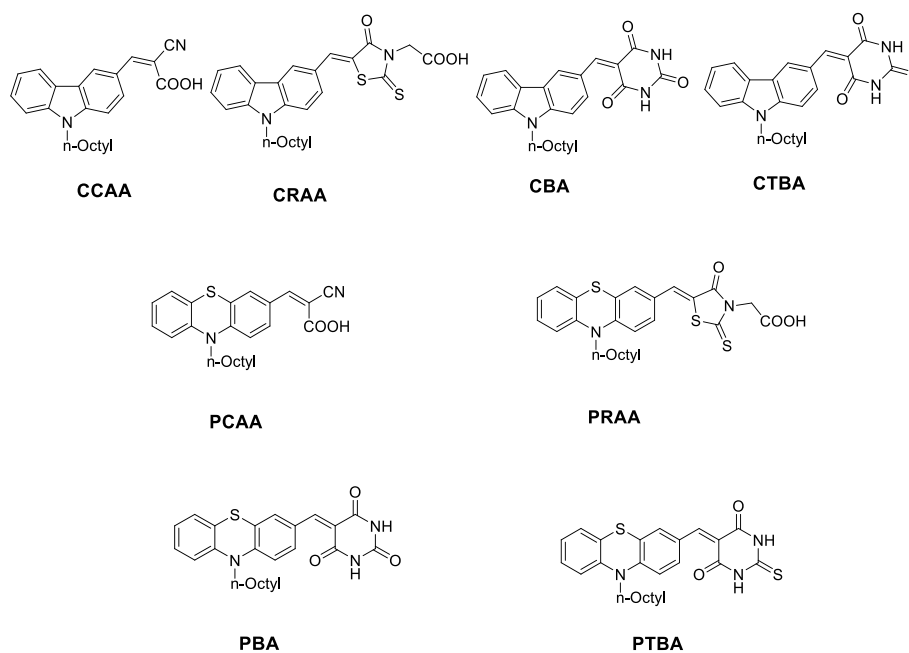


electron withdrawing groups into aromatic rings can induce a shift of the absorption spectrum into the visible region. Lee *et al.* reported that simple phenothiazine-based dyes with a directly connected anchoring group showed an absorption band which can cover almost the visible region than typical donor-acceptor type dyes with additional  $\pi$ -conjugated bridges.<sup>15</sup> Phenothiazine derivatives are potential hole transporting material in organic devices<sup>16-21</sup> as well as a promising organic sensitizer for DSSCs their excellent photoresponse in the visible region. Keeping all this in mind, we have designed and synthesized a series of metal free organic dyes composed of carbazole and phenothiazine as a donor and barbituric acid and thiobarbituric acid as acceptor. We are focussing the photovoltaic application of synthesised dyes in this chapter. The present chapter report the study on the application of these molecules in DSSC and are compared with 9-octylcarbazole and 10-octylphenothiazine based dyes having cyanoacrylic, rhodanine-3-acetic acid.

### 3.3 Results and Discussion

The carbazole dyes (CCAA, CRAA, CBA, and CTBA) and phenothiazine dyes (PCAA, PRAA, PBA and PTBA) contain an octyl group as the substituent on the donor group. Such long alkyl chains as substituents on the dye were reported to prevent aggregation of the dyes on the TiO<sub>2</sub> semiconductor surface and thus to control the energy wasting back electron transfer during the operation of the cell. Moreover, the enhanced hydrophobicity due to the long alkyl chain is expected to act as

a barrier to prevent  $I_3^-$  or moisture from reaching the semiconductor and thereby reducing the leakage of dark current.<sup>22</sup>

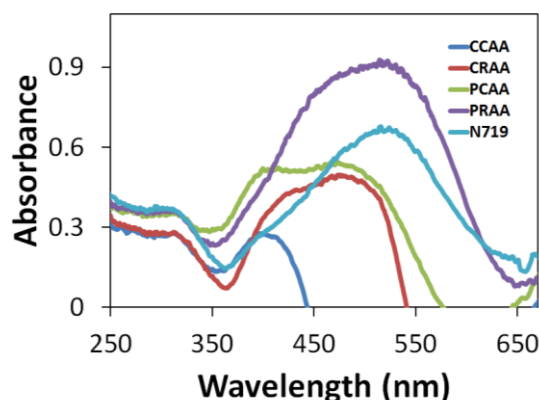


**Scheme 3.1** Heterocyclic donor- $\pi$ -acceptor systems

### 3.3.1 UV–Visible Absorption Properties

The UV–Vis absorption spectra of all the dyes in  $\text{CHCl}_3$  solution (§ 2.3.2.1 and 2.3.2.4) as well as adsorbed on  $\text{TiO}_2$  films have been recorded (Figure 3.4), and the detailed spectroscopic data is presented earlier in chapter 2 (§ 2.3.2.1, 2.3.2.2, 2.3.2.4 and 2.3.2.5). All the dyes exhibited broad absorption bands in the range of 300–700 nm. They all possess high molar extinction coefficient ( $\epsilon$ ) with values greater than  $2.7 \times 10^4 \text{ M}^{-1} \text{ cm}^{-1}$ , with relatively lower values for phenothiazine dyes which are similar or higher than that of reported standard ruthenium dyes

N3 and N719 ( $1.39 \times 10^4$  and  $1.4 \times 10^4 \text{ M}^{-1} \text{ cm}^{-1}$ , respectively).<sup>23</sup> When these dyes are adsorbed onto the nanocrystalline  $\text{TiO}_2$  films, the absorption bands display a slight red-shift with respect to those in solutions.



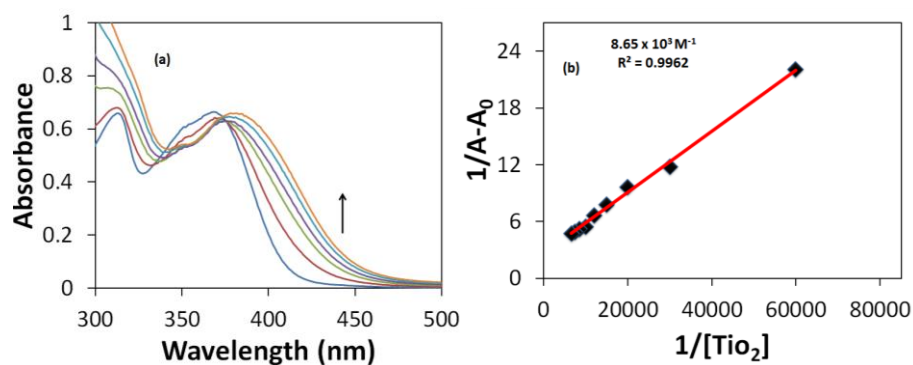
**Figure 3.1** Absorption spectra of the dyes adsorbed on  $\text{TiO}_2$

### 3.3.2 Evaluation of the Binding Properties of the Dyes with $\text{TiO}_2$

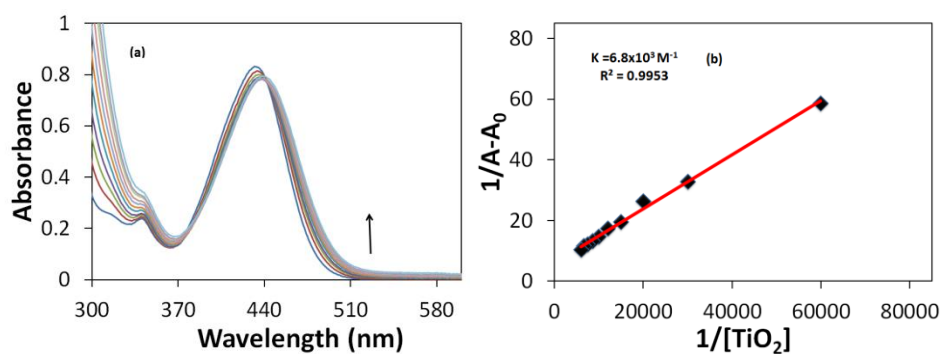
#### 3.3.2.1 Absorption Spectral Properties

From the absorption spectral studies of the sensitizers, we confirmed that the introduction of acceptors to the sensitizers resulted in the visible range absorption, thus satisfying one of the main requirements for the DSSC application. Binding between the sensitizers and the semiconductor  $\text{TiO}_2$  is another deciding factor for DSSC efficiency.<sup>24</sup> It was reported earlier that the 'COOH' of cyanoacrylic acid and rhodanine-3-acetic acid bind with  $\text{TiO}_2$  involves prior deprotonation. Barbituric acid and thiobarbituric acid do possess strong acid character and is expected to interact with  $\text{TiO}_2$  by deprotonation of the amide

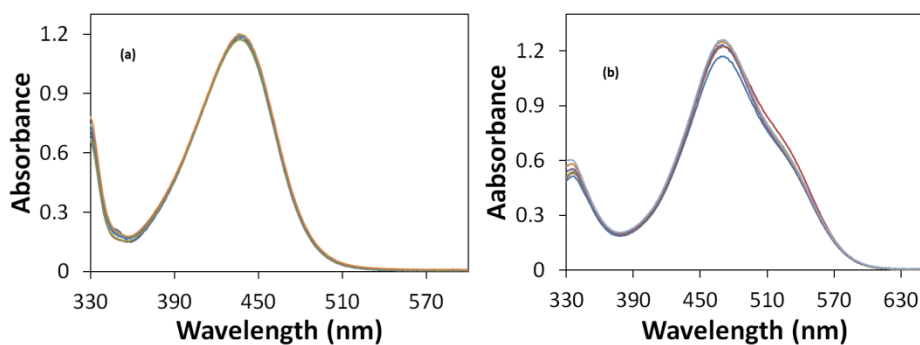
functionality. This is expected to serve as the main anchoring mechanism with  $\text{TiO}_2$ . To study this, absorption measurements were carried out by adding colloidal  $\text{TiO}_2$  to the respective solutions of the dyes. Figure 3.2a shows the absorption spectrum of CCAA in the presence of colloidal  $\text{TiO}_2$ . It was observed that with increasing the concentration of  $\text{TiO}_2$ , the absorbance of CCAA increased with the appearance of an isosbestic point at 373 nm and a red shift of 20 nm. Similarly, the absorption spectrum of CRAA also changed with an isosbestic point at 440 nm and a 20 nm red shift (Figure 3.3a). These changes clearly indicate the binding interaction between the sensitizers and  $\text{TiO}_2$ . Similar results were obtained for PCAA and PRAA (Figure 3.5 & 3.6). However, for CBA, CTBA, PBA and PTBA no significant changes were observed in the absorption spectrum (Figure 3.4 & 3.7). The spectrum remained unchanged even after adding a high concentration (334  $\mu\text{M}$ ) of  $\text{TiO}_2$ . This clearly indicates the weak binding interaction between these dyes and  $\text{TiO}_2$ . The binding constants (K) were calculated using the model described in (§ 3.5.3) and the results are tabulated in Table 3.1.



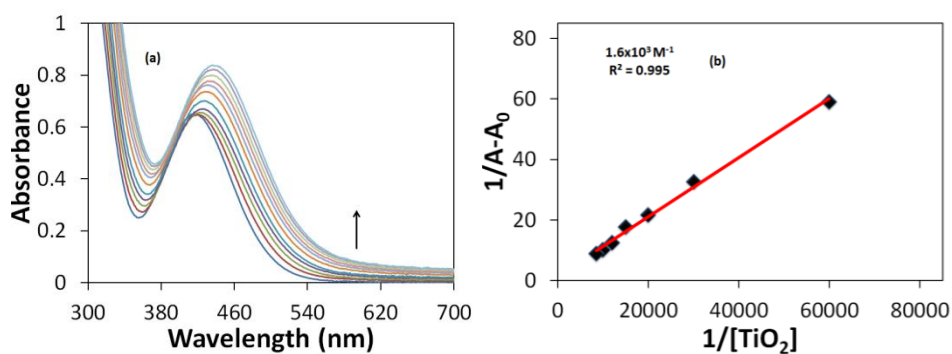
**Figure 3.2** (a) Absorption spectrum of CCAA (24.8  $\mu\text{M}$ ) with  $\text{TiO}_2$  in the concentration range of (16.7 $\mu\text{M}$  - 300.6  $\mu\text{M}$ ) M in MeOH (b) Absorbance ratio ( $1/A - A_0$ ) as the inverse concentration of  $\text{TiO}_2$  in MeOH



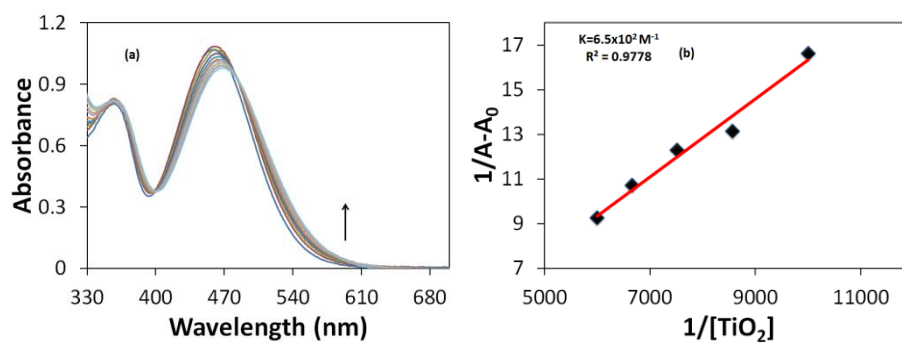
**Figure 3.3** (a) Absorption spectrum of CRAA (19.3  $\mu\text{M}$ ) with  $\text{TiO}_2$  in the concentration range of (16.7  $\mu\text{M}$  - 334  $\mu\text{M}$ ) in MeOH. (b) Absorbance ratio ( $1/A - A_0$ ) as the inverse concentration of  $\text{TiO}_2$  in MeOH



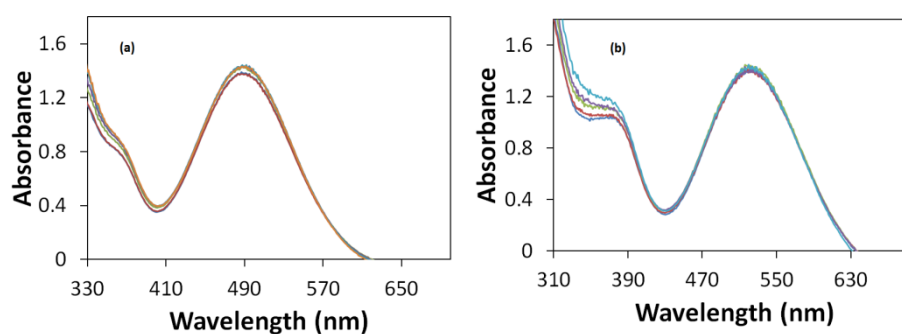
**Figure 3.4(a)** Absorption spectrum of CBA (30.8 μM) and **(b)** CTBA (29.8 μM) with TiO<sub>2</sub> in the concentration range of (16.7 μM – 334 μM) in MeOH



**Figure 3.5(a)** Absorption spectrum of PCAA (43.9 μM) with TiO<sub>2</sub> in the concentration range of 16.7 μM to 334 μM in MeOH. **(b)** Absorbance ratio (1/A - A<sub>0</sub>) as the inverse concentration of TiO<sub>2</sub> in MeOH



**Figure 3.6(a)** Absorption spectrum of PRAA (34.8  $\mu\text{M}$ ) with  $\text{TiO}_2$  in the concentration range of 16.7  $\mu\text{M}$  to 334  $\mu\text{M}$  in MeOH. **(b)** Absorbance ratio ( $1/A-A_0$ ) as the inverse concentration of  $\text{TiO}_2$  in MeOH



**Figure 3.7(a)** Absorption spectrum of PBA (64.9  $\mu\text{M}$ ) and **(b)** PTBA (122.6  $\mu\text{M}$ ) with  $\text{TiO}_2$  in the concentration range of 16.7  $\mu\text{M}$  to 334  $\mu\text{M}$  in MeOH.

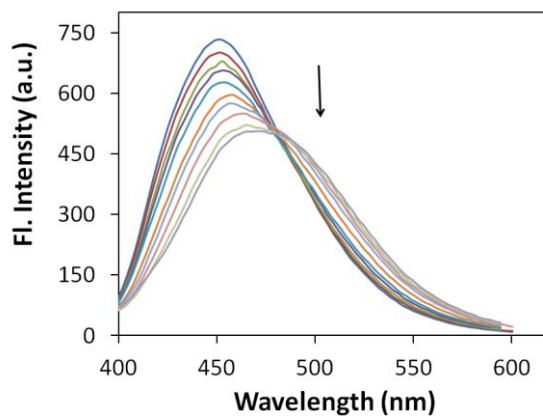
**Table 3.1** Calculated binding constants

Dye	Binding Constant ( $10^3 \text{ M}^{-1}$ )
CCAA	8.65
CRAA	6.8
PCAA	1.6
PRAA	0.65

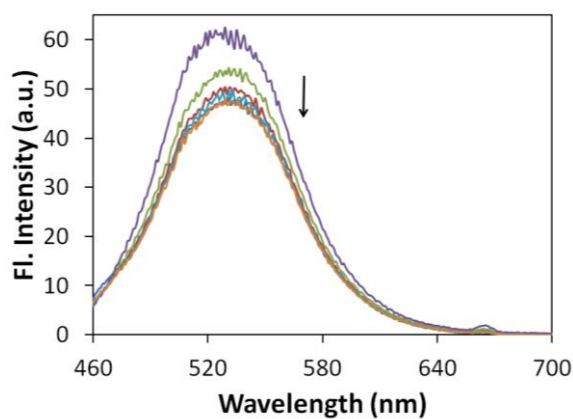
### 3.3.2.2 Electron Transfer and Electrochemical Properties

Normally, when the sensitizers are photoexcited, an electron from the ground state of the sensitizers will transfer to its excited state. Hence it is essential to study the excited state interaction of the sensitizers with  $\text{TiO}_2$ . Fluorescence quenching measurements have been commonly used to analyse the feasibility of electron transfer between the molecules in their excited state<sup>25,26</sup> and  $\text{TiO}_2$ . Figure 3.8 shows the emission spectrum of CCAA in the absence and presence of  $\text{TiO}_2$ . The emission intensity of CCAA was significantly reduced by  $\text{TiO}_2$  at different concentrations (16.7  $\mu\text{M}$  to 1 mM). Similar results were observed for CRAA, PCAA, and PRAA (Figures 3.9, 3.10 and 3.11). The decrease in fluorescence intensity of the sensitizers in the presence of  $\text{TiO}_2$  is usually attributed to electron transfer to the conduction band of semiconductor nanoparticles.<sup>27</sup>

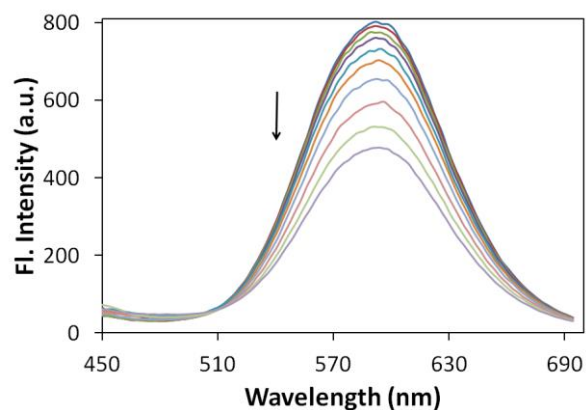




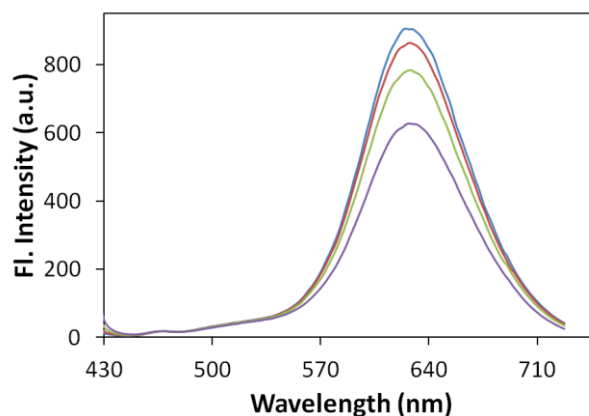
**Figure 3.8** Fluorescence quenching of CCAA (35.5 μM;  $\lambda_{\text{ex}} = 374 \text{ nm}$ ;  $\lambda_{\text{emi}} = 449 \text{ nm}$ ) in the presence of TiO<sub>2</sub> (16.7 μM to 1000 μM) in MeOH



**Figure 3.9** Fluorescence quenching of CRAA (10 μM;  $\lambda_{\text{ex}} = 440 \text{ nm}$ ;  $\lambda_{\text{emi}} = 532 \text{ nm}$ ) in the presence of TiO<sub>2</sub> (16.7 μM to 200 μM) in MeOH



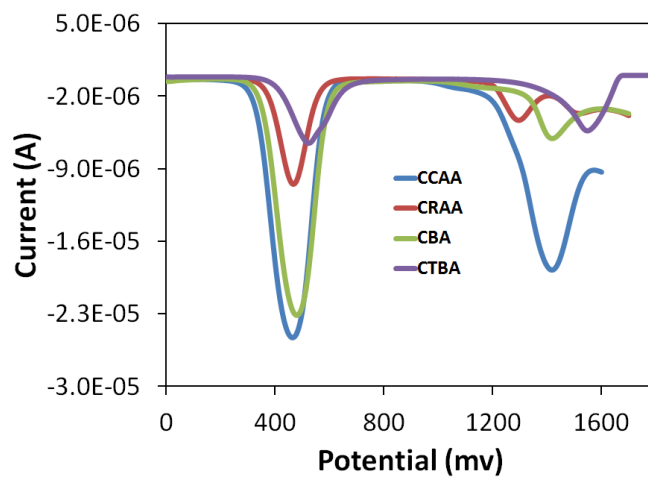
**Figure 3.10** Fluorescence quenching of PCAA ( $24.5\mu\text{M}$ ;  $\lambda_{\text{ex}} = 390\text{ nm}$ ;  $\lambda_{\text{emi}} = 590\text{ nm}$ ) in the presence of  $\text{TiO}_2$  ( $16.7\mu\text{M}$  to  $830\mu\text{M}$ ) in MeOH.



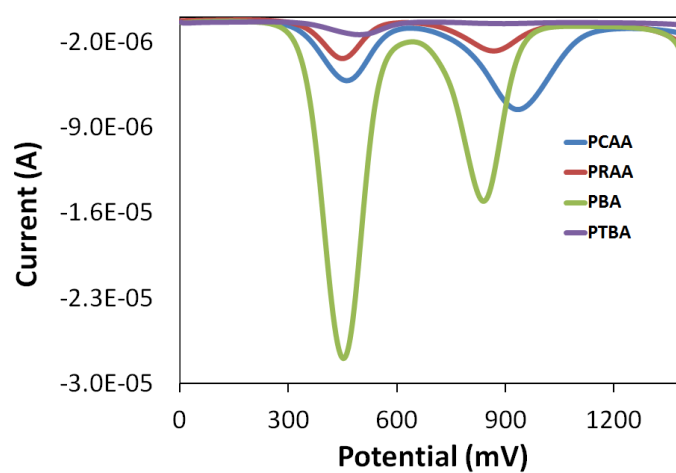
**Figure 3.11** Fluorescence quenching of PRAA ( $18.8\mu\text{M}$ ;  $\lambda_{\text{ex}} = 400\text{ nm}$ ;  $\lambda_{\text{emi}} = 623\text{ nm}$ ) in the presence of  $\text{TiO}_2$  ( $16.7\mu\text{M}$  to  $233.8\mu\text{M}$ ) in THF.

In order to assess the feasibility of electron transfer between the excited sensitizers and  $\text{TiO}_2$ , an energy level diagram has been constructed using HOMO and LUMO energy of the sensitizers. These energy levels were determined by square wave voltammetry measurements of the oxidation potentials. The oxidation potential was

determined against  $\text{Fc}/\text{Fc}^+$  was converted to potential against NHE (§ 3.5) to obtain the HOMO energy ( $E(\text{S}^+/\text{S}, \text{V})$  vs NHE or HOMO in eV). Since oxidation is a single electron transfer, the value obtained in V is directly converted to eV. The values obtained for all the compounds are tabulated in Table 3.2. The energy of LUMO was obtained from the corresponding value of HOMO energy and HOMO-LUMO energy gap ( $E_{0-0}$ ) is estimated from the onset of the UV-visible absorption spectra by the equation  $E_{(0-0)} = \frac{1240}{\lambda}$ , where,  $\lambda$  is obtained from the intersection point of absorption and emission spectra or from the end of the absorption spectrum. The energy levels of the dyes are compared with the energy of the conduction band of the semiconductor and the redox level of the electrolyte and are given in Figure 3.12 and 3.13 for carbazole and phenothiazine dyes respectively. The analysis of the diagram reveals that the LUMO levels of all the dyes except CTBA are more negative than the conduction band edge (CB) of  $\text{TiO}_2$  ( $-0.5 \text{ V}$  vs NHE), making the electron injection from the excited dye molecules to the conduction band of  $\text{TiO}_2$  exergonic (Figure 3.15 & 3.16). In the case of CTBA, the electron injection to the conduction band of  $\text{TiO}_2$  is endergonic and thus is not feasible (Figure 3.15). Similarly, the HOMO levels of the dyes are suitably placed to effect the regeneration of the dye by the electrolyte (iodide/triiodide) during the operation of the cell.



**Figure 3.12** Square wave voltamogram of carbazole based dyes



**Figure 3.13** Square wave voltamogram of phenothiazine based dyes

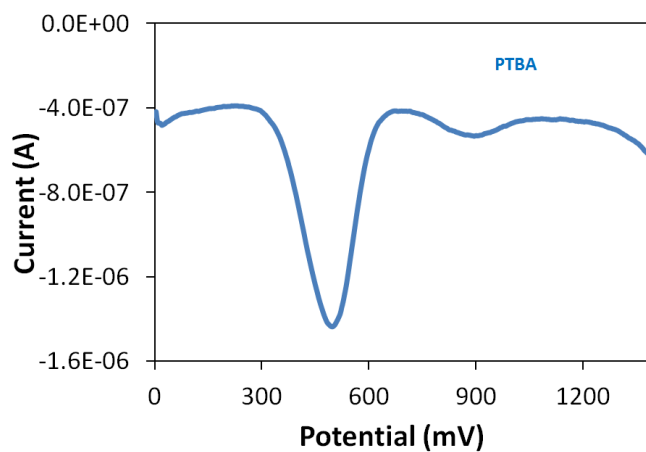


Figure 3.14 Square wave voltamogram of PTBA

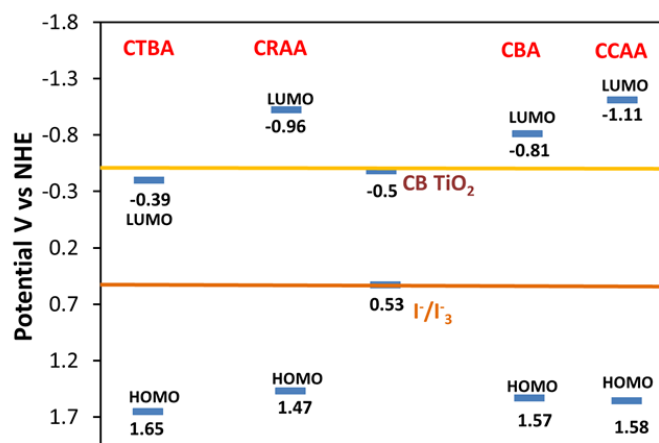
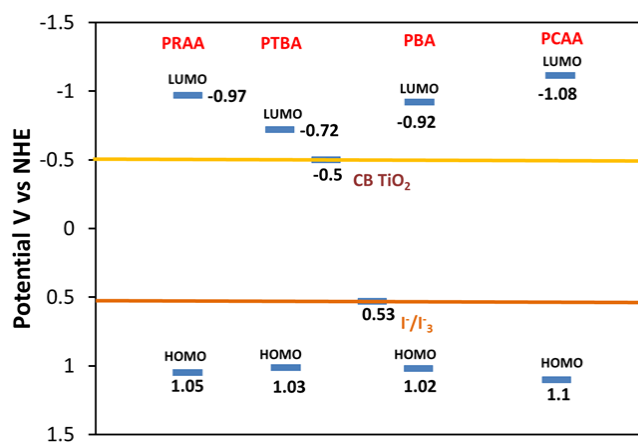


Figure 3.15 Energy level diagrams of carbazole based dyes.



**Figure 3.16** Energy level diagrams of phenothiazine based dyes.

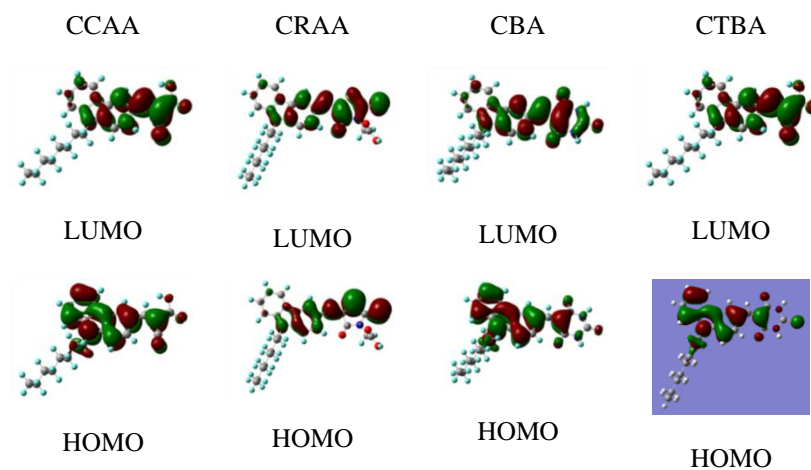
**Table 3.2** Electrochemical parameters and energy levels of dyes.

Dye	$E_{ox}$ vs. Fc/Fc <sup>+</sup> (V)	$E(S^+/S)$ vs NHE/V	$E_{0-0}$ (eV)	LUMO vs NHE/eV	Egap/ V	HOMO (IP)/eV	LUMO (EA)/eV Vacuum
CCAA	0.95	1.58	2.69	-1.11	0.61	-6.38	-3.69
CRAA	0.84	1.47	2.43	-0.96	0.46	-6.27	-3.84
CBA	0.94	1.57	2.38	-0.81	0.31	-6.37	-3.99
CTBA	1.02	1.65	2.04	-0.39	-0.11	-6.45	-4.41
PCAA	0.47	1.10	2.18	-1.08	0.58	-5.9	-3.72
PRAA	0.42	1.05	2.02	-0.97	0.47	-5.85	-3.83
PBA	0.39	1.02	1.94	-0.92	0.42	-5.82	-3.88
PTBA	0.40	1.03	1.75	-0.72	0.22	-5.83	-4.08

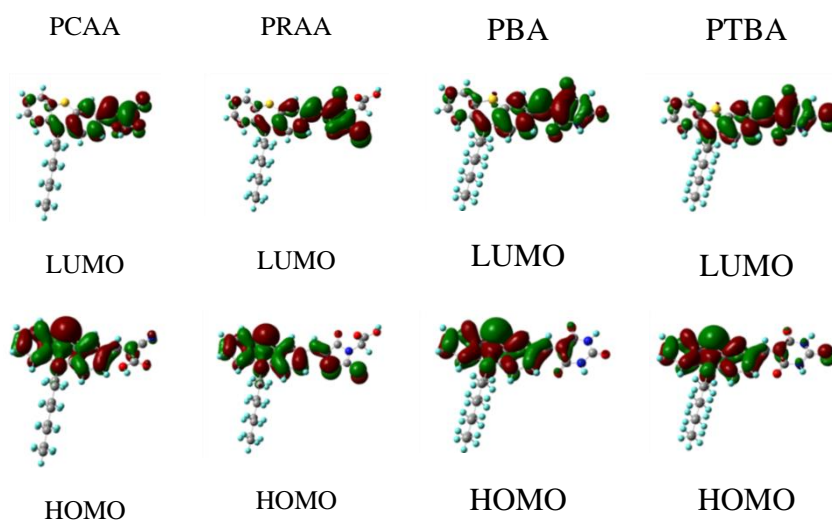
### 3.3.4 Theoretical Calculations

In order to assess the directionality of charge transfer within the dye, we have calculated and mapped the HOMO and LUMO orbitals by Density Functional Theory (DFT). The structures of the dyes were fully optimized without constraints by using B3LYP exchange correlation functions and 6-311g (d, p) basis on GUASSIAN-09 programme.<sup>28,29</sup> All the dyes showed HOMO orbitals centered on the donor and the LUMO on the acceptor group. The HOMO and LUMO surfaces of carbazole dyes are given in Table 3.3 and those of phenothiazine dyes are given in Table 3.4.

**Table 3.3** Frontier molecular orbitals of the HOMO and LUMO of carbazole based sensitizers calculated using B3LYP exchange correlation functions and 6-311g (d, p) basis on GUASSIAN-09 programme



**Table 3.4** Frontier molecular orbitals of the HOMO and LUMO of phenothiazine based sensitizers calculated using B3LYP exchange correlation functions and 6-311g (d, p) basis on GUASSIAN-09 programme



### 3.3.5 Photovoltaic Performance

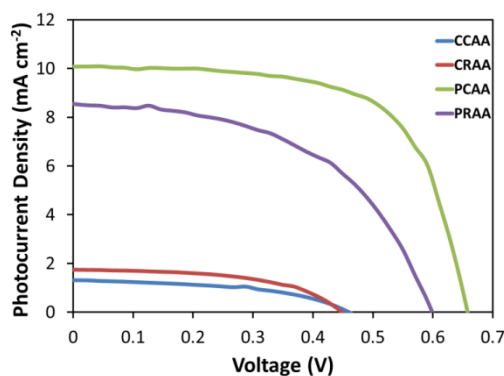
In order to investigate the photovoltaic performance of the dyes, a series of DSSCs have been fabricated as described in the experimental section (§ 3.5.4) and tested under normal conditions (AM 1.5 G, 100 mW cm<sup>-2</sup>). The cell parameters of fabricated DSSCs with the dyes synthesised, i.e.,  $J_{sc}$ ,  $V_{oc}$ , fill factor (FF), and PCE ( $\eta$ ) are summarized in Table 3.2. The photocurrent–voltage (J–V) plots are shown in Figure 3.17 & 3.18. The results obtained were compared with the standard dye N719, for which we got an efficiency of 6.18% ( $J_{sc} = 14.96 \text{ mA cm}^{-2}$ ,  $V_{oc} = 0.65\text{V}$ , FF= 60%). Among the synthesized sensitizers, the cell based



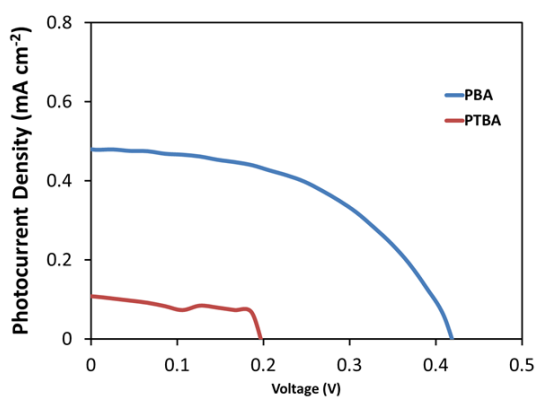
on PRAA exhibits the highest  $\eta$  of 2.63% ( $J_{sc} = 8.53 \text{ mA cm}^{-2}$ ,  $V_{oc} = 0.775 \text{ V}$ ,  $FF = 0.689$ ). For the sake of comparison of efficiencies based on acceptor moieties as well as anchoring groups, the efficiency of dye PCAA was also estimated under identical conditions, and we got an efficiency of 4.28% as against 4.87%, reported for the molecule.<sup>30</sup> For the dyes CCAA and CRAA, the photo conversion efficiency is 0.3 and 0.41%, respectively. Very low photoconversion efficiencies for the sensitizers which hold barbituric acid and thiobarbituric acid as acceptor groups are due to their weak binding affinities on  $\text{TiO}_2$ , even though the absorption spectrum of these dyes covers the entire visible region.

**Table 3.5** Photovoltaic parameters of DSSCs under full sunlight illumination.

Dye	$J_{sc}(\text{mA cm}^{-2})$	$V_{oc}(\text{V})$	FF (%)	$\eta$ (%)
N719	14.96	0.65	60	6.18
CCAA	1.31	0.45	48	0.30
CRAA	1.74	0.44	53	0.41
PCAA	<b>10.08</b>	<b>0.66</b>	<b>62</b>	<b>4.28</b>
PRAA	8.53	0.59	51	2.63
PBA	0.48	0.42	46	0.055
PTBA	0.11	0.19	58	0.012



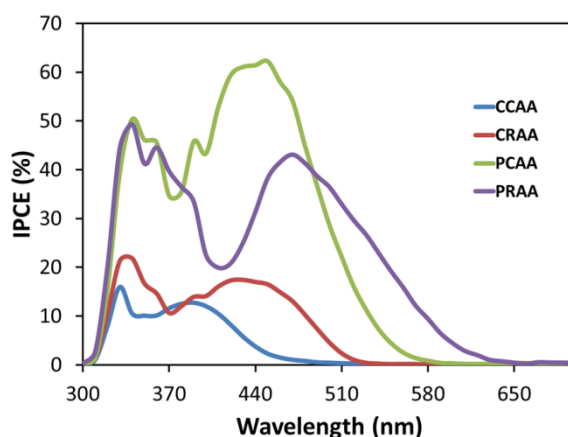
**Figure 3.17** Photocurrent–voltage (J–V) plots obtained with the sensitizers PCAA, PRAA, CCAA, CRAA



**Figure 3.18** Photocurrent–voltage (J–V) plots obtained with the sensitizers PBA and PTBA

Figure 3.19 shows the incident photon-current conversion efficiencies (IPCEs) for the sensitizers in DSSCs as a function of the wavelength of the light. The IPCEs of PCAA shows a broadband in the region 370–580 nm with values mostly > 60%, whereas, PRAA exhibits a broadband in the region of 400–650 nm with values > 40%. In the case of CCAA, the incident photocurrent conversion efficiency is only 10%

and CCAA exhibits a broadband activity in the region 340-460 nm. For CRAA the IPCE is above 18% and the spectrum shows a band in the region 370-510 nm. The curves show good correlation with the absorption spectrum of the dyes on TiO<sub>2</sub>. The low photo conversion efficiency is due to the less coverage of absorption spectra of carbazole dyes.



**Figure 3.19** Incident photon-to-current efficiency (IPCE) curves of DSSCs based on the new dyes

### 3.4 Conclusions

A series of carbazole and phenothiazine based D- $\pi$ -A systems by changing the acceptor moieties were successfully synthesized and characterized by photophysical and electrochemical analysis. The dyes exhibit a distinct donor- $\pi$ -acceptor behaviour comprising of carbazole and phenothiazine derivatives as electron donors and cyano acetic acid, rhodamine-3-acetic acid, barbituric acid and thiobarbituric acid as electron acceptors. Under simulated AM 1.5 G irradiation, the PRAA

based DSSC exhibits a short-circuit photocurrent of  $8.53 \text{ mA cm}^{-2}$ , an open-circuit photovoltage of  $0.59 \text{ V}$ , a fill factor of  $0.51$ , corresponding to a power conversion efficiency (PCE) of  $2.63\%$ . The very low power conversion efficiency for the dyes which hold barbituric acid and thiobarbituric acid as acceptors is due to the weak binding affinities on to  $\text{TiO}_2$  surface.

## 3.5 Experimental Section

### 3.5.1 Materials and Reagents

All solvents and reagents were purchased from Sigma-Aldrich Company and Spectrochem Pvt. Ltd., used as received without further purification. Dye *cis*-bis(isothiocyanato)bis(2,2'-bipyridyl-4,4'-dicarboxylato)-ruthenium-(II)-bis-tetrabutylammonium (coded as N719), iodide-based liquid electrolyte (DHS-E23) and TiO<sub>2</sub> paste were purchased from Solaronix SA.

### 3.5.2 Electrochemical Characterization

The square wave voltammograms (SWV) were measured with Bas W 50 electrochemical workstation using a normal three-electrode cell with a glassy carbon electrode, a Pt wire counter electrode, and an Ag/Ag<sup>+</sup> reference electrode. The supporting electrolyte was 0.1 M tetra-n-butylammonium hexafluorophosphate in acetonitrile solution. The potential of the reference electrode was calibrated using ferrocene after each set of measurements, and all potentials mentioned in the work were against the normal hydrogen electrode by using the following conversion:

$$E \text{ (HOMO or LUMO)} = [-e (E_{1/2}(x \text{ vs. Ag/AgCl}) - E_{1/2}(\text{Fc/Fc}^+ \text{ vs. Ag/AgCl}))] - 4.80\text{eV}$$

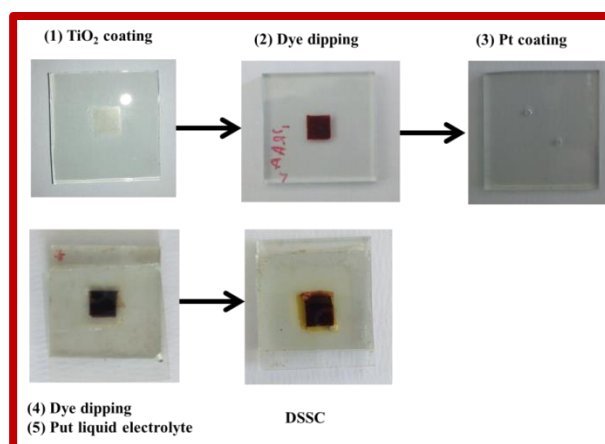
### 3.5.3 Determination of Binding Constants

The binding affinities between dyes and TiO<sub>2</sub> were calculated using Benesi–Hildebrand (BH plot) equation.<sup>27</sup>

$$\frac{1}{(A-A_0)} = \frac{1}{K(A-A_{max})[TiO_2]} + \frac{1}{(A-A_{max})}$$

where, K is the binding constant,  $A_0$  is the absorbance of the dye, A is the observed absorbance in the presence of  $TiO_2$  and  $A_{max}$  is the absorbance at saturation. The linear dependence of  $\frac{1}{(A-A_0)}$  on the reciprocal of the  $[TiO_2]$  concentration indicates the formation of a 1:1 binding stoichiometry between the dye and  $TiO_2$ .

### 3.5.4 Fabrication and Characterization of Cells



All the photoanode thin films for the DSSCs were made by following standard protocol, which is composed of a 12  $\mu\text{m}$  thick transparent layer of  $TiO_2$  with an area of 0.16  $\text{cm}^2$ .  $TiO_2$  thin films were made from a titania paste by the doctor-blade technique. A layer of  $\sim 6$   $\mu\text{m}$  thick  $TiO_2$  paste was doctor bladed onto the FTO conducting glass and kept at room temperature for 3 min before heating to 150  $^\circ\text{C}$  and kept for 6 min; this procedure was repeated again by coating another  $\sim 6$   $\mu\text{m}$  thick  $TiO_2$  paste to achieve an overall film thickness of  $\sim 12$   $\mu\text{m}$ . The

electrodes were then slowly heated to 275 °C and kept at this temperature for 10 min, at 325 °C for 10 min, 400 °C for 10 min, 450 °C for 10 min and 500°C for 30 min to remove the binders present in the titania paste. The film thus formed is a three-dimensional TiO<sub>2</sub> nanoparticle network. After cooling down to ~80 °C, the electrodes were immersed into a  $3 \times 10^{-4}$  M solution of the dye in MeOH. For the N719 dye, a solution in acetonitrile/tertbutyl alcohol (volume ratio, 1:1) was used. The films were kept in the dye solutions for 16 h in the dark. The dye-coated films were thoroughly washed with MeOH to remove the unadsorbed dye molecules and dried in air. Pt coated counter electrodes were prepared by painting platisol onto FTO followed by sintering at 500 °C. Two holes (1 mm in diameter) were predrilled on the FTO glass used for coating Pt. These holes are meant for introducing the electrolyte. The dye-adsorbed TiO<sub>2</sub> electrode and Pt-counter electrode were assembled into a sandwich type cell and sealed at about 100 °C with a hot-melt parafilm. The composition of the liquid electrolyte used was 0.1 M LiI, 0.05 M I<sub>2</sub> in a mixture of acetonitrile and 4-tert-butylpyridine (1:1 volume ratio).

## References

1. Kotchapradist, P.; Prachumrak, N.; Tarsang, R.; Jungsuttiwong, S.; Keawin, T.; Sudyoasuk, T.; Promarak, V. *J. Mater. Chem. C* **2013**, *1*, 4916.
2. Cui, L.-S.; Dong, S.-C.; Liu, Y.; Li, Q.; Jiang, Z.-Q.; Liao, L.-Z. *J. Mater. Chem. C* **2013**, *1*, 3967.
3. Thomas, K. R. J.; Lin, J. T.; Tao, Y.-T.; Ko, C.-W. *J. Am. Chem. Soc.* **2001**, *123*, 9404.
4. Ooyama, Y.; Inoue, S.; Nagano, T.; Kushimoto, K.; Ohshita, J.; Imae, I.; Komaguchi, K.; Harima, Y. *Angew. Chem., Int. Ed.* **2011**, *50*, 7429.
5. Ooyama, Y.; Nagano, T.; Inoue, S.; Imae, I.; Komaguchi, K.; Ohshita, J.; Harima, Y. *Chem. Eur. J.* **2011**, *17*, 14837.
6. Venkateswararao, A.; Thomas, K. R. J.; Lee, C.-P.; Ho, K.-C. *Tetrahedron Lett.* **2013**, *54*, 3985.
7. Wang, H.-Y.; Liu, F.; Xie, L.-H.; Tang, C.; Peng, B.; Huang, W.; Wei, W. *J. Phys. Chem. C* **2011**, *115*, 6961.
8. Huang, H.; Fu, Q.; Pan, B.; Zhuang, S.; Wang, L.; Chen, J.; Ma, D.; Yang, C. *Org. Lett.* **2012**, *14*, 4786.
9. Brunner, K.; van Dijken, A.; Börner, H.; Bastiaansen, J. J. A. M.; Kiggen, N. M. M.; Langeveld, B. M. W. *J. Am. Chem. Soc.* **2004**, *126*, 6035.
10. Teng, C.; Yang, X.; Li, S.; Cheng, M.; Hagfeldt, A.; Wu, L.; Sun, L. *Chem. Eur. J.* **2010**, *16*, 13127.
11. Lee, W.; Cho, N.; Kwon, J.; Ko, J.; Hong, J.-I. *Chem. Asian J.* **2012**, *7*, 343.



12. Venkateswararao, A.; Justin Thomas, K. R.; Lee, C- P.; Li, C-T.; Ho, K-C. *ACS Appl. Mater. Interfaces* **2014**, *6*, 2528.
13. Sathiyam, G.; Sivakumar, E. K. T.; Ganesamoorthy, R.; Thangamuthu, R.; Sakthivel, P. *Tetrahedron Lett.* **2016**, *57*, 243.
14. Venkateswararao, A.; Justin Thomas, K. R. Carbazole-Based Organic Dyes for Dye-Sensitized Solar Cells: Role of Carbazole as Donor, Auxiliary Donor and  $\pi$ -Linker Solar Cell *Nanotechnology* ISBN: 978-1-118-84578-3
15. Lee, J.; Kwak, J.; Ko, K.C.; Park, J.H.; Ko, J.H.; Park, N.; Kim, E.; Ryu, D.H.; Ahn, T.K.; Lee, J.Y.; Son, S.U. *Chem. Commun.*, **2012**, *48*, 11431.
16. Birel, Ö. *EJOVOC : Electronic Journal of Vocational Colleges - May/Mayıs 2015*
17. Huang, Z. H.; Meier, H.; Cao, D. *J. Mater. Chem. C* **2016**, *4*, 2404.
18. Chang, Y. J.; Chou, P. T.; Lin, Y. Z.; Watanabe, M.; Yang, C. J.; Chin, T. M.; Chow, T. J. *J. Mater. Chem.* **2012**, *22*, 21704.
19. Dai, X. X.; Feng, H. L.; Huang, Z. S.; Wang, M. J.; Wang, L.; Kuang, D. B.; Meier, H.; Cao, D. *Dyes Pigm.* **2015**, *114*, 47.
20. Hua, Y.; Chang, S.; Wang, H.; Huang, D.; Zhao, J.; Chen, T.; Wong, W. Y.; Wong, W. K.; Zhu, X. *J. Power Source* **2013**, *243*, 253.
21. Wu, W.; Yang, J.; Hua, J.; Tang, J.; Zhanng, L.; Long, Y.; Tian, H. *J. Mater. Chem.* **2010**, *20*, 1772
22. Hua, Y.; Chang, S.; Huang, D.; Zhou, X.; Zhu, X.; Zhao, J.; Chen, T.; Wong, W. Y.; Wong, W. K. *Chem. Mater.* **2013**, *25*, 2146.

23. Nazeeruddin, M. K.; Baranoff, E.; Grätzel, M. *Solar Energy* **2011**, *85*, 1172.
24. Daphnomili, D.; Landrou, G.; Prakash Singh, S.; Thomas, A.; Yesudas, K.; Bhanuprakash, K.; Sharma, G. D.; Coutsolelos, A. G. *RSC Adv.* **2012**, *2*, 12899.
25. Wu, H.; Wang, H.; Xue, L.; Li, X. *J. Colloid Interf. Sci.* **2011**, *353*, 476.
26. Shown, I.; Ujihara, M.; Imae, T. *J. Colloid Interf. Sci.* **2010**, *352*, 232.
27. Jagadeeswari, S.; Paramaguru, G.; Thennarasu, S.; Renganathan, R. *J. Mole. Struct.* **2014**, *1060*, 191.
28. Becke, A.D. *J. Chem. Phys.* **1993**, *98*, 5648.
29. Gaussian 09, Revision D.01, M. J. Frisch, G. W. Trucks, H. B. Schlegel, G. E. Scuseria, M. A. Robb, J. R. Cheeseman, G. Scalmani, V. Barone, B. Mennucci, G. A. Petersson, H. Nakatsuji, M. Caricato, X. Li, H. P. Hratchian, A. F. Izmaylov, J. Bloino, G. Zheng, J. L. Sonnenberg, M. Hada, M. Ehara, K. Toyota, R. Fukuda, J. Hasegawa, M. Ishida, T. Nakajima, Y. Honda, O. Kitao, H. Nakai, T. Vreven, J. A. Montgomery, Jr., J. E. Peralta, F. Ogliaro, M. Bearpark, J. J. Heyd, E. Brothers, K. N. Kudin, V. N. Staroverov, T. Keith, R. Kobayashi, J. Normand, K. Raghavachari, A. Rendell, J. C. Burant, S. S. Iyengar, J. Tomasi, M. Cossi, N. Rega, J. M. Millam, M. Klene, J. E. Knox, J. B. Cross, V. Bakken, C. Adamo, J. Jaramillo, R. Gomperts, R. E. Stratmann, O. Yazyev, A. J. Austin, R. Cammi, C. Pomelli, J. W. Ochterski, R. L. Martin, K. Morokuma, V. G. Zakrzewski, G. A.

Voth, P. Salvador, J. J. Dannenberg, S. Dapprich, A. D. Daniels, O. Farkas, J. B. Foresman, J. V. Ortiz, J. Cioslowski, and D. J. Fox, *Gaussian, Inc.*, Wallingford CT, **2013**.

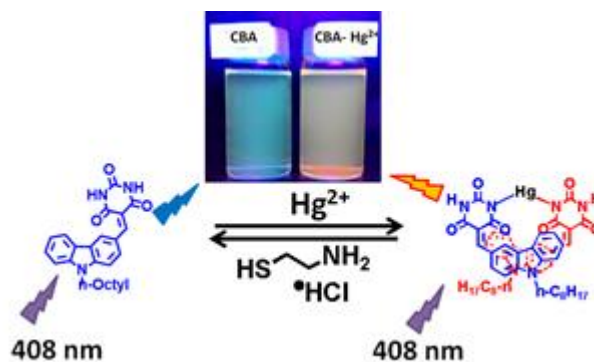
30. Dai, X.-X.; Feng, H.-L.; Chen, W. J.; Yang, Y.; Nie, L.-B.; Wang, L.; Kuang, D.- B.; Meie, H.; Cao, D. *Dyes Pigm.* **2015**, *122*, 13.

## Chapter 4

### A Carbazole Based “Turn on” Fluorescent Sensor for Selective Detection of $\text{Hg}^{2+}$ in an Aqueous Medium

---

#### 4.1 Abstract



Developed a multimode  $\text{Hg}^{2+}$  selective sensor system based on carbazole-barbituric acid conjugate (CBA). Its colorimetric and fluorescent behaviour for  $\text{Hg}^{2+}$  ions in both aqueous methanol and fully aqueous (micelle) media were investigated. Upon  $\text{Hg}^{2+}$  binding, CBA exhibited a considerable aggregation induced absorption spectral changes along with an enhanced emission (AIE) at 593 nm in aqueous methanol. Job's plot analysis of the complexation showed that CBA had a 2:1 binding stoichiometry in aqueous methanol medium, while in the micellar medium a 1:2 binding stoichiometry. In both the media, CBA exhibited a selective and sensitive detection of  $\text{Hg}^{2+}$  without any interference from the other metal ions.

## 4.2 Introduction

Heavy metals, which are toxic to the environment and ecosystem, have been dangerously accumulating in the biosphere as a result of human activity. They contaminate the food chain and cause persistent damages to the living beings. Hence, investigations on the mechanism of accumulation and transmission of toxic metals in the environment and precautionary measures thereby are active areas of research in these days. With the advent of sensitive optical imaging tools, which are capable of assaying heavy and transition metal ions in biological samples, there is a renewed interest in the development of selective and sensitive fluorescent chemosensors for the rapid identification of the toxic heavy metal ions, such as the  $\text{Pb}^{2+}$ ,  $\text{Cd}^{2+}$ , and  $\text{Hg}^{2+}$ .<sup>1-3</sup> Among these, mercury contamination is found to be widespread and originates from a variety of natural as well as anthropogenic sources including volcanic eruptions, incineration of urban solid wastes, mining and improper management of e-wastes. Mercury ends up in the marine environment, by bacterial action gets converted into organic mercury (methylmercury), which is lipophilic and easily enters into the food chain and thus accumulates in higher organisms, in particular, large fishes. Mercury poisoning through food-chain and high dose exposure can result in several diseases, including acrodynia, Hunter-Russell syndrome, and Minamata disease.<sup>4</sup> Studies carried out in patients inflicted with mercury poisoning have shown that mercury concentrates more in blood and brain, as seen in the case of certain patients with Alzheimer's disease.<sup>5</sup> The maximum

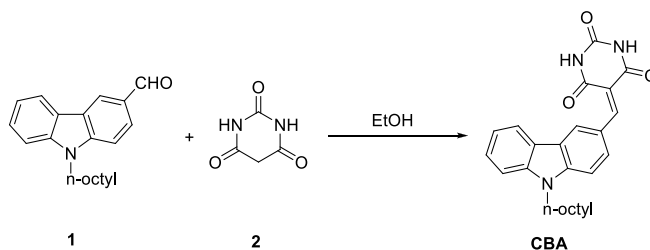
permitted level of mercury (II) ions in potable water prescribed by EPA is 2 ppb.<sup>6,7</sup> Detection and quantification of mercury are thus necessary for monitoring and preventing the contamination of the environment and the living world.

Fluorescent chemosensors of metal ions consist of a fluorophore and a receptor moiety. The fluorescence emission gets altered in terms of energy or intensity as a result of metal ion binding. Depending on the design of the chemosensor system, such changes in the fluorescence may be due to photoinduced electron/charge transfer, energy transfer, excimer/excimer formation or dissociation or charge induced changes in the polarity of the environment etc.<sup>8-11</sup> The commonly used fluorophores are 1,8-naphthalimide, coumarin, pyrene, anthracene, BODIPY, squaraine, xanthenes, cyanine, rhodamine, fluorescein etc.<sup>12-19</sup> As fluorescent chemosensors are hydrophobic in nature, most of them require organic solvents for proper operation due to low solubility in aqueous medium. In recent years, hydrophilic biomolecules such as amino acids, peptides, and DNA have been used as receptors in the design of fluorescent chemosensors. These molecules and supramolecular assemblies of natural origin have potent binding affinities to specific metal ions, higher solubility in aqueous and other polar solvents and biological compatibility required for *in vivo* or *in vitro* tissue imaging applications and such chemosensors showed sensitive responses to heavy metal ions in aqueous solutions.<sup>20</sup> For practical applications, two major requirements to avoid filter effects are, having a long wavelength emission maximum along with enhanced emission intensity

in the presence of the metal ion. A majority of fluorescent chemosensors show quenching of fluorescence due to the heavy atom effect. In 2013, S. Li and co-workers<sup>21</sup> reported a barbituric acid derivative (AnB) having anthracene as the fluorophore which can selectively detect mercury cation, by spectrofluorometric method via the formation of  $\text{Hg}^{2+}$ -AnB coordination polymers. We report for the first time a cost effective carbazole based chemosensor (CBA) which can detect  $\text{Hg}^{2+}$  ions with a high degree of sensitivity and selectivity in aqueous methanol medium, showing over 100 fold enhancement in emission.

## 4.3 Results and Discussions

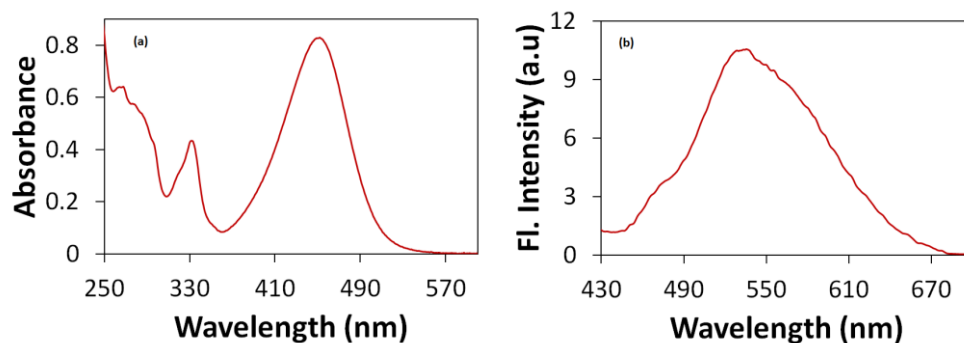
### 4.3.1 Photophysical Properties



**Scheme 4. 1**

The carbazole barbituric acid derivative (CBA) synthesized by Knoevenagel condensation between 9-octyl-9H-carbazole-3-carbaldehyde (1) and barbituric acid (2) in ethanol (Scheme 4.1) as reported elsewhere.<sup>22</sup>

The absorption spectrum of CBA is characteristic of a  $\pi$ -conjugated Donor-Acceptor molecule with a prominent charge transfer band at 438 nm ( $\epsilon_{\text{max}}$ ,  $3.16 \times 10^4 \text{ cm}^{-1} \text{ M}^{-1}$ ) in methanol and is sensitive to solvent polarity. In order to assure an aqueous medium for the metal binding studies, a methanol water mixture of 1:1 (v:v) ratio was used. It was observed that as the water content increased, the precipitation of the dye resulted. The variation in the aqueous content during the addition of metal ions was kept at 0.19%. Blank experiments showed that no changes in the absorption and emission properties of the dye in the measured range. The absorption maximum observed for the dye in this solvent composition was at 452 nm. The observed emission was very weak and broad with a maximum at 533 nm (Figure 4.1).

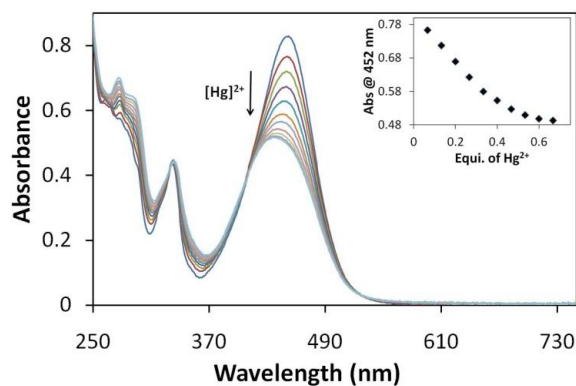


**Figure 4.1** Absorption (a) and emission (b) spectra of CBA in 1:1 MeOH H<sub>2</sub>O,  $\lambda_{\text{ex}} = 408 \text{ nm}$

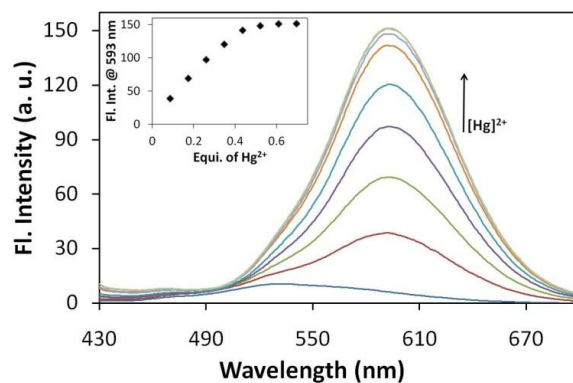


### 4.3.2 Metal ion binding studies of CBA in 1:1 MeOH/H<sub>2</sub>O

The interaction of CBA with an aqueous solution of mercury (II) acetate was investigated by spectrophotometric and spectrofluorometric titrations in aqueous methanol (Figure 4.2). During the photometric titration of mercury ions to CBA, the light yellow solution turned colourless along with a blue-shift of the long-wavelength absorption maximum from 452 nm to 438 nm. The isosbestic point at 408 nm indicates the formation of a complex with Hg<sup>2+</sup> ions which is in equilibrium with the free ligand. No further change in the absorbance was observed after the addition of about 0.7 equivalence of Hg<sup>2+</sup> (Figure 4.2 inset). Since this value is less than one, it can be assumed that a 2:1 complex between CBA and Hg<sup>2+</sup> ie., CBA-Hg-CBA by replacing two acetate anions is formed. The blue-shift in the absorption spectrum is indicative of the formation of an aggregate of CBA or the reduced the electron affinity of the pyrimidine moiety due to complexation with Hg<sup>2+</sup> ions.

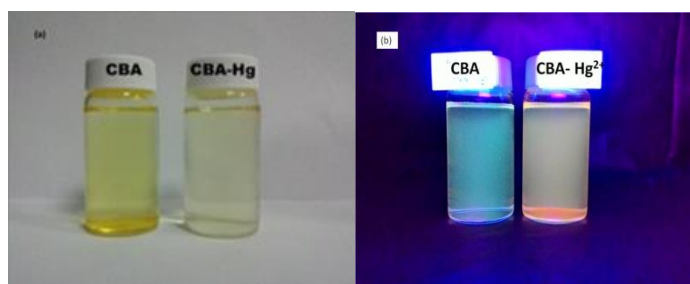


**Figure 4.2** Evolution of absorption spectra of CBA in the presence of increasing concentration of an aqueous solution of  $\text{Hg}(\text{OAc})_2$  in 1:1 MeOH  $\text{H}_2\text{O}$  ( $[\text{CBA}] = 30 \mu\text{M}$ ,  $[\text{Hg}(\text{OAc})_2] = 0\text{--}19 \mu\text{M}$ ). Arrows indicate the direction change in the absorbance.



**Figure 4.3** Evolution of fluorescence spectra of CBA in the presence of increasing concentration of an aqueous solution of  $\text{Hg}(\text{OAc})_2$  in 1:1 MeOH  $\text{H}_2\text{O}$  ( $[\text{CBA}] = 10 \mu\text{M}$ ,  $[\text{Hg}(\text{OAc})_2] = 0\text{--}8 \mu\text{M}$ ,  $\lambda_{\text{ex}} = 408 \text{ nm}$ ). Arrows indicate the direction change in the fluorescence intensity.

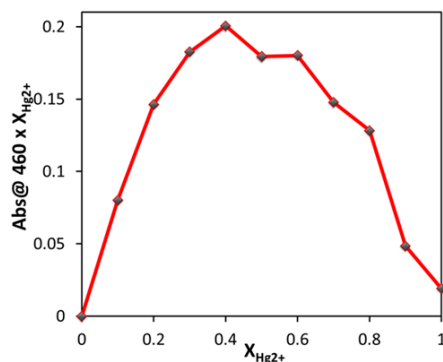
We further investigated the emission spectral characteristics and its response to  $\text{Hg}^{2+}$  in aqueous methanol solutions. Fluorescence spectra were recorded by exciting optically matched solutions of CBA ( $1.0 \times 10^{-5}$  M) at the isosbestic point (408 nm). This was done to rule out fluorescence intensity variation due to changes in the absorbance at the excitation wavelength. With increasing the concentration of  $\text{Hg}^{2+}$  ions, the weak fluorescence intensity of CBA was found to increase along with a red shift in the emission maximum to 593 nm (Figure 4.3). A dramatic 150 fold enhancement in the intensity is observed and this has reached a plateau after the addition of about 0.7 equivalents of  $\text{Hg}^{2+}$  ions (Figure 4.3 inset). This result agrees with the outcome of spectrophotometric titration and suggests that CBA showed a very strong affinity to  $\text{Hg}^{2+}$  ions. The colorimetric response as well as the fluorescence response under UV illumination of CBA to  $\text{Hg}^{2+}$  in 1:1 methanol water solution, is visible even with the naked eye as shown in the photographs (Figure 4.4).



**Figure 4.4** Photographs of CBA and CBA in the presence of  $\text{Hg}^{2+}$  ions under (a) normal light and (b) UV (365 nm) light.

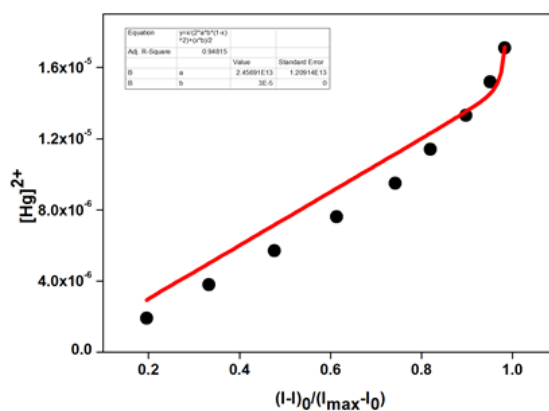
### 4.3.2.1 Stoichiometry and Reversibility of Complexation

The stoichiometry of the complex formed between CBA and  $\text{Hg}^{2+}$  ions were analysed through Job's plot analysis and the binding constant was calculated through nonlinear least square fit analysis. The CBA formed a 2:1 complex in the presence of 0.5 equivalents of  $\text{Hg}^{2+}$  ions, the binding geometry is proved by Jobs plot. The maximum on the plot correspond to the stoichiometry of the two species in the complex and in the present study, the maximum is at the mole fraction of  $\text{Hg}^{2+}$  as 0.4 which confirms the 2:1 binding stoichiometry (Figure 4.5). Nonlinear least square fit analysis gave spectrophotometrically an association constant,  $K$  of  $2.45 \times 10^{13} \text{ M}^{-2}$  (Figure 4.6) and spectrofluorimetrically an association constant,  $K$  of  $8.73 \times 10^{13} \text{ M}^{-2}$  (figure 4.7) for 2:1 complex. A remarkably high value of  $8.73 \times 10^{13} \text{ M}^{-2}$  ( $R^2 = 0.996$ ) is obtained, which shows the very high affinity of CBA to  $\text{Hg}^{2+}$  ions.

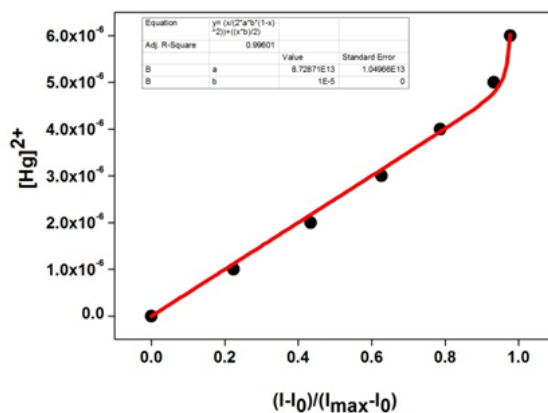


**Figure 4.5** Job's plot analysis of CBA with  $\text{Hg}^{2+}$  showing a 2:1 binding geometry.

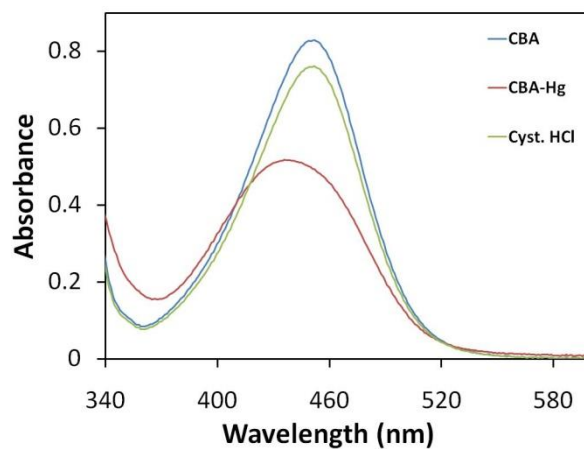
To investigate the reversibility of the complexation of CBA with mercuric ions, cysteamine hydrochloride, (Cys HCl) was used as the complexing agent. To verify this, CBA-Hg<sup>2+</sup>-CBA solution was subsequently treated with excess cysteamine hydrochloride, which holds a thiol group, a strong ligand to Hg<sup>2+</sup> ions. The strong fluorescence of the CBA-Hg<sup>2+</sup>-CBA was almost quenched and the absorption spectrum showed a red shift indicating a decomplexation and releasing of free CBA and thus demonstrating the possibility of using CBA as a reversible chemosensor (Figure 4.8 & 4.9).



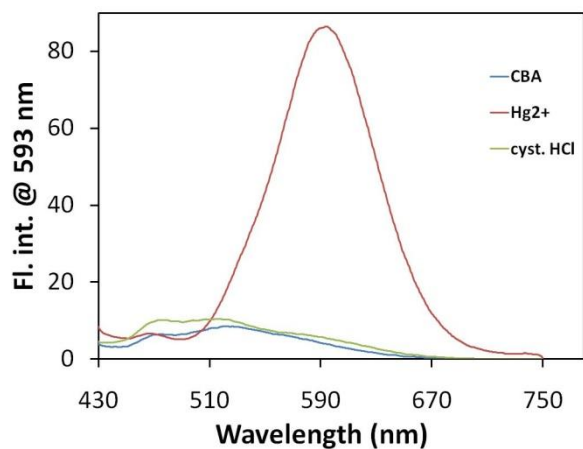
**Figure 4.6** A plot of absorbance ratio ( $I-I_0/I_{\max}-I_0$ ) vs. concentrations of Hg<sup>2+</sup> in (1:1) MeOH/H<sub>2</sub>O.



**Figure 4.7** A plot of fluorescence intensity ratio  $(I-I_0/I_{max}-I_0)$  vs. concentrations of  $Hg^{2+}$  in (1:1) MeOH/ $H_2O$ .



**Figure 4.8** Absorption spectrum of CBA,  $CBA-Hg^{2+}$  complex and in the presence of cysteamine hydrochloride.



**Figure 4.9** Emission spectra of CBA, CBA-Hg<sup>2+</sup> complex, and in the presence of cysteamine hydrochloride. The excitation wavelength is 408 nm.

#### 4.3.2.2 Nature of Complexation

Completion of binding interaction at lower Hg<sup>2+</sup> equivalents suggests a 2:1-CBA:Hg<sup>2+</sup> stoichiometry for the complex formation. In a related work, Li and co-workers have identified the formation of a coordination polymer of Hg<sup>2+</sup> ions with an anthracene-barbituric acid conjugate. According to this report, the polymer formation involved deprotonation of N-H protons of the barbituric acid moiety and the interaction was proposed to have a 1:1 stoichiometry.<sup>21</sup> Our study of spectrophotometric titration data by continuous variation of mole fraction of Hg<sup>2+</sup> in comparison to CBA and the Job's plot thus obtained, fitted very well with a model corresponding to a 2:1 CBA-Hg<sup>2+</sup>-CBA complex. This result indicates a mechanism that involves deprotonation of NH protons of the barbituric acid moiety. The complex

formation could be a stepwise formation of the 1:1 complex CBA-Hg<sup>2+</sup>-OAc followed by the formation of the 2:1 complex CBA-Hg<sup>2+</sup>-CBA. In this mechanism two possibilities exist. In the first one, the two binding interactions occur with comparable rate constants and in the second mode, one of the binding interactions is very fast compared to the second binding. However, the observation of the well-focused isobestic point at 408 nm with a very small standard deviation (0.003 absorbance units) suggests the second mechanism. Here an apparent equilibrium between CBA and CBA-Hg<sup>2+</sup>-CBA is involved and the formation of the 1:1 complex is not observed by the steady state UV-Vis spectroscopy.

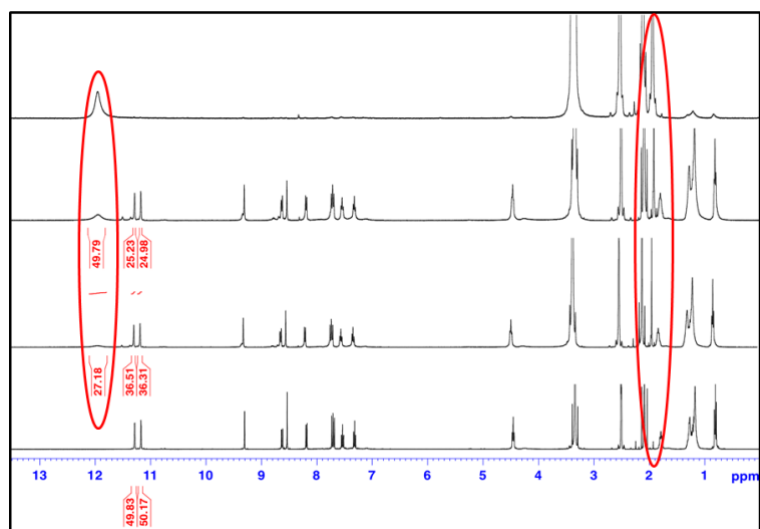
In order to add further insight into the structure of the complex formed between the CBA and Hg<sup>2+</sup> ions and the complexation mechanism, we have recorded <sup>1</sup>H-NMR spectrum in DMSO-d<sub>6</sub> in the presence of increasing concentration of Hg (II) acetate. Figure 4.10 shows <sup>1</sup>H-NMR spectrum of CBA and mixtures of CBA and Hg (II) acetate at different ratios from 0 to 0.5 equivalents of Hg<sup>2+</sup>. The spectrum of free CBA is characterized by two distinct peaks corresponding to the two NH protons at 11.15 ppm and 11.27 ppm. Analysis of the spectra evolved in the presence of Hg<sup>2+</sup> acetate shows new resonance peaks at 12 ppm, 11.5 ppm, and 1.95 ppm. The peak at 12 ppm is assigned to the -OH proton of acetic acid which is indicative of a mechanism of Hg<sup>2+</sup> binding involving the deprotonation of NH of the barbituric acid moiety releasing a molecule of acetic acid. Moreover, the binding event led to deprotonation of N-H on CBA as indicated by the decrease in the peak area of two N-H protons and a



proportional increase in the area of the peak corresponding to the –OH proton of acetic acid. A careful look at these spectra reveals the appearance of a small peak at 11.5 ppm after the addition of  $\text{Hg}^{2+}$  acetate and this may be due to the 1:1 CBA- $\text{Hg}^{2+}$ -OAc complex. This is observed probably due to the relatively high concentrations used for the NMR experiments or the second reaction may be slow enough leaving some 1:1 complex to be observed on the time scale of the NMR experiment. When 0.5 equivalents of  $\text{Hg}(\text{OAc})_2$  was added, the two NH protons completely vanished and the CBA- $\text{Hg}^{2+}$ -CBA complex precipitated which is undoubtedly seen in  $^1\text{H}$ -NMR, ie, only acetic acid peaks and solvents peaks are seen in the resulting spectrum.  $^1\text{H}$  NMR of the precipitate was taken in THF-d8 was indicative of a symmetrical structure with one free NH proton (Figure 4.11). This further confirms the 2:1 binding stoichiometry.

Further corroborative evidence for the mercury complex was observed in the MALDI-TOF mass spectrum which showed a mass peak at  $m/z=1082.0839$  corresponding to  $[2\text{CBA}+\text{Hg}+2\text{H}+2\text{Na}-2\text{H}]$  fragment, where the calculated molecular weight is 1082.3584 and 1066.1122 corresponding to  $[2\text{CBA}+\text{Hg}+\text{MeOH}-2\text{H}]$  fragment, where the calculated molecular weight is 1066.3917 (Figure 4.12 and Table 4.1). The results of the  $^1\text{H}$ -NMR titration and MALDI-TOF suggest a 2:1 binding stoichiometry of CBA with  $\text{Hg}^{2+}$ . Such mercuration by deprotonation and insertion between T-T base pairs has observed in DNA double helices with a linear T-Hg-T geometry.<sup>23,24</sup> Similarly, in thiamine-graphene conjugates, a mercury

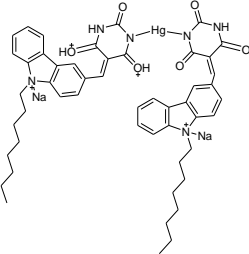
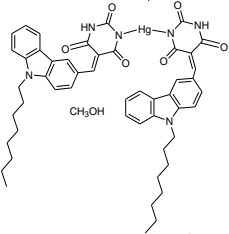
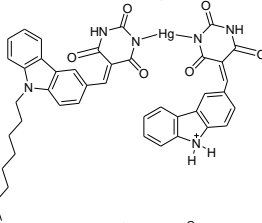
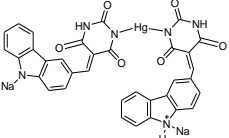
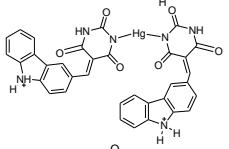
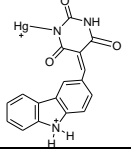
induced deprotonation and formation of a 2:1 complex with a bend structure has been reported.<sup>25</sup>



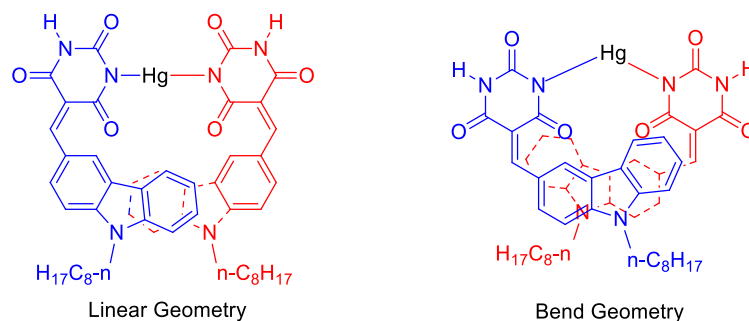
**Figure 4.10** The  $^1\text{H}$ -NMR spectra of the CBA and CBA in the presence of 0.13, 0.25, 0.5 equivalents of  $\text{Hg}^{2+}$  acetate (400 MHz,  $\text{DMSO-d}_6$ )



**Table 4.1** Fragment ions observed in MALDI-TOF.

Peak No.	Fragment	Expected Mass	Observed Mass
1		1082.3584	1082.0839
2		1066.3917	1066.1122
3		923.2475	923.3328
4		855.0862	855.0875
5		812.1296	812.4752
6		507.0496	507.3012

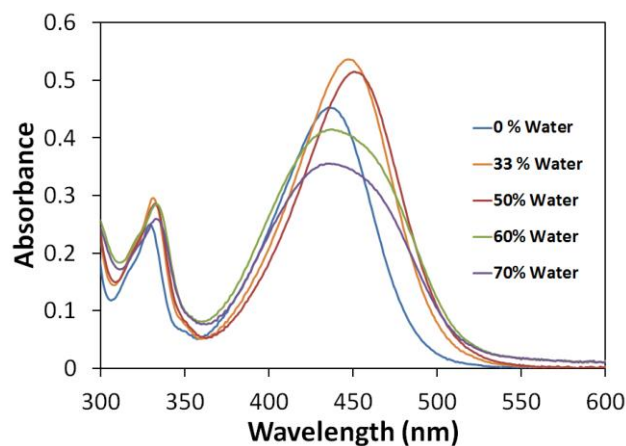
The observation of fluorescence enhancement is contrary to what generally reported. Usually, heavy metals quench the fluorescence of the molecules due to heavy atom effect. A plausible reason for the enhanced emission could be the aggregate formation or a CBA-mercury complex having a linear or bend geometry (Figure 4.12). Such geometries can lead to close interaction between two carbazole moieties. Further, an association of non-polar n-octyl chains assists in bringing two carbazole moieties closer favouring aggregation induced emission.



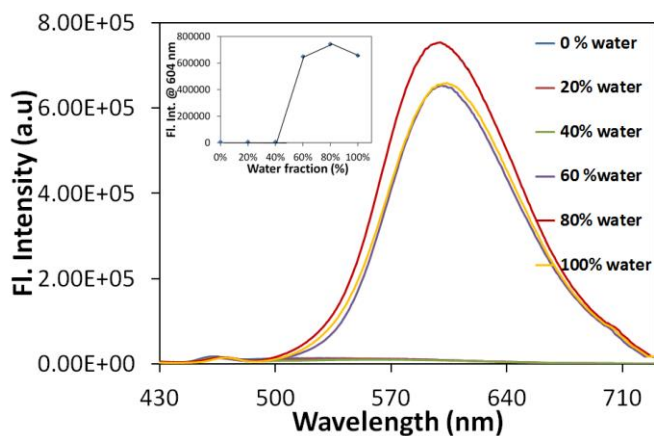
**Figure 4.12** Proposed geometry for the CBA-Hg-CBA complex.

Most of the fluorescent organic dyes are reasonably highly emissive in the solution state and drop their emission in the solid state or in the aggregated structures as a result of aggregation induced quenching. Conversely, in recent times, Tang and co-workers<sup>26-28</sup> and Park and co-workers<sup>29,30</sup> have individually presented that some flexible molecular systems with weak emission are capable of showing strong fluorescence at high concentration due to aggregation. This phenomenon finds applications

in numerous designs of fluorescent sensors and solid state lighting devices. Aggregation of barbituric acid or its derivatives via hydrogen bonding networks has been well documented in the literature.<sup>31,32</sup> Aggregation induced emission enhancement (AIEE) results from the controlled movement of molecules in close-packed structures suppressing non-radiative relaxation pathways. To establish aggregation induced emission enhancement (AIEE) of a compound,<sup>33,34</sup> its fluorescent behaviour is studied with a poor solvent added to a solution of the compound. As CBA is insoluble in water, increasing the water fraction in the mixed solvent can change its existing form from a solution state in pure MeOH to aggregated particles in mixtures with high water content. The emission spectra of CBA in the MeOH/H<sub>2</sub>O mixtures with different water contents are shown in Figure 4.13. Figure 4.12 is the absorption spectral changes observed as a function of water content. Here the absorption spectrum initially showed a red shift to 450 nm, typical for a charge transfer band that responds to increase in polarity. However, the addition of water above 50% lead to a blue shift to 435 nm for 70% of water and higher water content made the spectrum flatter and finally the dye gets precipitated. The fluorescence emission showed a sudden enhancement in the intensity for a 60% water-methanol mixture along with a red shift to 600 nm. This enhancement in luminescence is due to the aggregation effects and it is clear that the aggregation can lead to such enhancement in emission with the possibility of such stacking between two CBA units is achievable in the CBA-Hg<sup>2+</sup>-CBA complex.



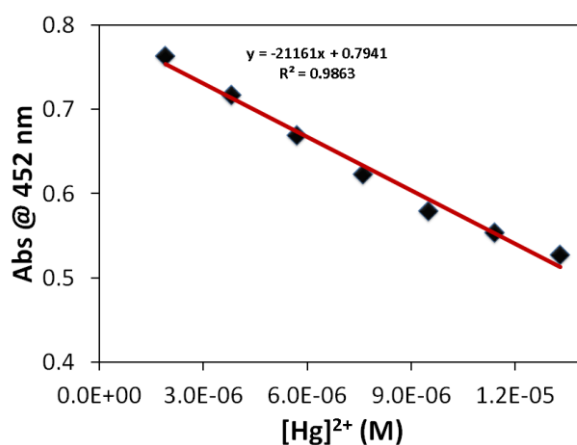
**Figure 4.12** Changes in the absorption spectra of CBA in MEOH/H<sub>2</sub>O mixture as a function of solvent composition in percentage.



**Figure 4.13** Changes in the emission spectra of CBA in MeOH/H<sub>2</sub>O mixture as a function of solvent composition in percentage ( $\lambda_{ex} = 408$  nm). (Inset: Fluorescence intensity @ 604nm vs % water).

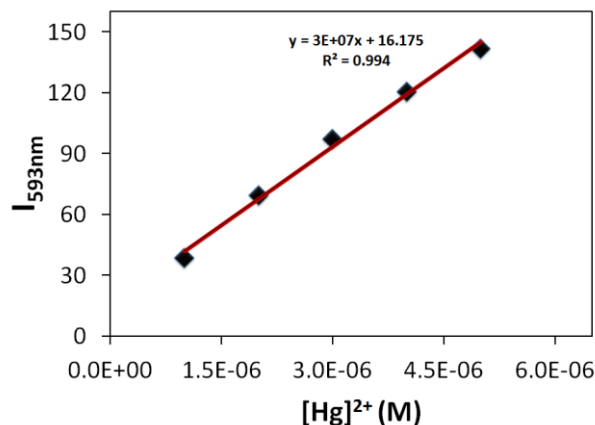
#### 4.3.2.3 Determination of Lowest Detection Limit

The variation in the absorbance and the fluorescence intensity show a linear dependence with the  $\text{Hg}^{2+}$  in the concentration range 0-12  $\mu\text{M}$  and 0-6  $\mu\text{M}$  respectively. Each of this response was plotted and the detection limit was calculated from the slope of the fitted curve. The results show that CBA can be used to detect and quantify  $\text{Hg}^{2+}$  with a detection limit of 8.89 nM by fluorescence and 1.7  $\mu\text{M}$  by absorption spectroscopy (Figure 4.14 & 4.15).



**Figure 4.14** A plot showing a variation of Absorbance at 452 nm as a function of concentrations of  $\text{Hg}^{2+}$  in MeOH/ $\text{H}_2\text{O}$  (1:1).

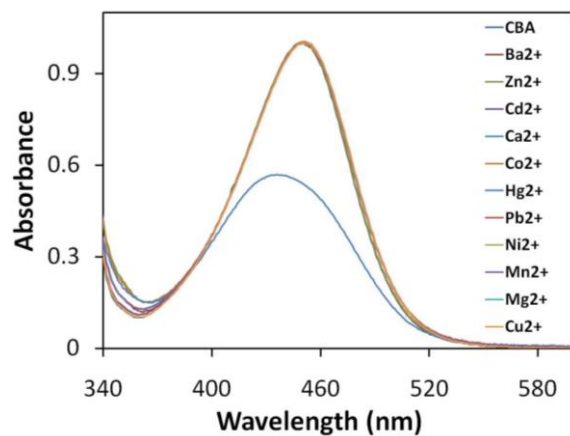




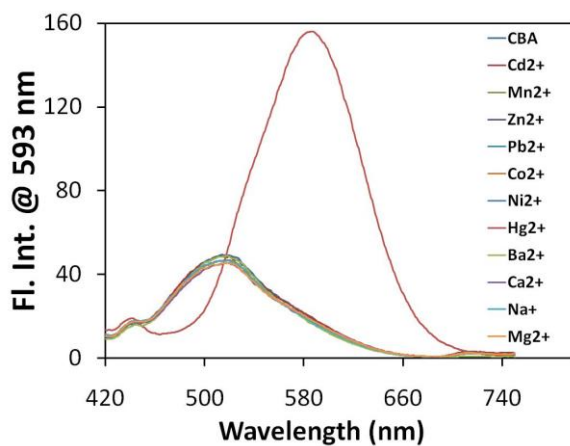
**Figure 4.15** A plot showing a variation of Fluorescence intensity at 593 nm as a function of concentrations of  $\text{Hg}^{2+}$  in MeOH/ $\text{H}_2\text{O}$  (1:1).

#### 4.3.2.4 Selectivity of Metal ion Recognition

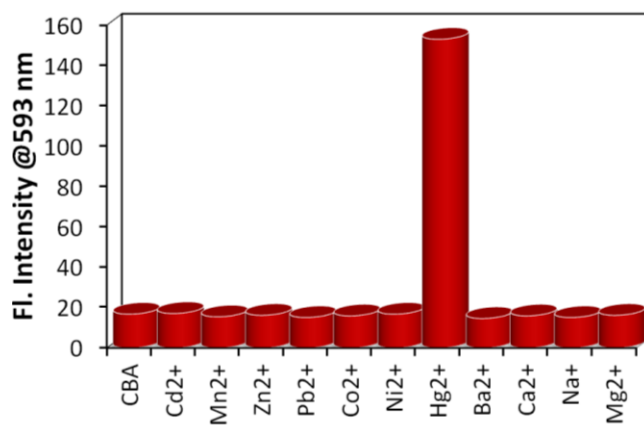
To demonstrate the selectivity of CBA for  $\text{Hg}^{2+}$  ions, we have investigated the interactions of dyes CBA with other environmentally important metal ions such as  $\text{Na}^+$ ,  $\text{Mg}^{2+}$ ,  $\text{Ca}^{2+}$ ,  $\text{Cd}^{2+}$ ,  $\text{Zn}^{2+}$ ,  $\text{Ni}^{2+}$ ,  $\text{Ba}^{2+}$ ,  $\text{Cu}^{2+}$ ,  $\text{Pb}^{2+}$ ,  $\text{Co}^{2+}$ , and  $\text{Mn}^{2+}$  ions in 1:1 MeOH/ $\text{H}_2\text{O}$ . The influence of the addition of acetate salts of  $\text{Na}^+$ ,  $\text{Mg}^{2+}$ ,  $\text{Ca}^{2+}$ ,  $\text{Cd}^{2+}$ ,  $\text{Zn}^{2+}$ ,  $\text{Ni}^{2+}$ ,  $\text{Ba}^{2+}$ ,  $\text{Cu}^{2+}$ ,  $\text{Pb}^{2+}$ ,  $\text{Co}^{2+}$ , and  $\text{Mn}^{2+}$  on the absorption and emission properties of CBA was studied (Figure 4.16 & 4.17). No change in fluorescence intensity was observed for a metal ion concentration up to 35  $\mu\text{M}$  except for the  $\text{Hg}^{2+}$  salts. The chloride, sulfate and perchlorate salts of mercury were also used and showed similar enhancement in fluorescence. The bar diagram in Figure 4.18 illustrates the selectivity feature of CBA in the detection of  $\text{Hg}^{2+}$  ions.



**Figure 4.16** Absorption spectra of CBA recorded in the presence of various metal ions (Metal ion concentration =  $35\mu\text{M}$ ,  $[\text{CBA}] = 26\mu\text{M}$ ) in MeOH/H<sub>2</sub>O (1:1).



**Figure 4.17** Emission spectra of CBA recorded in the presence of various metal ions (Metal ion concentration =  $35\mu\text{M}$ ,  $[\text{CBA}] = 26\mu\text{M}$ ,  $\lambda_{\text{ex}} = 408 \text{ nm}$ ) in MeOH/H<sub>2</sub>O (1:1).



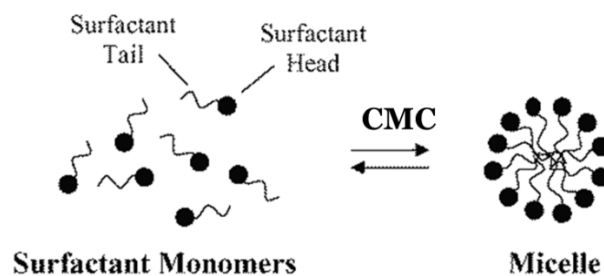
**Figure 4.18** The bar diagram showing the metal ion binding selectivity of CBA.

### 4.3.3 Study of the Effect of Microheterogeneous Medium on the Metal Binding Properties of CBA

CBA showed unusual sensitivity and selectivity for  $\text{Hg}^{2+}$  ions and forms a 2:1 complex with mercury in 1:1 MeOH/H<sub>2</sub>O mixture. The calculated lowest detection limit was 8.89 nM by fluorescence. However, the range of detection is only up to 0.5 equivalents of  $\text{Hg}^{2+}$ . To achieve a higher range of detection, a barrier to complexation can be introduced. Microheterogeneous medium such as micelles offers such a possibility, where the hydrophobic CBA molecule can be solubilized within the micelle, limiting easy access to metal ions. This is expected to control the stoichiometry of binding by choosing appropriate surfactant concentration.

A micelle is an aggregate of amphiphilic surfactant molecules having a polar head and non-polar tail groups dispersed in a liquid. A typical micelle in aqueous solution forms an aggregate with the hydrophilic "head" group in contact with surrounding water, sequestering the hydrophobic tail in the core of the aggregate. This type of micelle is known as a normal-phase micelle (oil-in-water micelle). Inverse micelles have the polar head groups at the core with the tail groups extending out (water-in-oil micelle). Micelles are approximately spherical in shape. Other phases, including shapes such as ellipsoids, cylinders, and bilayers, are also possible. The shape and size of a micelle is a function of the molecular geometry of its surfactant molecule and solution conditions such as surfactant concentration, temperature, pH, and ionic strength. Most commonly, surfactants are classified according

to the nature of their polar head groups. Non-ionic surfactants are neutral molecules with a polar head group. Ionic surfactants are charged molecules and carries either a positive or a negative charge. When the charge is negative, the surfactant molecules assemble in an aqueous medium to form a micelle with an anionic outer surface. Similarly, when the charge positive it forms a micelle with a positively charged surface.

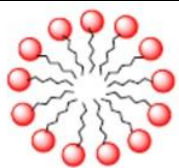


The **critical micelle concentration (CMC)** and aggregation number ( $N_{\text{agg}}$ ) are two important parameters that describe a surfactant molecule. CMC is defined as the concentration of surfactants above which micelles form. The value of the **CMC** for a given surfactant in a given medium depends on temperature, pressure, and (sometimes strongly) on the presence and concentration of other surface active substances and electrolytes. For example, the value of **CMC** for sodium dodecyl sulfate in water (in the absence of other additives or salts) at 25 °C and 1 atm pressure, is  $8 \times 10^{-3} \text{ mol L}^{-1}$ . The aggregation number ( $N_{\text{agg}}$ ) is the number of surfactant molecules present in a micelle once the critical micelle concentration (CMC) is reached.

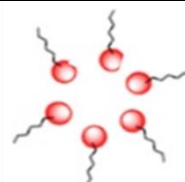
---

### Types of Micelle

---



Normal Phase Micelle



Inverse Phase micelle

---

### Shapes of micelle

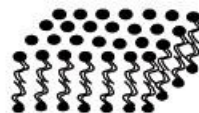
---



Spherical Micelle



Cylindrical Micelle

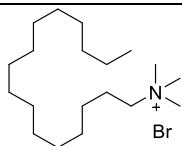


Bilayer

---

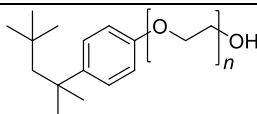
### Types of Surfactants

---



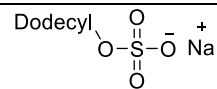
CTAB

Cationic surfactant



Triton X-100

Neutral Surfactants



SDS

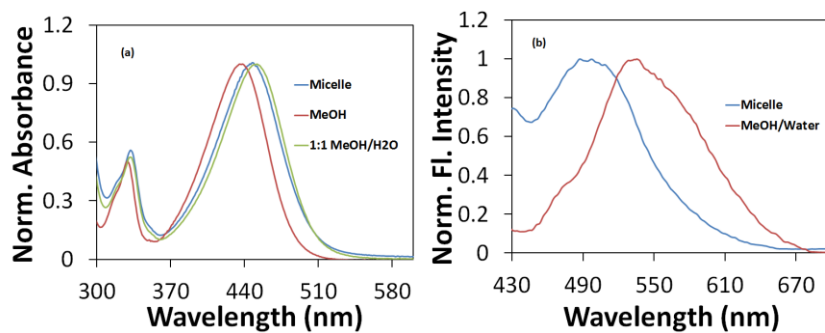
Anionic Surfactants

CBA by nature is amphiphilic and is expected to get solubilised within the micelle with a topology that keeps the octylcarbazol in the hydrophobic core and the polar barbituric acid moiety aligned along the

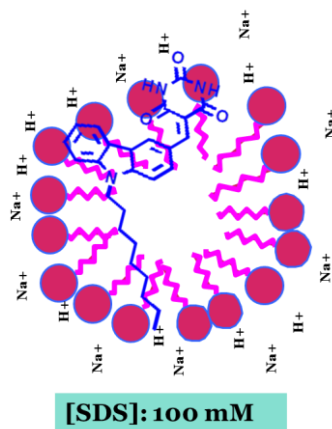
surface. For a prospective binding of positively charged metal ions, it is better to use anionic micelles. The inherent negative charge on the surface of the micelle is also expected to assist in bringing metal ions closer to the chelating groups on CBA. With this objective, we choose anionic surfactant sodium dodecyl sulphate (SDS) in this study. Of all the conditions examined, it has been observed that a 100 mM aqueous SDS micellar medium is very effective in the present case.

#### 4.3.3.1 Photophysical Properties of CBA in Micellar Medium

The absorption and emission spectrum of CBA in SDS micelle were recorded. The absorption spectrum showed a maximum at 448 nm which is 10 nm red shifted in comparison to the maximum obtained in methanol and 4 nm less than that observed in 1:1 MeOH/H<sub>2</sub>O mixture (Figure 4.19a). Thus the polar environment experienced by the CBA molecule is similar or slightly lesser to that of 1:1 MeOH/H<sub>2</sub>O mixture. This indicates that the topology of micellisation of CBA is one in which the polar pyrimidine group aligned with the anionic surface of the micelle. The fluorescence spectrum also showed a similar trend with maximum at 494 nm which is 39 nm less than that observed in 1:1 MeOH/H<sub>2</sub>O mixture and same as that observed in methanol (Figure 4.19b). This further confirms the micellisation of CBA in SDS.



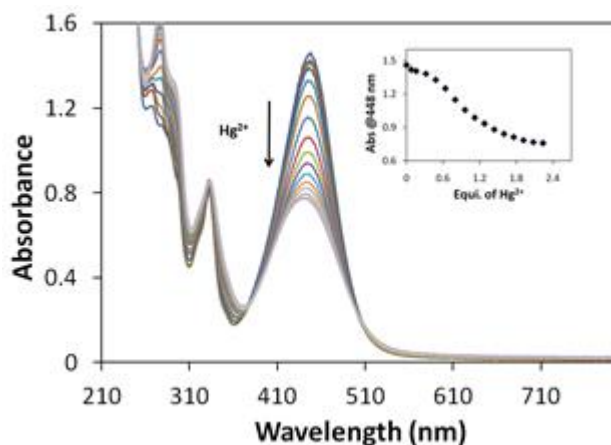
**Figure 4.19** Absorption spectra (a) and emission spectra (b) of CBA in methanol, 1:1 MeOH/H<sub>2</sub>O and in 100 mM SDS. The excitation wavelength is 408 nm.



**Figure 4.20** Cartoon showing the topology of micellisation of CBA in SDS micelles.



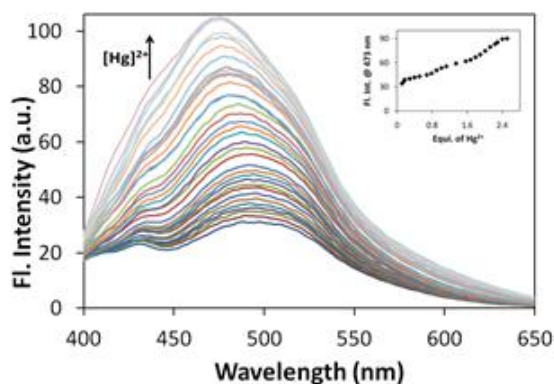
## 4.3.3.2 Metal ion binding studies of CBA in 100 mM SDS



**Figure 4.21** Evolution of absorption spectra of CBA in the presence of increasing concentration of an aqueous solution of  $\text{Hg}(\text{OAc})_2$  in 100 mM SDS ( $[\text{CBA}] = 37.6 \mu\text{M}$ ,  $[\text{Hg}(\text{OAc})_2] = 0\text{--}78 \mu\text{M}$ ). The arrow indicates the direction change in the absorbance.

Figure 4.21 shows the changes in the absorption spectrum of CBA in 100 mM SDS with the addition of  $\text{Hg}^{2+}$  ions. As the concentration of  $\text{Hg}^{2+}$  ions increased, we observed a decrease in the absorbance of the band at 448 nm with a small blue shift of 7 nm. Less focussed Isosbestic points at 376 nm and 511 nm indicate the formation of a complex of stoichiometry different from a 1:1 complex structure. A complete change in the absorbance required about 2 equivalents of  $\text{Hg}^{2+}$  (Figure 4.21). Inset in the Figure 4.21 shows the response of absorbance at 448 nm against the equivalents of  $\text{Hg}^{2+}$  used for the study. Similarly, with an increase in the concentration of  $\text{Hg}^{2+}$

ions, we observed a gradual increase in the fluorescence intensity of CBA (Figure 4.22). The addition of  $\text{Hg}^{2+}$  ions up to  $43.2 \mu\text{M}$  i.e., 2.4 equivalents gave about 4-fold enhancement in the fluorescence intensity along with a hypsochromic shift of 20 nm. This enhancement in fluorescence is useful for the detection of  $\text{Hg}^{2+}$  ions in aqueous medium. The range of detection is now modified from 0.5 equivalents to 2.4 equivalents when used in the presence of 100 mM SDS.

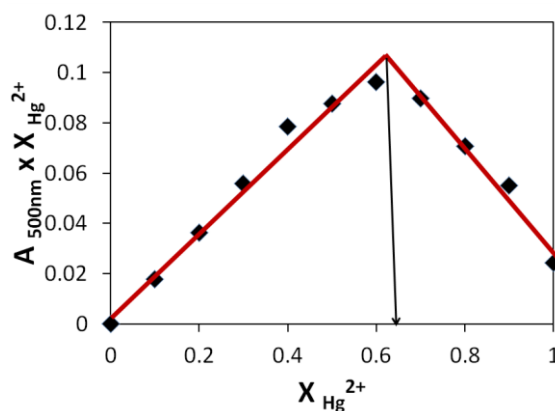


**Figure 4.22** Evolution of fluorescence spectra of CBA in the presence of increasing concentration of an aqueous solution of  $\text{Hg}(\text{OAc})_2$  in 100 mM SDS ( $[\text{CBA}] = 17.6 \mu\text{M}$ ,  $[\text{Hg}(\text{OAc})_2] = 0\text{--}43.2 \mu\text{M}$ ,  $\lambda_{\text{ex}} = 376 \text{ nm}$ ). The arrow indicates the direction change in the fluorescence intensity.

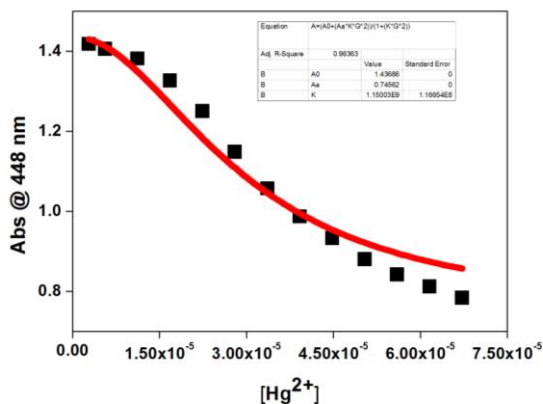
#### 4.3.3.3 Stoichiometry and Reversibility of Complexation in Micellar Medium

In order to understand the stoichiometry of the complex formed, Job's plot analysis was carried out. In micellar medium Job's plot showed a

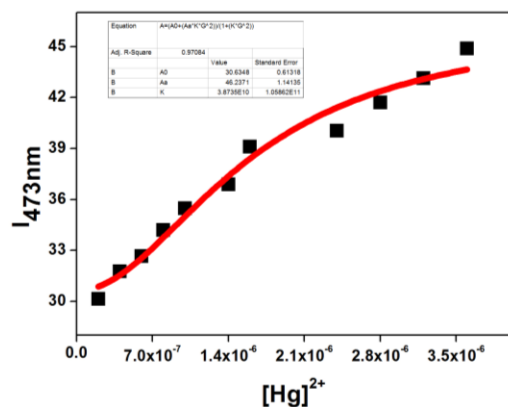
maximum at the mole fraction of  $\text{Hg}^{2+}$  as 0.65 which is an indicative of 1:2 or 2:1 binding stoichiometry. However, the association constant  $K_a$  was determined by a non-linear least square fit to a model described for 1:2 complexation stoichiometry and hence we concluded that the stoichiometry of the complex formed between CBA and  $\text{Hg}^{2+}$  ions in SDS micellar was found to be 1:2 (Figure 4.23). The nonlinear least square fit analysis of the absorbance changes at 448 nm gave an association constant ( $K_a$ ) of  $1.15 \times 10^9 \text{ M}^{-2}$  (Figure 4. 24). Similarly, the fluorescence intensity change at 473 nm was also fitted to a model corresponding to 1:2 binding stoichiometry resulting an association constant ( $K$ ) of  $10.6 \times 10^9 \text{ M}^{-2}$  in micellar medium (Figure 4.25).



**Figure 4.23** Job's plot analysis of CBA with  $\text{Hg}^{2+}$  showing 1:2 binding stoichiometry in 100 mM SDS.



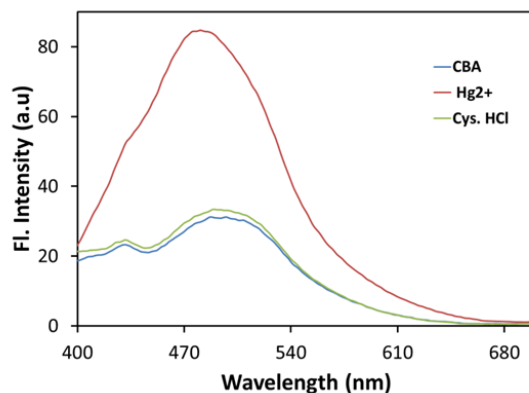
**Figure 4.24** A plot of absorbance at 448 nm vs. concentrations of  $\text{Hg}^{2+}$  in 100 mM SDS.



**Figure 4.25** A plot of fluorescence intensity at 473 nm vs. concentrations of  $\text{Hg}^{2+}$  in 100 mM SDS.

Cysteamine hydrochloride (Cys. HCl) was used as a competing chelating agent to explore the reusability of CBA in  $\text{Hg}^{2+}$  sensing. The weakly fluorescent CBA in 100 mM SDS was mixed with 2 equivalents of

$\text{Hg}^{2+}$  and about 5 equivalents of cysteamine hydrochloride (Cys. HCl) was added. The fluorescence spectrums of the solutions were recorded before and after the addition of cysteamine hydrochloride (Cys. HCl). While the addition of cysteamine hydrochloride, the enhanced fluorescence intensity in the presence of  $\text{Hg}^{2+}$  was restored to the initial intensity recorded for the free CBA in 100 mM SDS. This result demonstrated that CBA shows reversibility of the complexation in the presence of cysteamine hydrochloride in micellar medium (Figure 4.26).



**Figure 4.26** Emission spectra of CBA, CBA-Hg complex and CBA-Hg complex in the presence of cysteamine hydrochloride in 100 mM SDS. The excitation wavelength is 376 nm.

#### 4.3.3.4 Nature of Complexation in Micellar Medium

##### Distribution of Probes in Micelles

Given the discrete number of micelles present at a given total surfactant concentration, introduction of probes leads to their solubilization in the available number of micelles. Knowledge of this distribution of probes among the micelles is essential for the interpretation of various excited state bimolecular processes such as fluorescence quenching, excimer formation, energy and electron transfer.

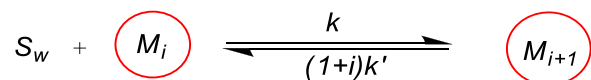
Given the average number of solutes per micelle  $\bar{n} = \frac{[CBA]}{[M]}$  where [CBA] is the total concentration of CBA introduced, [M] is the concentration of micelle.

$$[M] = \frac{[SDS]}{N_{agg}}$$

Where [SDS] is the concentration of surfactant,  $N_{agg}$  is the aggregation number<sup>35,36</sup>

The determination of the probability  $P_i$  of finding  $i$  probes in a given micelle can find out by several distribution laws such as geometric, binomial and Poissonian distributions.<sup>35,36</sup> Poissonian distribution is the most widely used model for the distribution of probes in micelles. According to Poissonian distribution model for the distribution of probes in micelles the

following dynamic equilibrium of probe  $S$  with micelle can be represented as

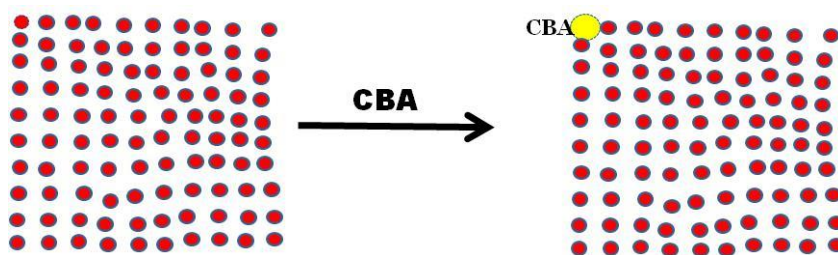


Where  $S_w$  is the probe molecule in water,  $M_i$  is the micelle assembly containing  $i$  number of probe molecules. The rate  $k$  is a second order rate constant which describes the rate of entry of probes in the micelles. The  $k'$  is the exit rate of one probe and is assumed to be independent of occupation no  $i$ . The rate at which the probes leave the micelle containing several of them is assumed to be linearly dependent on the number of probes, ie.,  $rate = (1+i)k'$ . There is no limit to the maximum number of probes that may occupy a given micelle. Writing equilibrium expressions for all values of  $i$ , it is easy to obtain the fraction of micelles that are occupied by  $i$  probes as

$$\frac{[M_i]}{[M]} = \frac{\bar{n} e^{-\bar{n}}}{i!}$$

This equation shows that the distribution of probes in micelles to be governed by a Poisson distribution. At a low value of  $\bar{n} = 0.1$ , most of the micelles are empty and only 10% of micelles contain one or more probes. When  $\bar{n} = 1$ , ie., there is equal concentrations of probes and micelles, 37% of micelles are still empty but about 26% of them contain two or more probes. In this type of distribution aggregation of probes and bimolecular self-quenching of the excited states are possible. To avoid this  $\bar{n}$  should be much

less than 0.5. In our study, we used a surfactant concentration of 100 mM i.e., concentration of micelle is  $1.33 \times 10^{-3}$  M and the probe concentration of  $\sim 10^{-5}$  M which makes the  $\bar{n}$  to have a value of 0.0132 which is  $\ll 0.1$ . Thus, the probe molecules are distributed in such a way that there is large excess of empty micellar assemblies ruling out multiple occupancies of probe molecules and thus aggregation effects (Figure 4.27).

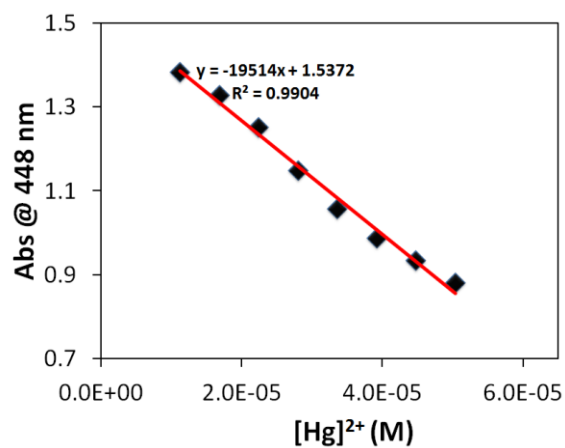


**Figure 4.27** Cartoon showing the occupation of CBA in 100mM SDS micellar solution.

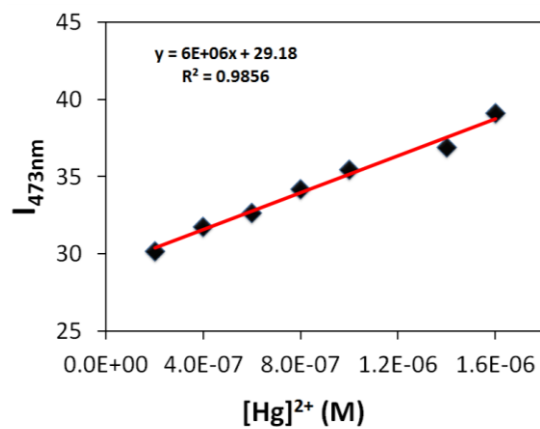
#### 4.3.3.5 Determination of Lowest Detection Limit in Micellar Medium

The variation in the absorbance and the fluorescence intensity show a linear dependence with the  $\text{Hg}^{2+}$  in the concentration range 10-50  $\mu\text{M}$  and 0.2-1.66  $\mu\text{M}$  respectively. Each of this response was plotted and the detection limit was calculated from the slope of the fitted curve. The results show that CBA can be used to detect and quantify  $\text{Hg}^{2+}$  with a detection limit of 44.5 nM by fluorescence and 2.3  $\mu\text{M}$  by absorption spectroscopy (Figure 4.28 & 4. 29).





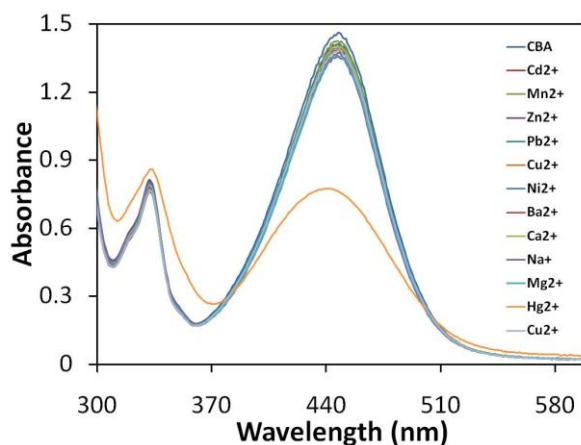
**Figure 4.28** A plot showing a variation of Absorbance at 448 nm as a function of concentrations of  $\text{Hg}^{2+}$  in 100 mM SDS in water.



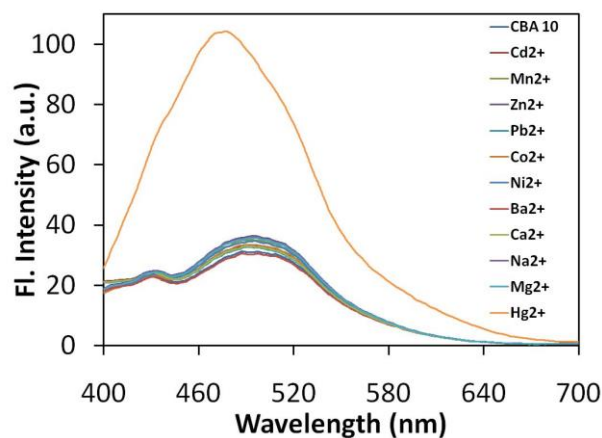
**Figure 4.29** A plot showing a variation of Fluorescence intensity at 473 nm as a function of concentrations of  $\text{Hg}^{2+}$  in 100 mM SDS.

#### 4.3.3.6 Selectivity of Metal ion Recognition by CBA in SDS micelles

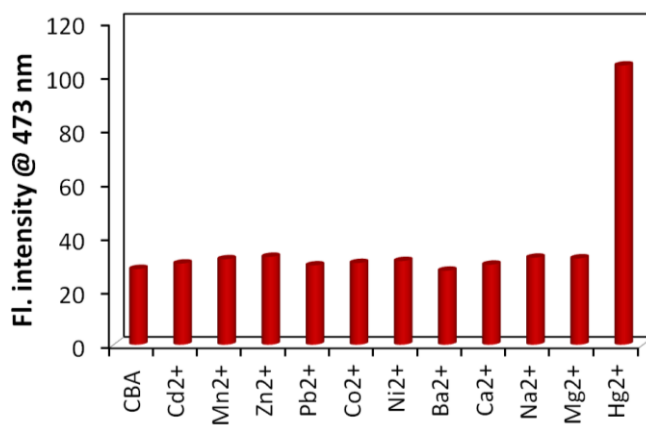
To verify the selectivity of metal binding by CBA for  $\text{Hg}^{2+}$  ions, we have investigated the interactions of CBA with other metal ions such as  $\text{Na}^+$ ,  $\text{Mg}^{2+}$ ,  $\text{Ca}^{2+}$ ,  $\text{Cd}^{2+}$ ,  $\text{Zn}^{2+}$ ,  $\text{Ni}^{2+}$ ,  $\text{Ba}^{2+}$ ,  $\text{Cu}^{2+}$ ,  $\text{Pb}^{2+}$ ,  $\text{Co}^{2+}$ , and  $\text{Mn}^{2+}$  ions in 100 mM SDS. Figure 4.30 & 4.31 shows the relative changes in the absorption as well as fluorescence intensity of CBA with the addition of two equivalents of different metal ions. As evident from the figure, the addition of other metal ions caused negligible changes in the absorption and emission bands of CBA. The bar-diagram in Figure 4.32 illustrates the selectivity feature of CBA in the detection of  $\text{Hg}^{2+}$  ions in 100 mM SDS.



**Figure 4.30** Absorption spectra of CBA recorded in the presence of various metal ions in 100 mM SDS. (Metal ion concentration =  $78\mu\text{M}$ ,  $[\text{CBA}] = 37\mu\text{M}$ )



**Figure 4.31** Emission spectra of CBA recorded in the presence of various metal ions in 100 mM SDS. (Metal ion concentration = 44  $\mu$ M, [CBA] = 17.6  $\mu$ M).  $\lambda_{\text{ex}} = 376$  nm.



**Figure 4.32** The bar diagram showing the metal ion binding selectivity of CBA in 100 mM SDS in water.

## 4.4 Conclusions

We have investigated the metal ion binding properties of CBA with various mono- and bivalent metal ions. CBA molecule, which contains a barbituric acid fragment having a cyclic amide structure act as a ligand for metal ions. CBA shows unusual selectivity for the  $\text{Hg}^{2+}$  ions among the various metal ions investigated. Our investigations revealed that the metal ion complexation involves the deprotonation of NH protons of the chelating site as characterized by  $^1\text{H}$  NMR spectral analysis. The unusual selectivity of the CBA for the  $\text{Hg}^{2+}$  ions may be due to the high affinity of pyrimidines to  $\text{Hg}^{2+}$  illustrated earlier for DNA double strands. Upon addition of  $\text{Hg}^{2+}$  in 1:1 MeOH/ $\text{H}_2\text{O}$  medium an enhancement in fluorescence emission was observed and the complex formed was having a 2:1 binding stoichiometry. The observed enhanced emission could be due to the formation of an aggregate or a complex having a linear or bend geometry. Such geometries can lead to close interaction between two carbazole moieties favouring aggregation induced emission (AIE). In a microheterogeneous medium such as 100 mM SDS an enhancement in the emission was observed in the presence of  $\text{Hg}^{2+}$  ions. However, this enhancement in emission was ascribed to a complex having 1:2 geometry. This result indirectly supports our argument that in 1:1 MeOH/ $\text{H}_2\text{O}$  the observed enhancement in emission is indeed due to the aggregation or stacking of carbazole units possible in a complex with 2:1 binding stoichiometry. In both medium, we obtained comparatively high binding constant for  $\text{Hg}^{2+}$  binding. The chemosensor

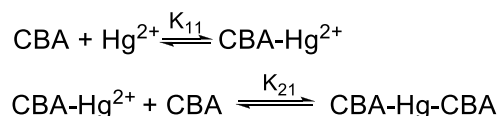
developed is very sensitive to  $\text{Hg}^{2+}$  with a detection limit of 8.89 nm which is less than 2 ppb, the EPA recommended maximum limit allowed for  $\text{Hg}^{2+}$  in potable water.

## 4.5 Experimental Section

### 4.5.1 General Photophysical Studies

A stock solution of CBA with the concentration of  $4.3 \times 10^{-3}$  M was prepared in tetrahydrofuran (THF) and stored in a cool and dark place. This stock solution was used for all spectrofluorimetric titrations after appropriate dilution. Absorption spectra were recorded using Evolution 201 UV-visible spectrophotometer. Fluorescence emission spectra of the samples were measured using Perkin-Elmer Fluorescence spectrophotometer (model LS 45).

### 4.5.2 Determination of Association Constant for 2:1 Stoichiometry



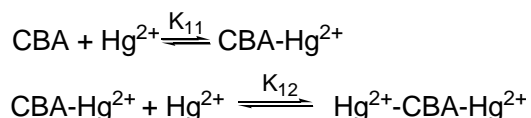
The association constant was calculated based on the absorbance or fluorescence titration curve of CBA with metal ions. Association constant was determined by a nonlinear least-squares fit of the data with the following equation as described elsewhere.<sup>37</sup>

$$y = \frac{x}{2ab(1-x)^2} + \frac{xb}{2}$$

where  $x$  is  $(I - I_0) / (I_{max} - I_0)$ ,  $y$  is the concentration of  $\text{Hg}^{2+}$  ions,  $a$  is the association constant  $K_{21}$ , and  $b$  is the concentration of CBA. Here  $I$  is the

absorption or emission intensity at particular  $\text{Hg}^{2+}$  concentration,  $I_0$  is the initial absorbance or emission intensity and  $I_{max}$  is the final absorbance or emission intensity from the titration of CBA with  $\text{Hg}^{2+}$ .

#### 4.5.3 Determination of Association Constant for 1:2 Stoichiometry



The association constant was calculated based on the absorbance or fluorescence titration curve of CBA with metal ions. Association constant was determined by a nonlinear least-squares fit of the data with the following equation as described elsewhere.<sup>38</sup>

$$A = \frac{A_0 + A_\infty K_{12} [G]^2}{1 + K_{12} [G]^2}$$

Where A is absorbance/fluorescence signal,  $A_0$  and  $A_\infty$  are the initial and final absorbance or fluorescence signal,  $[G]$  is total concentration of the metal ion.

#### 4.5.4 Job's Plot by UV-vis Method

A series of solutions containing CBA and  $\text{Hg}(\text{OAc})_2$  were prepared to keep sum of concentration  $[\text{Hg}^{2+}]$  ion and  $[\text{CBA}]$  a constant, whereby, the

mole fraction (X) of  $\text{Hg}^{2+}$  was varied from 0.1 to 1.0. The Job's plot is obtained by plotting the absorbance ( $A_{460 \text{ nm}} \times X_{\text{Hg}^{2+}}$ ) at 460nm against the molar fraction of the  $\text{Hg}^{2+}$ .<sup>39</sup> The value of mole fraction corresponding to the maximum on the Job's plot thus obtained was 0.4 indicative of a 2:1 binding stoichiometry.<sup>15</sup>

#### 4.5.5 Detection Limit Calculations Experimental Procedure

The detection limit was calculated based on the fluorescence titration. To calculate the S/N ratio, the emission intensity of CBA in the absence of  $\text{Hg}^{2+}$  was measured 10 times and the standard deviation ( $\sigma$ ) of blank measurements was determined. Three independent duplication measurements of emission intensity at 600 nm in the presence of  $\text{Hg}^{2+}$  and the average value of the intensities was plotted against the concentration of  $\text{Hg}^{2+}$  for determining the slope ( $m$ ). The detection limit is then calculated with the following equation.<sup>15</sup>

$$\text{Detection limit} = 3\sigma/m$$



## 4.6 References

1. Moura, N. M. M.; Núñez, C.; Santos, S. M.; Faustino, M. A. F.; Cavaleiro, J. A. S. Neves, M. G. P. M. S.; Capelo, J. L. Lodeiro, C. *Inorg. Chem.* **2014**, *53*, 6149.
2. Li, C. Y.; Zhou, Y.; Li, Y. F.; Kong, X. F.; Zou, C. X.; Weng, C. *Anal. Chim. Acta.* **2013**, *774*, 79.
3. Harada, M. *Crit. Rev. Toxicol.* **1995**, *25*, 1.
4. Hardy, S.; Jones, P. *J. Chromatogr. A.* **1997**, 333.
5. *Guidelines for drinking-water quality, 3rd ed.*; World Health Organization, Geneva, **2004**, p 188
6. *US Environmental Protection Agency, EPA Office of Water*, Washington, DC. (<http://www.epa.gov/ogwdw000/contaminants/index.html#mcls>).
7. Nolan, E. M.; Lippard, S. *Chem. Rev.* **2008**, *108*, 3443.
8. Kim, H. N.; Ren, W. X.; Kim, J. S.; Yoon, J. Y. *Chem. Soc. Rev.* **2012**, *41*, 3210.
9. Karuppanan, S.; Chambron, J. C. *Chem. Asian J.* **2011**, *6*, 964.
10. Zhao, Q.; Li, F.; Huang, C. *Chem. Soc. Rev.* **2010**, *39*, 3007.
11. Tian, M.; Liu, L.; Li, Y.; Hu, R.; Liu, T.; Liu, H.; Wang, S.; Li, Y. *Chem. Commun.* **2014**, *50*, 2055.
12. Bera, K.; Das, A. K.; Nag, M.; Basak, S. *Anal. Chem.* **2014**, *86*, 2740.

13. Bhalla, V.; Kumar, R. M.; Sharma, P. R.; Kaur, T. *Inorg. Chem.* **2012**, *51*, 2150.
14. Sanjoy, M.; Pakkirisamy, T. *Chem. Commun.* **2013**, *49*, 7292.
15. Yang, M. H.; Thirupathi, P.; Lee, K. H. *Org. Lett.* **2011**, *13*, 5028.
16. Wu, D.; Huang, W.; Duan, C.; Lin, Z.; Meng, Q. *Inorg. Chem.* **2007**, *46*, 1538.
17. Lee, M. H.; Lee, S. W.; Kim, S. H.; Kang, C.; Kim, J. S. *Org. Lett.* **2009**, *11*, 2101.
18. Chen, X.; Meng, X.; Wang, S.; Cai, Y.; Wu, Y.; Feng, Y.; Zhua, M.; Guob, Q. *Dalton Trans.* **2013**, *42*, 14819.
19. Lee, M. H.; Cho, B. K.; Yoon, J.; Kim, J. S. *Org. Lett.* **2007**, *9*, 4515.
20. Neupane, L. N.; Park, J. Y.; Park, J. H.; Lee, K. H. *Org. Lett.* **2013**, *15*, 254.
21. Wang, J.; Zhang, L.; Qi, Q.; Li, S.; Jianga, Y. *Anal. Methods* **2013**, *5*, 608.
22. Tehfe, M. A.; Dumur, F.; Graff, B.; Savary, F. M.; Gigmès, D.; Fouassier, J. P.; Lalevee, J. *Polym. Chem.* **2013**, *4*, 3866.
23. Ono, A.; Torigoe, H.; Tanaka, Y.; Okamoto, I. *Chem. Soc. Rev.* **2011**, *40*, 5855.
24. Marino, T. *J. Mol. Model* **2014**, *20*, 2303.
25. Dinda, D.; Shaw, B. K.; Saha, S. K. *ACS Appl. Mater. Interfaces* **2015**, *7*, 14743.

26. Luo, J.; Xie, Z.; Lam, J. W. Y.; Cheng, L.; Chen, H.; Qin, C.; Kwok, H. S.; Zhan, X.; Liu, Y.; Zhu, D.; Tang, B. Z. *Chem. Commun.* **2001**, 1740.
27. Hong, Y.; Lam, J. W. Y.; Tang, B. Z. *Chem. Commun.* **2009**, 4332.
28. Shi, J.; Chang, N.; Li, C.; Mei, J.; Deng, C.; Luo, X.; Liu, Z.; Bo, Z.; Dong, Y. Q.; Tang, B. Z. *Chem. Commun.* **2012**, 48, 10675.
29. An, B. K.; Kwon, S. K.; Jung, S. D.; Park, S. Y. *J. Am. Chem. Soc.* **2002**, 124, 14410.
30. An, B. K.; Kwon, S. K.; Park, S. Y. *Angew. Chem. Int. Ed.* **2007**, 46, 1978.
31. Lu, R.; Jiang, Y.; Duo, J.; Chai, X.; Yang, W.; Lu, N.; Cao, Y.; Li, T. *Supramol. Sci.* **1998**, 5, 737.
32. Ramondo, F.; Pieretti, A.; Gontrani, L.; Bencivenni, L. *Chem. Phys.* **2001**, 271, 293.
33. Zhang, X.; Chi, Z.; Zhang, J.; Li, H.; Xu, B.; Li, X.; Liu, S.; Zhang, Y.; Xu, J. *J. Phys. Chem. B* **2011**, 115, 7606.
34. Singh, G.; Bhalla, V.; Kumar, M. *Phys. Chem. Chem. Phys.* **2015**, 17, 22079.
35. Kalyanasundaram, K. *Photochemistry in Microheterogeneous Systems ISBN: 978-0-12-394995-0*
36. Manju, T.; Manoj, N.; Gejo, J. L.; Braun, A. M.; Oliveros, E. *Photochem. Photobiol. Sci.* **2014**, 13, 281.
37. Kubo, Y.; Kato, M.; Misawa, Y.; Tokita, S. *Tetrahedron Lett.* **2004**, 45, 3769.

38. Park, J.; In, B.; Lee, K. H. *RSC Adv.* **2015**, *5*, 56356.
39. Maity, D.; Govindaraju, T. *Chem. Commun.* **2010**, *46*, 4499.

## Chapter 5

### Highly Selective Ratiometric and Colorimetric Detection of Mercury (II) ions in Aqueous Medium with a Carbazole Thiobarbituric acid based Fluorescent Probe

---

#### 5.1 Abstract



Developed a multimode ratiometric  $\text{Hg}^{2+}$  selective chemosensor system based on carbazole-thiobarbituric acid conjugate (CTBA). Its colorimetric and fluorescent behavior for  $\text{Hg}^{2+}$  ions in both homogeneous and microheterogeneous media were investigated. A ratiometric mode of response in absorption as well as fluorescence in acetonitrile and 9:1 THF/ $\text{H}_2\text{O}$  medium was observed in the presence of  $\text{Hg}^{2+}$  ions. A dramatic colour change was detected visually on the addition of  $\text{Hg}^{2+}$  ions in both the media

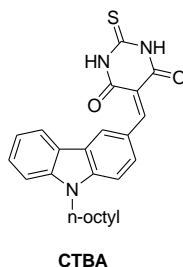
made it an excellent colorimetric chemosensor for selective detection of  $\text{Hg}^{2+}$  ions. Similar results were observed with slightly higher detection limit and extended concentration range of detection when used in microheterogeneous medium such as anionic SDS micelles. Interestingly, the sensing mechanism is reversible and free CTBA can be regenerated in the presence of competing chelating agent such as cysteamine hydrochloride. The metal binding interaction is more selective with mercuric ions, while a less dramatic change observed for  $\text{Cd}^{2+}$ . Other biologically and environmentally important mono- and divalent metal ions did not show any binding interaction. Job's plot analysis of the complexation showed that the complex formed has a 1:2 binding stoichiometry.

## 5.2 Introduction

The demand for advanced detection methods of heavy and transition metal ions are growing nowadays. Especially,  $\text{Hg}^{2+}$  ion considered as one of the most toxic metal ions<sup>1-4</sup> as it pollute the environment and cause major human health problems. In recent years, numerous efforts have been made to develop various chemosensors, particularly for  $\text{Hg}^{2+}$  ion detection.<sup>5,6</sup> However, some of the most sensitive analytical methods such as inductively coupled plasma mass spectrometry (ICP-MS), inductively coupled plasma atomic emission (ICP-AES) or atomic absorption spectrometry are very expensive or involved tedious sample preparation methods. The commercially available mercury analyzers use chemical reduction of  $\text{Hg}^{2+}$  ions to metallic Hg. The volatile zero mercury in the gaseous form is then

analyzed by absorption spectroscopy. This method is less sensitive and often requires concentrating the samples to overcome the sensitivity limit of the technique. A modification of the method involves emission measurement where the gaseous Hg vapor is excited by UV light and by monitoring its characteristic emission bands in the UV or visible region. The later technique is more sensitive compared to the detection by absorption spectroscopy. All these techniques have inherent disadvantages that make them less effective in online monitoring of Hg pollution and limit field based detection techniques.<sup>7,8</sup> Colorimetric or Turn-on fluorescence based chemosensors for Hg<sup>2+</sup> ion are attractive in terms of their potential use in optoelectronic devices for online/real-time or field based analysis of mercury pollution. Such methods offer simple detection with a naked eye, inexpensive instrumentation thus reducing the cost of environmental monitoring.<sup>9-23</sup> The bioaccumulation of Hg<sup>2+</sup> in living organisms including human population occur mainly through contamination of water. So, an ideal colorimetric chemosensors for Hg<sup>2+</sup> ions should be usable in aqueous solutions and sensitively detect low levels of Hg<sup>2+</sup> ions in aqueous solutions. Such systems should have high thermal as well as hydrolytic stability. Most colorimetric chemosensors suffer from interference of other metal ions because of a low binding affinity for Hg<sup>2+</sup> ions in aqueous solutions.<sup>9-23</sup> In addition, effective colorimetric detection of Hg<sup>2+</sup> ion in aqueous solution was typically achieved by chemodosimeters, however they irreversibly detected Hg<sup>2+</sup> ions.<sup>11-16, 23</sup>

In fluorescent sensors, the method that most of the fluorogenic chemosensors depend on responses such as quenching, enhancement, or ratiometric changes in the fluorescence intensity. Ratiometric sensing is the most desirable as it is sensitive as well as self-calibrating. However, chemosensors having ratiometric capability in fluorescence is rare.<sup>24-32</sup> To date, the majority of mercury sensors detect  $\text{Hg}^{2+}$  by means of either through a turn-off response or by a turn-on response. Most of the ratiometric sensors of  $\text{Hg}^{2+}$  known hitherto suffer from the interference of  $\text{Ag}^+$  or  $\text{Cu}^{2+}$  ions and low sensitivity.<sup>25-31</sup> Hence, the development of new reversible colorimetric and ratiometric chemosensors for  $\text{Hg}^{2+}$  ions having high sensitivity and selectivity is a major challenge. Fluorescent chemosensors for heavy metals generally use peptides, cyclic amides and cyclic thioamides as the recognition sites.<sup>32-44</sup> The present work employ a donor – acceptor molecule based on carbazole and thiobarbituric acid conjugate (CTBA) having intramolecular charge transfer property. Here, the thiobarbituric acid moiety acts as the recognition site and exploit the perturbation in the intramolecular charge transfer due to the presence of heavy metals as the signaling event.

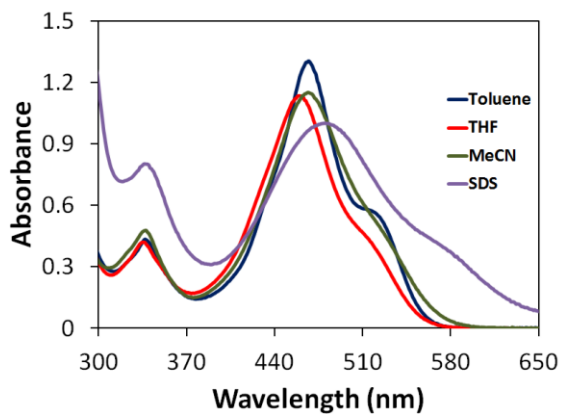


**Scheme 5. 1**

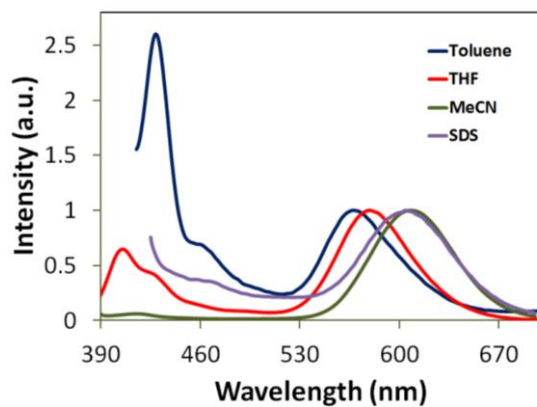


## 5.3 Results and Discussion

### 5.3.1 Intramolecular Charge Transfer and Dual Emission in CTBA



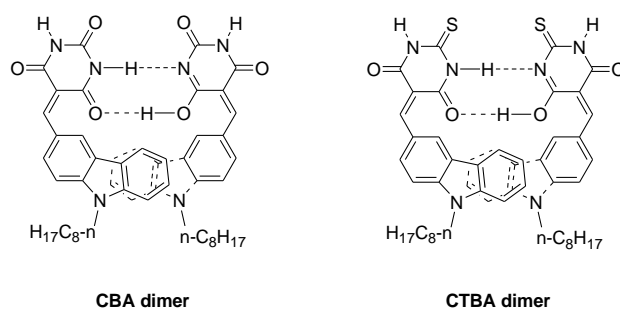
**Figure 5.1** Absorption spectrum of CTBA in different solvents and in 100 mM SDS.



**Figure 5.2** Emission spectrum of CTBA in different solvents and in 100 mM SDS.

Based on the experimental and theoretical studies on the excited state properties of CTBA presented in chapter 2 of the present thesis (§2.3.2.3) we have concluded that CTBA possess dual emission. This dual emission is attributed to a pre-twisted tautomeric form having a twisted excited state giving rise to a carbazole type emission (CE) around 425 nm and another long wavelength emission at around 600 nm due to a twisted charge transfer state. The CE emission maximum was found to be independent of solvent polarity and the ICT emission maximum was found to be solvent polarity dependent. However, this polarity dependence was not seen in the absorption spectrum of CTBA and is largely affected by hydrogen bond accepting nature of the solvents. Figure 5.1 and 5.2 show the absorption and emission spectra of CTBA in Toluene, THF, MeCN and in SDS micelles. Though we have assigned the dual emission in CTBA to the carbazole based CE emission and the ICT emission there exists a second possibility. In the structurally similar carbazole – barbituric acid conjugate CBA, a similar redshifted emission band is observed in the solid state and also in 60:40 H<sub>2</sub>O:THF mixture. This emission is assigned to the presence of an aggregate formed possibly due to dimerization of two CBA molecules held through a two hydrogen bonds as showed in Scheme 5.2 In such assemblies, stacking of two carbazole moieties are possible and an aggregation induced emission is observed and is also feasible in CTBA. In order to rule out this, we studied the effect of micelles on the absorption and emission properties of CTBA. We choose 100 mM anionic SDS surfactant solution for the solubilisation of 47 μM CTBA. At this surfactant concentration the number of micellar

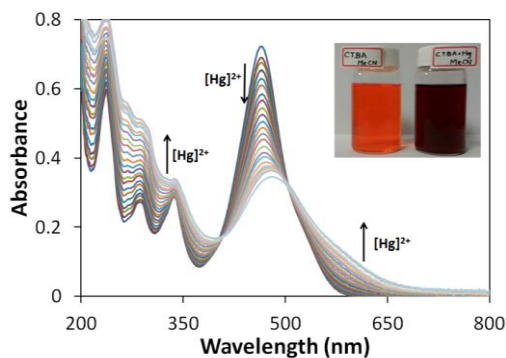
assemblies having multiple occupancies of CTBA is less probable (*vide infra* § 4.3.3.4). Figure 5.1 shows the absorption spectrum of CTBA in SDS which is 15 nm red shifted compared to that observed in MeCN. This illustrates that CTBA is micellised with a topology where the polar thiobarbituric acid unit closer to the anionic surface and the hydrophobic octyl carbazole in the core of the micelle. The emission spectra did not show any significant shift in the long wavelength emission band. Since we ruled out the possibility of multiple occupancy of CTBA in micelles, at this surfactant concentration and the concentration of CTBA, the observed emission band at 604 nm is solely due to the ICT excited state. As showed in Chapter 2 (*vide infra* § 2.3.3) that CTBA respond to the presence of  $\text{Hg}^{2+}$  exhibiting changes in its absorption spectrum. **The major objective of the present chapter is to study the effect of  $\text{Hg}^{2+}$  on the absorption and emission behavior of CTBA and to explore the possibility of using dual emission property of CTBA in ratiometric sensing of  $\text{Hg}^{2+}$  ions.**



Scheme 5.2

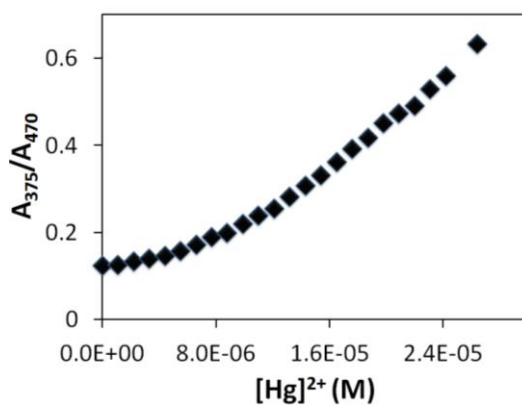
### 5.3.2 Metal ion Binding Studies of CTBA in MeCN

The effect of  $\text{Hg}^{2+}$  on the absorption and emission properties of CTBA was studied in MeCN solutions. During the photometric titration of mercury ions to CTBA, the orange solution turned dark brown along with a red-shift of the long-wavelength absorption maximum from 465 nm to 482 nm (Figure 5.3). Not so well focused isosbestic points at 408 nm and 502 nm indicates the formation of a complex with  $\text{Hg}^{2+}$  ions which is in equilibrium with the free ligand. No further change in the absorbance was observed after the addition of about 2 equivalence of  $\text{Hg}^{2+}$ . The red-shift in the absorption spectrum is indicative of the formation of an aggregate of CTBA or due to the changes in the electron affinity of the pyrimidine moiety due to complexation with  $\text{Hg}^{2+}$  ions.



**Figure 5.3** Evolution of absorption spectra of CTBA in the presence of increasing concentration of an aqueous solution of  $\text{Hg}(\text{OAc})_2$  in MeCN ( $[\text{CTBA}] = 14.4 \mu\text{M}$ ,  $[\text{Hg}(\text{OAc})_2] = 0\text{--}26.4 \mu\text{M}$ ). Arrows indicate the direction change in the absorbance.

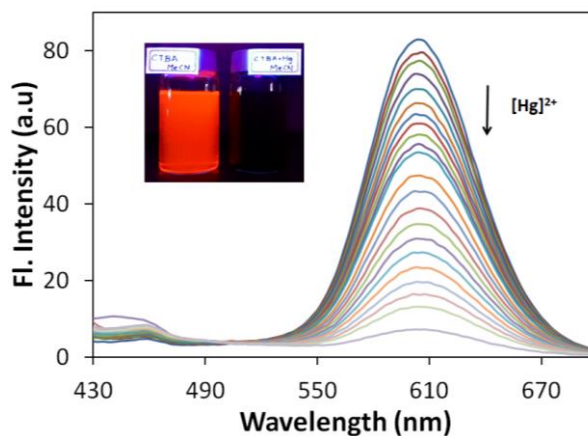
The ratio of the absorbance at 375 nm and 470 nm and its change as a function of  $\text{Hg}^{2+}$  concentration in acetonitrile medium can be used for ratiometric determination of Hg ions. The ratiometric plot for the absorbance changes at 375 nm and 470 nm is depicted in Figure 5.4.



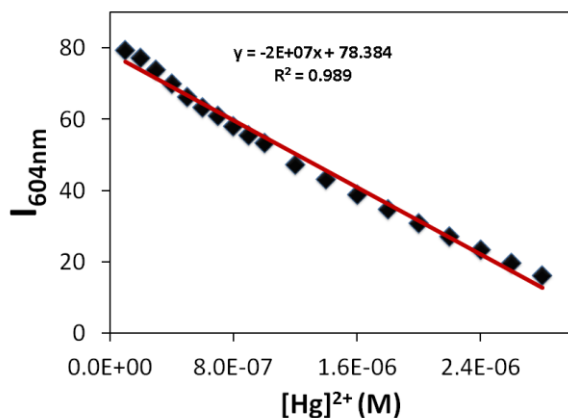
**Figure 5.4** A plot of absorbance ratio ( $A_{375}/A_{470}$ ) vs concentrations of  $\text{Hg}^{2+}$  in MeCN.

We further investigated the emission spectral characteristics and its response to  $\text{Hg}^{2+}$  in MeCN. Fluorescence spectra were recorded by exciting optically matched solutions of CTBA ( $5.8 \times 10^{-6}$  M) at the isosbestic point (408 nm). The evolution of the emission spectrum of CTBA as a function of  $\text{Hg}^{2+}$  show an interaction that lead to quenching of the fluorescence emission (Figure 5.5). This is manifested as a decrease in the emission intensity of the band at 604 nm. The decreased emission intensity was continued to be observed even after the addition of about 1.7 equivalents of  $\text{Hg}^{2+}$ . As seen in Figure 5.6, the intensity at 604 nm decreases linearly as a function of the

concentration of  $\text{Hg}^{2+}$  ions. This result agrees with the outcome of spectrophotometric titration and suggests that CTBA showed a very strong affinity towards  $\text{Hg}^{2+}$  ions. The colorimetric response as well as the fluorescence response under UV illumination of CTBA to  $\text{Hg}^{2+}$  in MeCN is visible even with the naked eye as shown in the photographs as insets of Figures 5.3 and 5.5.

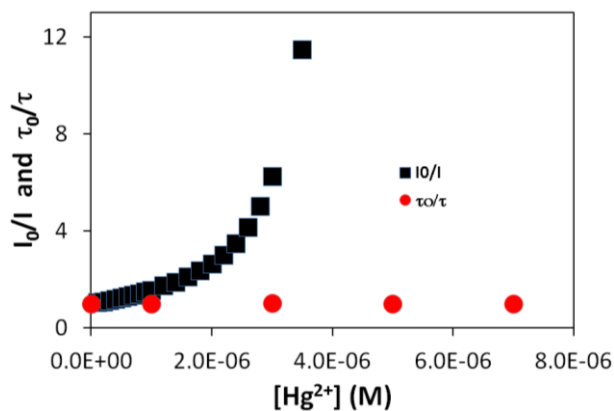


**Figure 5.5** Evolution of fluorescence spectra of CTBA in the presence of increasing concentration of an aqueous solution of  $\text{Hg}(\text{OAc})_2$  MeCN ( $[\text{CTBA}] = 5.8 \mu\text{M}$ ,  $[\text{Hg}(\text{OAc})_2] = 0\text{--}9.8 \mu\text{M}$ ,  $\lambda_{\text{ex}} = 404 \text{ nm}$ ). Arrows indicate the direction change in the fluorescence intensity.



**Figure 5.6** The fluorescence intensity changes at 604 nm as a function of  $\text{Hg}^{2+}$  concentration.

To get more insight into the mechanism of interaction of  $\text{Hg}^{2+}$  with CTBA, a Stern – Volmer analysis was performed. A plot of  $I_0/I$  vs concentration of  $\text{Hg}^{2+}$  was not linear but showed an upward curvature (Figure 5.7.). However, a similar plot obtained by time-resolved fluorescence emission measurements yielded a straight line slope zero. Thus it is clear that the emission observed in the presence of  $\text{Hg}^{2+}$  is solely due the presence of free CTBA molecules and the CTBA- $\text{Hg}^{2+}$  complex is non-fluorescent. The upward curvature of the SV plot obtained by steady-state emission measurements could be due to enhanced quenching by a 1:1 CTBA- $\text{Hg}^{2+}$  and the added  $\text{Hg}^{2+}$ . This behavior clearly indicates the formation of a 1:2 complex involving one CTBA molecule and two  $\text{Hg}^{2+}$  ions.



**Figure 5.7** Stern–Volmer plot obtained for the quenching of fluorescence of CTBA by Hg<sup>2+</sup> ions by Steady–State fluorescence measurements and time resolved emission measurements.

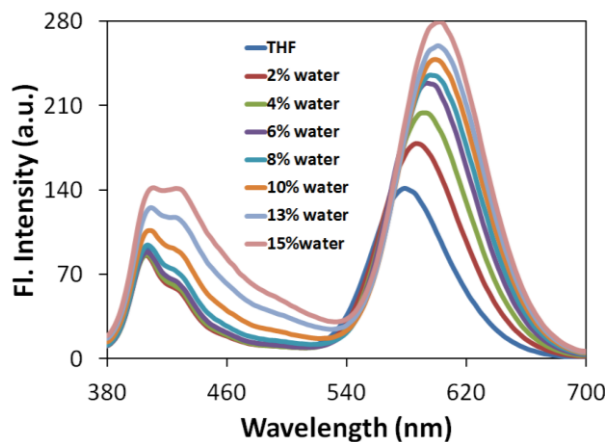
A similar fluorescence quenching process was observed for CTBA in methanol. In order to explore the possibility of using the chemosensing property in an aqueous medium, we studied the binding interaction in water-methanol or water-acetonitrile mixtures. No significant change was observed in comparison to the binding behavior in pure MeOH and MeCN.

### 5.3.3 Effect of Water on the Emission Spectrum of CTBA in THF

The fluorescence spectrum of CTBA is a characteristic one where dual emission was observed. An emission corresponding to the local emission due to carbazole moiety at around 425 nm and the long wavelength emission was observed at 600 nm. With the addition of water, both these emission bands were found to enhance the intensity of emission along with a



25 nm red shift in the band due to the CT excited state. This red shift in the CT emission is due to the stabilization of the CT excited state in a more polar environment and the enhancement in both emission bands may also due to higher quantum yield of emission or due to an increase in the absorbance or  $\epsilon$  in this solvent composition.

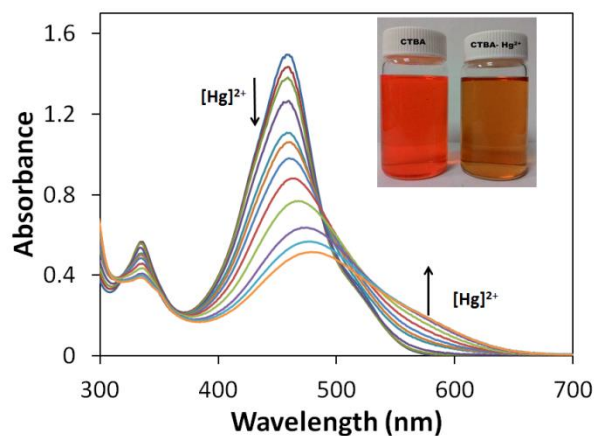


**Figure 5.8** Evolution of the emission spectrum of CTBA in THF as a function of water content.  $\lambda_{\text{ex}} = 360 \text{ nm}$

#### 5.3.4 Metal ion Binding Studies of CTBA in 9:1 THF/H<sub>2</sub>O

To extend the present study of metal–CTBA interaction in aqueous THF, we choose 9:1 THF water mixture. As shown in Figure 5.2a, the solution of CTBA in 9:1 THF/ H<sub>2</sub>O was orange in colour and exhibited an absorption maximum at 458 nm. The absorption maximum is altered to 478 nm with a concomitant decrease in the absorbance intensity is observed by the addition of Hg<sup>2+</sup> (Figure. 5.9). The colour of the solution was also

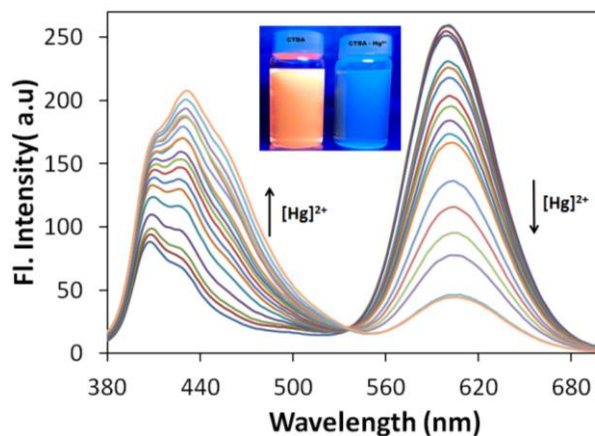
changed from orange to light brown (Figure.5.9, inset). The unfocused isosbestic point at 360 nm and at around 500 nm suggests that the complex formed between CTBA and  $\text{Hg}^{2+}$  is not having 1:1 stoichiometry. The visual change in color of the solution makes CTBA in 9:1 THF/ $\text{H}_2\text{O}$  an ideal system for naked eye detection of  $\text{Hg}^{2+}$ .



**Figure 5.9** Evolution of absorption spectra of CTBA in the presence of increasing concentration of an aqueous solution of  $\text{Hg}(\text{OAc})_2$  in 9:1 THF/ $\text{H}_2\text{O}$  ( $[\text{CTBA}] = 30 \mu\text{M}$ ,  $[\text{Hg}(\text{OAc})_2] = 0\text{--}71 \mu\text{M}$ ). Arrows indicate the direction of change in absorbance.

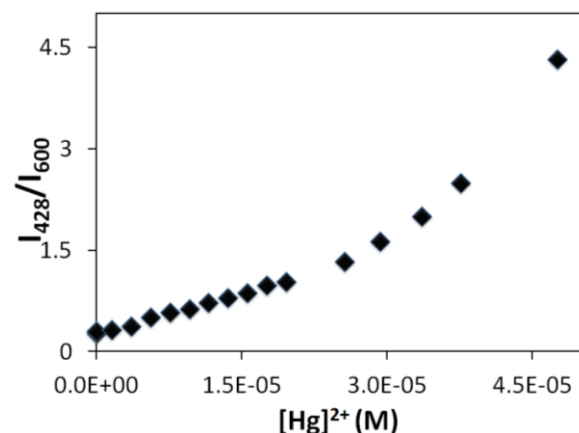
The changes observed in the emission spectrum were more dramatic in this medium. With the addition of  $\text{Hg}^{2+}$  ions, the intensity of the CT emission decreased along with an associated increase in intensity of the band due to carbazole based local excited state. The evolution of the emission spectra is characterized by an iso-emissive point at 535 nm (Figure 5.10).

This offers the possibility to use the CTBA in 9:1 THF/H<sub>2</sub>O as a ratiometric probe for Hg<sup>2+</sup>.



**Figure 5.10** Evolution of fluorescence spectra of CTBA in the presence of increasing concentration of an aqueous solution of Hg(OAc)<sub>2</sub> in 9:1 THF/H<sub>2</sub>O ([CTBA] = 30 μM, [Hg(OAc)<sub>2</sub>] = 0–51 μM, λ<sub>ex</sub> = 360 nm). Arrows indicate the direction change in the fluorescence intensity.

The ratiometric behavior of CTBA in THF/H<sub>2</sub>O is illustrated in Figure 5.11. The upward curvature in the plot may be due to the highly emissive nature of the mercury-CTBA complex or due to an accelerated quenching of the CT emission of free CTBA molecules by Hg<sup>2+</sup> as well as the 1:1 CTBA-Hg<sup>2+</sup> complex.

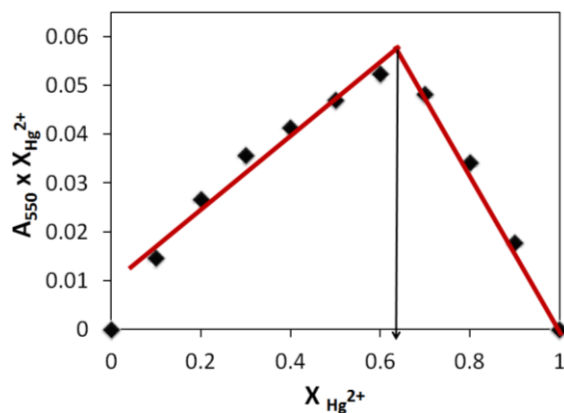


**Figure 5.11** A plot of fluorescence intensity ratio ( $I_{428}/I_{600}$ ) vs concentration of  $\text{Hg}^{2+}$  in 9:1 THF/ $\text{H}_2\text{O}$ , ( $\lambda_{\text{ex}} = 360 \text{ nm}$ )

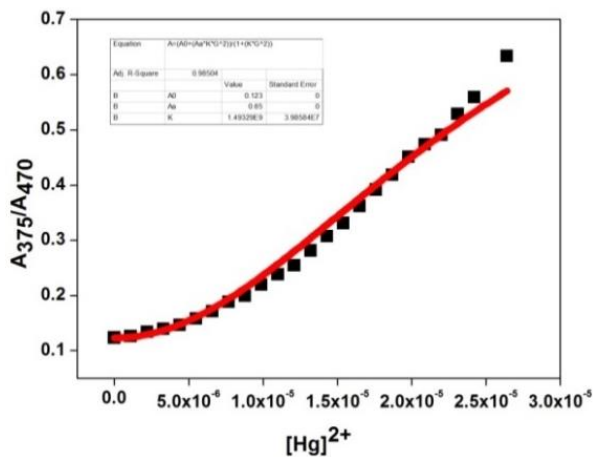
#### 5.3.4.1 Stoichiometry of Complexation

The stoichiometry of the complex formed between CTBA and  $\text{Hg}^{2+}$  ions was analyzed by Job's plot, the method of continuous variation of mole fraction of interacting partners and its effect on the absorbance. Job's plot showed a maximum corresponding to the mole fraction 0.65 which is an indication of 1:2 binding stoichiometry (Figure 5.12). The binding constant was determined by nonlinear least square fit analysis of the ratiometric response to  $\text{Hg}^{2+}$  by absorption and emission to a model corresponding to a 1:2 CTBA:Hg complex. The result shows very good correlation with the model and this further supports the formation of a 1:2 CTBA:Hg complex. The results of the analysis also yielded the binding constant as  $1.49 \times 10^9 \text{ M}^{-2}$  by absorption spectroscopy and  $0.58 \times 10^9 \text{ M}^{-2}$  by fluorescence

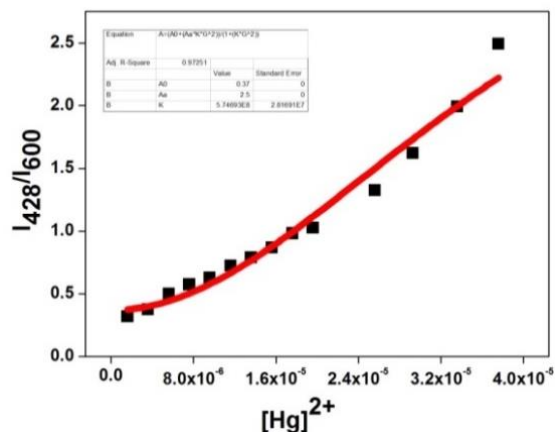
spectroscopy (Figures 5.13 and 5.14). Such a high value of binding constant shows that CTBA is very sensitive to  $\text{Hg}^{2+}$  ions.



**Figure 5.12** Job's plot analysis of CTBA with  $\text{Hg}^{2+}$  showing a 1:2 binding geometry in 9:1 THF/ $\text{H}_2\text{O}$



**Figure 5.13** A plot of absorbance ratio ( $A_{375}/A_{470}$ ) vs concentrations of  $\text{Hg}^{2+}$  in MeCN.

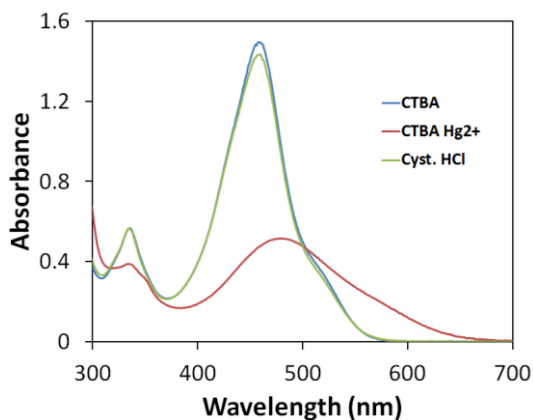


**Figure 5.14** A plot of fluorescence intensity ratio ( $I_{428}/I_{600}$ ) vs concentrations of  $\text{Hg}^{2+}$  in 9:1 THF/ $\text{H}_2\text{O}$ .

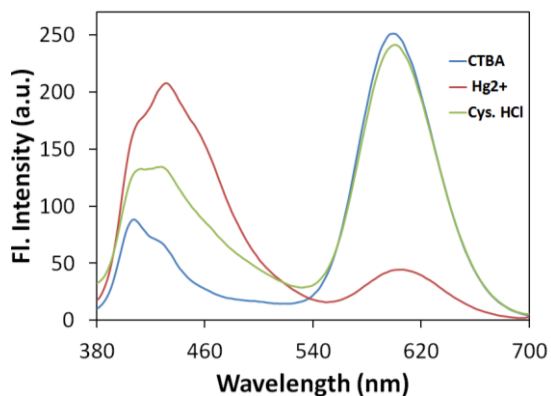
#### 5.3.4.2 Reversibility of Complexation

For practical applications, reversibility, the ability to regenerate the free probes from the complex, is also an important parameter for fluorescent probes. To validate the reversibility of complexation of CTBA and  $\text{Hg}^{2+}$  in 9:1 THF/ $\text{H}_2\text{O}$ , competing ligand such as cysteamine hydrochloride, having a thiol group was added. The absorbance of CTBA- $\text{Hg}^{2+}$  complex increased gradually with a blue shift and an absorption spectrum which matches with the absorption spectrum of CTBA (Figure 5.15) was obtained. A similar effect was also observed in the fluorescence spectrum of the CTBA- $\text{Hg}^{2+}$  complex. The fluorescence at 428 nm turned off gradually and fluorescence at 600 nm was restored as in the emission spectrum of free CTBA (Figure

5.16). These results demonstrate that CTBA can serve as a reversible probe for  $\text{Hg}^{2+}$ .



**Figure 5.15** Absorption spectra of CTBA, CTBA- $\text{Hg}^{2+}$  complex and CTBA- $\text{Hg}^{2+}$  complex in the presence of cysteamine hydrochloride in 9:1 THF/ $\text{H}_2\text{O}$ .

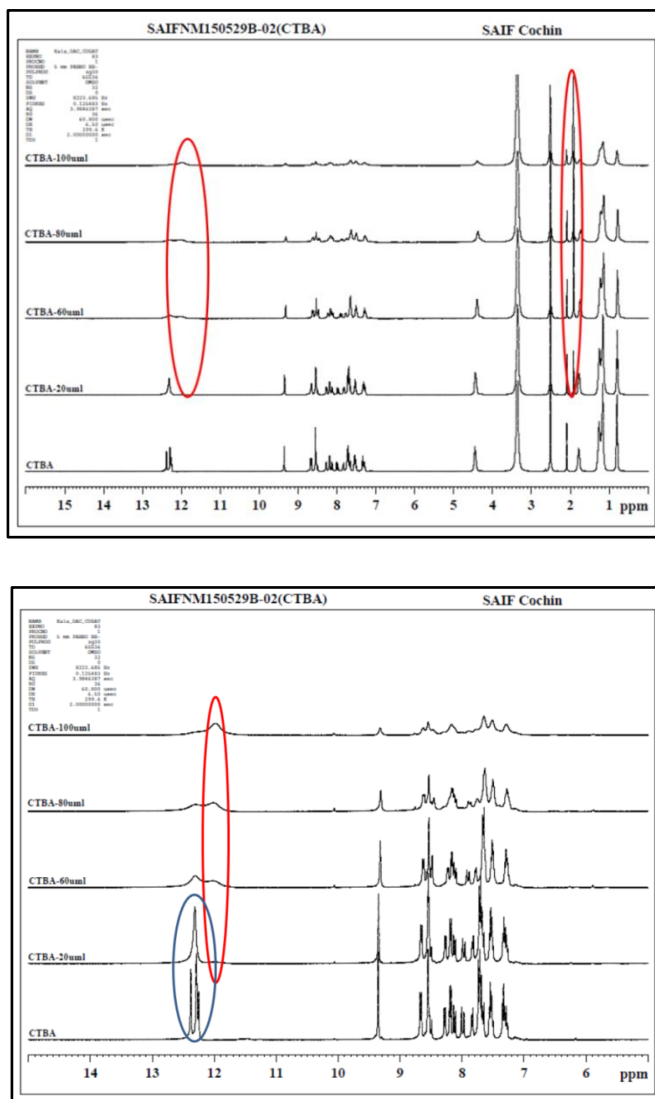


**Figure 5.16** Emission spectra of CTBA, CTBA- $\text{Hg}^{2+}$  complex and CTBA- $\text{Hg}^{2+}$  complex in the presence of cysteamine hydrochloride in 9:1 THF/water.  $\lambda_{\text{ex}} = 360 \text{ nm}$

### 5.3.4.3 Mechanism of Complexation

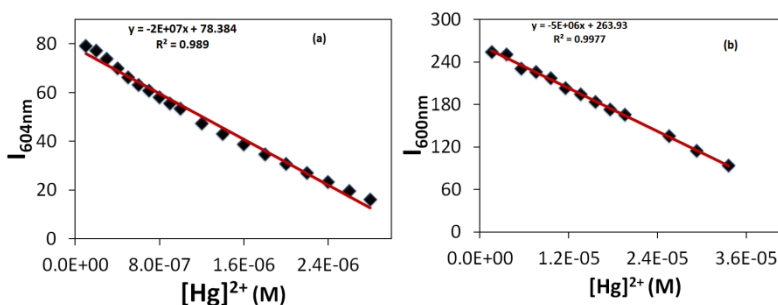
To understand the nature of the complexation, we monitored the  $^1\text{H}$  NMR spectral changes of CTBA in the absence and presence of different concentrations of  $\text{Hg}^{2+}$  ions. We have recorded  $^1\text{H}$ -NMR spectrum in  $\text{DMSO-d}_6$  in the presence of increasing concentration of  $\text{Hg}$  (II) acetate. Figure 5.17 shows  $^1\text{H}$ -NMR spectrum of CTBA and mixtures of CTBA and  $\text{Hg}$  (II) acetate at different ratios from 0 to 2 equivalents of  $\text{Hg}^{2+}$ . The spectrum of free CTBA is characterized by two distinct peaks corresponding to two NH protons at 12.25 ppm and 12.4 ppm. Analysis of the spectra evolved in the presence of  $\text{Hg}^{2+}$  acetate shows new resonance peaks at 12 ppm, 12.3 ppm and 1.95 ppm. The peaks corresponding to two NH protons become one and appeared at 12.3 ppm by the addition of  $\text{Hg}^{2+}$  ions initially. The peak at 12 ppm is assigned to the  $-\text{OH}$  proton of acetic acid which is indicative of a mechanism of  $\text{Hg}^{2+}$  binding involving the deprotonation of NH of the thiobarbituric acid moiety releasing a molecule of acetic acid. Moreover, the binding event led to deprotonation of both N-H protons on CTBA as indicated by the decrease in the peak area of the peak at 12.3 ppm. When two equivalents of  $\text{Hg}(\text{OAc})_2$  was added, the resonance due to NH proton completely vanished and the  $\text{Hg}^{2+}$ -CTBA- $\text{Hg}^{2+}$  complex precipitated which is undoubtedly seen in  $^1\text{H}$ -NMR, *ie.* only acetic acid peaks and solvents peak are seen in the resulting spectrum. This further confirms the 1:2 binding stoichiometry.





**Figure 5.17** a) The <sup>1</sup>H-NMR spectra of the CTBA and CTBA in the presence of 0-2 equivalents of Hg<sup>2+</sup> acetate (400 MHz, DMSO-d<sub>6</sub>) b) Expanded spectrum in the aromatic region.

#### 5.3.4.4 Determination of Lowest Detection Limit



**Figure 5.18** A plot showing variation of fluorescence intensity at 604 nm and 600 nm as a function of concentrations of  $\text{Hg}^{2+}$  in MeCN and 9:1 THF/H<sub>2</sub>O respectively.

The variation in the absorbance and the fluorescence intensity show a linear dependence with the  $\text{Hg}^{2+}$  in the concentration range 0-2.4  $\mu\text{M}$  and 0-35  $\mu\text{M}$  respectively. Each of this response was plotted and the detection limit was calculated from the slope of the fitted curve. The results show that CTBA can be used to detect and quantify  $\text{Hg}^{2+}$  with a detection limit of 13.35 nM by fluorescence in MeCN and 53.34 nM in 9:1 THF/H<sub>2</sub>O (Figure 5.18). The results of the calculation by absorption emission and ratiometry are summarized in Table 5.1.

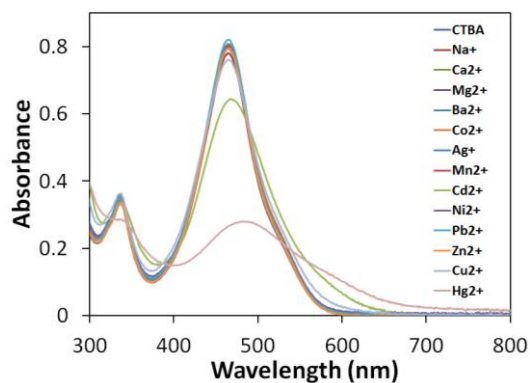
**Table 5.1** Lowest detection limit obtained for CTBA in MeCN and 9:1 THF/H<sub>2</sub>O

Method	Detection Limit MeCN	Detection Limit 9:1 THF/ H <sub>2</sub> O
Fluorimetry	13.35 nM	53.34 nM
Colorimetry	1.10 μM	2.62 μM
Ratiometry	2.23 μM (UV)	1.60 μM (FI)

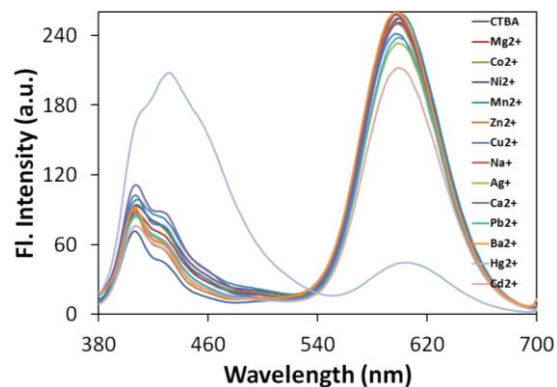
#### 5.3.4.5 Selectivity of Recognition of Hg<sup>2+</sup> Ions

In addition to Hg<sup>2+</sup> metal ion, binding studies were also carried out with Cd<sup>2+</sup>, Mn<sup>2+</sup>, Pb<sup>2+</sup>, Zn<sup>2+</sup>, Cu<sup>2+</sup>, Ag<sup>+</sup>, Co<sup>2+</sup>, Na<sup>+</sup>, Ba<sup>2+</sup>, Mg<sup>2+</sup> and Ni<sup>2+</sup> ions in 9:1 THF/H<sub>2</sub>O at a CTBA concentration of  $2.8 \times 10^{-5}$  M. To study the selectivity of detection, other metal ions were also added and recorded the absorption and emission spectra of CTBA (Figure 5.19 & 5.20). All metal ions were studied except Hg<sup>2+</sup> and Cd<sup>2+</sup> did not show any obvious change in the absorbance or fluorescence emission. Cd<sup>2+</sup> showed a weak quenching of emission band at 600 nm. The ratiometric fluorescence response ( $I_{428}/I_{600}$ ) of CTBA was also unaffected by the metal ions other than Hg<sup>2+</sup> and Cd<sup>2+</sup> (Figure 5.20). Most of the reported ratiometric sensors for Hg<sup>2+</sup> show cross-sensitivities to heavy metal ions such as Ag<sup>+</sup> and Cu<sup>2+</sup> whereas CTBA showed a very sensitive response to Hg<sup>2+</sup> with a weak interference by Cd<sup>2+</sup>. The selectivity of CTBA to Hg<sup>2+</sup> is illustrated in the bar diagram (Figure

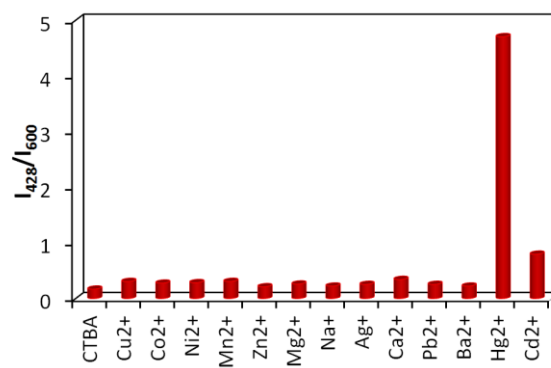
5.21) plotted with the fluorescence intensity obtained for different metal ions at a concentration of  $5.6 \times 10^{-5} \text{M}$ .



**Figure 5.19** Absorption spectra of CTBA recorded in the presence of various metal ions in 9:1 THF/H<sub>2</sub>O. (Metal ion concentration = 65  $\mu\text{M}$ , [CTBA] = 30  $\mu\text{M}$ )



**Figure 5.20** Fluorescence spectra of CTBA recorded in the presence of various metal ions in 9:1 THF/H<sub>2</sub>O. (Metal ion concentration = 65  $\mu\text{M}$ , [CTBA] = 30  $\mu\text{M}$ )  $\lambda_{\text{ex}} = 360 \text{ nm}$ .



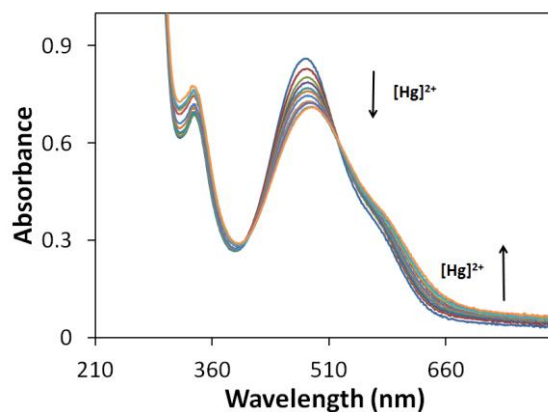
**Figure 5.21** The bar diagram showing the selectivity of CTBA in the detection of Hg<sup>2+</sup> ions

### 5.3.5 Detection of $\text{Hg}^{2+}$ Ions in Aqueous Medium Containing Micelles

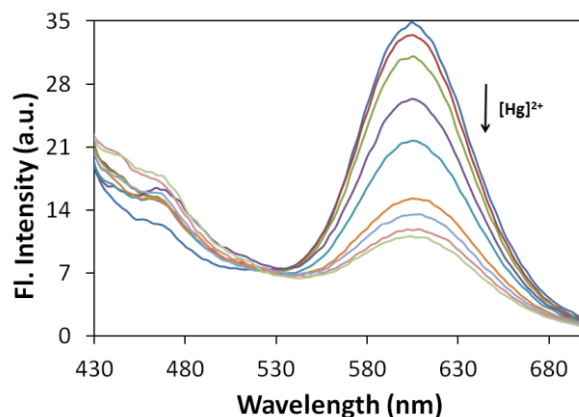
The CTBA was found to be sensitive for  $\text{Hg}^{2+}$  ions in MeCN and in THF/ $\text{H}_2\text{O}$ . In order to explore the applicability of CTBA as a chemosensor to be used in aqueous medium its interaction with metal ions were studied in 100 mM SDS micelles. The concentration of CTBA used for the study was  $\sim 50 \mu\text{M}$  and by Poissonian statistics the average occupancy of CTBA in the micellar assemblies is *ca.* 0.0375 which is  $\ll 0.1$ . Thus, CTBA molecules are distributed in such a way that there is large excess of empty micellar assemblies ruling out multiple occupancies of probe molecules and thus any aggregation effects. By using such micro-heterogenous medium, one could also enhance the usable range as the micellisation of the probe introduce a barrier to free access of metal ions to CTBA. The anionic surfactant, sodium dodecyl sulfate (SDS) is chosen for this study so that the positively charged metal ions will be assisted by the anionic micellar surface in its interaction with CTBA.

Figure 5.22 shows the changes in the absorption spectra of CTBA in 100 mM SDS with the addition of  $\text{Hg}^{2+}$  ions. We observed similar changes in the absorption spectra as in homogenous media such as MeCN. As the concentration of  $\text{Hg}^{2+}$  ions increased, we observed a regular decrease in the absorbance of CTBA at 488 nm with a concomitant increase in absorbance at 338 nm and observed isosbestic points at 405 and 525 nm. Similarly, with an increase in the concentration of  $\text{Hg}^{2+}$  ions, we observed a gradual

decrease in the fluorescence intensity of CTBA (Figure 5.23). Addition of two equivalents of  $\text{Hg}^{2+}$  ions gave quenching of fluorescence intensity.



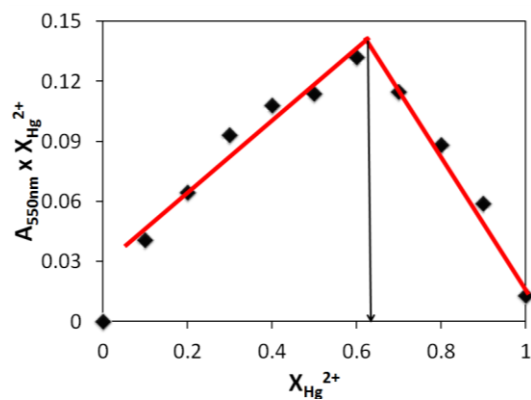
**Figure 5.22** Evolution of absorption spectra of CTBA in the presence of increasing concentration of an aqueous solution of  $\text{Hg}(\text{OAc})_2$  in 100 mM SDS ( $[\text{CTBA}] = 47.7 \mu\text{M}$ ,  $[\text{Hg}(\text{OAc})_2] = 0\text{--}85.56 \mu\text{M}$ ). Arrow indicates the direction change in the absorbance.



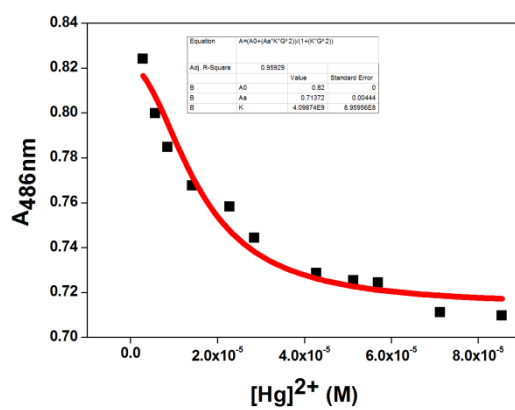
**Figure 5.23** Evolution of fluorescence spectra of CTBA in the presence of increasing concentration of an aqueous solution of  $\text{Hg}(\text{OAc})_2$  in 100 mM SDS ( $[\text{CTBA}] = 19.2 \mu\text{M}$ ,  $[\text{Hg}(\text{OAc})_2] = 0\text{--}22.8 \mu\text{M}$ ,  $\lambda_{\text{ex}} = 405 \text{ nm}$ ). Arrow indicates the direction change in the fluorescence intensity.

The stoichiometry of binding was analyzed by the method of Job's plot and obtained a curve that indicates a CTBA: Hg binding stoichiometry of 1:2 (Figure 5.24). The association constant  $K_a$  was determined by non-linear least square fit of absorbance change at 486 nm and fluorescence intensity changes at 605 nm to a model described for 1:2 binding stoichiometry. The data fitted well to the model with very good correlation (Figure 5.25 & 5.26). By spectrophotometry, an association constant ( $K_{12}$ ) of  $4.09 \times 10^9 \text{ M}^{-2}$  and spectrofluorimetrically an association constant ( $K_{12}$ ) of  $9.58 \times 10^9 \text{ M}^{-2}$  was obtained for the CTBA:  $\text{Hg}^{2+}$  with 1:2 binding stoichiometry in micellar medium.

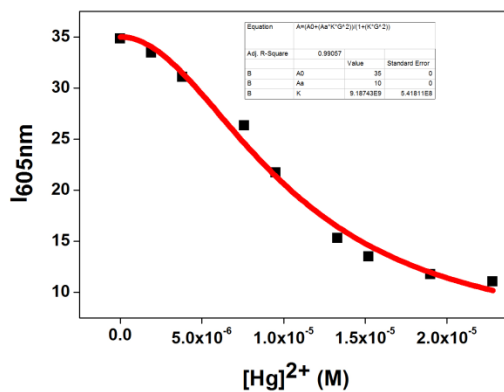




**Figure 5.24** Job's plot analysis of CTBA with  $\text{Hg}^{2+}$  showing a 1:2 binding stoichiometry in 100 mM SDS.

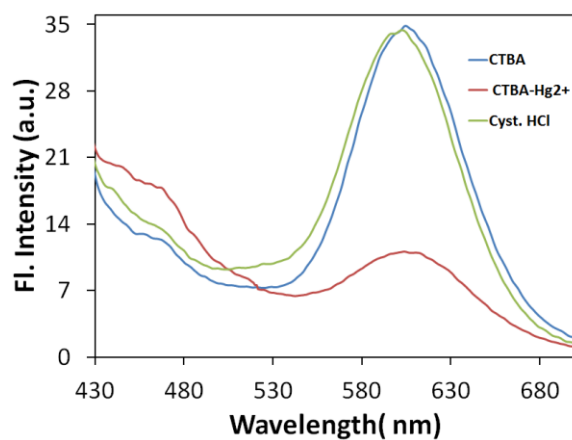


**Figure 5.25** A plot of absorbance at 486 nm vs. concentrations of  $\text{Hg}^{2+}$  in 100 mM SDS.

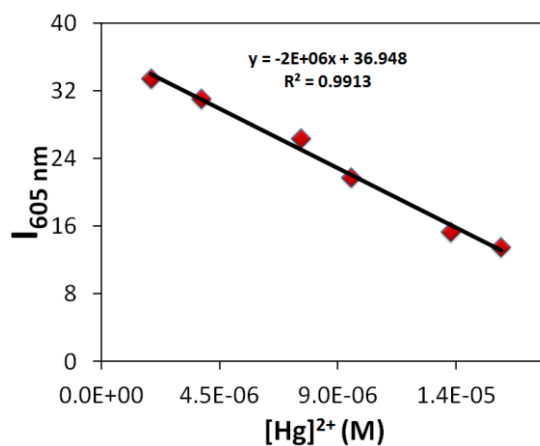


**Figure 5.26** A plot of fluorescence intensity at 605 nm vs. concentrations of  $\text{Hg}^{2+}$  in 100 mM SDS.

The complex formed was found to react with cysteamine hydrochloride and released free CTBA establishing reusability of the chemosensor in practical applications (Figure 5.27). The lowest detection limit in the SDS micellar medium was also estimated by fitting the linear response region of the fluorescence intensity variation against concentration of  $\text{Hg}^{2+}$  to a straight line. A value of 133.5 nM was the detection limit calculated for CTBA mercury interaction in 100 mM SDS micellar medium (Figure 5.28).

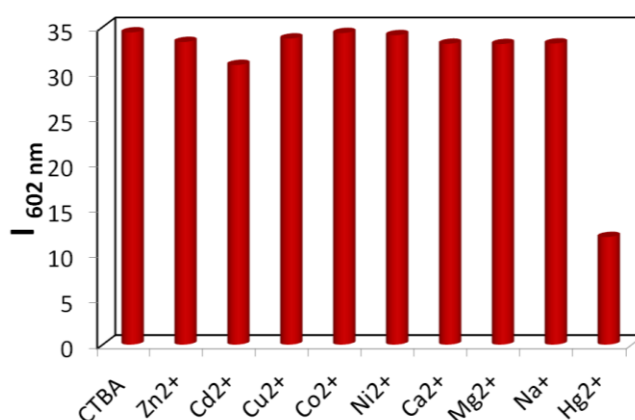


**Figure 5.27** Emission spectrum of CTBA, CTBA-Hg complex and in presence of cysteamine hydrochloride in 100 mM SDS in water. Excitation wavelength is 405 nm



**Figure 5.28** A plot showing variation of fluorescence intensity at 605 nm as a function of concentrations of  $\text{Hg}^{2+}$  in 100 mM SDS

We observed a similar response in selectivity as in homogeneous medium and the CTBA in SDS showed response to  $\text{Hg}^{2+}$  as well as to  $\text{Cd}^{2+}$  with much higher sensitivity to  $\text{Hg}^{2+}$ . The bar diagram showing fluorescence responses to different metal ions are given in Figure 5.29.



**Figure 5.29** The bar diagram showing the selectivity of CTBA in the detection of  $\text{Hg}^{2+}$  ions in 100mM SDS

## 5.4 Conclusions

We developed a reusable, ratiometric and fluorescence Turn-off carbazole thiobarbituric acid conjugate (CTBA) for selective detection of  $\text{Hg}^{2+}$  and  $\text{Cd}^{2+}$ . Among the two metal ions CTBA is more sensitive to  $\text{Hg}^{2+}$ . The complex formed between CTBA and  $\text{Hg}^{2+}$  has a stoichiometry of 1:2. The binding mechanism was established by  $^1\text{H}$  NMR, Jobs plot analysis and fitting the absorption and fluorescence responses to a model describing 1:2

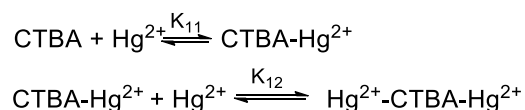
stoichiometry. Clear visual colour changes on metal binding make it a very good indicator for naked eye detection of  $\text{Hg}^{2+}$  ions.

## 5.5 Experimental Section

### 5.5.1 General Photophysical Studies

A stock solution of CTBA with concentration of  $6.9 \times 10^{-3}$  M was prepared in tetrahydrofuran (THF) and stored in a cold and dark place. This stock solution was used for all spectrofluorimetric titrations after appropriate dilution. Absorption spectra were recorded using Evolution 201 UV-visible spectrophotometer. Fluorescence emission spectrum of a sample was measured using a Perkin Elmer luminescence spectrophotometer (model LS 45). Metal ion stock solutions were prepared in the respective medium and used with appropriate dilution.

### 5.5.2 Determination of Association Constant for 1:2 Stoichiometry



The association constant<sup>46</sup> was calculated based on the absorbance or fluorescence titration curve of CTBA with metal ions. Association constant was determined by a nonlinear least squares fit of the data with the following equation as described elsewhere.

$$A = \frac{A_0 + A_\infty K_{12} [G]^2}{1 + K_{12} [G]^2}$$

Where A is absorbance/fluorescence signal,  $A_0$  and  $A_\infty$  are the initial and final absorbance/ fluorescence signal, [G] is total concentration of metal ion

### 5.5.3. Job's Plot by UV-vis Method

A series of solutions containing CTBA and  $\text{Hg}(\text{OAc})_2$  were prepared and kept sum of concentration  $[\text{Hg}^{2+}]$  ion and  $[\text{CTBA}]$  as a constant, whereby, the mole fraction (X) of  $\text{Hg}^{2+}$  was varied from 0.1 to 1.0. The Job's plot<sup>47</sup> is obtained by plotting the absorbance ( $\text{Abs}_{550} \times X_{\text{Hg}^{2+}}$ ) at 550 nm against the mole fraction of the  $\text{Hg}^{2+}$ . The value of mole fraction corresponding to the maximum on the Job's plot thus obtained was 0.67 is an indication of a 1:2 binding stoichiometry.<sup>42</sup>

### 5.5.4 Detection Limit Calculation's Experimental Procedure

The detection limit<sup>42</sup> was calculated based on the fluorescence titration. To calculate the S/N ratio, the emission intensity of CTBA in the absence of Hg(II) was measured 10 times and the standard deviation ( $\sigma$ ) of blank measurements was determined. Three independent duplication measurements of emission intensity at 600 nm in the presence of Hg(II) and the average value of the intensities was plotted against concentration of Hg(II) for determining the slope (**m**). The detection limit is then calculated with the following equation.

$$\text{Detection limit} = 3\sigma/m$$

## 5.6 Reference

1. Amendola, V.; Fabbrizzi, L.; Forti, F.; Licchelli, M.; Mangano, C.; Pallavicini, P.; Poggi, A.; Sacchi, D.; Taglieti, A. *Coord. Chem. Rev.* **2006**, *250*, 273.
2. Valeur, B.; Leray, I. *Coord. Chem. Rev.* **2000**, *205*, 3.
3. De Silva, A. P.; Gunaratne, H.Q.N.; Gunnlaugsson, T.; Huxley, A. J. M.; McCoy, C. P.; Rademacher, J. T.; Rice, T. E. *Chem. Rev.* **1997**, *97*, 1515.
4. De Silva, A. P.; Fox, D. B.; Huxley, A. J. M.; Moody, T. S. *Coord. Chem. Rev.* **2000**, *205*, 41.
5. Hutchinson, T. C.; Meema, K. M. *Lead, mercury, cadmium and arsenic in the environment*; Wiley: New York, **1987**.
6. Scoullou, G. H.; Vonkeman, M. J.; Thornton, L.; Makuch, Z. *In Mercury, Cadmium, and Lead: Handbook for Sustainable Heavy Metals Policy and Regulation (Environment & Policy)*; Kluwer Academic: Norwell, MA, **2001**; Vol. 31.
7. Lo, J. M.; Yu, J. C.; Hutchison, F. I.; Wai, C. M. *Anal. chem.*, **1982**, *54*, 2536.
8. Anderson, K. A. *Mercury analysis in environmental samples by cold vapor techniques, in Encyclopedia of analytical chemistry*, ed. R. A. Meyers, Wiley, New York, **2006**.
9. Kim, H. N.; Ren, W. X.; Kim, J. S.; Yoon, J. *Chem. Soc. Rev.* **2012**, *41*, 3210.



10. Sareen, D.; Kaur, P.; Singh, K. *Coord. Chem. Rev.* **2014**, *265*, 125.
11. Nolan E. M.; Lippard, S. *J. Chem. Rev.* **2008**, *108*, 3443.
12. Jun, M. E.; Roy, B.; Ahn, K. H. *Chem. Commun.* **2011**, *47*, 7583.
13. Kaur, K.; Saini, R.; Kumar, A.; Luxami, V.; Kaur, N.; Singh, P.; Kumar, S. *Coord. Chem. Rev.* **2012**, *17*, 1992.
14. Prodi, L.; Bolletta, F.; Montalti, M.; Zaccheroni, N. *Coord. Chem. Rev.* **2000**, *205*, 59.
15. Chen, X.; Pradhan, T.; Wang, F.; Kim, J. S.; Yoon, J. *Chem. Rev.* **2012**, *112*, 1910.
16. Cho, D.; Sessler, J. L. *Chem. Soc. Rev.* **2009**, *38*, 1647.
17. Jiang, J.; Liu, W.; Cheng, J.; Yang, L.; Jiang, H.; Bai, D.; Liu, W. *Chem. Commun.* **2012**, *67*, 8371.
18. Coronado, E.; Galan-Mascaros, J. R.; Marti-Gastaldo, C.; Palomares, E.; Durrant, J. R.; Vilar, R.; Gratzel, M.; Nazeeruddin, M. K. *J. Am. Chem. Soc.* **2005**, *127*, 12351.
19. Zhu, M.; Yuan, M.; Liu, X.; Xu, J.; Lv, J.; Huang, C.; Liu, H.; Li, Y.; Wang, S.; Zhu, D. *Org. Lett.* **2008**, *10*, 148.
20. Moon, S. Y.; Cha, N. R.; Kim, Y. H.; Chang, S. J. *J. Org. Chem.* **2004**, *69*, 181.
21. Yang, H.; Zhou, Z.; Li, F.; Yi, T.; Huang, C. *Inorg. Chem. Commun.* **2007**, *10*, 1136.
22. Park, J. Y.; In, B. G.; Neupane, L. N.; Lee, K. *Analyst*, **2015**, *140*, 744.
23. Yang, Y.; Yook, K.; Tae, J. *J. Am. Chem. Soc.* **2005**, *127*, 16760.

24. Coskun, A.; Akkaya, E. U. *J. Am. Chem. Soc.* **2006**, *128*, 14474.
25. Wang, J.; Qian, X.; Cui, J. *J. Org. Chem.* **2006**, *71*, 4308.
26. Nolan, E. M.; Lippard, S. J. *J. Mater. Chem.* **2005**, *15*, 2778.
27. Tian, M.; Ihmels, H. *Chem. Commun.* **2009**, 3175.
28. Kim, J. S.; Choi, M. G.; Song, K. C.; No, K. T.; Ahn, S. D.; Chang, S. K. *Org. Lett.* **2007**, *9*, 1129.
29. Liu, B.; Tian, H. *Chem. Commun.* **2005**, 3156.
30. Yuan, M.; Li, Y.; Li, J.; Li, C.; Liu, X.; Lv, J.; Xu, J.; Liu, H.; Wang, S.; Zhu, D. *Org. Lett.* **2007**, *9*, 2313.
31. Zhang, X.; Xiao, Y.; Xuhong, Q. *Angew. Chem., Int. Ed.* **2008**, *47*, 8025.
32. Zhou, Y.; Zhu, C.; Gao, X.; You, X.; Yao, C. *Org. Lett.* **2010**, *12*, 2566.
33. Shults, M. D.; Pearce, D. A.; Imperiali, B. *J. Am. Chem. Soc.* **2003**, *35*, 10591.
34. White, B. R.; Liljestr and, H. M.; Holcombe, J. A. *Analyst* **2008**, *1*, 65.
35. Jang, S.; Thirupathi, P.; Neupane, L. N.; Seong, J.; Lee, H.; Lee, W. I.; Lee, K. *Org. Lett.* **2012**, *18*, 4746.
36. Neupane, L. N.; Thirupathi, P.; Jang, S.; Jang, M. J.; Kim, J. H.; Lee, K. *Talanta* **2011**, *3*, 1566.
37. Neupane, L. N.; Park, J.; Park, J. H.; Lee, K. *Org. Lett.* **2013**, *2*, 254.
38. Kim, D.; Seong, J.; Lee, H.; Lee, K. *Sens. Actuators, B* **2014**, *196*, 421.

39. Hatai, J.; Pal, S.; Jose, G. P.; Bandyopadhyay, S. *Inorg. Chem.* **2012**, *19*, 10129.
40. Kim, J.; Lohani, C. R.; Neupane, L. N.; Choi, Y.; Lee, K. *Chem. Commun.* **2012**, *48*, 3012.
41. Joshi, B. P.; Lohani, C. R.; Lee, K. *Org. Biomol. Chem.* **2010**, *8*, 3220.
42. Yang, M.; Thirupathi, P.; Lee, K. *Org. Lett.* **2011**, *19*, 5028.
43. Lohani, C. R.; Kim, J. M.; Lee, K. *Tetrahedron* **2011**, *67*, 4130.
44. Li, Y.; Zhang, X.; Zhu, B.; Xue, J.; Yan, J. *J. Fluoresc.* **2011**, *21*, 1343.
45. Tehfe, M. A.; Dumur, F.; Graff, B.; Savary, F. M.; Gimes, D.; Fouassier, J. P.; Lalevee, J. *Polym. Chem.* **2013**, *4*, 3866.
46. Park, J.; In, B.; Lee, K. H. *RSC Adv.* **2015**, *5*, 56356.
47. Maity, D.; Govindaraju, T. *Chem. Commun.* **2010**, *46*, 4499.

## Summary and Conclusion

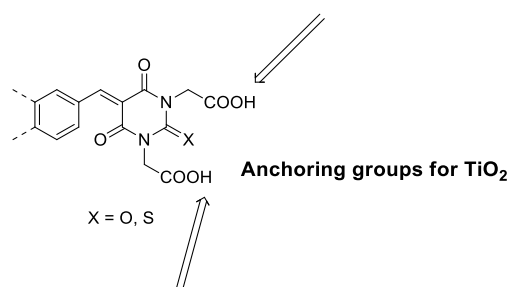
The thesis entitled “**STUDIES ON THE PHOTOVOLTAIC AND METAL ION BINDING PROPERTIES OF A FEW HETEROCYCLIC DONOR- $\pi$ -ACCEPTOR SYSTEMS**” embodies the results of the investigations carried out to study the heterocyclic donor–acceptor systems. The thesis launched with a review of the application of organic donor-acceptor systems in photovoltaics with special emphasis on applications in dye sensitised solar cells and D- $\pi$ -A based sensor for heavy metal ions are outlined in chapter 1.

A simple donor- $\pi$ -acceptor strategy has used for the synthesis of BA and TBA based potential dyes. The direct covalent bonding between the donor and the acceptor moieties leads to an effective overlap between the HOMO and the LUMO energy levels which ensured wide absorption properties to the proposed dyes. In this thesis, eight D- $\pi$ -A systems having either N-octylcarbazole or N-octylphenothiazine as the donor and cyanoacetic acid, rhodanine-3-acetic acid, barbituric acid or thiobarbituric acid as the acceptor units were synthesised and characterised as described in chapter 2. We have selected barbituric and thiobarbituric acid as the acceptor groups, for bringing the excitation energy considerably down and thereby ensure better overlap with the visible solar spectrum.

Appropriately architected D-A moieties in the synthesised dyes leads to the substantial improvement in the absorption properties with elevated molar extinction coefficients are significant for typical ICT

states, which overlap well with the visible region of the solar spectrum is the subject matter of chapter 3.

The prospective dyes having BA and TBA as acceptors showed suitable absorption characteristics and can be found to be useful as sensitizers in solar energy harvesting application. However, low power conversion efficiency was obtained for the barbituric acid and thiobarbituric acid based dyes due to their weak binding interaction with the semiconductor  $\text{TiO}_2$  surface. We can manipulate the binding mode and the interaction ability by suitably placing the NH group in BA and TBA systems with the aid of better anchoring moieties like COOH group (Scheme1). We did an attempt as described but the system couldn't get stabilized and our group is still working on this to stabilise the modified system.



**Scheme 1**

All BA and TBA derivatives show affinity towards heavy metal ion,  $\text{Hg}^{2+}$  and the carbazole barbituric acid and thiobarbituric acid derivatives CBA and CTBA showed solid state emission under UV illumination whereas CTBA showed dual emission. Systematic metal ion binding investigations have been carried out and included in Chapter 4

and 5. In the fourth chapter, we presented the metal ion binding properties of CBA with various mono- and bivalent metal ions as well as their unusual selectivity for the  $\text{Hg}^{2+}$  ions. With increasing concentration of  $\text{Hg}^{2+}$  ion in 1:1 MeOH/ $\text{H}_2\text{O}$  medium, almost 150 fold enhancement in fluorescence emission was observed and the analysis showed a 2:1 binding stoichiometry of the complex formed between and  $\text{Hg}^{2+}$  ions. The enhanced emission intensity can be attributed to the formation of an aggregate or a complex with linear or bend geometry, thereby lead to close interaction between two carbazole moieties favouring aggregation induced emission (AIE). In a microheterogeneous medium such as 100 mM SDS, an enhancement in the emission was observed with increasing concentration of  $\text{Hg}^{2+}$  ions. Furthermore, the enhancement in emission was ascribed to a complex having 1:2 stoichiometry between and ions evidenced that in 1:1 MeOH/ $\text{H}_2\text{O}$  system, the enhancement in emission is indeed due to the aggregation or stacking of carbazole units in the complex with 2:1 binding stoichiometry. The main advantages of this sensor are

- Naked eye detection
- Very sensitive to  $\text{Hg}^{2+}$  ion with a detection limit of 8.89 nm which is less than 2 ppb (the EPA recommended maximum limit allowed for  $\text{Hg}^{2+}$  ion in potable water).

Investigation on the interaction of thiobarbituric acid based derivatives with various heavy metal ions forms the subject matter of the fifth chapter in the thesis. The successive addition of  $\text{Hg}^{2+}$  to a 9:1 THF/ $\text{H}_2\text{O}$  and fully aqueous solutions of thiobarbituric acid based dye

showed a significant change in absorption with an almost 100% quenching of the ICT emission intensity. We obtained ratiometric behaviour during the absorption as well as fluorescence titration of CTBA with  $\text{Hg}^{2+}$  ions in acetonitrile and 9:1 THF/ $\text{H}_2\text{O}$  medium. The analysis showed a 1:2 binding stoichiometry with a high binding constant as  $1.49 \times 10^9 \text{ M}^{-2}$  in all medium studied. Based on the detailed investigations we have developed a reusable, ratiometric and fluorescence turn-off sensor for the selective naked eye detection of  $\text{Hg}^{2+}$  with a lowest detection limit as 13.35 nM. The molecule can be used as a sensor in both aqueous and organic media.

## Publications

1. **K. Kala** and N. Manoj, “A Carbazole Based “Turn on” Fluorescent Sensor for Selective Detection of Hg<sup>2+</sup> in an Aqueous Medium” *RSC Adv.*, **2016**, 6, 22615–22619
2. **Kala K.**, Parvathy O.C, Manoj N. “Colorimetric Detection of Hg (II) Ions using a Simple Barbituric Acid Based Sensor” *MATCON 2016 International Conference on Materials for the Millennium* January 14 -16, 2016. (ISBN 978-93-80095-738)
3. Aswathy A., Vineetha P. K., **Kala K.** Manoj “Pyran-Pyrimidinetrione Conjugate for Heavy Metal Ion Detection” *MATCON 2016 International Conference on Materials for the Millennium* January 14 -16, 2016. (ISBN 978-93-80095-738)
4. **K. Kala** and N. Manoj “Highly selective ratiometric and colorimetric detection of mercury (II) ions in aqueous medium with a carbazole thiobarbituric acid based fluorescent probe” *Journal of Materials Chemistry B*, (under publication)
5. **K. Kala** and N. Manoj “Synthesis and study of phenothiazine and carbazole sensitized organic solar cells: Effect of different dye anchoring group on the cell performance” *Dyes and Pigments* (under publication)

## Oral and Poster Presentations

1. Metal Enhanced Fluorescence: Study of Pyran-Pyrimidinetrione Conjugates for Selective Detection of Mercury, **K. Kala**, Ajayakumar Aswathy, P. K. Vineetha, N. Manoj **oral presentation** *TriPS 2015 UGC sponsored National Seminar* at Sree Sankara college Kalady, Kerala, India
2. Synthesis and Characterization of Rhodamine Appended S-triazine Derivative: Application in Singlet Oxygen Generation, **K. Kala**, O. C. Parvathy, James Kiran, N. Manoj, **Poster Presentation** *TriPS 2015 UGC sponsored National Seminar* at Sree Sankara College Kalady, Kerala, India.



3. Synthesis and characterization of triazine based donor acceptor system, **K. Kala** , O. C. Parvathy and N .Manoj, **Poster Presentation** CTriC 2014 National seminar at Cochin University of Science and Technology, Kerala, India
4. Design and Development of Cyanuric Chloride based Organic catalyst for Asymmetric Catalysis, S. Varun , **K. Kala** and N .Manoj, **Poster Presentation** CTriC 2013 National seminar at Cochin University of Science and Technology, Kerala, India.